


CHANGES IN EXTREME HYDROCLIMATE EVENTS IN INTERIOR ALASKAN BOREAL
FORESTED WATERSHEDS

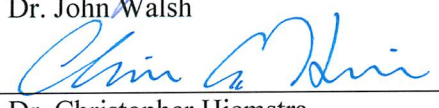
By

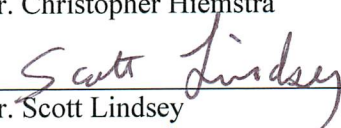
Katrina E. Bennett

RECOMMENDED:









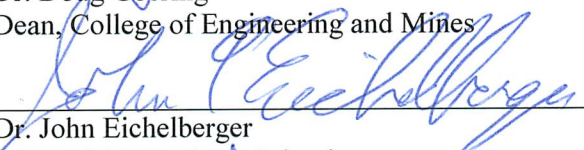






APPROVED:







CHANGES IN EXTREME HYDROCLIMATE EVENTS IN INTERIOR ALASKAN BOREAL
FOREST WATERSHEDS

A

DISSERTATION

Presented to the Faculty
of the University of Alaska Fairbanks

in Partial Fulfillment of the Requirements

for the Degree of

DOCTOR OF PHILOSOPHY

By

Katrina E. Bennett, M.Sc.

Fairbanks, Alaska

December 2014

Abstract

The high latitude regions of the globe are responding to climate change at unprecedented magnitudes and rates. As the climate warms, extreme hydroclimate events are likely to change more than the mean events, and it is the extreme changes that present a risk to society, the economy and the environment of the north. The subarctic boreal forest is one of the largest ecosystems in the world and is greatly understudied with respect to hydroclimate extremes. Thus, defining a baseline for changing extremes is the first step towards planning and implementing adaptation measures to reduce risk and costs associated with the changing extremes. This thesis focuses on quantitative analysis of extreme events using historical data and future model projections of changing temperature, precipitation and streamflow in the Interior forested region of boreal Alaska.

Historically, shifts in the climate have resulted in declining magnitudes of peak flow for snow dominated and glacial Interior Alaskan basins. However, changes are variable and dependent upon watershed topography, permafrost conditions, and glacial extents. Therefore, adjacent basins respond in considerably different ways to the same climate drivers. For example, peak streamflow events in the adjacent Salcha and Chena River basins had different responses to changes in climate. In the higher elevation Salcha basin, maximum streamflow increased as spring temperatures increased but in the lower elevation Chena, winter precipitation was a control on increases in maximum streamflow, while both were influenced by the Pacific Decadal Oscillation. Analysis of hydrologic change must take this variability into account to understand extreme hydroclimate responses and correctly account for process shifts.

To examine future changes in peak streamflow, the implementation and parameterization of hydrologic models to simulate hydroclimate extremes is required. In the northern latitudes of the world, there is a sparse observational station network that may be used for evaluation and correction of hydrologic models. This presents a limitation to science in these regions of the globe and has led to a paucity of research results and consequently, a lack of understanding of the hydrology of northern landscapes. Input of observations from remote sensing and the implementation of models that contain parameterizations specific to northern regions (i.e. permafrost) is one aim of this thesis. Remote sensing of snow cover extent, an important indicator of climate change in the north, was positively validated at snow telemetry sites across Interior Alaska. Input of the snow cover extent observations into a hydrologic model used by the Alaska Pacific River Forecast Center for streamflow flood forecasting improved discharge estimates for poorly observed basins, whereas the discharge estimates in basins with good quality river discharge observations improved little. Estimates of snow water equivalent were improved

compared to station results and the adaptation of the model parameters indicated that the model is more robust, particularly during the snowmelt period when model simulations are error prone.

Use of two independent hydrologic models and multiple global climate models (GCMs) and emission scenarios to simulate changes in future hydroclimate extremes indicated that large regime shifts are projected for snowmelt dominated basins of Interior Alaska. The Chena River basin, nearby Fairbanks, Alaska, is projected to be rainfall dominated by the 2080s, with smaller snowmelt peaks. Return intervals for flooding will increase by one-and-one half to double the flow volume magnitude compared to the historical return interval. Frequency of extreme streamflow events will increase five times the mean increase. These changes in extreme streamflow events necessitate further research on the implications for infrastructure, ecology and economy to constrain risk associated with the projected regime shift in boreal forested watersheds of Interior Alaska.

Table of Contents

	Page
Signature Page.....	i
Title Page	iii
Abstract.....	v
Table of Contents	vii
List of Figures.....	xiii
List of Tables	xv
Acknowledgements	xvii
CHAPTER 1	1
1.1 General Introduction	1
1.2 Literature Review	6
1.2.1 Climate Change.....	8
1.2.2 Extreme Event Analysis.....	11
1.2.3 Hydrologic Models	13
1.2.4 Remote Sensing of Snow.....	16
1.3 Structure of this Thesis.....	18
1.4 Figures.....	19
1.5 References.....	21
CHAPTER 2 : SPATIAL AND TEMPORAL CHANGES IN INDICES OF EXTREME PRECIPITATION AND TEMPERATURE FOR ALASKA.....	33
Abstract.....	33
2.1 Introduction.....	34
2.2 Study Area	36
2.3 Methods.....	37
2.3.1 Selection of Global Climate Models	37

2.3.2	Future Forcing Scenarios	38
2.3.3	Reanalysis Data	38
2.3.4	ClimDEX Calculations	39
2.3.5	Processing ClimDEX.....	40
2.4	Results and Discussion.....	41
2.4.1	Historical Observations and Simulations of Extreme Temperature and Precipitation	41
2.4.2	Projected Changes in Extreme Temperature and Precipitation	43
2.5	Conclusions.....	47
2.6	Acknowledgments	49
2.7	Figures.....	51
2.8	Tables	61
2.9	References.....	67
CHAPTER 3 : HISTORICAL TRENDS AND EXTREMES IN REGIONAL SCALE INTERIOR AND WESTERN ALASKA RIVER BASINS		71
Abstract.....		71
3.1	Introduction.....	72
3.2	Methods.....	74
3.2.1	Study Area	74
3.2.2	Data Sources	75
3.2.3	Analysis	76
3.2.3.1	Trend Analysis	76
3.2.3.2	Generalized Extreme Value Theorem Analysis	77
3.2.3.3	Covariate Analysis	79
3.3	Results	81
3.3.1	Trends	81
3.3.2	Generalized Extreme Value Analysis	82

3.3.3	Covariates Analysis: Climate Variability	83
3.3.4	Covariate Analysis: Precipitation and Temperature.....	84
3.4	Discussion.....	84
3.5	Conclusions.....	87
3.5.1	Implications	88
3.6	Acknowledgements	89
3.7	Figures.....	91
3.8	Tables	101
3.9	References.....	103
 CHAPTER 4 : ESTIMATING, VERIFYING AND PREDICTING SNOW COVER DEPLETION IN BOREAL WATERSHEDS OF INTERIOR ALASKA FROM REMOTE SENSING, <i>IN SITU</i> MEASUREMENTS AND STATISICAL MODELING.....		111
	Abstract.....	111
4.1	Introduction.....	112
4.2	Methods.....	115
4.2.1	Study Area	115
4.2.2	Data Sources	116
4.2.3	Analysis	118
4.3	Results	121
4.3.1	Nonlinear Model.....	122
4.3.2	Nonlinear Logistic Parameters Regression Models	123
4.4	Discussion.....	124
4.5	Conclusions.....	128
4.6	Acknowledgements	129
4.7	Figures.....	131
4.8	Tables	137

4.9	References	141
CHAPTER 5 : USING MODIS ESTIMATES OF FRACTIONAL SNOW COVER EXTENT TO IMPROVE RIVER FORECASTING MODELS IN INTERIOR ALASKA.....		
	Abstract	151
5.1	Introduction	152
5.2	Methods	154
5.2.1	Study Area	154
5.2.2	Data	154
5.2.3	Models	156
5.2.3.1	SNOW17	156
5.2.3.2	SAC-SMA	158
5.2.3.3	Community Hydrologic Prediction System	159
5.2.4	Calibration and Validation	160
5.2.5	Analysis	161
5.3	Results	162
5.3.1	Model Results	162
5.3.2	Parameters	162
5.3.3	SASC and SWE	163
5.3.4	Streamflow Estimates	164
5.3.5	Sensitivity to Parameter SCTOL	165
5.4	Discussion	166
5.5	Conclusions	169
5.6	Acknowledgements	170
5.7	Figures	171
5.8	Tables	183
5.9	References	191

CHAPTER 6 : CLIMATE CHANGE IMPACTS ON EXTREME EVENTS IN A SNOW DOMINATED WATERSHED OF BOREAL INTERIOR ALASKA	195
Abstract.....	195
6.1 Introduction.....	196
6.2 Methods.....	199
6.2.1 Study Area	199
6.2.2 Climate and Topographic Data	199
6.2.3 Models	200
6.2.3.1 SAC-SMA	200
6.2.3.2 VIC	202
6.2.4 GCMs	205
6.2.5 Verification	206
6.2.6 Analysis	206
6.3 Results	207
6.3.1 Calibration and Verification	207
6.3.2 Temperature and Precipitation	208
6.3.3 Streamflow.....	210
6.3.4 Median to Maximum Flow Changes	211
6.3.5 Relationship of Maximum Streamflow to ClimDEX Indices.....	211
6.4 Discussion.....	212
6.5 Conclusions.....	214
6.6 Figures.....	217
6.7 Tables	227
6.8 References.....	235
CHAPTER 7	245
7.1 General Discussion.....	245

7.2	Implications	248
7.3	Conclusions.....	250
7.4	Figures.....	251
7.5	References	253

List of Figures

Figure 1.1 Ecoregions of Alaska.....	19
Figure 1.2 Changes in extremes.....	20
Figure 2.1 Focus sites in Alaska.....	51
Figure 2.2 DJF, MAM, JJA and SON seasonal results for Rx5 versus TNn for RCP 8.5.....	52
Figure 2.3 DJF, MAM, JJA and SON seasonal results for Rx5 versus TXx for RCP 8.5.....	53
Figure 2.4 Graphical plots of TNn for all seasons.....	54
Figure 2.5 Graphical plots of TXx for all seasons.....	55
Figure 2.6 Graphical plots of Rx5 for all seasons.....	56
Figure 2.7 Plots of average daily minimum temperature.....	57
Figure 2.8 Plots of average daily maximum temperature.....	58
Figure 2.9 Plots of maximum 5 day precipitation.....	59
Figure 3.1. Stations analyzed in the study.....	91
Figure 3.2 Streamflow hydrographs shown for 11-day composites for all eight stations.....	92
Figure 3.3 Maximum streamflow trends (%) for the period of record for all eight stations.....	93
Figure 3.4 Minimum streamflow trends (%) for the period of record for all eight stations.....	94
Figure 3.5 GEV results for maximum streamflow for the annual time period.....	95
Figure 3.6 GEV results for maximum streamflow in AMJ.....	96
Figure 3.7 Susitna and Talkeetna river basins elevation ranges.....	97
Figure 3.8 GEV climate variability results for maximum streamflow for AMJ.....	98
Figure 3.9 GEV results for maximum streamflow in MAM, temperature or precipitation covariates.....	99
Figure 4.1 Study sites and their geographic location in Alaska.....	131
Figure 4.2 SNOTEL, NARR, snow course, and MODIS data for all index stations.....	132
Figure 4.3 Inter-comparison with NARR data at the Caribou Poker Creek Research Watershed.....	133
Figure 4.4 Example of the nonlinear regression function.....	134
Figure 4.5 Model fits for the midpoint logistic parameter, predicted versus observed.....	135
Figure 4.6 The Fairbanks GCHN climate station MODIS SCE observed and estimated.....	136
Figure 5.1 Map of the four study basins with upper and lower divisions shown.....	171
Figure 5.2 Snow cover fractional extents based on MOD10A1.....	172
Figure 5.3 Simulated model output for SWE (mm) versus SNOTEL SWE (mm).....	173
Figure 5.4 Study area areal extent of snow cover in the CHPS model framework.....	174
Figure 5.5 Study area basin SWE (in) estimates in CHPS model framework.....	175
Figure 5.6 Streamflow evaluation and validation statistics.....	176

Figure 5.7 Upper Chena River basin simulated versus observed flows.....	177
Figure 5.8 Chatanika River basin simulated versus observed flows.....	178
Figure 5.9 Little Chena River basin simulated versus observed flows.....	179
Figure 5.10 Salcha River basin simulated versus observed flows.....	180
Figure 5.11 Goodpaster River basin simulated versus observed flows.....	181
Figure 6.1 Chena River basin, Interior Alaska, U.S.A.....	217
Figure 6.2 Climatological data.....	218
Figure 6.3 Historical and future hydrological variables.....	219
Figure 6.4 Time series of ClimDEX extremes compared to mean values.....	220
Figure 6.5 Streamflow average historical monthly differences.....	221
Figure 6.6 Chena River Basin SAC model.....	222
Figure 6.7 Chena River Basin VIC model.....	223
Figure 6.8 Chena River basin return intervals for 5, 20, 50 and 100 year return periods.....	224
Figure 6.9 ClimDEX indices and streamflow correlation plot.....	225
Figure 7.1 Large scale climate forcing when applied through landscape filters.....	251

List of Tables

Table 2.1 The six GCMs used in this study	61
Table 2.2 ClimDEX indices selected for use in this study.....	62
Table 2.3 Average seasonal minimum seasonal and annual daily minimum temperature.....	63
Table 2.4 Average seasonal maximum seasonal and annual daily maximum temperature	64
Table 2.5 Average seasonal and annual five-day maximum precipitation	65
Table 2.6 Comparison of changes in extreme values (ClimDEX indices) and mean values.....	66
Table 3.1 Table of station information.....	101
Table 3.2 Monthly, seasonal and annual trends results for the period of records.....	102
Table 4.1 Stations used in the study with physiographic information (2000-2012).	137
Table 4.2 Climate variables and climate indices used to estimate asym, midpt and slope	138
Table 4.3 Training and testing results for RF and GBM for all stations.....	139
Table 4.4 Snowmelt timing statistics for all sites based on the MODIS SCE nonlinear regression.....	140
Table 5.1 Sub-basin characteristics.....	183
Table 5.2 SNOTEL stations.....	184
Table 5.3 Range of parameter values in the SNOW17 model for APRFC and MODIS runs.	185
Table 5.4 Parameters for the MOD10A1 calibration.	186
Table 5.5 Parameters employed in the MODSCAG calibration.	187
Table 5.6 April-May-June monthly calibration statistics.....	188
Table 5.7 Comparison between RMSE (%) and NSE (in brackets) based on AMJ	189
Table 6.1 Chena River basin characteristics	227
Table 6.2 Maximum and minimum temperature weighting factors.....	228
Table 6.3 Calibration and verification results.....	229
Table 6.4 ClimDEX indices, codes, definitions and units.	230
Table 6.5 Regional values for gridded downscaled ensemble	231
Table 6.6 ClimDEX indices for the 2050s and the 2080s.....	232
Table 6.7 The 99th, 95th, 5th, and 50th (median) exceedances.....	233

Acknowledgements

I would like to first and foremost thank my major advisor, Larry Hinzman and my committee members, Jessica Cherry, John Walsh, Christopher Hiemstra and Scott Lindsey for the mentorship, guidance and support you have given me through the degree process. I would also like to thank the Alaska Pacific River Forecast Center for their collaborative spirit during the project. A very special shout out to the different folks at University of Alaska Fairbanks within the IARC, ARSC, GINA and SNAP groups for aiding me along the way. Thank you very much, particularly to Scott Rupp and the Alaska Climate Science Center, along with the National Science and Engineering Council of Canada, for providing me financial support to carry out the bulk of this degree program. All those at PCIC and those who have moved on, your friendship and tutelage in the early days gave me the tools and the skills to apply myself and I am grateful for my time with you all. My family and friends were steadfast pillars of strength for me that I relied upon heavily to get through this time – you’ve been far away but you are always close to my heart. I cannot thank my parents enough for believing in me, for letting me dream and explore in life and for always being there for me. Dad, thanks for encouraging me to become a scientist and not an artist, although I will always strive to find art in the work that I do.

CHAPTER 1

1.1 General Introduction

Extreme hydroclimate events are one of the major ways in which society, the economy and the environment will experience climate change impacts. Changes in extreme events have received great attention in recent years in the literature (CCSP, 2008; Coumou and Rahmstorf, 2012; IPCC, 2012; Peterson et al., 2013; Stocker et al., 2013; Zhang et al., 2011), however there has been little focus on extremes in Alaska's boreal forest region, despite the evidence of an amplified response to climate change at the northern latitudes (ACIA, 2005; Hinzman et al., 2005; Serreze and Barry, 2011). The challenges of understanding changing extreme events in Northern regions are related to the lack of a dense, high quality station network (Cherry et al., 2007; Goodison et al., 1997; Yang et al., 2005) with which to examine both historical trends and model future changes. However, even when and where station records are available, the complexities of the basic hydrologic functions in boreal landscapes including soil moisture regimes in discontinuous permafrost (Ye et al., 2009; Zhang et al., 2005), changing snow characteristics (Liston and Hiemstra, 2011; Zhang, 2005), precipitation and evapotranspiration balances (Rawlins et al., 2010; Serreze et al., 2006; Slater et al., 2007) and the influence of changing permafrost conditions (Osterkamp, 2005; Romanovsky et al., 2010; Smith et al., 2005) on runoff and baseflow contributions (St. Jacques and Sauchyn, 2009; Walvoord and Striegl, 2007), and associated feedbacks and interactions are still poorly understood (Hinzman et al., 2005; Woo et al., 2008).

Understanding changes in extreme hydroclimate (temperature, precipitation and streamflow) in subarctic regions is important because of the risks and costs associated with changing events. A study examining the costs associated with impacts to Alaskan infrastructure as a result of climate change using an economic modeling framework, which included a simple extreme events scalar, estimated expenditures between \$5.6-\$7.6 billion dollars by the 2080s, with up to 45% reduction possible by adaptation strategies (Larsen et al., 2008). Additionally, an increase in extreme hydroclimate events will have an effect on ecology and wildlife in Alaska. For example, floods are associated with increased sedimentation that affects aquatic habitat, while low flows cause increased stream temperature which impacts fish and macroinvertebrates, leading to increased morbidity (Mantua et al., 2010). Caribou die-offs have been noted to occur when freezing rain or deep snow is encountered (Klein, 1991; Miller and Barry, 2009). Moisture regimes impact permafrost thaw rates (Bonan, 1989) and are linked to changes in tree growth in Alaska (Lloyd and Fastie, 2002; Soja et al., 2007; Walker et al., 1987). Floods resulting from ice jams have the propensity to cause enormous damage to settlements located along rivers susceptible to these types of floods (Prowse and Beltaos, 2002). Increased winter baseflow and associated groundwater upwelling may lead to more dangerous ice conditions along river ways, which are used as primary

transportation corridors during the winter (Jones, 2014). Flood events may have the propensity to cause increased degradation of permafrost substrates and thermokarst along stream banks and flood plains that could alter land surfaces (Walker et al., 1987; Yarie et al., 1998). In Alaska, cities and villages are largely located along rivers or close to water sources and therefore Alaskan's will be affected by changing extreme temperature, precipitation and streamflow, including their ability to use rivers for economic, transport and industrial needs.

The study of changes to peak stream flow has been limited to regions outside of Alaska, or very high latitude northern basins. Changes to spring snowmelt peaks have been well documented, and most research indicates an earlier peak stream flow associated with an earlier snowmelt (Stewart et al., 2005) and decreases in snow cover extents (Brown et al., 2010). A number of studies examining peak flooding associated with summer rainfall events in the Kuparuk River basin linked the events to high rainfall occurring across the entire watershed (Kane et al., 2008; Kane et al., 2003). Changes to streamflow, temperature and precipitation extremes in Alaska are limited to a few studies (Stewart et al., 2013), although shifts have been examined in the context of global studies (i.e. IPCC, 2012; Sillmann et al., 2013a; Sillmann et al., 2013b). Regional studies focused on basin responses have not been undertaken, despite the differences that locally scaled inputs may have on the response of extreme hydroclimate (Bürger et al., 2012).

One of the major means by which to examine extreme changes in hydroclimate is to utilize a hydrologic model that simulates energy balances and moisture fluxes to develop scenarios of historical and future changes. To drive models under future conditions, gridded data sets of temperature and precipitation must be developed and tested (Hamlet and Lettenmaier, 2005; Liston and Elder, 2006b), and then coarse scale global models must be downscaled to these data (Hayhoe, 2010). Downscaling has its own inherent uncertainty associated with it, and the type of downscaling procedure can impact how extreme event are represented in models (Bürger et al., 2012; Bürger et al., 2013). Future climate estimates from global models must also be considered for specific regions as some models perform better than others within regions of the globe (Overland et al., 2011). There are additional concerns regarding the accuracy of models to estimate some of the most sensitive components of the hydrologic cycle, e.g. snow and frozen ground (Andreadis et al., 2009; Essery et al., 1999; Liston and Elder, 2006a; Liston and Sturm, 2002; Nicolsky et al., 2007; Pomeroy and Li, 2000; Verseghy, 2009; Verseghy et al., 2000). One approach to deal with this is to use remotely sensed observations of snow cover extent to update hydrologic models. Obtaining improved estimates of snow cover from observations as opposed to relying upon conceptual schemes to estimate the extent of snow has been applied in several studies in the past, with various degrees of success (Andreadis and Lettenmaier, 2006; Parajka and Blöschl, 2008). An additional uncertainty in hydrologic models is the parameterization of frozen ground processes and in

particular, discontinuous permafrost found in the region of Interior Alaska. These outstanding issues in modeling require careful attention as inaccuracies may result in incorrect representation of changes in modeling future climate and in particular, extremes.

The objectives of this thesis are to address these challenges and present an examination of changes in extreme hydroclimate events in Interior Alaskan watersheds, considering:

- historical changes in extremes of temperature and precipitation within the context of the broader Alaskan landscape
- changes in historical extreme streamflow through an analysis of trends and generalized extreme value theory
- validation of remote sensing of snow cover extent at Interior Alaskan sites, and presentation of an approach to model snowmelt timing, which has a large impact on changing flood conditions, using non-linear regression techniques and estimates of regression parameters from reanalysis-based climate variables to simulate snowmelt timing
- insertion of snow cover extent observations from remotely sensed snow cover data sets into a hydrological framework utilized in Alaska for streamflow forecasting
- modeling streamflow extremes to estimate future changes in return levels using downscaled global climate model projections of temperature and precipitation and hydrologic models implemented over a watershed located in a boreal forest watershed surrounding Fairbanks, Alaska

The first paper is entitled “Spatial and temporal changes in indices of extreme precipitation and temperature for Alaska”, and was published in the *International Journal of Climatology* in 2014 (Chapter 2). Future projections of extreme temperature and precipitation are analyzed for Alaska based on the ClimDEX suite of indices and an Environment Canada database of recently released global climate models (GCMs). Extreme minimum temperature changes were greater during all seasons and annually (Alaska, +14.3°C for the 2080s under emission scenario RCP 8.5) and larger than the changes in the mean temperature (+7.4°C for the 2080s under emission scenario RCP 8.5) although this was not true for maximum temperature (+4.4°C compared to +7.4°C for the 2080s under emission scenario RCP 8.5). Spatial variability across the state was observed, with extreme temperature changes generally larger in the north during the cold season and larger in the south during the warm season. An index of 5-day precipitation showed strong increases in absolute values in southern Alaska (annually +25 mm for the 2080s under emission scenario RCP 8.5), but the greatest percentage change occurred in the north (up to +40% at Barrow in some seasons for the 2080s under emission scenario RCP 8.5). Changes were 2-4 times that of inter-GCM standard deviations for all three indicators analyzed, indicating robust projected changes for all GCMs. Model interannual variability in temperature changes decline with time to 2100, hypothesized to be occurring due to reduced sea ice and snow cover in the models by that time.

“Historical trends and extremes in regional scale Interior and Western Alaska river basins” (Chapter 3) details a study using nonparametric trends analysis and generalized extreme value theorem to examine maximum and minimum streamflow changes over the past 50/60 years for eight Interior and Western Alaskan river basins. Increasing maximum streamflow during early April and in late fall and declining late spring, summer and annual flow were documented at stations through Interior Alaska. Variability identified from the nonparametric trends analysis could be linked to regime type. Snow dominated systems and glacial basins exhibited strong declines in maximum streamflow over time, while complex systems such as the Tanana and the Yukon did not exhibit clear trends except flow increases in the fall. Minimum flows were generally increasing, although fewer trends in minimum flow were statistically significant compared to maximum flow trends. Analysis of trends using a complementary approach, generalized extreme value (GEV) theorem, supported the findings of the nonparametric trend study. An investigation of spring maximum streamflow changes revealed that linear nonstationary models best represent trends at almost all stations where trends could be identified (four out of the eight stations). The positive Pacific Decadal Oscillation (PDO) led to lower maximum streamflow values in snowmelt dominated basins and the Arctic Oscillation (AO) was linked to changes in a lake dominated watershed but the rest of the basins did not respond to climate drivers. On the other hand, all basins responded to either temperature or precipitation changes, as expected, with glacially dominant and high elevation snow pack systems largely responding to increased temperatures in April-May-June and snow dominated basins responding to winter precipitation. The study highlights the need for consideration of flow regime when examining trends in streamflow across multiple systems, in-depth analysis utilizing multiple toolsets to verify results and the use of multiple time scales (days to seasons to years) to understand process shifts within river basins.

Chapter 4, “Estimating, verifying and predicting snow cover depletion in boreal watersheds of Interior Alaska from remote sensing, *in situ* measurements and statistical modeling” describes an analysis of snow cover depletion timing in Interior Alaska based on remote sensing of snow cover to estimate snowmelt characteristics using a nonlinear regression approach. Snow cover extent is an important driver to the hydrology of snow dominated systems of the north. Remote sensing tools are available to observe snow cover extent (SCE) across Alaska and show promise when compared against station results at 38 sites across Interior Alaska. The Moderate Resolution Imaging Spectroradiometer (MODIS) remote sensing of (SCE) data were analyzed by using a simple nonlinear regression approach to quantify characteristics of the snow melt depletion curve, including the date of melt onset, and the rate of change (melt) over the snowmelt season. One of these derived indices, the date of snow depletion initiation, was significantly correlated with snow depth in February, March, December-January-February and over the October to mid-April season from results at Global Historical Climate Network (GHCN) stations (2000-

2012), indicating these statistics could be useful for identifying changing snow conditions within these systems. The logistic parameters of the nonlinear regression were then estimated using gradient boosting and tree regression approaches and NARR climate reanalysis data, identifying temperature, albedo, and wind speed in conjunction with topographic features (namely slope and aspect) as important tools to characterize the three parameters in the model. Using the estimate, the nonlinear regression was recreated over the 1970-2012 period and used to produce trends and identify snow timing changes over time across multiple indicators, with most stations having strong and significant changes in melt timing indices over a standardized 30 year period. On the other hand, only one station (Eagle) showed a statistically significant decrease in the snow depth captured at the station (-53 mm). Insertion of these data into modeling tools is deemed reliable and the data are shown to be a useful tool to examine snowmelt timing in Interior Alaskan river basins.

“Using MODIS estimates of fractional snow cover extent to improve river forecasting models in Interior Alaska” describes a study employing the United States National Weather Service’ Alaska Pacific River Forecast Center (APRFC) modeling framework to test the influence of integrating remotely sensed observations of snow cover fractional extent into a snow model and using this output to force a rainfall runoff model to generate streamflow simulations in Interior river basins of Alaska (Chapter 5). The integration of MODIS remote sensing of SCE into the APRFC modeling framework resulted in discernable improvements within sites lacking long term, high quality river gaging records (i.e. Chatanika River basin, +12% RMSE during the calibration period), while sites with quality streamflow gaging records that were calibrated with skill showed little or no improvement. Snow water equivalent estimates matched the melt timing at upper elevation snow telemetry sites located across the Chena River basin. Two different MODIS products were considered in the analysis; MOD10A1 slightly underperformed in basins where improvements in streamflow simulations were observed, whereas MODSCAG performed slightly better, however the results were similar between the two products and it appears that both estimates of snow cover extent work adequately at the basin scale in this region of boreal forest. The use of the semi-lumped model applied may be obscuring improvements that may be possible using a distributed approach. The study results are anticipated to be useful to the APRFC for verification of areal extent of snow cover depletion through the snowmelt season, a time when the model estimates are believed to be uncertain.

A climate change analysis is presented in Chapter 6, “Climate change impacts on extreme events in a snow dominated watershed of boreal Interior Alaska” utilizing two hydrologic models, six downscaled GCMs, two emission scenarios and two time periods to consider changing extreme streamflow for one river basin in Interior Alaska. Results indicate that by the 2050s, a snow melt peak is still projected to occur, although the volume magnitude of the flow is reduced and is similar to the

magnitude of the rainfall peak. However by the 2080s, a complete regime shift to a rainfall dominant system is projected for the Chena River basin. The distributed model that included frozen ground simulations projected a more severe change, while the semi-lumped rainfall-runoff model was better calibrated to current conditions and matched the peak flows with higher accuracy (NSE 0.73 versus 0.51 for 1970-2005). Return interval analysis based on the GEV approach indicated that the 5-year flood event will increase in flow volume by 1.6 times, and the 100-year flow event will double in magnitude by the 2080s. Differences between uncertainty around the return interval based on the range of GCM changes are largest for the 5-year return interval in the 2050s compared to the 2080s. These differences are due the variable representation of snow water equivalent (SWE) in the models, with cooler, wetter projections retaining more snow and warmer, drier models having lower estimates. However the remainder of the results provided similar ranges of uncertainty for both time periods, although for different reasons. Uncertainty during the 2050s is likely due to the range in model response to variable input forcings from the GCMs, and the variable simulation of snow pack changes, while in the 2080s the range is due to differences in the across GCM representations of precipitation. ClimDEX indices examined in the work illustrated large changes in minimum temperatures indices and in (increased) warm spells. Precipitation indices show the greatest changes in the indicators representing moderate extremes compared to the highest precipitation extremes. Maximum streamflow increases were related to total precipitation (increases) and days when minimum temperature is greater than the 90th percentile. This indicates the dominance over time of increasing maximum summer and fall streamflow driven by a rainfall dominant regime in the future.

1.2 Literature Review

Alaska's Interior is part of a broader ecozone referred to as the Lowland Boreal or Taiga region (Figure 1.1). The Alaskan Lowland Boreal extends from the Bering Sea in the west to the Richardson Mountains in the Yukon Territory on the east and bounded by the Brooks Range on the north and the Alaska Range on the south. The region includes the Tanana, Kuskokwim, and Yukon River basins, all of which contain glaciers in their headwaters and therefore are heavily impacted by silt outwash. The Susitna and Talkeetna River basins are located below the Alaska Range and are strongly impacted by large glacial complexes located in their upper headwater regions. The Yukon River is the fourth largest basin in North America and the fifth largest in terms of volume (Schumm and Winkley, 1994). Its headwaters are located in British Columbia, Canada and it flows through the Yukon Territory and Alaska to drain into the Bering Sea at the Yukon-Kuskokwim delta. The basin is considered to be of importance economically and culturally to the peoples of Canada and Alaska (Brabets et al., 2000). Although considered one of the major freshwater inputs to the Arctic Ocean, the overall contribution of the Yukon basin is relatively low

in comparison to other large Eurasian rivers and the Mackenzie (Lammers et al., 2001; McClelland et al., 2006, Peterson et al., 2002). The Susitna and Talkeetna rivers flow into Cook Inlet and the Gulf of Alaska, while the Kuskokwim River flows south west to exit in Kuskokwim Bay west of the Aleutian Islands. Via the Alaska current, inflow from these rivers may contribute minor fresh water inputs to the Bering Sea and the Arctic Ocean.

The Interior of Alaska as a whole is comprised of rolling hills and lowlands, and low, moderate and high mountains (Brabets et al., 2000). Discontinuous permafrost underlies most of the region, with permafrost generally found on north-facing slopes and absent from south-facing slopes and flood plain environments (Jorgenson et al., 2008; Smith et al., 2010). The permafrost though this region is considered to be warm permafrost, with temperatures close to 0°C (Smith et al. 2010). Through the low elevation sections of the Interior, periglacial features such as pingos, thermokarst, ice-wedge polygons and hummocks are found (Kautz and Taber, 2004). Interior river basins such as the Salcha and Chena are considered part of the Yukon-Tanana Uplands ecoregion. The region is described as containing broad, rounded mountains of moderate height, with sharp ridges at higher elevations (Kautz and Taber, 2004). The region is underlain by bedrock and coarse rubble on ridges, with colluvium on lower slopes and fluvial deposits and slope alluvium in the valleys (Nowacki et al., 2001). Loess silts overtop these geological features, deepest at the valley bottoms and shallowest on the slopes. Loess silt has its origin in the late Quaternary and is considered eolian (wind deposited, Muhs and Budahn, 2006). Soils are primarily gelisols (52%, poorly drained), inceptisols (32%, well drained), and entisols (10%); soil temperature and moisture regimes are pergelic or cryic and aquic or udic (Kautz and Taber, 2004). Vegetation consists of white spruce, birch and aspen on south-facing slopes, and black spruce on north-facing slopes (Nowacki et al., 2001). Black spruce woodlands and tussock forming sedges and scrub bogs dominate valley bottoms while the floodplains environments consist of white spruce, balsam poplar, alder, and willows. Above treeline, low birch-ericaceous shrubs and *Dryas*-lichen tundra are found (Nowacki et al., 2001). The two other major ecoregions of Tanana, Kuskokwim, and Susitna river basins are the Tanana-Kuskokwim Lowlands, and the Alaska Range. The Tanana-Kuskokwim Lowlands is an alluvial terraced floodplain environment. Towards the southern part of the Kuskokwim, isolated permafrost dominates (Jorgenson et al., 2008). Eolian loess silt underlies soils and forest cover of similar composition to the Yukon-Tanana Uplands ecoregion. Floodplains contain white spruce, balsam poplar with higher incidence of black spruces on north slopes, in cooler bog environments and tamarack, paper birch, shrubs, and sedge tussocks are found on permafrost flats. Hills and low relief mountains are scattered throughout the region (Kautz and Taber, 2004). The Alaska Range, on the other hand, is a steep mountainous region comprised of metamorphic rocks, with foothills surrounding mountain bases (Kautz and Taber, 2004). Large valley glaciers, icefields and perennial snowpacks make up about 15% of the

area (Kautz and Taber, 2004). Mountain colluvium and alluvium, moraines, drift and outwash deposits are common. The eolian silt present in other ecoregions is confined to the river valleys. Soils are similar to the Tanana Uplands with lesser amounts of the first two soil orders and spodosols (7%) comprising the third. Alpine tundra communities dominate in this environment, with shrubs, willow, birch and alder at lower elevations; permafrost is not present on steep mountainous slopes. More minor parts of the basins include the Kluane Range, Wrangell Mountains, Kuskokwim Mountains, Lime Hills and the Ahklun Mountains. Although the Wrangell Mountains are only a small part of the Tanana River basin, the extensive glacier complexes contribute high amounts glacial runoff, in addition to those glacier systems within the Alaska Range.

The climate in Interior Alaska is continental, featuring cold, long and dark winters with short sunny summers. Monthly average air temperature in Fairbanks ranges from a low of -28°C in the winters to a high of 23°C in July (Shulski and Wendler, 2007). Due to its continental location and position behind the Alaska Range, average annual precipitation is low (254 mm), with an average annual snowfall of 173 cm, hence the region is considered to be semi-arid (Shulski and Wendler, 2007). Large diurnal temperature variability is not uncommon during winter months. Inversions, where the coolest temperatures are found at low elevations and higher temperatures in the hills, are a unique feature of the Fairbanks climate (Shulski and Wendler, 2007). Wind speeds also tend to be low within this region, less than 2 m/s in the winter on average, with higher values (4 m/s) occurring during the summer (Shulski and Wendler, 2007).

1.2.1 Climate Change

Climate change impacts in Alaska reflect the changing Arctic, with strongly increasing global temperature changes and shifts in precipitation variability anticipated. Alaska has warmed more than two times the rate of the rest of the US since the 1950s (Karl et al., 2009). Interior Alaska has warmed the most of all regions in Alaska, increasing by 4°C in winter and 1.9°C annually from 1949-2011 (Stewart et al., 2013). Future projections for Interior Alaska indicate that temperatures will rise by 2-3°C by the 2050s and 4.2-5.3°C by the 2080s under emission scenario A2 of the Coupled Model Intercomparison Project version 3 (CMIP3), based on a multi-model ensemble (Stewart et al., 2013). Annual precipitation estimates from four different data sets analyzing the 60-90°N latitudes indicate that precipitation increased weakly (0.63 +/- 1.27 mm/yr) relative to the 1981-2000 climatology from 1951-2008 (earlier time periods not available due to a lack of observations, see Figure 2.28 in Hartmann et al., 2013). Precipitation for Alaska specifically shows an increase of approximately 10%, with the most amount of change observed in recent decades (Shulski and Wendler 2007, Stewart et al., 2013). McAfee et al. (2013) documented results from seven research studies where precipitation changes were presented as either positive or negative,

with varying levels of statistical significance, for Alaska's Interior (Table 1 in McAfee et al., 2013). Trend analysis indicated non-significant increases in precipitation of 6% and 13.4% for the Fairbanks and McGrath stations, respectively (1950-2010, McAfee et al. 2013). Annual precipitation is projected to increase in Alaska's Interior region by approximately 10-15% by the 2050s and by 20-25% by the 2080s under the A2 CMIP3 ensemble scenario (Stewart et al., 2013) while a 20-40% increase is projected for the 2080s under CMIP5's RCP 8.5 scenario (Walsh et al. 2014). The values presented in the Walsh et al. (2014) report are similar to those numbers projected by ACIA in its 2005 report for the region of the globe north of 60°N for the B2 scenario (ACIA, 2005). Due to the difficulty in measuring solid precipitation, there are major challenges in the historical records and estimates of this variable (Cherry et al., 2007; Goodison, 1978).

Snowpack extents and duration in Alaska have decreased over time by 18% (1966-2012) due to an earlier snow melt (SWIPA, 2012). These value are higher than the 10% decline in snow cover extent presented for the Northern Hemisphere based on data from 1972-2003 (ACIA, 2005). It is unclear if snow depth is increasing or decreasing. Over the North American Arctic, snow depth has decreased since 1950 however there is regional variation in these results (SWIPA, 2012). Snowfall was reported to be increasing in Canada's North, but decreasing in the rest of the country (Mekis and Vincent, 2011). A recent study by Liston and Hiemstra (2011) documented declining snow precipitation based on analysis of MERRA-driven SnowModel results for the entire Arctic. The Fairbanks region exhibited a decrease in snowfall of 1-2% per decade and snow duration declined by 5-10 days per decade over the 30 year period of analysis from 1979-2009. Snow onset was delayed by 2-5 days and snow-off dates were earlier by 2-5 days (Figures 9 and 10 in Liston and Hiemstra, 2011). SWE is mostly declining in the Interior of Alaska, although the trends were weaker than for snow precipitation. Rain on snow events were increasing in some interior regions and decreasing in others (Liston and Hiemstra, 2011). Shrubiness has been noted to be changing in the Arctic and subarctic, which is linked to increases in snow as the shrubs tend to influence drifting and redistribution of moisture. The influence of vegetation on moisture fluxes may lead to altered feedbacks in tussock tundra locations (comprising a small component of boreal ecosystems, Marsh et al., 2010; Pomeroy et al., 2006; Sturm et al., 2001). Future projections of snow cover indicate that by the 2071-2090 period declines of 9-18% (across GCMs) will occur (ACIA, 2005). Seasonality in the change is present, with the greatest declines occurring in April and November, March and December (ACIA, 2005).

Even small changes in snowpack are anticipated to have large and variable impacts to the hydrology and ecology of Alaskan watersheds (Chapin III et al., 2005; Hinzman et al., 2005). Snow insulates the ground during the winter and provides a 'blanket' over the permafrost which guards against cold temperatures from penetrating deep into the soils. Snow has a high albedo such that declines in snow

cover reduce the albedo of the ground surface and cause an increase in energy absorption (Armstrong and Brun, 2008). The snow-albedo feedback has a great influence in the spring when incoming radiation is high (Groisman et al., 1994) and will lead to enhanced warming of the Arctic as a whole (Déry and Brown, 2007). There is a potential for clouds to interact with this feedback as well, as snow albedo can increase under cloudy conditions, leading to enhanced snowmelt and changes in snowmelt timing in the subarctic (Zhang et al., 1996). This is due to changes in incoming shortwave radiation, which is reflected by cloud tops and a corresponding increase in longwave radiation associated with greater emissivity of clouds versus clear sky conditions.

Other climate changes include shifts in permafrost, glaciers and fire regimes. Changes in temperature and snow are affecting frozen ground, and leading to decreases in the permafrost. The temperature of the permafrost near Fairbanks Alaska has risen by 2-4°C from 1930-2003 (Figure 6.22 by Romanovksy 2004 in ACIA 2005). Additionally, the active layer has begun to deepen in some areas. Sixty seven glaciers in Alaska were observed to be thinning with a resulting volumetric change of $-52 \pm 15 \text{ km}^3/\text{yr}$ between the 1950s and the 1990s, with the rate of change observed to be increasing since the 1990s (Arendt et al., 2002). Glacial meltwater contributions are anticipated to rise as a result of continued thinning and melting (ACIA 2005). Fires in Alaska doubled in area during the 2000s compared with other time periods post the 1940s (Kasischke et al., 2010). Permafrost conditions are projected to experience considerable warming, leading to the degradation of permafrost in many areas across Interior Alaska (Stewart et al., 2013). These changes all have consequences for hydrologic regimes in Alaska.

Rivers in north western Canada were observed to have declining magnitudes of annual snowmelt peaks (Cunderlik and Ouarda, 2009). However, in the Mackenzie River basin, no obvious trends were found in terms of changing flow magnitudes from 1973-1999, although variability was noted to be increasing (Woo and Thorne, 2003; Zhang et al., 2001). This was linked to a lack of change in the precipitation minus evaporation (P-E) relationships in these basins (Serreze et al., 2000). On the other hand, Déry and Wood (2005) found decreased streamflow discharge trends from 1964-2003 at coastal stations in Arctic Canada associated with declining precipitation in the region, and stated that these sites are dominated by recent changes in precipitation and not changes in evapotranspiration. However, an updated paper in 2009 revealed a trend reversal towards increasing flows and flow variability when the time series was extended by four years (1964-2007, Déry et al., 2009). These trends were attributed to an ‘intensification’ of the hydrologic cycle that could lead to an increase in peak flows in the Northern American high latitudes (Huntington, 2006; Rawlins et al., 2010). This intensification of hydrology in the Arctic has been associated with climate change driven shifts the water vapor feedback, permafrost extent, snowpack, evapotranspiration, and soil moisture (Rawlins et al., 2010). Baseflow (winter) or low flow values were observed to be increasing in high latitude, western North American river systems (St. Jacques

and Sauchyn, 2009; Walvoord and Striegl, 2007) owing to permafrost thaw (Smith et al., 2007) although precipitation changes are also discussed as a cause (Zhang et al., 2000). Breakup dates on rivers have been noted to be occurring earlier, this is discussed further in the next section (ACIA 2005, Zhang et al., 2001). Challenges in defining streamflow trends and linkages to increased precipitation may be due in part to the consequence of sparse measurements and cold season biases in precipitation observations (Adam and Lettenmaier, 2003; Cherry et al., 2007; Yang et al., 2005).

1.2.2 Extreme Event Analysis

Extreme weather events are defined by the Intergovernmental Panel on Climate Change (IPCC) in their Fifth Assessment Report (AR5, Stocker et al., 2013) as,

An event that is rare at a particular place and time of year. Definitions of rare vary, but an extreme weather event would normally be as rare as or rarer than the 10th or 90th percentile of a probability density function estimated from observations. By definition, the characteristics of what is called extreme weather may vary from place to place in an absolute sense. When a pattern of extreme weather persists for some time, such as a season, it may be classed as an extreme climate event, especially if it yields an average or total that is itself extreme (e.g., drought or heavy rainfall over a season).

The US Climate Change Science Program “synthesis and assessment products” (SAPs) report defined climate extremes similarly, but considered changes over a seasonal or longer term time period (CCSP, 2008). This definition is important because it reinforces that to characterize extreme events we need to define a target set of weather events on which to develop a statistical understanding of their distribution(s). Additionally, the definition makes clear that extreme events analysis must be pursued on a regional basis and across temporal scales to determine the baseline distributions on which to develop a study of changes. Definitions of events that cause impacts are relative to time and space; a return interval event that can cause a flood in one region or basin at one point in time may not necessarily create a flood in another basin at a different time (Lavell et al., 2012). Finally, extreme events are rare by nature and thus the methodology and approaches to determine changes in events must be carefully considered in order to assess impacts correctly and present reliable results for decision making purposes (Zhang and Zwiers, 2013).

Extreme events have been changing with respect to climate shifts and have the capacity to cause deleterious impacts to society and the environment. Extreme events in particular are thought to have a more dramatic effect than changes in mean climate; as first documented by Katz and Brown (1992) and illustrated in SAP Figure ES.I (Figure 1.2 this chapter, CCSP, 2008). Climate extremes have particularly high risks associated with them because many systems are managed (human) and adapted (human and

ecological) according to the frequency and intensity at which they occurred over the historical time or a baseline period in the past. As the climate changes, we are moving into uncharted territory where the historical baseline may be a poor indicator of the magnitude, return interval and timing of climate events.

Due to the concern about changing extreme events, a number of recent synthesis reports and research papers have presented overviews of extreme events occurring at regional, national and global scales. At the global level, Working Groups I (WGI) and II (WGII) of the IPCC's Special Report on Managing the Risks of Extreme Events and Disasters to Advance Climate Change Adaptation (SREX) was released in 2012 (IPCC, 2012). Chapter three of this report specifically details how extremes are changing, with emphasis on shifts in temperature, precipitation, droughts and floods. Temperature extremes have changed - cold days and nights have decreased while warm days and nights have increased and the length of warm spells or heat waves has increased in many regions and in particular in the high latitude Northern Hemisphere region (Alexander et al., 2006; Trenberth et al., 2007). Brown et al. (2008) found extreme trends in land area annual daily maximum temperature maximums and minimums to be increasing across most of the Arctic (1.64-1.95°C), with annual daily minimum temperature maximums and minimums exhibiting the greatest change over the largest percentage of the area (1.98-2.49°C) based on gridded data from 1950-2004. Trends in the number of days above the 90th percentile of minimum temperature for Alaska are for 1-3 more days per decade, with the southern region around Anchorage exhibiting the greatest trends (>2.7 days/decade, Peterson et al., 2008). Extreme temperatures were found to be changing at all stations analyzed in Interior Alaska, with the greatest increases (decreases) occurring in the frequency of warm (cold) extremes occurring in spring and winter (Stewart et al., 2013). Future projected extreme temperature examined globally, including results for Alaska, indicates that most GCMs agree that the fraction of warm days and warm nights will increase, and the fraction of cool days and cool nights will decrease, with the strongest changes projected for the cool indicators annually and for the summer (Orlowsky and Seneviratne, 2012). Kharin et al. (2007) also noted increases in annual daily maximum temperature maximums under different emission scenarios on the order of 2-4°C by the 2090s based on results of 12 CMIP3 GCMs.

Globally, heavy precipitation events have strong regional variation although statistically significant increases are more common than statistically significant decreases (Alexander et al., 2006). In Alaska, heavy precipitation extremes have been increasing south of 62°N, based on the 99.7 percentile of daily precipitation (37%) since the 1950s, although the results were not statistically significant (Groisman et al., 2005). The 95th percentile threshold was noted to have increased by 18%, and total precipitation increased by 10.3%, both statistically significant results. The Canadian Arctic as a whole was analyzed by Stone et al. (2000), measuring large changes (increases) in precipitation events over that region from 1950 onward. Peterson et al. (2008) documented slight decreases in precipitation intensity based on the Simple

Daily Intensity Index (an index value of heavy precipitation) for parts of southern Interior Alaska to the coast, with increases in the rest of the state, although these results were not statistically significant. Extreme precipitation was noted by Stewart et al. (2013) to be highly variable, with only 50% (33%) of stations in Interior Alaska showing increasing trends in heaviest 1% of three day precipitation for spring, summer and fall (winter). Model projections of daily precipitation indicate that wet day intensity, percentage of days with precipitation > 95th quantile, and fraction of days > 10 mm are all increasing in Alaska, with 90% of the 12 CMIP3 GCMs analyzed agreeing on the results (Orlowsky and Seneviratne 2012). Kharin et al. (2007) provided projections of return intervals for daily maximum precipitation rates, and presented results indicating that Alaska and Western Canada would experience an increase in return values between 10 to 30% by the 2080s. One study used downscaled precipitation data to examine extremes, finding a decrease in the probability of extreme precipitation over Alaska; however the authors' suggest that their findings are not robust due to the lack of climate stations in the region (Wang and Zhang, 2008).

Extreme streamflow events have been analyzed across the globe, with no evidence supporting a world-wide or a US/Canada increase in flooding, with most of the changes occurring in low flows or baseflow values (Lins and Slack, 1999; McCabe and Wolock, 1999; McCabe and Wolock, 2002). On the other hand, melt season peak flow in snow-dominated and glacial fed systems is occurring earlier (Regonda et al., 2005; Rosenzweig et al., 2007; Stewart et al., 2005) and earlier breakup is occurring with respect to river ice (Beltaos and Prowse, 2009; Smith, 2000; Zhang et al., 2001). Burn (2008) examined multiple timing measures for changes in peak streamflow in the Mackenzie River basin and found the strongest trends in spring freshet (earlier) across most of the stations for all three time periods (between 1961-2005). Peak flow studies from the Kuparuk River basin in northern Alaska describe two extreme streamflow events that occurred due to high amounts of rainfall falling across the entire river basin (Kane et al., 2008; Kane et al., 2003). Kane argues that while snowmelt peaks are more common, the largest floods will occur during summer rainfall events due to the rainfall amount and intensity coupled with continuous permafrost conditions which retard infiltration.

1.2.3 Hydrologic Models

Hydrologic models are the primary way researchers study and understand climate change impacts on extreme events. There are several classifications of hydrologic models; two main categories are distributed, 'physically' based models and lumped or semi-lumped conceptual models. The semi-lumped conceptual Sacramento Soil Moisture and Accounting (SAC-SMA) model is a widely used rainfall-runoff model that was designed for the US River Forecast Centers for forecasting with a response time greater than 12 hours (Burnash et al., 1973). The model partitions inflow from rain and snow into various upper

and lower compartments that treat water in various ways. The model's upper partition consists of interception, tension water and free water storage. The tension water storages represent water held by capillary force in either the upper or lower zones. Free water percolates from the upper to the lower zone as well as to interflow and surface water runoff. Baseflow occurs from either the primary free water storage or the supplementary free water storages. Direct runoff is also possible. The model requires an estimate of temperature, precipitation, and evapotranspiration at a six-hourly timestep. SAC-SMA is coupled with a temperature index based snow model, referred to as SNOW17 (Anderson, 2006). SNOW17 computes melt as either rain or snow as inflow into the SAC-SMA model. Both SAC-SMA and SNOW17 have parameters that are estimated based on either recommended values or standard settings, or calibrated using the observed streamflow. The Variable Infiltration Capacity (VIC) hydrologic model is a distributed, physically based model that was originally developed as a land surface scheme (Liang et al., 1994; Liang et al., 1996). The model uses the physical understanding of processes that affect the runoff including infiltration, evapotranspiration, snow accumulation and ablation, canopy conductance and frozen ground to develop fluxes of runoff and baseflow on a grid cell basis. The model can be run in full energy balance mode, and with or without the frozen ground module for specific grid cells. Model inputs are precipitation, minimum and maximum temperature and wind speed. Soils, vegetation and topography must be supplied for each grid cell; only vegetation and topography is supplied at a sub-grid cell scale.

Determining the best choice of model for a particular application, such as extreme event analysis, is challenging. Users must weigh the pros and cons of each model and there are literally dozens of hydrologic models available for use (Beven, 2001; Bourdin et al., 2012; Singh and Woolhiser, 2002). A recent study attempting to elucidate why people choose models highlighted the importance of model function, availability, and familiarity (Fleming, 2009). The Distributed Model Intercomparison Project (DMIP) were established specifically to assist the National Weather Service in determining the most suitable model for a specific application, namely river forecasting (Reed et al., 2004; Smith et al., 2004). There are two phases of the project, Phase 1 and Phase 2. Both the SAC-SMA model and a version of the VIC model were included in Phase 1 of the study, although the VIC model results are only provided for daily streamflow for one calibrated river basin (Reed et al., 2004). Out of the twelve models tested, the lumped models performed better than the distributed models, however well calibrated distributed models performed better than the calibrated lumped models at times. For the calibrated model results, the three models that exhibited the best performance in mid-sized watersheds all used the SAC-SMA model for soil moisture accounting. With regards to peak flow runoff statistics, again the lumped models performed better than the distributed models. On the other hand, distributed models outperformed the lumped models for peak flow in basins with distinguishable physiography and soils. Generally, calibrated models that combined conceptual rainfall-runoff approaches with physically based distributed routing performed

best for all basins, with the exception of small watersheds (Reed et al., 2004). In a follow up study (Phase 2), Smith et al. (2012) outlines a comparison of 16 lumped versus distributed models that were part of the Oklahoma DMIP2 study. The findings concluded that while lumped models still outperformed distributed models, the distributed models had improved and they would continue to improve over time. The distributed models performed poorly, in particular, for peak flow estimation, highlighting the challenge of modeling extreme streamflow events.

One particularly challenging aspect of modeling is the problem with model calibration and susceptibility to user error (Smith et al., 2012). This refers to the fact that the model intercomparison studies are not just tests of the model, but also tests of the implementation, calibration and verification of models (i.e. both the model structure and how it was set up). Another issue with regards to comparison of different models is the ways in which they are distinguished, which can be misleading. For example, distributed, 'physically-based' models that contain numerous parameters are in fact, closer to conceptual models because they may not be calibrated uniquely for an each grid cell, or rely upon empirical tools to determine their parameters. This can obscure the true differences between models. This issue is particularly true for domains such as Alaska, where there is a lack of field-based observations with which to develop parameters for distributed, physically-based models.

For climate change studies, a number of other factors with regards to modeling must be considered, and these factors were not included as a part of the National Weather Service's DMIP1 and 2 studies. For example, conceptual models have parameters that are calibrated to streamflow but may be sensitive towards the selection of parameters under different calibration conditions (i.e. wet and dry, Wilby, 2005). Ludwig et al. (2009) assessed three different hydrologic models of varying complexity specifically with respect to the uncertainties related to climate change impacts. The lumped conceptual model overestimated evapotranspiration, while the physical models operated in a reasonable range. The other issue with respect to conceptual models is that it is unclear if their parameterizations, developed and calibrated on current climate, will hold up under a future climate. Current research indicates that parameter uncertainty under future climate is similar to that obtained by recent past climate (Poulin et al., 2011). On the other hand, Ludwig et al. (2009) found that uncertainties across models of increasing complexity can be in the same range as climate scenarios, and thus process descriptions are needed to provide robust predictions of future climate. A more recent study in Quebec found that low flow response was greatly impacted by the selection of hydrologic model, although high flows were much less sensitive (Velázquez et al., 2013). Catchment properties, however, also lent considerably to uncertainty across models (Bloschl and Montanairi, 2010, DMIP studies) These findings have obvious implications for the Arctic, where P-E relationships dictate the response of streamflow to climate change forcings (Serezze et

al., 2000) and where catchments have variable hydrologic conditions in terms of permafrost distributions, geology, topographic position and other factors (e.g. distance from the coast, vegetation).

1.2.4 Remote Sensing of Snow

Approximately 40–50% of the Northern Hemisphere is covered with snow during midwinter, making snow cover the most prevalent land-cover type during the season (Lemke et al., 2007). The accurate capture of snow at a landscape scale remains one of the most important components in the water balance of northern river basins. However, one of the key unknowns in the modeling of hydrology is the model representation of snow across the landscape. One potential approach to addressing this is to replace the modeled snow simulations with remotely sensed observations of snow. Remotely sensed snow measurements began in the 1970s, and more sensors have been added since the early 2000s (Armstrong and Brodzik, 2001), in particular for the North (Romanov et al., 2000). The most recently deployed remote sensors to observe snow is the Visible/Infrared Imager Radiometer Suite (VIIRS) on board the Suomi National Polar-Orbiting Partnership (NPP) satellite (Cao et al., 2013).

Remote sensing of snow is possible due to the primary factors that influence spectral reflectivity and scattering in snow. These include grain size, grain texture, snow depth, snow metamorphism such as aging and albedo, snow stratigraphy (textural and crystal structure changes such as ice lenses, depth hoar), snow liquid water content (or lack thereof), and the physiographic situation of the snowpack itself (topography, aspect, slope, soil and vegetation characteristics of the underlying substrate to the pack, Hall and Martinec, 1985; Sturm et al., 1995). Snow grain size and crystal shapes affect scattering properties in both the visible and the microwave spectral ranges. In the visible spectrum, melting and refreezing in the snow that leads to changes in snow texture and grain sizes can reduce reflectance, which is the main property allowing researchers to correctly identify snow in the visible spectrum (Foster et al., 2005). Grain size differences also lead to an increase in variability of reflectance properties, obscuring the signal (Dozier, 1989). Metamorphism can lead to changes in snow density, crystal shape/texture and changes in liquid water content, which all reduce its reflectivity.

Clouds are also major issue in terms of blocking the visualization of snow or confusion in terms of snow classification (Frei et al., 2012). Clouds reflect a higher proportion of shortwave infrared, and thus have a different reflectivity than snow. However, cloud properties themselves, such as ice crystals, cloud depth, type of cloud (high cirrus, stratocumulus) can also influence reflectance. Techniques to separate these affects from snow properties must be adopted in different terrain types and regions to determine if the algorithms are accurately correcting for the presence of clouds. The near-infrared bands can be used to distinguish between snow and clouds as the near-infrared reflectance of clouds is generally high while the near-infrared reflectance of snow is low (Hall et al., 2010; Hall et al., 2002).

Topography, including slope, aspect and other characteristics of the ground surface (vegetation) can also change the reflectivity of snow on the ground, limiting the use or reducing the accuracy of remote sensing tools (Frei et al., 2012). Shading of snow can produce a change in snow reflectance properties, making it difficult to detect using automatic classification techniques. Additionally, topography can introduce shading effects variably across a landscape. Vegetation such as forest cover, shrubs and exposed bare soils or rocky alpine outcrops (i.e. mountain tops with exposed/blowing snow) can also affect spectral properties by lowering surface albedo, creating issues in terms of detection and classification (Hall et al., 1998). Forest cover, in particular, is a major issue as the sensor cannot see under the canopy to determine snow properties (Chang et al., 1996; Klein et al., 1998).

In the microwave ranges, snow properties influence the scattering of microwave wavelengths proportional to the grain size, which is one of the main properties that allow for microwave detection of snow cover (Chang et al., 1987). The scattering properties of snow become reduced as grain sizes grow larger, which permits estimates of snowpack volume (snow water equivalent, SWE). Passive microwave remote sensing does not require daylight conditions and can penetrate non-liquid forming clouds, which is ideal for northern applications where cloudiness and daylight are issues (Frei et al., 2012). However, the presence of liquid water in the snow pack can change as a result of metamorphism and this can affect the absorption of microwaves in the snow (Foster et al., 1999). Thus wet snow conditions limit the use of passive microwave techniques. Snow depth can also have an effect on the microwave emission properties, setting an upper limit to the maximum snow depth that can be analyzed using microwave remote sensing techniques (Derksen, 2008). Finally, depth hoar also affects scattering properties of the snow and may lead to an over estimation of SWE (Clifford, 2010).

Some of these biases in passive microwave remote sensing products can be overcome by combining these tools with optical sensors, or with active microwave that may compensate for the limitations. Active microwave can be used to map snow-cover characteristics of wet snow but dry snow cannot be identified (Wang et al., 2008). When dry snow is mapped using active microwave data, microwaves pass through the snow and detect/reflect the ground conditions under the snow (König et al., 2001). Off-nadir scatter also affects reflectance properties, which can cause some vegetated surfaces and rock faces to be interpreted as snow at these locations. These require proper correction and adjustment in imagery. Despite this, active sensors can capture snow at high spatial resolutions, reduced swath widths (50–500 km) and have frequent pass overs (König et al., 2001).

The MODIS products are one of the most widely used today to map snow cover extent. The MODIS sensor is situated onboard NASA's Earth Observing System (EOS) Terra satellite, and has been used to calculate snow cover extent since 1999. One algorithm to detect snow in MODIS is based on the normalized difference snow index (NDSI). The suite of MODIS data served up by the National Snow and

Ice Data Center rely upon this algorithm for their MOD10A1 data product. NDSI is calculated as a difference of band 4 and band 6, divided by the sum of band 4 and band 6 (Hall et al., 2002); a threshold NDSI value of 0.4 is used to indicate snow/no snow. The algorithm can detect the difference between clouds and snow, because the reflectance of snow is low while the reflection of clouds remains high on MODIS band 6 (Terra only). Procedures to map the fractional extent of snow cover are based on linear regression for NDSI and were developed from analysis of Landsat scenes (Salomonson and Appel, 2004). Another algorithm to detect snow cover is the MODIS Snow-Covered Area and Grain size (MODSCAG) model (Painter et al., 2009). MODSCAG is a linear spectral mixing model that utilizes snow, rock, soil, vegetation and lake ice endmembers to determine the best model fit based on the spectral characteristics of two or more endmembers. There are several other types of fractional products and combined products that hold great promise for remote sensing of snow (i.e. Foster et al., 2011; Hall et al., 2012).

1.3 Structure of this Thesis

This thesis is paper-based in structure. Chapters 2-6 describe the results of five studies that are included in this thesis as individual manuscripts. The final chapter (Chapter 7) is a summary and synthesis of all five chapters, including implications of the study with respect to infrastructure in Alaska. Individual chapters (Chapters 2-6) contain an abstract, introduction, study area description, and results and discussion sections. Figures, tables and references follow each chapter.

1.4 Figures

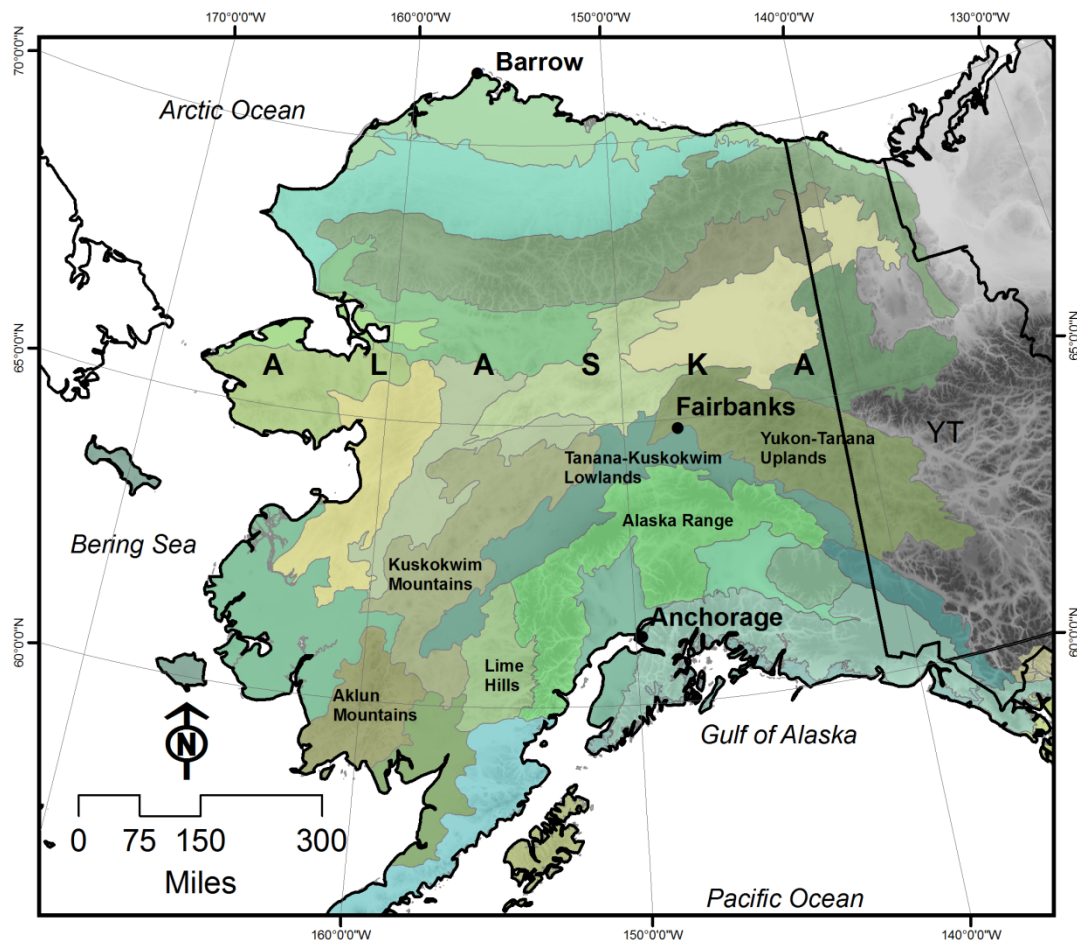


Figure 1.1 Ecoregions of Alaska. Major cities of Anchorage and Fairbanks and the village of Barrow are illustrated.

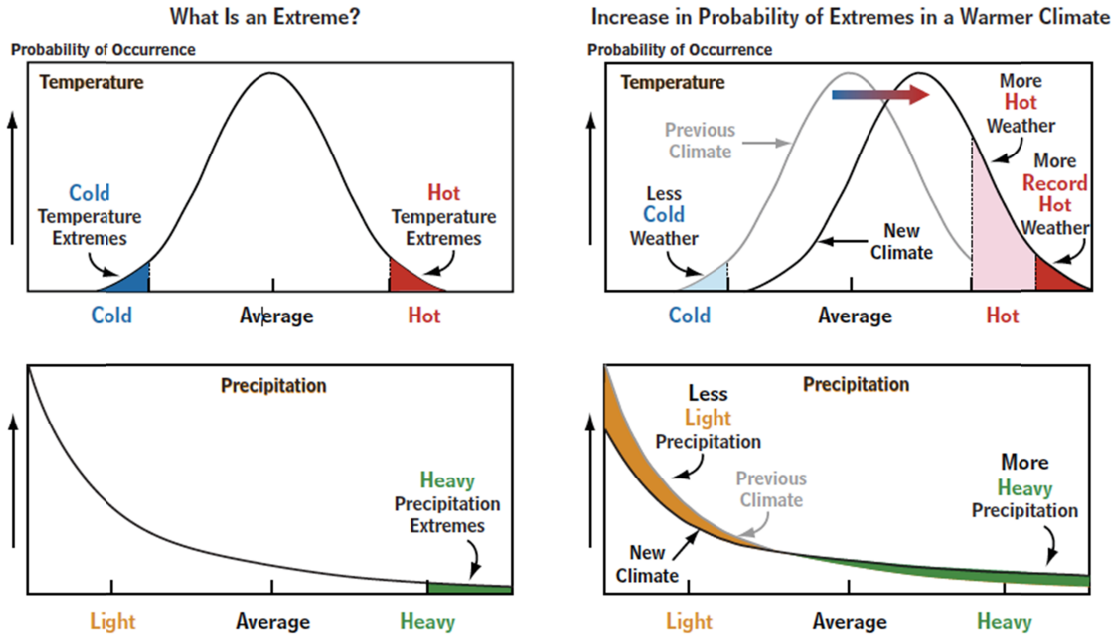


Figure 1.2 Changes in extremes in terms of probability of occurrence. As mean climate changes (right hand panels) the tails of the distributions exhibit greater changes than shifts in the mean of the distribution. Excerpted from CCSP, 2008, Figure ES.1.

1.5 References

- ACIA, 2005. Chapter 6: Cryosphere and Hydrology. In: Walsh, J.E. (Ed.), *The Arctic Climate Impact Assessment*. Cambridge University Press, pp. 1042.
- Adam, J., Lettenmaier, D.P., 2003. Adjustment of global gridded precipitation for systematic bias. *J. Geophys. Res.*, 108 (9): 4257-4271.
- Alexander, L.V., Zhang, X., Peterson, T.C., Caesar, J., Gleason, B., Klein Tank, A.M.G., Haylock, M., Collins, D., Trewin, B., Rahimzadeh, F., Tagipour, A., Rupa Kumar, K., Revadekar, J., Griffiths, G., Vincent, L., Stephenson, D.B., Burn, J., Aguilar, E., Brunet, M., Taylor, M., New, M., Zhai, P., Rusticucci, M., Vazquez-Aguirre, J.L., 2006. Global observed changes in daily climate extremes of temperature and precipitation. *Journal of Geophysical Research: Atmospheres* (1984–2012), 111 (D5).
- Anderson, E., 2006. Snow Accumulation and Ablation Model - SNOW-17. http://www.nws.noaa.gov/oh/hrl/nwsrfs/users_manual/part2/_pdf/22snow17.pdf, NWS NOAA, pp. 44.
- Andreadis, K.M., Lettenmaier, D.P., 2006. Assimilating remotely sensed snow observations into a macroscale hydrology model. *Advances in Water Resources*, 29 (6): 872-886.
- Andreadis, K.M., Storck, P., Lettenmaier, D.P., 2009. Modeling snow accumulation and ablation processes in forested environments. *Water Resour. Res.*, 45 (5).
- Arendt, A.A., Echelmeyer, K.A., Harrison, W.D., Lingle, C.S., Valentine, V.B., 2002. Rapid wastage of Alaska glaciers and their contribution to rising sea level. *Science*, 297 (5580): 382-386.
- Armstrong, R., Brodzik, M., 2001. Recent Northern Hemisphere snow extent: A comparison of data derived from visible and microwave satellite sensors. *Geophys. Res. Lett.*, 28 (19): 3673-3676.
- Armstrong, R.L., Brun, E., 2008. *Snow and climate: physical processes, surface energy exchange and modeling*. Cambridge University Press.
- Beltaos, S., Prowse, T., 2009. River-ice hydrology in a shrinking cryosphere. *Hydrol. Process.*, 23 (1): 122-144.
- Beven, K.J., 2001. *Rainfall-runoff modelling: the primer*. John Wiley & Sons.
- Bonan, G.B., 1989. A computer model of the solar radiation, soil moisture, and soil thermal regimes in boreal forests. *Ecol. Model.*, 45 (4): 275-306.
- Bourdin, D.R., Fleming, S.W., Stull, R.B., 2012. Streamflow modelling: a primer on applications, approaches and challenges. *Atmosphere-Ocean*, 50 (4): 507-536.

- Brabets, T.P., Wang, B., Meade, R.H., 2000. Environmental and hydrologic overview of the Yukon River Basin, Alaska and Canada. Rep. WRIR 99-4204, US Department of the Interior, US Geological Survey, Anchorage, AK, pp. 106.
- Brown, R., Derksen, C., Wang, L., 2010. A multi-data set analysis of variability and change in Arctic spring snow cover extent, 1967–2008. *J. Geophys. Res.: Atmos.*, 115 (D16): D16111.
- Brown, S., Caesar, J., Ferro, C.A., 2008. Global changes in extreme daily temperature since 1950. *Journal of Geophysical Research: Atmospheres* (1984–2012), 113 (D5).
- Bürger, G., Murdock, T., Werner, A., Sobie, S., Cannon, A., 2012. Downscaling extremes-an intercomparison of multiple statistical methods for present climate. *J. Clim.*, 25 (12): 4366-4388.
- Bürger, G., Sobie, S., Cannon, A., Werner, A., Murdock, T., 2013. Downscaling Extremes: An Intercomparison of Multiple Methods for Future Climate. *J. Clim.*, 26 (10): 3429-3449.
- Burn, D.H., 2008. Climatic influences on streamflow timing in the headwaters of the Mackenzie River Basin. *Journal of Hydrology*, 352: 225-238.
- Burnash, R.J.E., Ferral, R.L., McGuire, R.A., 1973. A generalized streamflow simulation system, Joint Federal-State River Forecast Center, Sacramento, CA, pp. 204.
- Cao, C., Xiong, J., Blonski, S., Liu, Q., Uprety, S., Shao, X., Bai, Y., Weng, F., 2013. Suomi NPP VIIRS sensor data record verification, validation, and long-term performance monitoring. *J. Geophys. Res.: Atmos.*, 118 (20): 11,664-11,678.
- CCSP (Ed.), 2008. Weather and Climate Extremes in a Changing Climate. Regions of Focus: North America, Hawaii, Caribbean, and U.S. Pacific Islands. A Report by the U.S. Climate Change Science Program and the Subcommittee on Global Change Research., Karl, T.R. et al.(Eds.). Department of Commerce, NOAA's National Climatic Data Center, Washington, D.C. USA, 164 pp.
- Chang, A., Foster, J., Hall, D., 1987. Nimbus-7 SMMR derived global snow cover parameters. *Annals of Glaciology*, 9 (9): 39-44.
- Chang, A.T.C., Foster, J.L., Hall, D.K., 1996. Effects of forest on the snow parameters derived from microwave measurements during the Boreas winter field campaign. . *Hydrol. Process.*, 10 (12): 1565-1574.
- Chapin III, F.S., Sturm, M., Serreze, M.C., Mcfadden, J.P., Key, J.R., Lloyd, A.H., McGuire, A.D., Rupp, T.S., Lynch, A.H., Schimel, J.P., Beringer, J., Chapman, W.L., Epstein, H.E., Euskirchen, E.S., Hinzman, L.D., Jia, G., Ping, C.L., Tape, K.D., Thompson, C.D.C., Walker, D.A., Welker, J.M., 2005. Role of land-surface changes in arctic summer warming. *Science*, 310 (5748): 657-660.

- Cherry, J.E., Tremblay, L.B., Stieglitz, M., Gong, G., Déry, S.J., 2007. Development of the pan-arctic snowfall reconstruction: new land-based solid precipitation estimates for 1940-99. *J. Hydrometeorol.*, 8 (6): 1243-1263.
- Clifford, D., 2010. Global estimates of snow water equivalent from passive microwave instruments: history, challenges and future developments. *Int. J. Remote Sens.*, 31 (14): 3707-3726.
- Coumou, D., Rahmstorf, S., 2012. A decade of weather extremes. *Nature Climate Change*, 2 (7): 491-496.
- Cunderlik, J.M., Ouarda, T.B., 2009. Trends in the timing and magnitude of floods in Canada. *Journal of Hydrology*, 375 (3): 471-480.
- Derksen, C., 2008. The contribution of AMSR-E 18.7 and 10.7 GHz measurements to improved boreal forest snow water equivalent retrievals. *Remote Sens. Environ.*, 112 (5): 2701-2710.
- Déry, D., Brown, R.D., 2007. Recent North Hemisphere snow cover trends and implications for snow-albedo feedback. *Geophys. Res. Lett.*, 34: 1-6.
- Déry, S.J., Hernández-Henríquez, M.A., Burford, J.E., Wood, E.F., 2009. Observational evidence of an intensifying hydrological cycle in northern Canada. *Geophys. Res. Lett.*, 36 (13): L13402.
- Déry, S.J., Wood, E.F., 2005. Decreasing river discharge in northern Canada. *Geophys. Res. Lett.*, 32.
- Dozier, J., 1989. Spectral signature of alpine snow cover from the Landsat Thematic Mapper. *Remote Sens. Environ.*, 28: 9-22.
- Essery, R., Li, L., Pomeroy, J., 1999. A distributed model of blowing snow over complex terrain. *Hydrol. Process.*, 13 (1415): 2423-2438.
- Fleming, S.W., 2009. An informal survey of watershed model users: Preferences, applications, and rationales. *Streamline Watershed Management Bulletin*, 13 (1): 32-35.
- Foster, J.L., Hall, D.K., Chang, A.T., Rango, A., Wergin, W., Erbe, E., 1999. Effects of snow crystal shape on the scattering of passive microwave radiation. *Geoscience and Remote Sensing, IEEE Transactions on*, 37 (2): 1165-1168.
- Foster, J.L., Hall, D.K., Eylander, J.B., Riggs, G.A., Nghiem, S.V., Tedesco, M., Kim, E., Montesano, P.M., Kelly, R.E., Casey, K.A., 2011. A blended global snow product using visible, passive microwave and scatterometer satellite data. *Int. J. Remote Sens.*, 32 (5): 1371-1395.
- Foster, J.L., Sun, C., Walker, J.P., Kelly, R., Chang, A., Dong, J., Powell, H., 2005. Quantifying the uncertainty in passive microwave snow water equivalent observations. *Remote Sens. Environ.*, 94 (2): 187-203.
- Frei, A., Tedesco, M., Lee, S., Foster, J., Hall, D.K., Kelly, R., Robinson, D.A., 2012. A review of global satellite-derived snow products. *Adv. Space Res.*, 50 (8): 1007-1029.
- Goodison, B., Louie, P., Yang, D., 1997. The WMO solid precipitation measurement intercomparison. *World Meteorological Organization-Publications-WMO TD: 65-70.*

- Goodison, B.E., 1978. Accuracy of Canadian snow gauge measurements. *J. Appl. Meteor.*, 17: 1542-1548.
- Groisman, P.Y., Karl, T.R., Knight, R.W., Stenchikov, G.L., 1994. Changes of snow cover, temperature, and radiative heat balance over the Northern Hemisphere. *J. Clim.*, 7 (11): 1633-1656.
- Groisman, P.Y., Knight, R.W., Easterling, D.R., Karl, T.R., Hegerl, G.C., Razuvaev, V.N., 2005. Trends in intense precipitation in the climate record. *J. Clim.*, 18 (9): 1326-1350.
- Hall, D., Martinec, J., 1985. Remote sensing of snow and ice. *Principles and Applications of Imaging Radar*, edited by FM Henderson and AJ Lewis: 677-703.
- Hall, D.K., Foster, J.L., Kumar, S., Chien, J.Y., Riggs, G.A., 2012. Improving the accuracy of the AFWA-NASA (ANSA) blended snow-cover product over the Lower Great Lakes region. *Hydrol. Earth Syst. Sci. Discuss*, 9: 1141-1161.
- Hall, D.K., Foster, J.L., Verbyla, D.L., Klein, A.G., Benson, C.S., 1998. Assessment of Snow-Cover Mapping Accuracy in a Variety of Vegetation-Cover Densities in Central Alaska. *Remote Sens. Environ.*, 66 (2): 129-137.
- Hall, D.K., Riggs, G.A., Foster, J.L., Kumar, S.V., 2010. Development and evaluation of a cloud-gap-filled MODIS daily snow-cover product. *Remote Sens. Environ.*, 114 (3): 496-503.
- Hall, D.K., Riggs, G.A., Salomonson, V.V., DiGirolamo, N.E., Bayr, K.J., 2002. MODIS snow-cover products. *Remote Sens. Environ.*, 83 (1): 181-194.
- Hamlet, A., Lettenmaier, D.P., 2005. Production of temporally consistent gridded precipitation and temperature fields for the continental United States. *J. Hydrometeorol.*, 6: 330-336.
- Hartmann, D.L., A.M.G. Klein Tank, M. Rusticucci, L.V. Alexander, S. Brönnimann, Y. Charabi, F.J. Dentener, E.J. Dlugokencky, D.R. Easterling, A. Kaplan, B.J. Soden, P.W. Thorne, M. Wild, Zhai, P.M., 2013. Observations: Atmosphere and Surface. In: *Climate Change 2013: The Physical Science Basis. Contribution of Working Group I Fifth Assessment Report of the Intergovernmental Panel on Climate Change*. In: Stocker, T.F., D. Qin, G.-K. Plattner, M. Tignor, S.K. Allen, J. Boschung, A. Nauels, Y. Xia, V. Bex and P.M. Midgley (Ed.), Cambridge University Press, Cambridge, United Kingdom and New York, NY, USA.
- Hayhoe, K., 2010. A standardized framework for evaluating the skill of regional climate downscaling techniques, University of Illinois, Urbana-Champaign, 153 pp.
- Hinzman, L.D., Bettez, N.D., Bolton, W.R., Chapin, F.S., Dyrgerov, M.B., Fastie, C.L., Griffith, B., Hollister, R.D., Hope, A., Huntinton, H.P., Jensen, A.M., Jia, G.J., Jorgenson, T., Kane, D.L., Klein, D.R., Kofinas, G., Lynch, A.H., Lloyd, A.H., McGuire, A.D., Nelson, F.E., Oechel, W.C., Osterkamp, T.E., Racine, C.H., Romanovsky, V.E., Stone, R.S., Stow, D.A., Sturm, M.D., Walker, D.A., Webber, P.J., Welker, J.M., Winker, K.S., Yoshikawa, K., 2005. Evidence and

- implications of recent climate change in northern Alaska and other Arctic regions. *Clim. Change*, 72: 251-298.
- Huntington, T.G., 2006. Evidence for intensification of the global water cycle: Review and synthesis. *Journal of Hydrology*, 319: 83-95.
- IPCC, 2012. *Managing the Risks of Extreme Events and Disasters to Advance Climate Change Adaptation: A Special Report of Working Groups I and II of the Intergovernmental Panel on Climate Change (IPCC)*, Cambridge University Press, Cambridge, UK, and New York, NY, USA., pp. 582.
- Jorgenson, T., Yoshikawa, K., Kanevskiy, M., Shur, Y., Romanovsky, V., Marchenko, S., Grosse, G., Brown, J., Jones, B., 2008. Permafrost Characteristics of Alaska – A new permafrost map of Alaska, Ninth International Conference on Permafrost. Abstract. Institute of Northern Engineering, University of Alaska Fairbanks.
- Kane, D.L., Hinzman, L.D., Gieck, R.E., McNamara, J.P., Youcha, E.K., Oatley, J.A., 2008. Contrasting extreme runoff events in areas of continuous permafrost, Arctic Alaska. *Hydrology Research*, 39 (4): 287-298.
- Kane, D.L., McNamara, J.P., Yang, D.Q., Olsson, P.Q., Gieck, R.E., 2003. An extreme rainfall/runoff event in Arctic Alaska. *J. Hydrometeorol.*, 4 (6): 1220-1228.
- Karl, T.R., Melillo, J.M., Peterson, T.C., 2009. *Global climate change impacts in the United States*. Cambridge University Press.
- Kasischke, E.S., Verbyla, D.L., Rupp, T.S., McGuire, A.D., Murphy, K.A., Jandt, R., Barnes, J.L., Hoy, E.E., Duffy, P.A., Calef, M., 2010. Alaska's changing fire regime-implications for the vulnerability of its boreal forests This article is one of a selection of papers from *The Dynamics of Change in Alaska's Boreal Forests: Resilience and Vulnerability in Response to Climate Warming*. *Can. J. For. Res.*, 40 (7): 1313-1324.
- Katz, R.W., Brown, B.G., 1992. Extreme events in a changing climate: variability is more important than averages. *Clim. Change*, 21: 289-302.
- Kautz, D.R., Taber, P. (Eds.), 2004. *Land Resource Regions and Major Land Resource Areas of Alaska*. USDA - NRCS Alaska, Palmer, Alaska.
- Kharin, V.V., Zwiers, F.W., Zhang, X., Hegerl, G.C., 2007. Changes in temperature and precipitation extremes in the IPCC ensemble of Global Coupled Model simulations. *J. Clim.*, 20: 1419-1444.
- Klein, A.G., Hall, D.K., Riggs, G.A., 1998. Improving snow cover mapping in forests through the use of a canopy reflectance model. *Hydrol. Process.*, 12 (10-11): 1723-1744.
- Klein, D.R., 1991. Limiting factors in caribou population ecology. *Rangifer*, 11 (4): 30-35.

- König, M., Winther, J.G., Isaksson, E., 2001. Measuring snow and glacier ice properties from satellite. *Rev. Geophys.*, 39 (1): 1-27.
- Lammers, R.B., Shiklomanov, A.I., Vörösmarty, C.J., Fekete, B.M., Peterson, B.J., 2001. Assessment of contemporary Arctic river runoff based on observational discharge records. *Journal of Geophysical Research: Atmospheres* (1984–2012), 106 (D4): 3321-3334.
- Larsen, P.H., Goldsmith, S., Smith, O., Wilson, M.L., Strzepek, K., Chinowsky, P., Saylor, B., 2008. Estimating future costs for Alaska public infrastructure at risk from climate change. *Global Environ. Change*, 18 (3): 442-457.
- Lavell, A., Oppenheimer, M., Diop, C., Hess, J., Lempert, R., Li, J., Muir-Wood, R., Myeong, S., Field, C., Barros, V., 2012. Climate change: new dimensions in disaster risk, exposure, vulnerability, and resilience. *Managing the Risks of Extreme Events and Disasters to Advance Climate Change Adaptation*: 25-64.
- Lemke, P., J. Ren, R.B. Alley, I. Allison, J. Carrasco, G. Flato, Y. Fujii, G. Kaser, P. Mote, R.H. Thomas, Zhang, T., 2007. Observations: Changes in Snow, Ice and Frozen Ground. In: Solomon, S. et al. (Eds.), *Climate Change 2007: The Physical Science Basis. Contribution of Working Group I to the Fourth Assessment Report of the Intergovernmental Panel on Climate Change*. Cambridge University Press, Cambridge and New York.
- Liang, X., Lettenmaier, D.P., Wood, E.F., Burges, S.J., 1994. A simple hydrologically based model of land surface water and energy fluxes for general circulation models. *J. Geophys. Res.*, 99 (D7): 14,415-14,428.
- Liang, X., Wood, E.F., Lettenmaier, D.P., 1996. Surface soil moisture parameterization of the VIC-2L model: Evaluation and modification. *Global Planet. Change*, 13: 195-206.
- Lins, H.F., Slack, J.R., 1999. Streamflow trends in the United States. *Geophys. Res. Lett.*, 26 (2): 227-230.
- Liston, G.E., Elder, K., 2006a. A distributed snow-evolution modeling system (SnowModel). *J. Hydrometeorol.*, 7 (6): 1259-1276.
- Liston, G.E., Elder, K., 2006b. A meteorological distribution system for high-resolution terrestrial modeling (MicroMet). *J. Hydrometeorol.*, 7 (2): 217-234.
- Liston, G.E., Hiemstra, C.A., 2011. The changing cryosphere: Pan-Arctic snow trends (1979-2009). *J. Clim.*, 24 (21): 5691-5712.
- Liston, G.E., Sturm, M., 2002. Winter precipitation patterns in arctic Alaska determined from a blowing-snow model and snow-depth observations. *J. Hydrometeorol.*, 3 (6): 646-659.
- Lloyd, A.H., Fastie, C.L., 2002. Spatial and temporal variability in the growth and climate response of treeline trees in Alaska. *Clim. Change*, 52 (4): 481-509.

- Ludwig, R., May, I., Turcotte, R., Vescovi, L., Braun, M., Cyr, J.-F., Fortin, L.-G., Chaumont, D., Biner, S., Chartier, I., 2009. The role of hydrological model complexity and uncertainty in climate change impact assessment. *Advances in Geosciences*, 21 (21): 63-71.
- Mantua, N., Tohver, I., Hamlet, A., 2010. Climate change impacts on streamflow extremes and summertime stream temperature and their possible consequences for freshwater salmon habitat in Washington State. *Clim. Change*, 102 (1-2): 187-223.
- Marsh, P., Bartlett, P., MacKay, M., Pohl, S., Lantz, T., 2010. Snowmelt energetics at a shrub tundra site in the western Canadian Arctic. *Hydrol. Process.*, 24 (25): 3603-3620.
- McCabe, G.J., Wolock, D.M., 1999. General-circulation model simulations of future snowpack in the western United States. *Journal of The American Water Resources Association*, 35 (6): 1473-1484.
- McCabe, G.J., Wolock, D.M., 2002. A step increase in streamflow in the conterminous United States. *Geophys. Res. Lett.*, 29 (24): 38-1-38-4.
- McClelland, J.W., Déry, S.J., Peterson, B.J., Holmes, R.M., Wood, E.F., 2006. A pan-arctic evaluation of changes in river discharge during the latter half of the 20th century. *Geophys. Res. Lett.*, 33 (6).
- Mekis, É., Vincent, L.A., 2011. An overview of the second generation adjusted daily precipitation dataset for trend analysis in Canada. *Atmosphere-Ocean*, 49 (2): 163-177.
- Miller, F.L., Barry, S.J., 2009. Long-Term Control of Peary Caribou Numbers by Unpredictable, Exceptionally Severe Snow or Ice Conditions in a Non-Equilibrium Grazing System. *Arctic*, 62 (2): 175-189.
- Muhs, D.R., Budahn, J.R., 2006. Geochemical evidence for the origin of late Quaternary loess in central Alaska. *Canadian Journal of Earth Sciences*, 43 (3): 323-337.
- Nicolson, D., Romanovsky, V., Alexeev, V., Lawrence, D., 2007. Improved modeling of permafrost dynamics in a GCM land-surface scheme. *Geophys. Res. Lett.*, 34 (8): L08501.
- Nowacki, G., Spencer, P., Brock, T., Fleming, M., Jorgenson, T., 2001. Unified ecoregions of Alaska and neighboring territories. US Geological Survey Open-File Report 02-297. US Geological Survey, Anchorage, Alaska, USA.
- Orlowsky, B., Seneviratne, S.I., 2012. Global changes in extreme events: regional and seasonal dimension. *Clim. Change*, 110 (3-4): 669-696.
- Osterkamp, T., 2005. The recent warming of permafrost in Alaska. *Global Planet. Change*, 49 (3-4): 187-202.
- Overland, J.E., Wang, M., Bond, N.A., Walsh, J.E., Kattsov, V.M., Chapman, W.L., 2011. Considerations in the Selection of Global Climate Models for Regional Climate Projections: The Arctic as a Case Study*. *J. Clim.*, 24 (6): 1583-1597.

- Painter, T.H., Rittger, K., McKenzie, C., Slaughter, P., Davis, R.E., Dozier, J., 2009. Retrieval of subpixel snow covered area, grain size, and albedo from MODIS. *Remote Sens. Environ.*, 113 (4): 868-879.
- Parajka, J., Blöschl, G., 2008. The value of MODIS snow cover data in validating and calibrating conceptual hydrologic models. *Journal of Hydrology*, 358 (3): 240-258.
- Peterson, B.J., Holmes, R.M., McClelland, J.W., Vörösmarty, C.J., Lammers, R.B., Shiklomanov, A.I., Shiklomanov, I.A., Rahmstorf, S., 2002. Increasing river discharge to the Arctic Ocean. *Science*, 298 (5601): 2171-2173.
- Peterson, T., Anderson, D., Cohen, S., Cortez-Vázquez, M., Murnane, R., Parmesan, C., Phillips, D., Pulwarty, R., Stone, J., 2008. Why weather and climate extremes matter. Weather and climate extremes in a changing climate. *Regions of focus: North America, Hawaii, Caribbean, and US Pacific Islands*: 11-33.
- Peterson, T.C., Heim, R.R., Hirsch, R., Kaiser, D.P., Brooks, H., Diffenbaugh, N.S., Dole, R.M., Giovannetone, J.P., Guirguis, K., Karl, T.R., Katz, R.W., Kunkel, K., Lettenmaier, D., McCabe, G.J., Paciorek, C.J., Ryberg, K.R., Schubert, S., Silva, V.B.S., Stewart, B.C., Vecchia, A.V., Villarini, G., Vose, R.S., Walsh, J., Wehner, M., Wolock, D., Wolter, K., Woodhouse, C.A., Wuebbles, D., 2013. Monitoring and Understanding Changes in Heat Waves, Cold Waves, Floods, and Droughts in the United States: State of Knowledge. *B. Am. Meteorol. Soc.*, 94 (6): 821-834.
- Pomeroy, J., Bewley, D., Essery, R., Hedstrom, N., Link, T., Granger, R., Sicart, J.-E., Ellis, C., Janowicz, J., 2006. Shrub tundra snowmelt. *Hydrol. Process.*, 20 (4): 923-941.
- Pomeroy, J., Li, L., 2000. Prairie and Arctic areal snow cover mass balance using a blowing snow model. *Journal of Geophysical Research: Atmospheres (1984–2012)*, 105 (D21): 26619-26634.
- Poulin, A., Brisette, F., Leconte, R., Arsenault, R., Malo, J.-S., 2011. Uncertainty of hydrological modelling in climate change impact studies in a Canadian, snow-dominated river basin. *Journal of hydrology*, 409 (3): 626-636.
- Prowse, T.D., Beltaos, S., 2002. Climatic control of river-ice hydrology: a review. *Hydrol. Process.*, 16 (4): 805-822.
- Rawlins, M.A., Steele, M., Holland, M.M., Adam, J.C., Cherry, J.E., Francis, J.A., Groisman, P.Y., Hinzman, L.D., Huntington, T.G., Kane, D.L., Kimball, J.S., Kwok, R., Lammers, R.B., Lee, C.M., Lettenmaier, D.P., McDonald, K.C., Podest, E., Pundsack, J.W., Rudels, B., Serreze, M.C., Shiklomanov, A., Skagseth, O., Troy, T.J., Vorosmarty, C.J., Wensnahan, M., Wood, E.F., Woodgate, R., Yang, D.Q., Zhang, K., Zhang, T.J., 2010. Analysis of the Arctic System for Freshwater Cycle Intensification: Observations and Expectations. *J. Clim.*, 23 (21): 5715-5737.

- Reed, S., Koren, V., Smith, M., Zhang, Z., Moreda, F., Seo, D.-J., 2004. Overall distributed model intercomparison project results. *Journal of Hydrology*, 298: 27-60.
- Regonda, S.K., Rajagopalan, B., Clark, M., Pitlick, J., 2005. Seasonal cycle shifts in hydroclimatology over the Western United States. *J. Clim.*, 18: 372-384.
- Romanov, P., Gutman, G., Csiszar, I., 2000. Automated monitoring of snow cover over North America with multispectral satellite data. *J. Appl. Meteor.*, 39 (11): 1866-1880.
- Romanovsky, V.E., Smith, S.L., Christiansen, H.H., 2010. Permafrost thermal state in the polar Northern Hemisphere during the international polar year 2007–2009: a synthesis. *Permafrost and Periglacial Processes*, 21 (2): 106-116.
- Rosenzweig, C., G. Casassa, D.J. Karoly, A. Imeson, C. Liu, A. Menzel, S. Rawlins, T.L. Root, B. Seguin, P. Tryjanowski, 2007. Assessment of observed changes and responses in natural and managed systems. *Climate Change 2007: Impacts, Adaptation and Vulnerability. Contribution of Working Group II to the Fourth Assessment Report of the Intergovernmental Panel on Climate Change*, M.L. Parry, O.F. Canziani, J.P. Palutikof, P.J. van der Linden and C.E. Hanson, Eds., Cambridge University Press, Cambridge, UK, 79-131.
- Salomonson, V., Appel, I., 2004. Estimating fractional snow cover from MODIS using the normalized difference snow index. *Remote Sens. Environ.*, 89 (3): 351-360.
- Schumm, S., Winkley, B., 1994. The character of large alluvial rivers. *The variability of large alluvial rivers*: 1-9.
- Serreze, M.C., Barrett, A.P., Slater, A.G., Woodgate, R.A., Aagaard, K., Lammers, R.B., Steele, M., Moritz, R., Meredith, M., Lee, C.M., 2006. The large-scale freshwater cycle of the Arctic. *Journal of Geophysical Research: Oceans (1978–2012)*, 111 (C11).
- Serreze, M.C., Barry, R.G., 2011. Processes and impacts of Arctic amplification: A research synthesis. *Global Planet. Change*, 77 (1–2): 85-96.
- Serreze, M.C., Walsh, J.E., Chapin, F.S., Osterkamp, T., Dyrurgerov, M., Romanovsky, V., Oechel, W.C., Morison, J., Zhang, T., Barry, R.G., 2000. Observational evidence of recent change in the northern high-latitude environment. *Clim. Change*, 46 (1-2): 159-207.
- Shulski, M., Wendler, G., 2007. *The climate of Alaska*. University of Alaska Press.
- Sillmann, J., Kharin, V., Zhang, X., Zwiers, F., Bronaugh, D., 2013a. Climate extremes indices in the CMIP5 multi-model ensemble. Part 1: Model evaluation in the present climate. *J. Geophys. Res.: Atmos.*
- Sillmann, J., Kharin, V., Zwiers, F., Zhang, X., Bronaugh, D., 2013b. Climate extreme indices in the CMIP5 multi-model ensemble. Part 2: Future climate projections. *J. Geophys. Res.: Atmos.*

- Singh, V.P., Woolhiser, D.A., 2002. Mathematical Modeling of Watershed Hydrology. *J. Hydrolog. Eng.*, 7 (4): 270.
- Slater, A., Bohn, T., McCreight, J., Serreze, M., Lettenmaier, D., 2007. A multimodel simulation of pan-Arctic hydrology. *Journal of Geophysical Research: Biogeosciences* (2005–2012), 112 (G4).
- Smith, L.C., 2000. Trends in Russian Arctic river-ice formation and breakup, 1917 to 1994. *Physical Geography*, 21 (1): 46-56.
- Smith, L.C., Pavelsky, T.M., MacDonald, G.M., Shiklomanov, A.I., Lammers, R.B., 2007. Rising minimum daily flows in northern Eurasian rivers: A growing influence of groundwater in the high-latitude hydrologic cycle. *Journal of Geophysical Research: Biogeosciences*, 112 (G4): G04S47.
- Smith, M.B., Koren, V., Zhang, Z., Zhang, Y., Reed, S.M., Cui, Z., Moreda, F., Cosgrove, B.A., Mizukami, N., Anderson, E.A., 2012. Results of the DMIP 2 Oklahoma experiments. *Journal of Hydrology*, 418: 17-48.
- Smith, M.B., Seo, D.-J., Koren, V.I., Reed, S.M., Zhang, Z., Duan, Q., Moreda, F., Cong, S., 2004. The distributed model intercomparison project (DMIP): motivation and experiment design. *Journal of Hydrology*, 298 (1-4): 4-26.
- Smith, S., Romanovsky, V., Lewkowicz, A., Burn, C., Allard, M., Clow, G., Yoshikawa, K., Throop, J., 2010. Thermal state of permafrost in North America: A contribution to the International Polar Year. *Permafrost and Periglacial Processes*, 21 (2): 117-135.
- Smith, S.L., Burgess, M.M., Riseborough, D., Mark Nixon, F., 2005. Recent trends from Canadian permafrost thermal monitoring network sites. *Permafrost and Periglacial Processes*, 16 (1): 19-30.
- Soja, A.J., Tchepakova, N.M., French, N.H., Flannigan, M.D., Shugart, H.H., Stocks, B.J., Sukhinin, A.I., Parfenova, E., Chapin III, F.S., Stackhouse Jr, P.W., 2007. Climate-induced boreal forest change: predictions versus current observations. *Global Planet. Change*, 56 (3): 274-296.
- St. Jacques, J.-M., Sauchyn, D.J., 2009. Increasing winter baseflow and mean annual streamflow from possible permafrost thawing in the Northwest Territories, Canada. *Geophys. Res. Lett.*, 36 (1): L01401.
- Stewart, B., Kunkel, K.E., Stevens, L.E., Sun, L., Walsh, J.E., 2013. Regional Climate Trends and Scenarios for the U.S. National Climate Assessment. Part 7. Climate of Alaska., NOAA/NESDIS, Washington, D.C.
- Stewart, I.T., Cayan, D.R., Dettinger, M.D., 2005. Changes toward earlier streamflow timing across Western North America. *J. Clim.*, 18 (8): 1136-1155.
- Stocker, T., Qin, D., Plattner, G., Tignor, M., Allen, S., Boschung, J., Nauels, A., Xia, Y., Bex, B., Midgley, B. (Eds.), 2013. *Climate Change 2013: The Physical Science Basis. Contribution of*

- Working Group I to the Fifth Assessment Report of the Intergovernmental Panel on Climate Change (IPCC). Cambridge University Press, Cambridge, UK and New York, NY, USA, 1535 pp.
- Stone, D.A., Weaver, A.J., Zwiers, F.W., 2000. Trends in Canadian precipitation intensity. *Atmosphere-Ocean*, 38 (2): 321-347.
- Sturm, M., Holmgren, J., Liston, G., 1995. A Seasonal Snow Cover Classification System for Local to Global Applications. *J. Climate*, 8: 1261-1283.
- Sturm, M., Racine, C., Tape, K., 2001. Climate change: increasing shrub abundance in the Arctic. *Nature*, 411 (6837): 546-547.
- Trenberth, K.E., Jones, P.D., Ambenje, P., Bojariu, R., Easterling, D.R., Tank, A.K., Parker, D., Rahimzadeh, F., Renwick, J.A., Rusticucci, M., Soden, B., Panmao, Z. (Eds.), 2007. Observations: Surface and Atmospheric Climate Change. *Climate Change 2007: The Physical Science Basis. Contribution of Working Group I to the Fourth Assessment Report of the Intergovernmental Panel on Climate Change*, Solomon, S. et al.(Eds.). Cambridge University Press, United Kingdom and New York, NY, USA.
- Velázquez, J., Schmid, J., Ricard, S., Muerth, M., Gauvin St-Denis, B., Minville, M., Chaumont, D., Caya, D., Ludwig, R., Turcotte, R., 2013. An ensemble approach to assess hydrological models' contribution to uncertainties in the analysis of climate change impact on water resources. *Hydrology and Earth System Sciences*, 17 (2): 565-578.
- Verseghy, D., 2009. CLASS–The Canadian Land Surface Scheme (Version 3.4), Technical Documentation (Version 1.1). Climate Research Division, Science and Technology Branch, Environment Canada: 180.
- Verseghy, D.L., Saunders, I.R., Bowers, J., Huo, Z., Bailey, W., 2000. Application of the Canadian Land Surface Scheme (CLASS) to the simulation of energy and water fluxes over alpine tundra. *Atmosphere-Ocean*, 38 (1): 37-55.
- Walker, J., Arnborg, L., Peippo, J., 1987. Riverbank Erosion in the Colville Delta, Alaska. *Geografiska Annaler. Series A, Physical Geography*, 69 (1): 61-70.
- Walvoord, M.A., Striegl, R.G., 2007. Increased groundwater to stream discharge from permafrost thawing in the Yukon River basin: Potential impacts on lateral export of carbon and nitrogen. *Geophys. Res. Lett.*, 34 (12): L12402.
- Wang, J., Zhang, X., 2008. Downscaling and projection of winter extreme daily precipitation over North America. *J. Clim.*, 21 (5): 923-937.
- Wang, L., Derksen, C., Brown, R., 2008. Detection of pan-Arctic terrestrial snowmelt from QuikSCAT, 2000–2005. *Remote Sens. Environ.*, 112 (10): 3794-3805.

- Wilby, R.L., 2005. Uncertainty in water resource model parameters used for climate change impact assessment. *Hydrol. Process.*, 19 (16): 3201-3219.
- Woo, M.K., Kane, D.L., Carey, S.K., Yang, D.Q., 2008. Progress in permafrost hydrology in the new millennium. *Permafrost and Periglacial Processes*, 19 (2): 237-254.
- Woo, M.K., Thorne, R., 2003. Streamflow in the Mackenzie Basin, Canada. *Arctic*, 56 (4): 328-340.
- Yang, D., Kane, D., Zhang, Z., Legates, D., Goodison, B., 2005. Bias corrections of long-term (1973–2004) daily precipitation data over the northern regions. *Geophys. Res. Lett.*, 32: L19501.
- Yarie, J., Viereck, L., Cleve, K.v., Adams, P., 1998. Flooding and Ecosystem Dynamics along the Tanana River. *Bioscience*, 48 (9): 690-695.
- Ye, B.S., Yang, D.Q., Zhang, Z.L., Kane, D.L., 2009. Variation of hydrological regime with permafrost coverage over Lena Basin in Siberia. *Journal of Geophysical Research-Atmospheres*, 114: -.
- Zhang, T., Stamnes, K., Bowling, S.A., 1996. Impact of Clouds on Surface Radiative Fluxes and Snowmelt in the Arctic and Subarctic. *J. Clim.*, 9 (9): 2110-2123.
- Zhang, T.J., 2005. Influence of the seasonal snow cover on the ground thermal regime: An overview. *Rev. Geophys.*, 43 (4): -.
- Zhang, T.J., Frauenfeld, O.W., Serreze, M.C., Etringer, A., Oelke, C., McCreight, J., Barry, R.G., Gilichinsky, D., Yang, D.Q., Ye, H.C., Ling, F., Chudinova, S., 2005. Spatial and temporal variability in active layer thickness over the Russian Arctic drainage basin. *Journal of Geophysical Research-Atmospheres*, 110 (D16): -.
- Zhang, X., Alexander, L., Hegerl, G.C., Jones, P., Tank, A.K., Peterson, T.C., Trewin, B., Zwiers, F.W., 2011. Indices for monitoring changes in extremes based on daily temperature and precipitation data. *Wiley Interdisciplinary Reviews: Climate Change*, 2 (6): 851-870.
- Zhang, X., Harvey, D.K., Hogg, W.D., Yuzyk, T.D., 2001. Trends in Canadian streamflow. *Water Resour. Res.*, 37 (4): 987–998.
- Zhang, X., Vincent, L.A., Hogg, W., Niitsoo, A., 2000. Temperature and precipitation trends in Canada during the 20th century. *Atmosphere-Ocean*, 38 (3): 395-429.
- Zhang, X., Zwiers, F., 2013. Statistical Indices for the Diagnosing and Detecting Changes in Extremes. In: AghaKouchak, A., Easterling, D., Hsu, K., Schubert, S., Sorooshian, S. (Eds.), *Extremes in a Changing Climate*. Water Science and Technology Library. Springer Netherlands, pp. 1-14.

CHAPTER 2: SPATIAL AND TEMPORAL CHANGES IN INDICES OF EXTREME PRECIPITATION AND TEMPERATURE FOR ALASKA¹

Abstract

Extreme temperature and precipitation events in Alaska are examined in an ensemble of global climate models and an atmospheric reanalysis. Extreme monthly maximum and minimum temperature and the monthly maximum 5-day precipitation amount are evaluated for a 30-year historical period and two 30-year future timeslices (2050s, 2080s). Although biases exist, models capture the spatial pattern and seasonality of the extremes depicted by the ERA-40 reanalysis. Discrepancies between station data (Anchorage, Fairbanks, and Barrow) and GCMs/Reanalysis are larger than the model-reanalysis differences, and are consistent with (1) surface elevation differences arising from the models' resolution, and (2) gage undercatch of precipitation in the station data. GCMs project future changes that are two to four times larger than the across-model standard deviations. The largest changes projected by the GCMs are significantly different from the historical mean at the 95% confidence level. Changes in extreme minimum temperature and extreme 5-day precipitation projections are larger than changes in means. The extreme minimum temperatures are projected to increase two to three times as much as the extreme maximum temperatures in all seasons except summer, with the largest increases of extreme minima in coastal regions. By the 2080s, the increases in all three extremes indices are twice as large in the Representation Concentration Pathway (RCP) 8.5 as in the RCP 4.5 scenario. The magnitude of the projected increase of maximum 5-day precipitation is largest in southern and inland areas, although the percentage increase is largest in the north. In the RCP 8.5 simulations, the interannual variability of extreme temperatures narrows by the end of the century, most notably in autumn. Record 5-day precipitation events become more common in the RCP 8.5 than in the RCP 4.5 scenario.

¹ Bennett, K.E. and Walsh, J.E. 2014. Spatial and temporal changes in indices of extreme precipitation and temperature for Alaska. *International Journal of Climatology*. DOI: 10.1002/joc.4067.

2.1 Introduction

In recent years there has been an increasing demand from stakeholders and decision makers for more information on extreme weather events. Examples of such events include extremes of temperature, precipitation and wind. Hydroclimatic extremes are especially important because of associated flooding on the one hand and drought-related impacts such as water availability, vegetative stress and fire risk on the other hand. Due to the high physical and economic impacts of extreme events, decision makers (*e.g.*, emergency responders, the insurance industry, natural resource managers) recognize the need to better account for and predict such occurrences. The expectation of recurrence based on past observations forms the basis of building codes, infrastructure design and operation, and land-use zoning and planning. An increase in the number and consistency of analyses of historic events is needed to improve the baseline for assessments of likelihoods of extreme events. It is also important to consider future changes in extreme events, as these events generally have greater impacts on humans and ecosystems than do changes in climatic means. Impacts vary with the duration of the extreme event, complicating the definition of extreme events and the synthesis of information on them.

There is growing concern that changes in frequency and intensity of extreme weather and climate events are due to human activity (Trenberth and Jones, 2007). Part of the concern is due to the fact that changes in the mean of the distribution are expected to result in correspondingly larger percentage changes in the tails of distribution or the extremes (Katz and Brown, 1992; Zhang and Zwiers, 2013). Attribution of changes in these extreme events first requires determination of whether and where statistically significant changes are occurring. The Intergovernmental Panel on Climate Change (IPCC) Fourth Assessment Report (AR4), summarized much of the research on regional changes in extreme weather and climate events (Trenberth and Jones, 2007). All regions addressed by the IPCC (including the Arctic, examined by Groisman *et al.*, 2005) showed patterns of changes in extremes consistent with a general warming. Recent warming has been especially pronounced in northern high latitudes. Alaska experienced an overall warming of 1.7°C in its mean annual temperature from 1949 to 2012 (Bieniek *et al.*, 2014). Most of this warming has occurred in winter and spring, and the smallest change has occurred in autumn. The possibility that the mean warming is associated with changes in occurrences of extremes is one of the motivations of this study.

The change in four extreme indices in the IPCC AR4 report (Table 3.6 of Working Group I) indicated that the distribution of minimum and maximum temperature had not only shifted, but also changed shape, *i.e.*, the probability density function changed (IPCC, 2007). Minimum temperatures have shown a greater increase than maximum temperatures, which led to a reduction in the diurnal temperature range since 1951. Analyses for Canada excluded the high-latitude Arctic and found no identifiable trends

in extreme precipitation for the country as a whole, although the frequency of days with precipitation did significantly increase during the twentieth century (Vincent and Mekis, 2006; Zhang *et al.*, 2001). It is noteworthy that a focus on extreme events in the Arctic region is absent from the analyses presented in this section of the IPCC AR4.

In 2008, the former U.S. Climate Change Science Program (CCSP - now the United States Global Change Research Program) published a Synthesis and Assessment Product (SAP) 3.3 which addressed the topic of weather and climate extremes (CCSP, 2008). SAP 3.3 found the largest increases in the 90th percentile threshold temperature in the western part of North America from northern Mexico through the western United States and Canada and across Alaska for the observation period from 1950 to 2004. These results were statistically significant at the 95% confidence level across almost all of Alaska, with the exception of the Aleutian Islands. All of Alaska showed an upward trend in the number of days with unusually warm daily low temperatures for the period of record 1950-2004. For the United States and Canada, the largest increases in daily maximum and minimum temperatures were found to occur in the colder days of each month. More recently, Peterson *et al.* (2013) evaluated decadal frequencies in the occurrence of heat waves and cold waves (defined as once-in-five-year magnitude events) for various regions of the United States, including Alaska. Like the other regions of the western United States, Alaska has shown an increase in heat waves and a decrease of cold waves in recent decades (Figure 1 in Peterson *et al.*, 2013).

SAP 3.3 (together with 20 other SAPs produced by CCSP) was summarized into a national climate assessment, *Global Climate Change Impacts in the United States* (Karl *et al.*, 2009). General findings from this report include an expectation of a widespread trend toward more heavy downpours, with precipitation becoming less frequent and more intense, and more precipitation falling as rain rather than snow. As reported in Karl *et al.* (2009), Alaska showed a 23% increase in the amount of precipitation falling in very heavy precipitation events (highest 1% of all daily events) from 1958 to 2007. Alaska had the fourth highest increase behind the Northeast (67%), Hawaii (37%), and the Midwest (31%). Alaska also showed a 13% increase in the number of days with very heavy precipitation during the same period. The state once again had the fourth highest regional increase behind the Northeast (58%), Hawaii (46%), and the Midwest (27%). More recently, the Fifth Assessment Report (AR5) of the IPCC (2013) summarizes observed changes in extremes in its Chapter 2. The fact that the AR5's Chapter 11 on model projections is somewhat sparser in its treatment of future changes, especially in high latitudes, is one of the motivations of the present study.

As the atmosphere warms, evaporation increases, and the atmosphere's capacity to hold moisture also increases. This holding capacity increases by about seven percent for every 1°C rise in temperature (Karl *et al.*, 2009). Concordant with these changes in the water cycle, a corresponding increase in the

intensity of extreme heavy precipitation events is hypothesized, with associated hydrologic impacts (Rawlins *et al.*, 2010). A test of this hypothesis for the Alaskan region is another motivation of the present study.

Alaska is a natural focus for this study because (1) climatic extremes in the Arctic have received considerably less attention than climatic extremes in other areas, so an assessment of Alaskan extremes can serve as prototype for similar studies of other Arctic regions, and (2) Alaska is anticipated to experience larger mean changes as a result of Arctic amplification effects, which could have consequences in the tail ends of the distributions as well as in the means. Moreover, Alaskan extremes have yet to be assessed in a study that includes both historical and future extremes in a common analysis framework. Adding to the timeliness of the present study is the recent release of a compilation of a gridded database on climate model-derived climatic extremes (the ClimDEX archive of CMIP5 output), providing an opportunity to examine changes in extremes of hydroclimate drivers, *i.e.* temperature and precipitation extremes (Sillmann *et al.*, 2013a; Sillmann *et al.*, 2013b).

The over-arching objective of the present study is to document the spatial patterns of ongoing and projected changes in extremes in Alaska, and to assess the level of agreement among different models in the projections of changes in extremes. The focus will be on variables (maximum and minimum temperature, and maximum five-day precipitation) that are directly relevant to high-impact hydrologic events (floods, droughts), although one intent of the present study is to highlight the availability of GCM-derived information on extremes. An additional goal of the study is to provide an analysis of historical and projected occurrences of extremes in Alaska, within a consistent framework. In particular, our use of standard (ClimDEX) indices of extremes will enable comparisons with other regions across the U.S. and globally.

2.2 Study Area

The Alaska region is used as a case study for assessing changes in climatic extremes both in climate models and in reference (historical) data (Figure 2.1). The domain over which model output was analyzed is 55-75°N, 134-172°W. As reference data, we use reanalysis output as well as station-based observations along a north-south transect in Alaska. The transect extends from the coast of the Arctic Ocean (Barrow) to the southern portion of the Arctic mainland (Anchorage), which is only about 100 km north of the Gulf of Alaska. While Alaska's climate is characterized by large heterogeneities arising from topography, proximity to coasts and sea ice, as well as the large size of the state, it is also poorly sampled by a sparse network of first-order stations (Bieniek *et al.*, 2012). For this reason, we limit our selection of in-situ data to three first-order stations that have complete records for the historical period of interest (1971-2000) and that capture a cross section of the north-to-south range in the state's climate.

The station-based observations include the Anchorage International Airport (61.17N, 150.03W, 37 m, USW00026451, referred to in text and figures as ANC), the Fairbanks International Airport (64.80N, 147.88W, 132 m, USW00026411, referred to in text and figures as FAI), and the Barrow Airport (71.2834N, 156.7815W, 9 m, USW00027502, referred to in text and figures as BRW). The sites are not intended to illustrate the variability in climate conditions across the entire state, but rather were selected to show how the ClimDEX results correspond to station data at three widely different climate locations in Alaska. These stations were selected as examples and for comparison with statewide fields of temperature and precipitation from a major atmospheric reanalysis, described below.

2.3 Methods

2.3.1 Selection of Global Climate Models

A set of more than twenty global climate models (GCMs) from the CMIP5 archive were evaluated for their ability to simulate the historical climate of the Alaska region. The key metrics of evaluation were the seasonal cycles of surface air temperature, precipitation and sea level pressure over the Alaskan domain defined in the preceding section. The historical validation data were the climatological mean fields for 1981-2000 from the ERA-40 reanalysis (Uppala *et al.*, 2005). For each calendar month and each of the three variables, the root-mean-square error (RMSE, model minus reanalysis) was evaluated for all grid cells and then summed over the 12 calendar months. The GCMs were ranked from smallest to largest RMSE, and the ranks of each model for temperature, precipitation and sea level pressure were summed. The summed rankings provided an Alaskan performance metric which, together with the availability of the corresponding information on extremes in the ClimDEX archive, led to our identification of a subset of six GCMs for inclusion in our comparison of simulated extremes: Max-Planck Institute Earth System Model MPI-ESM-LR, the Community Climate System Model CCSM4, the Canadian Earth System Model CanESM2, Japan Meteorological Research Institute's MRI-CGCM3, Institut Pierre Simon Laplace Climate Model IPSL-CM5A-LR, and the Centre National de Recherches Météorologiques CNRM-CM5.1. The main attributes of these models are listed in Table 2.1.

It should be emphasized that the results of the GCM model evaluation pertain to Alaska only and would be different had different variables or even different metrics been used. In the context of the present paper, we note that simulated extremes were not used in this evaluation of the models. The relative performance of global climate models is known to vary with region, variable and metric (Reichler and Kim, 2008), and there is no “one size fits all” evaluation procedure (Overland *et al.*, 2011). Nevertheless, the procedure described above represents one practical means for selecting a subset of CMIP5 models to illustrate the across-model variations of simulations of extreme events in our region of

interest. For GCMs having an ensemble of available simulations, the first of those simulations was selected for analysis to both limit the computation effort and focus the discussion of results to differences between GCMs and not between multiple ensemble members from the same models. Across-model differences are generally much larger than differences among ensemble members from a single model (Walsh *et al.*, 2008). The considerable internal variability in climate models contributes to these differences and will be a factor in comparisons among ensemble members from a single climate model as well as in across-model comparisons (Deser *et al.*, 2012).

2.3.2 Future Forcing Scenarios

Future climate projections from global climate models require specifications of the external forcing, which are dependent on emission scenarios of greenhouse gases and aerosols, as well as land use, technology and economic development. Because the factors contributing to future external forcing are not known, a range of future forcing scenarios is generally used to obtain future projections of climate. The most recently developed set of forcing scenarios has been termed “Representative Concentration Pathways” or RCPs (Moss *et al.*, 2010). These scenarios are termed RCP 2.6, RCP 4.5, RCP 6.0 and RCP 8.5, with the numerical values (2.6, 4.5, etc.) indicating the end-of-century (year 2100) radiative forcing in Watts per m² resulting from anthropogenic inputs to the atmosphere (but not including changes in land use). The low-end RCP 2.6 scenario is considered highly unlikely by researchers, as it assumes a substantial reduction (~70%) in greenhouse gas emissions by 2050. The RCP 6.0 scenario is comparable to the mid-range A1B scenario of the previous generation of scenarios used in the Fourth Assessment Report of the IPCC (2007). In the present study, we use the RCP 4.5 and RCP 8.5, which can be loosely termed “low-end” and “high-end” emission scenarios, to illustrate the dependence of future occurrences of Alaskan extremes on the emission scenario. We note that present rates of greenhouse gas emissions are closest to the RCP 8.5 scenario.

2.3.3 Reanalysis Data

The European Centre for Medium-Range Weather Forecasts (ECMWF) Re-Analysis, (ERA-40), like other reanalysis products, directly assimilates observed air temperature and sea level pressure (SLP) observations into a gridded product spanning the period from 1958-2002. A subsequent product, ERA-Interim, continues beyond 2002 but is not used here because our historical reference period is 1971-2000. While temperature observations are assimilated directly into the simulations by the reanalysis model, precipitation measurements are not assimilated; rather, precipitation is computed by the reanalysis model for all grid cells at every time step. The ERA-40 provides one of the most consistent, available and accurate gridded representations of these variables and compares favorably with other reanalysis products

of the Arctic (Bromwich *et al.*, 2007). ERA-40 precipitation has been compared with NCEP-NCAR and satellite-based Global Precipitation Climatology project (GPCP) data by Serreze *et al.* (2005) in Arctic river basins. The study found that ERA-40 outperforms the other sources of precipitation information, particularly during January, April and October, although lower correlations were found for July (Cassano and Cassano, 2010). It is therefore, a logical choice for the observational analysis from which we determine the biases of late-twentieth-century surface air temperature and precipitation extremes. Data and documentation for the ERA-40 can be found online at <http://www.ecmwf.int/research/era/Products>. While the ERA-40 reanalysis was performed at T106 (~125 km) resolution with 60 levels, we use the version of the output archived on a 2.5° latitude x 2.5° longitude grid for compatibility with the GCM output.

2.3.4 ClimDEX Calculations

The Expert Team on Climate Change Detection and Indices (ETCCDI) developed a set of extreme indices that could be used for analysis of extreme events (Alexander *et al.*, 2006; Frich *et al.*, 2002; Klein Tank *et al.*, 2009; Zhang *et al.*, 2011). The purpose of the ETCCDI indices was to have a compilation of reproducible, common index variables that could be easily calculated and were based on available daily climate data such as air temperature and precipitation (Zhang and Zwiers, 2013). The ETCCDI indices can be classified into three categories: monthly or annual minimum or maximum values of temperature and maximum daily values of precipitation; counts of the number of days exceeding a specific baseline climatological threshold; and counts of the number of days exceeding a specific fixed threshold. There are 27 ClimDEX indices in total (Zhang and Zwiers, 2013).

The three ClimDEX indices on which this study focuses are from the first category only. These are considered high impact variables that are widely reported and thus can be compared with other quantities (*i.e.* mean temperature), and they have broad usage in terms of engineering design criteria (Zhang and Zwiers, 2013) and environmental indicators. The minimum of the daily minimum temperatures in a month or year (TNn), the maximum of the daily maximum temperatures within a month or year (TXx), and the maximum consecutive 5-day precipitation total in a month, Rx5 where chosen for this work. For each of these indices, there is a single value for each month/year and grid cell (or station from *in situ* observational data). TNn and TXx are archived in °C, while Rx5 is archived in millimeters; see Table 2.2 for a description of the statistics and their calculation. The data set was developed based on the R package `climdex.pcic` as documented at The Comprehensive R Archive Network (CRAN) website (Bronaugh, 2012). Station data were downloaded from the National Ocean and Atmosphere's (NOAA) Climate Data Online Global Historical Climate Network (GHCN) database and processed using the same

climdex.pcic package for R (version 0.6-2, not currently released on CRAN) using the time period 1971-2000.

2.3.5 Processing ClimDEX

Files of the monthly and yearly extreme indices were downloaded from Environment Canada's ClimDEX portal (<http://www.cccma.ec.gc.ca/data/climdex/>, Kharin *et al.*, 2013; Sillmann *et al.*, 2013a; Sillmann *et al.*, 2013b). Our analysis consists of two parts, the first focused on the extended ensemble of 22 GCMs that provided a larger sample for assessing inter-variable relationships in the projected changes. This enlarged subset includes all models available in the ClimDEX archive, subject to the requirement that the archive of output be complete for 1950 to 2100 for both the RCP 4.5 and RCP 8.5 simulations. Eleven GCMs were thus excluded from the analysis, leaving the 22-model subset consisting of ACCESS1-0, BNU-ESM, CanESM2, CCSM4, CESM1-BGC, CMCC-CM, CNRM-CM5, CSIRO-Mk3-6-0, GFDL-ESM2G, GFDL-ESM2M, GFDL-ESM2M, Inmcm4, IPSL-CM5A-LR, IPSL-CM5A-MR, IPSL-CM5B-LR, MIROC5, MIROC-ESM, MIROC-ESM-CHEM, MPI-ESM-LR, MPI-ESM-MR, MRI-CGCM3, and NorESM1-M.

In the first part of the analysis, all 22 models were used to generate the figures relating projected changes of TN_n versus Rx5 (Figure 2.2) and TX_x versus Rx5 (Figure 2.3). The second part of the analysis, which includes spatial patterns and time series from individual models, is limited to the smaller subset of six high performing models for Alaska (see Selection of global climate models) models in order to highlight these models and retain parsimony in the presentation of analytical results.

GCMs time series were subset to 1971-2000, 2041-2070 (2050s) and 2071-2100 (2080s) using Climate Data Operators (CDO) tools. Each global file was clipped to the Alaskan domain defined in Section 2. All files were then averaged over 30-year time periods seasonally and annually. Raw monthly output extending from 1850-2100 was subset for each of three specific sites (ANC, FAI and BRW) and averaged over each season.

For comparison with the projected changes in the extremes of temperature and precipitation (described by the ClimDEX indices), the corresponding changes in the models mean values were also calculated. These changes were the differences between the 30-year means for the future timeslices (2041-2070, 2071-2100) and the historical base period (1971-2000). These differences were evaluated using the temperature and precipitation output from the subset of six global climate models described above, under both the RCP 4.5 and RCP 8.5 scenarios. Percentage changes for both mean and extreme precipitation were calculated as the 2080s changes (from the 1971-2000 mean values) divided by the mean 1971-2000 values. Statistical significance of the differences in these changes in mean were calculated using the two-sided Wilcoxon rank-sum test (Table 2.3, Helsel and Hirsch, 2002).

In order to allow for comparison between GCMs and the reanalysis data (i.e. Table 2.3 results), all monthly fields of GCM temperature and precipitation were interpolated to a common grid (CCSM4's 0.94° latitude by 1.25° longitude grid). Geographic Information System (GIS) shape files were used to clip and average results for the grid boxes covering the Alaskan land area and particular subsets containing Anchorage, Fairbanks, and Barrow. Several grid boxes (3-4) were used to represent the conditions nearby those cities but without selecting ocean regions.

Maps (Figures 2.4-2.6) were plotted using NetCDF Command Language (NCL). Line plots (Figures 2.7-2.9) were calculated based on the average and the range of the minimum and maximum temperature or 5-day precipitation that occurred at our two focus locations with the most widely differing characteristics (ANC, BRW).

2.4 Results and Discussion

The following discussion of results is divided into two sections. In the first, we assess the occurrence of extreme temperatures and precipitation in Alaska over an historical period, 1971-2000. This section includes a comparison of the global climate models, the atmospheric reanalysis (ERA-40), and station observations for the same period. With this comparative assessment providing context, we then turn in the second section to the changes projected by the models under two scenarios of future climate forcing.

2.4.1 Historical Observations and Simulations of Extreme Temperature and Precipitation

Tables 2.3, 2.4 and 2.5 provide overviews of the historical occurrences as well as the projected changes for TNn, TXx and Rx5, respectively. Each table is partitioned into sections for the Alaska statewide average and for locations corresponding to three stations having essentially complete daily records for the 1971-2000 historical period: Anchorage (ANC), Fairbanks (FAI) and Barrow (BRW). These stations provide a 3-point transect from the southern coastal region to the northern coast. In the tables, the first three lines summarize the ClimDEX extremes for the 1971-2000 historical period as obtained from the station data, the ERA-40 reanalysis, and the aggregate (average) of the six models. Also included (line 4 of each table) are the across-GCM standard deviations for each index and for each season (and the full annual period). For the ERA-40 reanalysis and the climate models, the values listed for each station are for the grid cell containing the station location, averaged with the four surrounding grid cells, or in the case of Barrow, three grid cells (to exclude ocean cells). This averaging was done on regridded data and acted to smooth results and reduce bias that may be introduced by selecting one grid cell. Note that the tables do not contain statewide averages of the station values because of the sparseness of the station network.

Several notable findings emerge from a comparison of the first three lines of the tables. First, the models generally produce colder extreme minimum temperatures (TNn) than the reanalysis, except at the Barrow location. The magnitude of the cold bias is 5°C and even larger at Anchorage. By contrast, the reanalysis values are quite close to the station values at all three stations, except for a cold bias of about 5°C at Fairbanks in winter and autumn, an annual bias of about 5°C at Barrow and about 10°C at Fairbanks. The cold bias of the models relative to the reanalysis and stations is most likely a consequence of the relatively coarse resolution of the GCMs. The Anchorage station, for example, is at sea level while the major mountains (1 to 2 km in elevation) are found within 50 km of the station location and are therefore within the Anchorage grid cell of climate models run at 100-200 km resolution. Fairbanks is also located in a valley, with significant topography to the north, south and west, giving a GCM's corresponding grid cell a higher elevation and hence colder temperatures. Our inclusion of several grid cells surrounding each station's grid cell can add to the elevational discrepancy. Because the native grid of the ERA-40 reanalysis had a finer resolution, the ERA-40 bias, relative to the station data, is not as severe as the GCM bias. Comparisons between global climate model output and individual stations are subject to the caveat that station locations are often unrepresentative of the surrounding grid cell.

The TXx values of the GCMs and the ERA-40 reanalysis are generally quite close to each other, although the models are colder than ERA-40 by 3° to 5°C at Fairbanks in spring, summer and autumn. The models are also colder by about 3.5°C at Anchorage in the spring, winter and fall. As was the case with TNn, the models and the reanalysis are colder (by 5 ° to 10°C in some seasons) compared to the station data at Anchorage and Fairbanks, although the models and reanalysis are much closer to the station values at Barrow. By comparison, the standard deviations across the six models range from 1.26°C (Anchorage in winter) to 4.27°C (Barrow in winter). Thus model-reanalysis differences are generally within the spread of the models at Barrow, where there is little topography, but the cold biases relative to Anchorage and Fairbanks station data are much larger than the spread across GCMs. In view of the locations of the three stations relative to topography, together with the sign of the biases when the values are large, the station-to-model discrepancies support the argument that topography and grid-cell elevations are at least partially responsible for the cold biases.

The maximum 5-day precipitation amounts, Rx5, are considerably larger in the models and the reanalysis than in the station data. The GCM amounts are generally two to four times larger than the station amounts in the cold season at Anchorage and Barrow, with smaller positive biases at Fairbanks. The global climate model amounts are generally much closer to, although still larger than, most of the ERA-40 reanalysis amounts. It is well known that station measurements of frozen precipitation suffer from gage undercatch, especially in cold windy conditions (Goodison, 1978). Since the station amounts are not adjusted for gage undercatch, part of the model-to-station discrepancy is likely due to the fact that

the station amounts are artificially low. However, it is also likely that topography also accounts for part of the discrepancy. The mountains to the east of Anchorage often shelter the Anchorage climate station from precipitation in winter when low pressure systems to the south produce easterly winds in the Anchorage area. As noted earlier, the models' coarse resolution smoothes topography and also has the effect of giving Anchorage a spuriously high elevation. These topographic mis-representations would contribute to an over-simulation of precipitation at Anchorage in the models and in the reanalysis. Given the absence of topography near Barrow, the models' higher Rx5 values relative to the station values may well result primarily from gage undercatch.

Despite the biases, the models capture much of the seasonality and the geographic (south-to-north) variation of the three ClimDEX indices examined here. Moreover, at least some portions of the models' biases relative to station data should remain invariant as the simulations extend into the future (*i.e.*, topography will not change over the 21st-century timeframe of the projections to be examined here). For these reasons, and because the models' biases relative to ERA-40 are smaller than with respect to station data, the models offer the potential for useful inferences about changes in the indices of extremes during 21st-century simulations by the models.

2.4.2 Projected Changes in Extreme Temperature and Precipitation

Relationships between the statewide averages of seasonal changes in TNn vs. Rx5 and TXx vs. Rx5 for the 2050s and the 2080s for RCP 8.5 are illustrated for 22 models (Figure 2.2 and 2.3, respectively). These plots show how the top six models used to discuss the major findings of the work fit within the relative spread of all 22 models analyzed (highlighted using black, open circles). Overall, the subset of six selected models represents the ranges of increases in precipitation and temperature. The 2050s results (green) are clustered in the lower left quadrant of the plots, while the 2080s (blue) tend to be clustered in the upper right hand quadrant, although there is some overlap. Changes in all seasons for TXx except SON, and in MAM for TNn appear approximately symmetric about the 1:1 line (a 1°C change in temperature is associated with a 1mm increase in 5-day precipitation, Figures 2.2, 2.3); during winter, spring and summer for TNn, models fall above the 1:1 line and for autumn TXx, the models (generally) fall below the line. Model spreads are largest in the winter and autumn and for the 2080s. Temperature and precipitation changes in the winter and autumn for TNn and TXx are most strongly correlated.

Results in the scatterplots relating TNn vs. Rx5 and TXx vs. Rx5 can be compared to recent work by Westra *et al.* (2012), who used ClimDEX indices to examine the relationship between increasing 1-day precipitation events and increases in global temperature for over 8000 stations observing precipitation and air temperature over 30-year time periods. Westra *et al.* (2012) used a generalized extreme value theory

analysis to explore the association between precipitation extremes and air temperatures. The results indicated a statistically significant relationship between extreme precipitation and changes in near surface atmospheric temperature between 6-8% K⁻¹. Westra *et al.* (2012) also found that the greatest sensitivities have occurred in the high latitudes, and the tropics. A test was performed to determine if the significance of the results occurred due to random variability under the null hypothesis that the year-to-year extremes are distributed independent of each other, and the findings indicated that the magnitude of the sensitivity was significantly different than that obtained under the null hypothesis (Figure 11 in Westra *et al.* 2012). Westra *et al.*'s study found that two stations in Alaska with statistically significant results are positively associated with temperature (Figure 5 in Westra *et al.* 2012). This work suggests that the scatterplots in Figures 2.2 and 2.3 may be illustrating an association between precipitation changes and increasing temperatures in Alaska, particularly in autumn.

For RCP 8.5, BNU-ESM, CanESM2 and ACCESS1-0 have the largest change in warm and wet extremes in most seasons and for both variables (TNn and TXx). This could be due to biases in these models. A temperature bias in CanESM2 is discussed in Chylek *et al.* (2011) and shown in relation to CanCM3 and CCSM3, which are precursors for CanESM2. However, Arora *et al.* (2011) present global mean temperature (2m) and precipitation results for CanESM2 and show good agreement with historical data. This is also found in our study; CanESM2 has reasonable historical results in comparison to reanalysis data across Alaska. It may be that the lack of a sophisticated sea ice model in CanESM2 that is leading to the large changes in extreme precipitation and temperature (see Table 2.1, Figure 2.2, 2.3). However, ACCESS1.0 was noted to have a relatively sophisticated sea-ice component (Massonnet *et al.*, 2012) which suggests another mechanism is causing these model projections to fall within the upper ranges of the 22 model spread. BNU-ESM was noted however to have some oddities in terms of atmospheric moisture balance, which indicates that the high values offered by the other two models may be inaccuracies (Liepert and Lo, 2013). MRI-CGCM3 projects the smallest change in temperature and precipitation extremes for most of the seasons. These results indicate that while a particular GCM's changes in means may be similar to other models; its simulated changes in climate extremes could be quite different. This argues for presenting GCMs extremes, along with mean values when discussing global climate model performance.

Changes in minimum and maximum temperatures across Alaska for an ensemble of the six top models are summarized in Table 2.3, along with the results for Anchorage, Fairbanks and Barrow sites. TNn is projected to increase more than TXx, up to three times as much in winter (+14°C TNn compared to +4°C for TXx for RCP8.5, for example), and two times as much in spring and autumn (for example, +11°C TNn compared to +6°C for TXx for RCP 8.5). Increases in TNn were statistically significant at the 95% confidence level for all seasons and annually across Alaska. For TXx, the changes were mostly

significant at the 95% and 90% confidence level, with the exception of summer. Annually, TXx changes were only significant by the 2080s under the RCP 8.5 scenario.

This finding that increases of TNn exceed those of TXx was documented using historical gridded station data in Canada, where it is associated with a decline in the diurnal temperature range (Zhang *et al.*, 2000) and is projected to occur globally over land although the differences are greatest in northern regions such as Alaska (Kharin *et al.*, 2013; Sillmann *et al.*, 2013a). By the 2080s, the increases in both TNn and TXx are about two times as large under RCP 8.5 and under RCP 4.5, respectively. The large changes in TNn are linked to changing snow covers in the north by Sillmann *et al.* (2013a), as these large differences between TNn and TXx are not found in lower latitudes, tropical regions such as South America.

The models' projected increases of TNn are much larger than the corresponding changes in mean temperature projected by the models, as shown in Table 2.6 for the 2080s RCP 8.5 results (the ratios of ΔTNn to ΔT_{mean} are similar for the 2050s and for the RCP 4.5 scenario). The changes in the annual mean TNn are approximately twice as large in the statewide mean and at Anchorage and Barrow. Seasonally, the differences between the changes in TNn and the mean temperature are smallest in the summer and largest in the spring. By contrast, the changes in TXx are smaller than the changes in the corresponding mean temperatures. The gap between the changes in TXx and the mean is largest in winter, when the increases of TXx are less than half the changes in the mean for the statewide average and for all three specific locations.

Autumn and winter increases in TNn and TXx are largest in the north (BRW), and in spring and summer increases are largest in the south (ANC, Table 2.3, Figure 2.4-2.5). This is especially notable in Figure 2.4, which shows increased TNn along coastal regions of Alaska, particular in the western regions of the state. At all three of the study sites (ANC, FAI and BRW), TNn and TXx are projected to increase the most in autumn and winter. Projected changes are similar for spring and autumn, particularly towards the 2080s. In both seasons, the ensemble maps illustrate large changes over western Alaska for both TXn and TNn. Large changes are projected for the inland Bristol Bay region of southwestern Alaska by some models (not shown). Future projections of summer TXx by MRI-CGCM3 show slight cooling within the Interior of the state, while the rest of the models agree on the direction of future change (*i.e.*, an increase) across Alaska (map not shown). All models agree on increased maximum autumn temperatures (Figure 2.5). Projected changes in TNn at ANC are the least robust statistically, while the changes in TNn for FAI and BRW are almost all statistically significant at the 95% level. However, TXx projected changes are statistically significant for most seasons and annually at ANC, while the changes of TXx at FAI and BRW are not consistently significant until the 2080s under the RCP 8.5 scenario (with the exception being the annual signal at FAI). In all cases the season/scenario with the greatest amount of change was statically significant.

The increases in TNn and TXx overall are much larger (two to four times) than the across GCM standard deviations, indicating across-model robustness in the predicted changes in TNn and TXx. Standard deviations are generally lower for TXx than TNn. The models' ranges of extremes converge by the year 2100 at the focus sites for TNn and TXx, particularly in spring and fall, and for TXx in winter under the RCP 8.5 scenario (Figures 2.7 and 2.8, Fairbanks not shown for clarity). It should be noted that the models' standard deviations (variation between the 30-year means of the models) for the difference values are not getting smaller, rather the standard deviations increase from the 2050s to the 2080s (Table 2.3). In other words, that the across-GCM differences are actually larger by the 2080s, whereas the interannual variability in models' responses is generally decreases with time (Figures 2.7 and 2.8). The reason for the reduced range of the models' extremes by 2100 is likely related to the reduction of sea ice and snow cover in the models. In areas from which sea ice has been lost (e.g., the northern and western Alaskan coastal seas for increasingly long portions of the year), the temperatures are constrained to remain near the freezing temperature. This constraint will extend to land areas that are subject to maritime influences, thereby reducing the tendency for large excursions of surface air temperature. Similarly, reduced snow on land implies less inter-model variability of snow cover during the periods of stronger insolation (*i.e.*, spring, early summer), reducing the high-leverage effects of snow cover on surface air temperatures.

Precipitation indices (Rx5) suggest increases across the state of Alaska, especially in the fall and summer seasons (Table 2.3). The magnitude of the Rx5 increase is largest in the south (ANC), whereas the percent increase is largest in the north (BRW, Table 2.3). There is only a slight change in Rx5 projected by the models in the 2050s, largely in the southern and interior regions (Figure 2.6). However, by the 2080s much of Alaska is projected to experience increases in Rx5, and the increases are two times larger for RCP 8.5 compared to RCP 4.5 (Table 2.3). Projected changes are larger along the interior and along the coastal mountainous regions to the east of Anchorage in summer (Figure 2.6) and along the southern coastal region and western interior in the autumn (Figure 2.6). Winter increases are largely confined to the coastal regions (Figure 2.6). Record 5-day precipitation events become noticeably more common by the 2100s under RCP 8.5, but this is less detectible under RCP 4.5 (Figure 2.9). Changes projected for the wet seasons (SON/JJA) and annually are statistically significant for the Alaska-wide domain by the 2050s, and for all seasons and annually by the 2080s under the RCP 8.5 scenario (Table 2.3). Extreme precipitation at ANC during JJA is projected to increase less so than in other seasons, but those changes are statically significant. FAI and BRW increases in precipitation are all significant at 90-95% confidence level during fall and annually. At FAI, by the 2080s the spring, summer, fall and annual projected changes are significant under the RCP 8.5 scenario.

A striking feature of the increases in Rx5 is that they exceed the changes in mean precipitation by a factor of two or more (Table 2.6). While the increases in mean precipitation are typically 12-20%, the increases in Rx5 are generally in the range of 25-35%, and even more than 40% at some locations (e.g., Barrow in summer, autumn and the annual mean). The implication is that a greater percentage of the precipitation will occur in the heaviest precipitation events. This tendency for more extreme heavy precipitation events is consistent with the time series shown in Figure 2.9.

2.5 Conclusions

The ClimDEX database has enabled an evaluation of extremes simulated by global climate models over historical as well as future timeslices. Our focus in this paper has been on the simulations of extreme minimum and maximum surface air temperature, as well as 5-day maximum precipitation amounts over Alaska. While it is not surprising that a warming climate is accompanied by increasing values of extreme temperatures as well as by heavier extreme precipitation amounts, quantitative depictions of the changes must recognize regional, seasonal and climate scenario sensitivities such as those presented here. These sensitivities are important for impact assessments, as the rates and magnitudes of changes in extremes will determine the impacts and adaptation strategies of stakeholders.

In keeping with the paper's organization, two categories of findings will be summarized: the projected changes in the extreme indices for Alaska, and the interpretation of these projected changes in the context of station-based changes. In the first category, key findings include the following:

- Projected increases of all three indices (extreme maximum and minimum temperatures, extreme 5-day precipitation) are two to four times larger than the across-GCM standard deviations, both for the statewide averages and for the three specific locations examined in this work.
- The increases in extreme minimum temperatures are much greater than the increases in extreme maximum temperature (by factors of about two in spring and autumn, and about three in winter).
- The increases in extreme minimum temperature and extreme 5-day precipitation are much larger than the corresponding changes in mean temperature and precipitation. However, the increases in extreme maximum temperature are smaller than the changes in mean temperature.
- By the 2080s, increases in extreme temperatures are about twice as large under the RCP 8.5 forcing as under RCP 4.5 forcing.
- The projected changes of extreme temperature are larger in the north during autumn and winter, but larger in the south during spring and summer.
- For the three locations along a north-south transect in Alaska, the across-GCM interannual variability of the extreme maximum and minimum temperatures decreases by 2100, especially under RCP 8.5 forcing.

- While the magnitude of the projected increase of Rx5 is largest in the south, the percentage increase is larger in the north.
- By the 2080s, increases in Rx5 are about twice as large under RCP 8.5 as under RCP 4.5. Record-breaking 5-day precipitation events become noticeably more common by 2100 in RCP 8.5, less so in RCP 4.5.
- The linearity of the relationship between increases of Rx5 and extreme temperatures is strongest in autumn and winter and suggests an association between precipitation changes and increasing temperatures in Alaska
- The largest changes in future projected extreme minimum temperature and extreme 5-day precipitation are significantly different from the historical based on significance testing at the 95% confidence interval

The second category of findings, those related to GCM simulations and station-based changes, has implications for the utility of the results for local applications (i.e. for the three sites analyzed in Alaska: Anchorage, Fairbanks and Barrow). Notable findings include:

- There are substantial discrepancies between the ClimDEX indices (TNn, TXx, Rx5) computed from the global climate models and the station data. In general, the models' values of TNn are considerably colder.
- The global climate model-derived values of Rx5 tend to be much larger than the corresponding station-derived amounts.

In explaining the discrepancies between the GCM-derived and station, it is useful to distinguish two components: differences between the GCMs and the reanalysis, and differences between the reanalysis and the stations. In the case of TXx, the reanalysis-station differences are much larger than the GCM-reanalysis differences, suggesting that GCM resolution is a key part of the explanation of the discrepancies. In particular, the GCMs and reanalysis data grid cells containing Anchorage and Fairbanks have average elevations that exceed the elevations of the stations, resulting in spuriously high elevations in the models. This interpretation is supported by the fact that the reanalysis and GCMs differ from the station values by greater amounts at Anchorage and Fairbanks, which are both “topographically shaded” locations in reality but not in the models, and less at Barrow, where there is little topographic relief within 100 km of the station. Resolution-related topographic influences also explain the fact that the GCMs and reanalysis both produce values of Rx5 that are much larger than the station amounts, especially at Anchorage, which is known to be in a rain/snow “shadow” very often during the cold season. For TNn, the GCMs are much colder than the reanalysis in the cold season, while the reanalysis is closer to the station values. Since cold-season temperatures are strongly impacted by surface-based inversions, the

reanalysis evidently has a boundary layer parameterization and/or vertical resolution that enable improved capture of the near-surface temperature profile.

Given the GCM-station discrepancies noted above, how credible are the projections of changes in extreme temperatures and precipitation amounts? While the raw values of the model-derived ClimDEX indices are not optimal for applications, there are reasons why the changes from the present to the future may be more robust. Biases in the GCMs, which are related to topography and parameterizations as noted above, can be expected to remain relatively consistent as the simulations extend through the remainder of the present century. This assumption is indeed the basis for the success of the so-called “delta method” of global climate model downscaling (Hayhoe, 2010). While the assumption is not perfect, it justifies some confidence in the sign, if not the magnitude, of the projected changes. The same reasoning applies to the seasonality and the spatial patterns of the projected changes.

Perhaps the greatest need for applications of the results here is downscaling to the local scale. As explained above, locations near significant topographic features can have significantly different weather and climate from other locations in the same grid-cell area of a GCM. The use of grid-cell average elevations in GCMs creates substantial biases relative to actual values at locations with elevations substantially different from the grid-cell means. Statistical downscaling is now coming into widespread use (e.g. Stoner *et al.*, 2012), and the extension of the ClimDEX calculations to downscaled GCM output represents a potential future extension of the work described here.

2.6 Acknowledgments

The project described in this publication was supported by Grant/Cooperative Agreement Number GIOAC00588 from the United States Geological Survey’s Alaska Climate Science Center. Its contents are solely the responsibility of the authors and do not necessarily represent the official views of the USGS. Dennis Shea’s assistance with NCL graphical plots used in this paper is acknowledged. The contribution of John Walsh to this paper was supported by the Cooperative Institute for Alaska Research with funds from the Climate Program Office, National Oceanic and Atmospheric Administration through grant NA10OAR4310055, and by the National Science Foundation through grants ARC-1049225 and ARC-1023131.

2.7 Figures

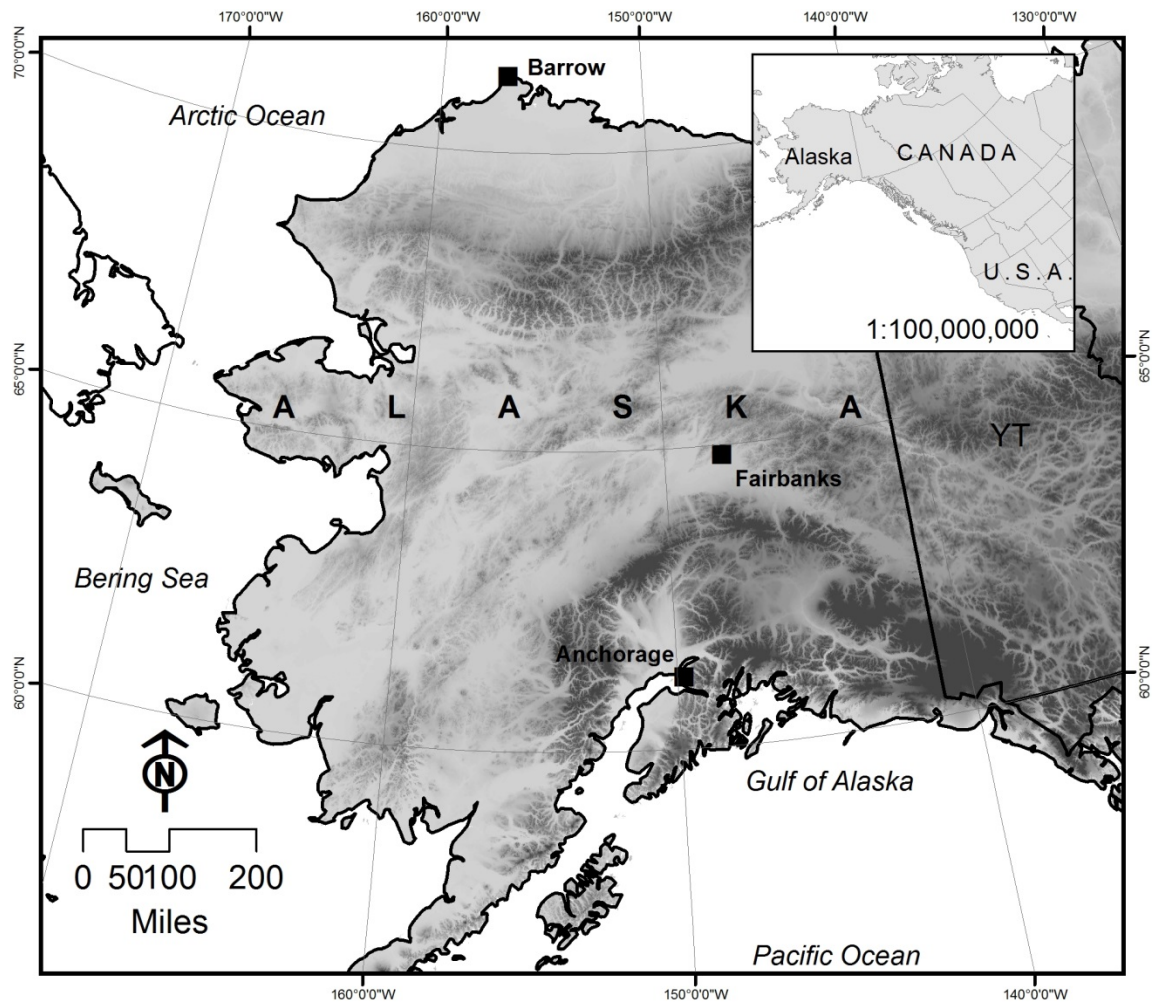


Figure 2.1 Focus sites in Alaska , Anchorage, Fairbanks and Barrow used in the text. Inset map shows Alaska in the context of continental USA and Canada. The Digital Elevation Model (DEM) in the background is the National Elevation Database (NED).

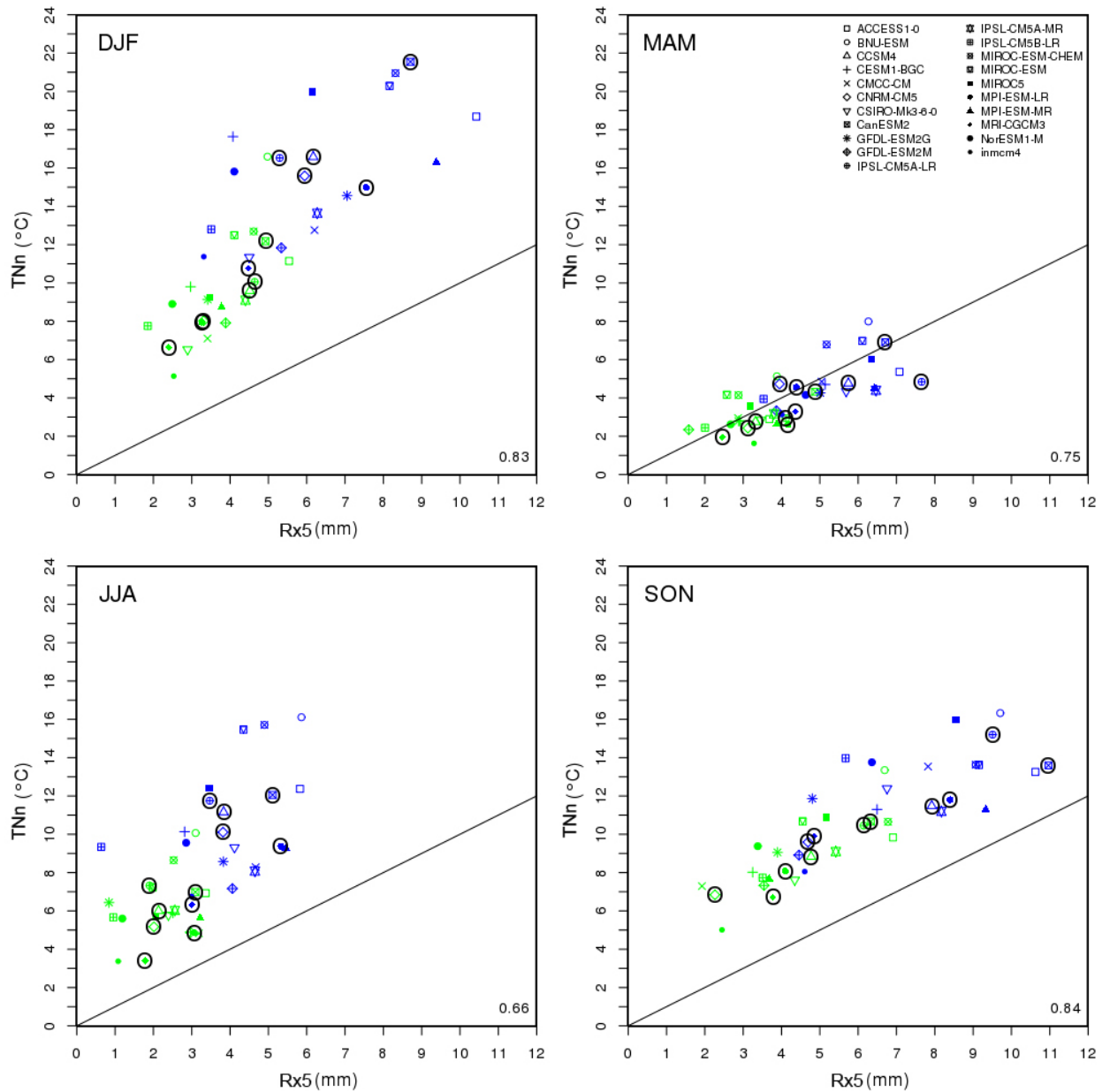


Figure 2.2 DJF, MAM, JJA and SON seasonal results for Rx5 versus TNn for RCP 8.5. The 2050s are shown in green, while the 2080s are shown in blue. The top six GCMs used in the primary analysis presented in this work are illustrated with circles around them. The 1:1 line is shown, and the correlation value is located in the bottom right hand corner of each plot. Symbology for each GCM is shown in the upper right hand corner of the MAM panel.

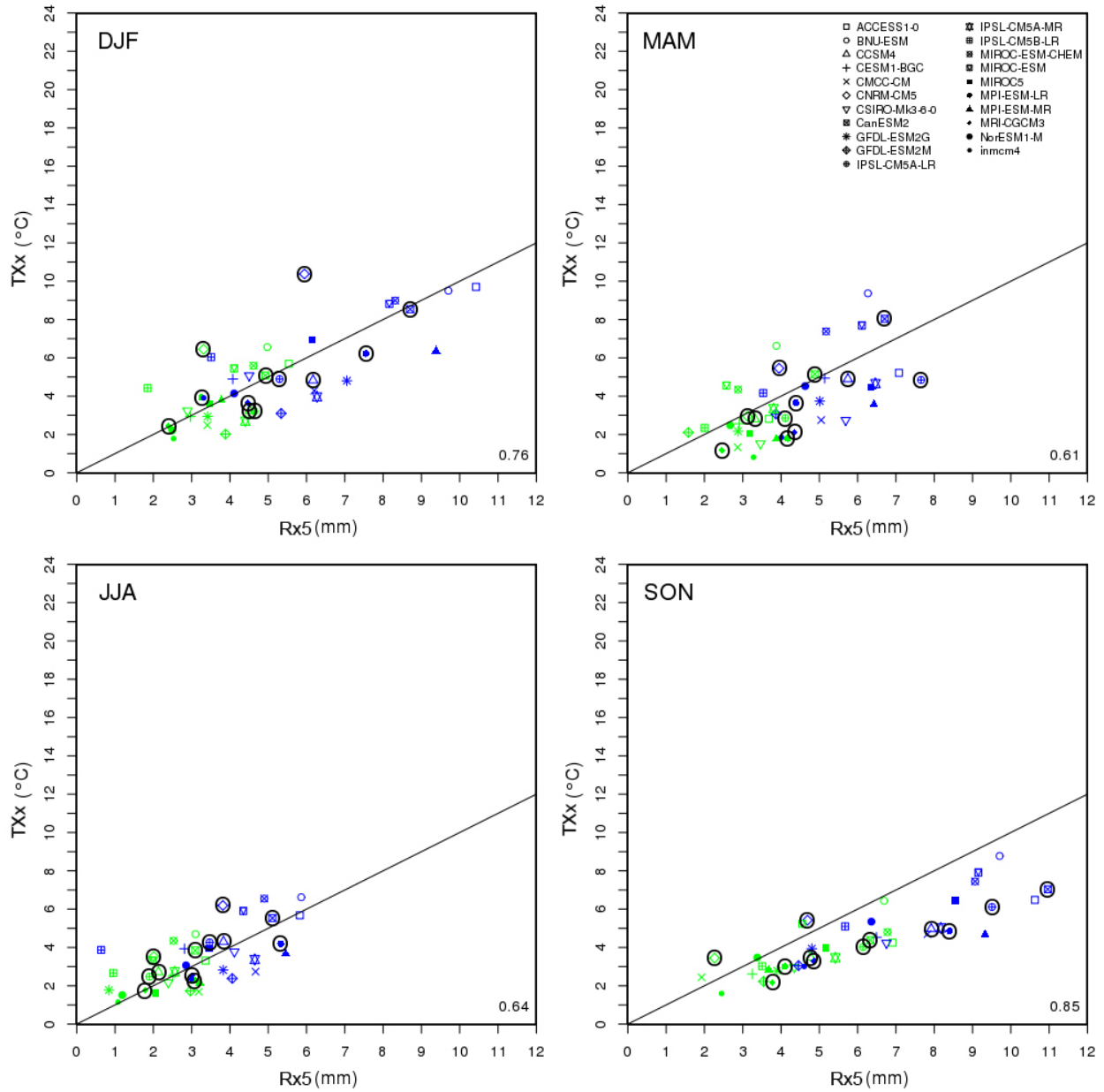


Figure 2.3 DJF, MAM, JJA and SON seasonal results for Rx5 versus TXx for RCP 8.5. The 2050s are shown in green, while the 2080s are shown in blue. The top six GCMs used in the primary analysis presented in this work are illustrated with circles around them. The 1:1 line is shown, and the correlation value is located in the bottom right hand corner of each plot. Symbology for each GCM is shown in the upper right hand corner of the MAM panel.

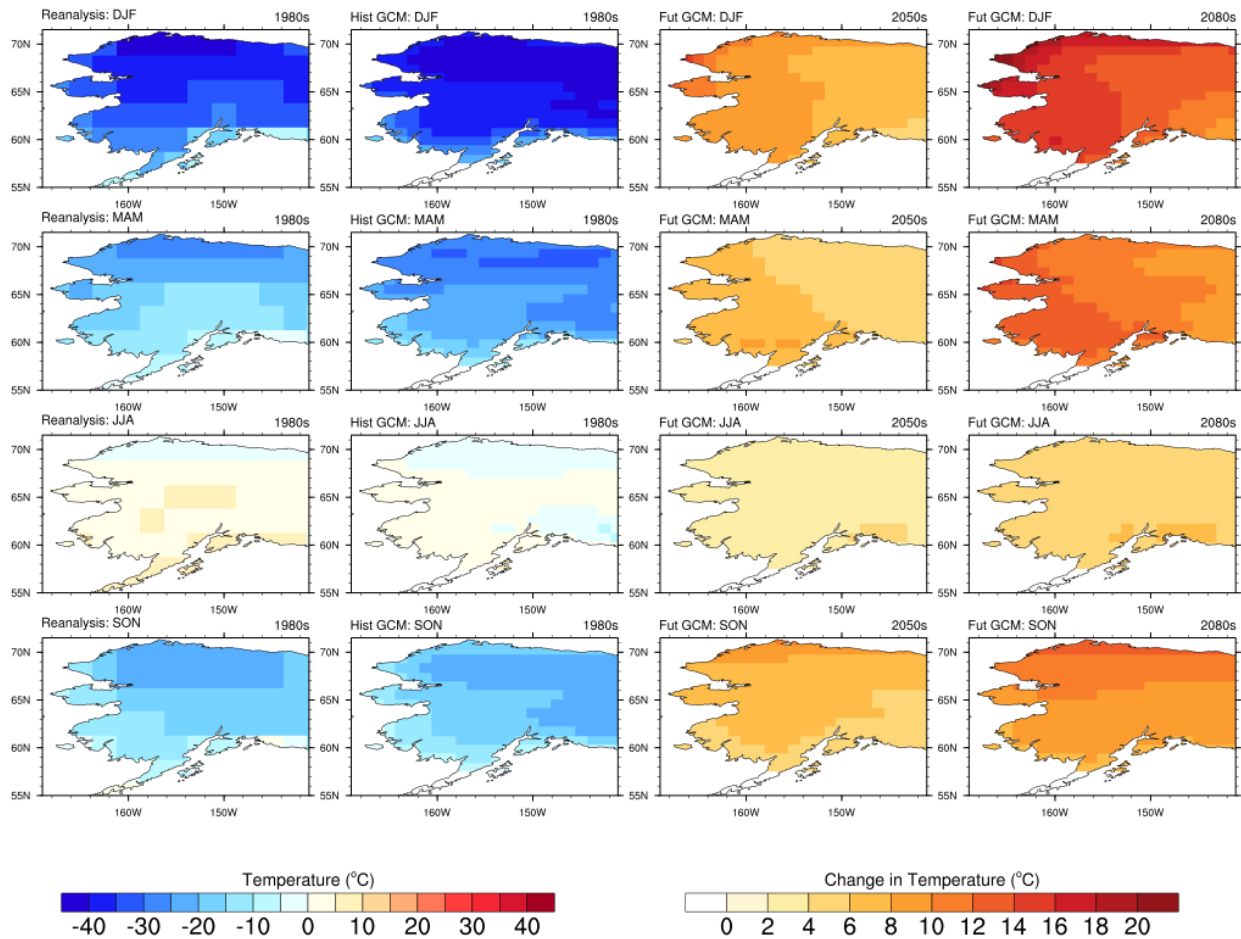


Figure 2.4 Graphical plots of TNn for all seasons. The first column shows the ERA-40 reanalysis historical (1971-2000, repeated down the rows), the second column is the ensemble GCM historical (1971-2000), and the third and fourth columns illustrate the differences between the future and historical climatology for the 2050s and the 2080s for the GCM ensemble (RCP 8.5). The legend is illustrated on the left bottom for the historical and reanalysis data, while the legend for the 2050s/2080s difference values is on the right bottom.

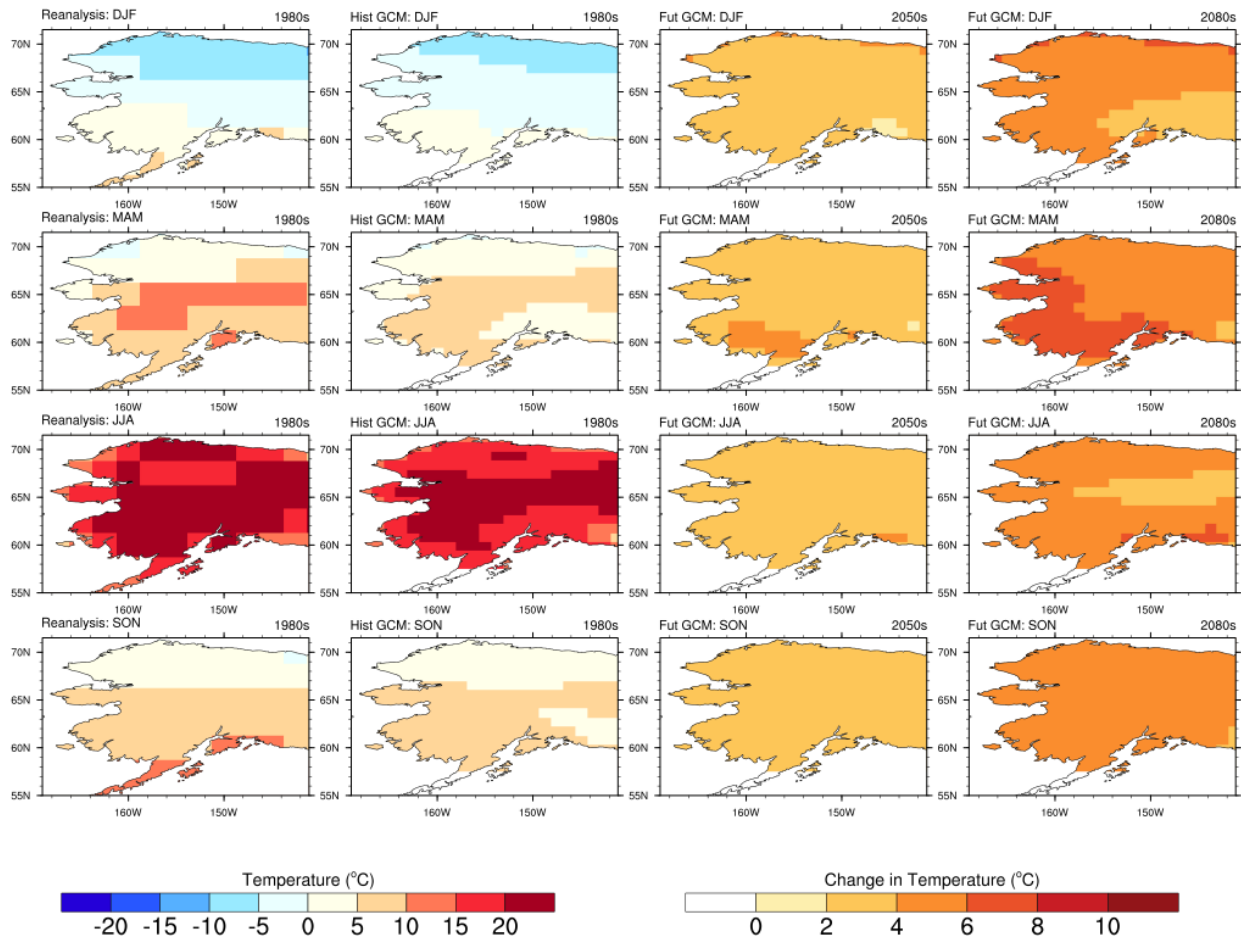


Figure 2.5 Graphical plots of TXx for all seasons. The first column shows the ERA-40 reanalysis historical (1971-2000, repeated down the rows), the second column is the ensemble GCM historical (1971-2000), and the third and fourth columns illustrate the differences between the future and historical climatology for the 2050s and the 2080s for the GCM ensemble (RCP 8.5). The legend is illustrated on the left bottom for the historical and reanalysis data, while the legend for the 2050s/2080s difference values is on the right bottom.

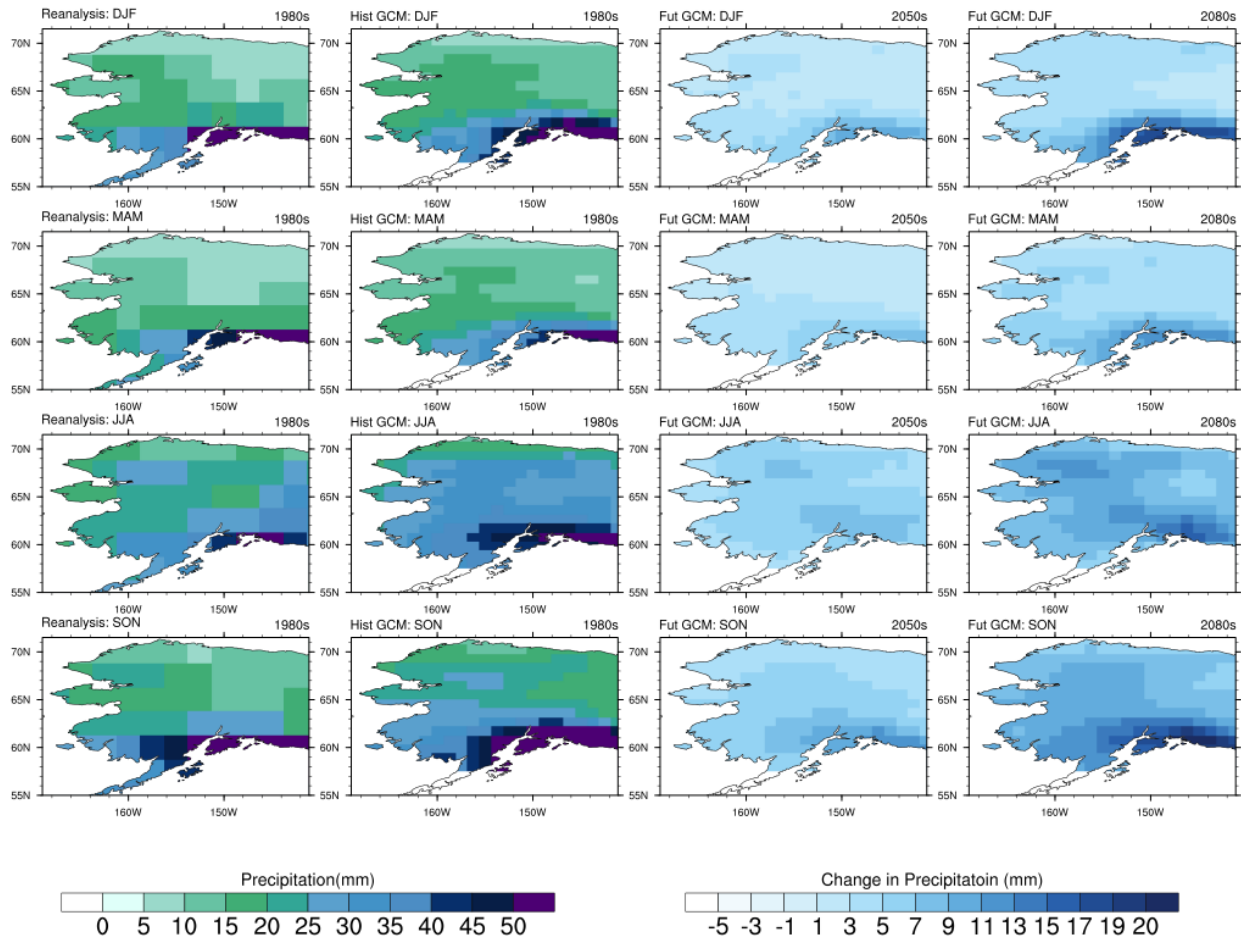


Figure 2.6 Graphical plots of Rx5 for all seasons. The first column shows the ERA-40 reanalysis historical (1971-2000, repeated down the rows), the second column is the ensemble GCM historical (1971-2000), and the third and fourth columns illustrate the differences between the future and historical climatology for the 2050s and the 2080s for the GCM ensemble (RCP 8.5). The legend is illustrated on the left bottom for the historical and reanalysis data, while the legend for the 2050s/2080s difference values is on the right bottom.

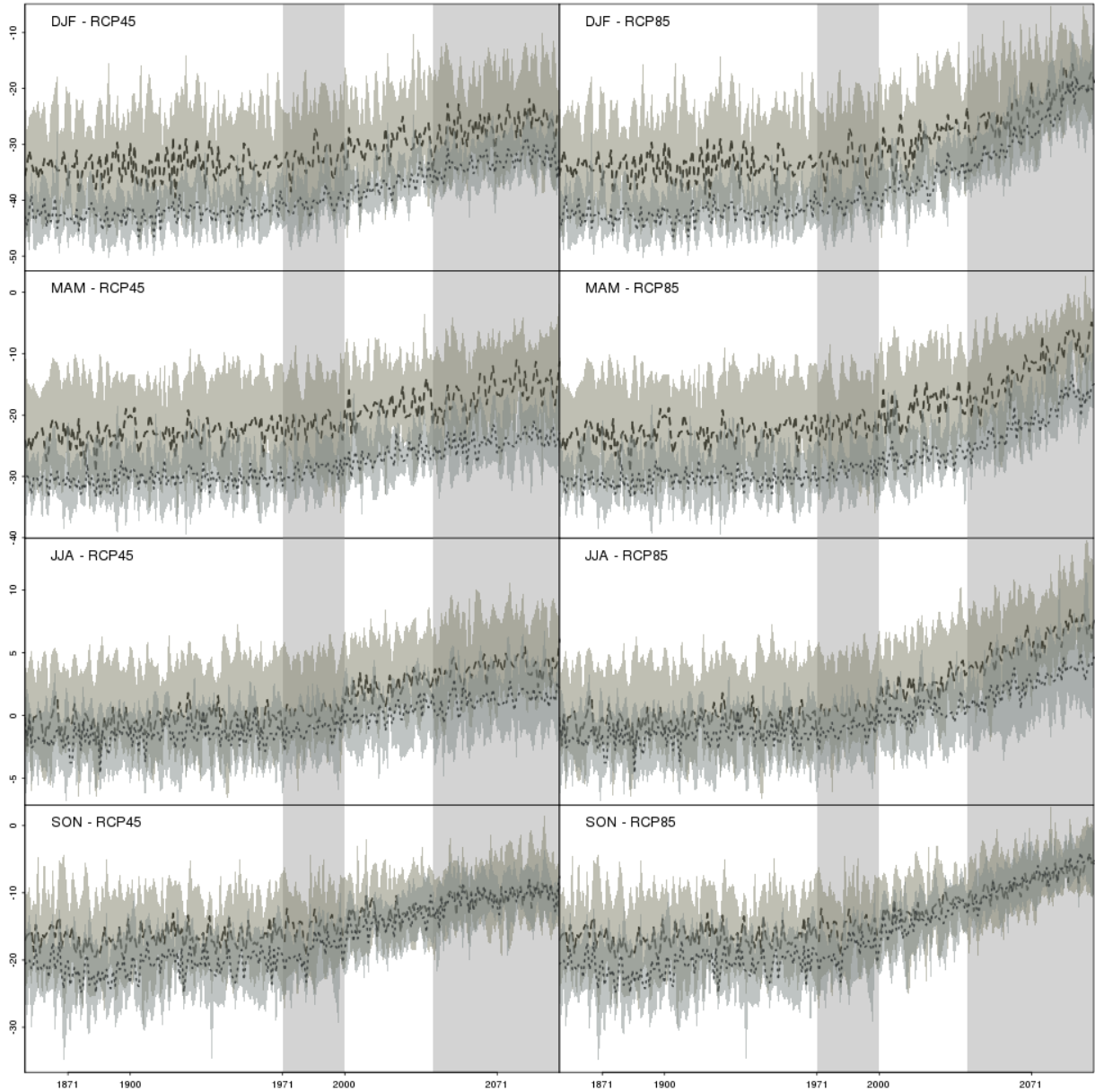


Figure 2.7 Plots of average daily minimum temperature median, maximum and minimum results for (dashed and dotted lines, Anchorage and Barrow respectively, T_n, °C) for Anchorage (light grey) and Barrow (dark grey) for each season DJF, MAM, JJA, and SON from 1850 to 2100. RCP 4.5 is shown on the left hand column and RCP 8.5 is shown on the right. Where locations overlap the colors are mixed. Gray bars indicate the historical (1971-2000), and future time periods (2041-2100).

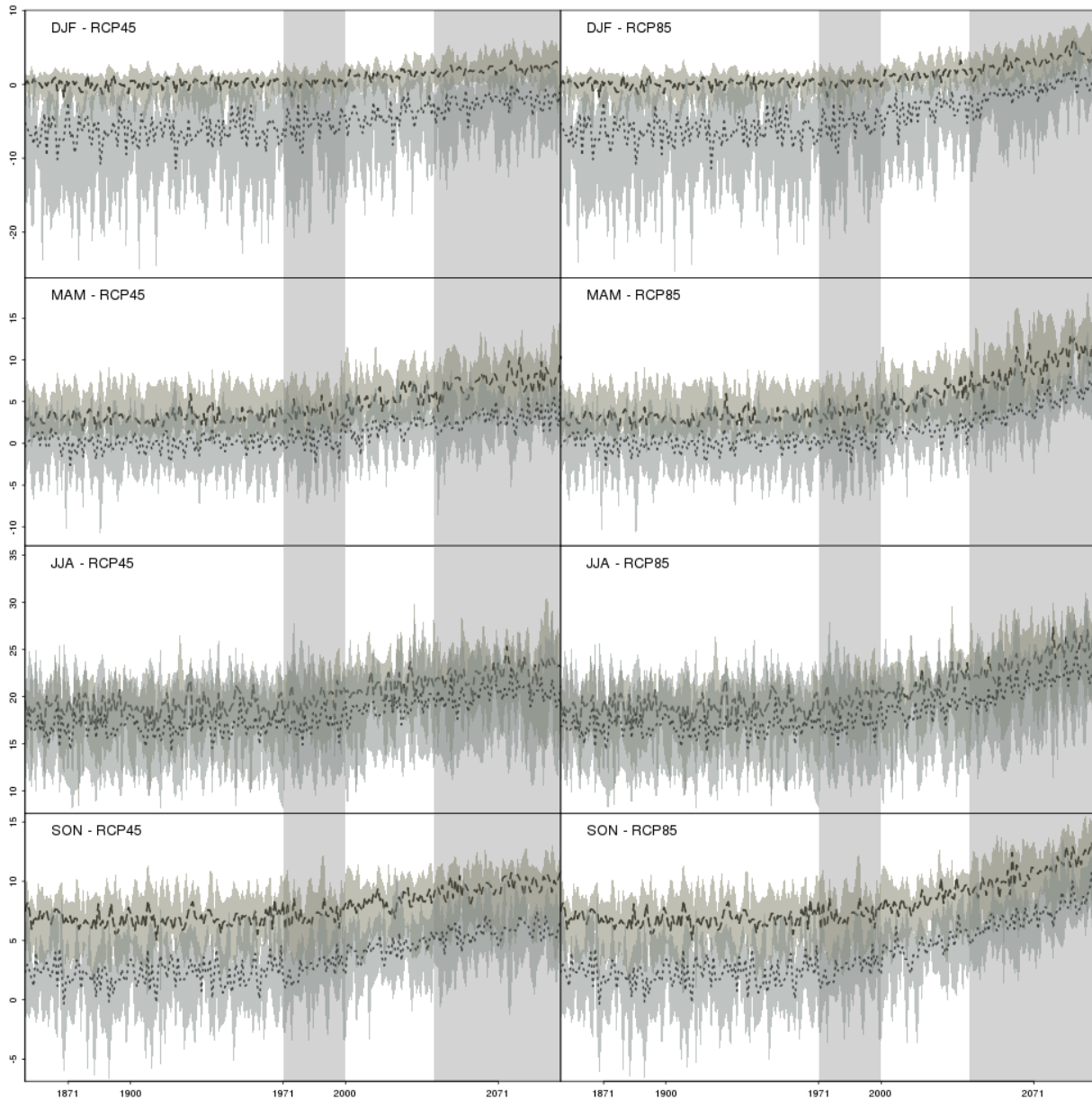


Figure 2.8 Plots of average daily maximum temperature median, maximum and minimum results for (dashed and dotted lines, Anchorage and Barrow respectively, T_{n} , $^{\circ}\text{C}$) for Anchorage (light grey) and Barrow (dark grey) for each season DJF, MAM, JJA, and SON from 1850 to 2100. RCP 4.5 is shown on the left hand column and RCP 8.5 is shown on the right. Where locations overlap the colors are mixed. Gray bars indicate the historical (1971-2000), and future time periods (2041-2100).

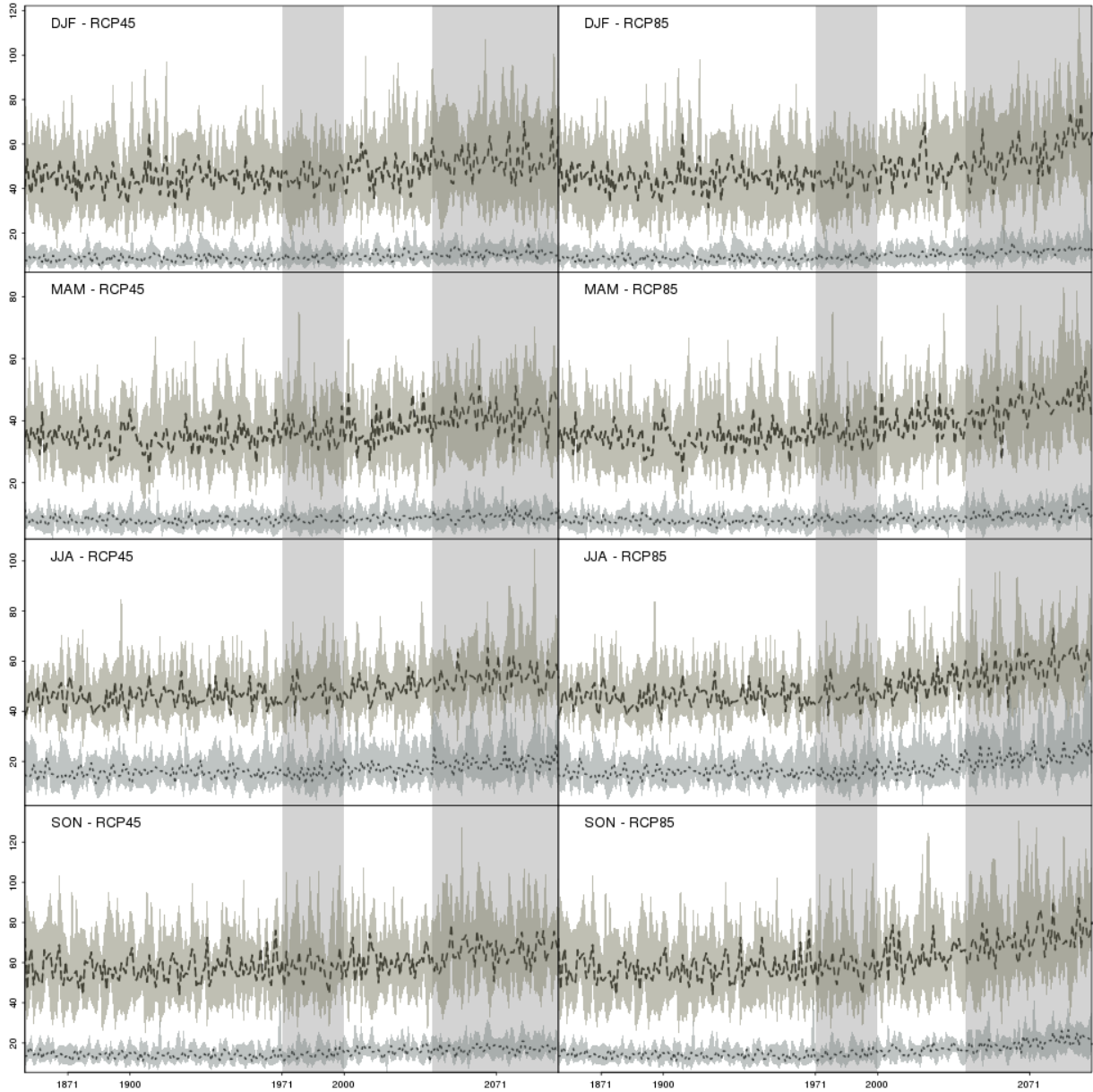


Figure 2.9 Plots of maximum 5 day precipitation median, maximum and minimum results (dashed and dotted lines, Anchorage and Barrow respectively, TNn, °C) for Anchorage (light grey) and Barrow (dark grey) for each season DJF, MAM, JJA, and SON from 1850 to 2100. RCP 4.5 is shown on the left hand column and RCP 8.5 is shown on the right. Where locations overlap the colors are mixed. Gray bars indicate the historical (1971-2000), and future time periods (2041-2100).

2.8 Tables

Table 2.1 The six GCMs used in this study, including model name, modeling center and primary reference, resolution of the GCMs and major model features, including the sea ice and land surface scheme employed.

Model Name	Modeling Center, Main Reference	Resolution	Major Model Features (sea ice and land surface schemes)
Community Climate System Model, Version 4 (CCSM4)	National Center for Atmospheric Research (NCAR), USA (Gent <i>et al.</i> , 2011)	0.9° x 1.25°	Sea Ice: Los Alamos Sea Ice Model Community Ice Code Version 4. Sub grid-scale ice thickness distribution and multiple layers. Land Surface: Community Land Model, version 4 (CLM4)
Centre National de Recherches Météorologiques Climate Model (CNRM-CM5.1)	Meteo France, National Centre for Meteorological Research, France (Voldoire <i>et al.</i> , 2011)	1.4° x 1.4°	Sea Ice: GELATO version 5. Four ice thickness categories are included. Ice slabs have 10 vertical layers, with increased resolution in upper layers. Land Surface: Interaction between Soil Biosphere and Atmosphere (ISBA) run in SURFEX.
Canadian Earth System Model CanESM2	Environment Canada's Canadian Center for Climate Modeling and Analysis (CCCma), University of Victoria, Canada (Arora <i>et al.</i> , 2011)	2.8° x 2.8°	Sea Ice: Mean thickness & concentration, no layers. Land Surface: Canadian Terrestrial Ecosystem Model (CTEM)
Institut Pierre Simon Laplace Climate Model, Low Res. (IPSL-CM5A-LR)	Institut Pierre Simon Laplace (IPSL), France (Dufresne <i>et al.</i> , 2012)	1.9° x 3.75°	Sea Ice: Version 3.2 Nucleus for European Modeling of the Ocean's (NEMO) Version 2 Louvain-la-Neuve Sea Ice Model (LIM2). Three layers (snow and ice). Land Surface: Organizing carbon and Hydrology In Dynamic Ecosystems (ORCHIDEE)
Max Plank Institute, Earth System Model, Low Res. (MPI-ESM-LR)	Max Plank Institute (MPI) for Meteorology, Germany (Giorgetta, 2012)	1.9° x 1.9°	Sea Ice: Max Planck Institute ocean model (MPIOM) Land Surface: JSBACH
Meteorological Research Institute Canadian Global Climate Model (MRI-CGCM3)	Meteorological Research Institute Japan, (Yukimoto <i>et al.</i> , 2012)	1° x 0.5°	Sea ice layers and thickness adopted from Los Alamos Sea Ice Model Community Ice Code Land Surface: Canadian Terrestrial Ecosystem Model (CTEM)

Table 2.2 ClimDEX indices selected for use in this study. ID is the identification code used in the text, description details fully each of the indices, units is the unit of measure for all of the indices, and details describes the calculations used to analyze all index values.

ID	Description	Unit	Details
TNn	Minimum daily minimum temperature, monthly or annual	°C	Monthly or annual minimum of daily minimum temperature. Let TNn be the daily minimum temperature in month k, period j. The minimum daily minimum temperature for each month is then: $TNn_{kj} = \text{minimum}(TNn_{kj})$.
TXx	Maximum of daily maximum temperature, monthly or annual	°C	Monthly or annual maximum of daily maximum temperature. Let TXx be the daily maximum temperatures in month k, period j. The maximum daily maximum temperature for each month is then: $TXx_{kj} = \text{maximum}(TXx_{kj})$.
Rx5	Maximum 5-day precipitation, monthly or annual	mm	Monthly or annual maximum 5-day consecutive precipitation. Let PR _{kj} be the precipitation amount for the 5-day interval ending k, period j. Then maximum 5-day values for period j are: $Rx5_j = \text{max}(PR_{kj})$.

Table 2.3 Average seasonal minimum seasonal and annual daily minimum temperature(TNn, °C) for (DJF=December, January, February, MAM=March, April, May, JJA=June, July, August, SON=September, October, November) and annual (ANN) results for Alaska, Anchorage (ANC), Fairbanks (FAI) and Barrow (BAR) for RCP 4.5 and RCP 8.5. The station average historical (1971-2000) is shown for ANC, FAI and BAR; statewide station values are not available (NA).. Historical mean from the Reanalysis and the mean and standard deviation (Stdev.) for the GCM is shown below. The 2050s and 2080s for both RCP 4.5 and RCP 8.5 is shown below, with the value as the difference (Diff.) from the 1971-2000 period shown first, followed by the standard deviation (Stdev.) from all GCMs. Italicized results indicate significance at the 90% confidence interval, while bold italicized values indicate 95% confidence intervals.

TNn	Alaska					Anchorage (ANC)				
	DJF	MAM	JJA	SON	ANN	DJF	MAM	JJA	SON	ANN
Station	NA	NA	NA	NA	NA	-23.34	-8.95	5.21	-10.42	-27.78
Historical (Reanalysis)	-32.49	-17.26	2.9	-15.73	-37.33	-22.24	-9.72	4.31	-10.45	-27.1
Historical (GCMs)	-37.42	-24.5	0.75	-18.06	-42.8	-32.52	-21.6	0.89	-15.3	-38.13
Historical Stdev.	3.7	2.86	1.54	1.75	3.34	6.48	5.93	2.72	3.91	6.17
2050s Diff. (RCP 4.5)	5.83	4.74	2.27	5.19	5.67	5.33	4.85	2.82	4.31	5.09
2050s Stdev. (RCP 4.5)	1.88	1.62	0.89	1.15	1.5	1.98	1.82	1.33	1.34	1.4
2050s Diff. (RCP 8.5)	8.19	5.98	3.02	6.47	8.07	7.32	6.3	3.85	<i>5.46</i>	7.11
2050s Stdev. (RCP 8.5)	1.87	1.96	1	1.26	1.87	2.3	2.34	1.54	1.41	2.26
2080s Diff. (RCP 4.5)	7.49	6.13	2.82	6.25	7.03	7.01	<i>6.74</i>	<i>3.47</i>	<i>5.56</i>	<i>6.49</i>
2080s Stdev. (RCP 4.5)	1.74	1.2	0.98	0.99	1.49	2.03	1.81	1.49	1.02	1.64
2080s Diff. (RCP 8.5)	14.03	11.1	5.03	9.73	14.26	12.78	11.95	5.96	8.51	13.12
2080s Stdev. (RCP 8.5)	3.13	2.78	1.34	1.32	3.05	3.85	4.29	1.93	1.81	3.81
	Fairbanks (FAI)					Barrow (BRW)				
Station	-39.24	-17.3	4.19	-21.38	-49.35	-39.19	-29.69	-3.23	-23.26	-48.43
Historical (Reanalysis)	-34.55	-15.23	4.34	-16.71	-39.85	-39.95	-26.87	-1.07	-20.91	-43.85
Historical (GCMs)	-39.49	-24.08	1.78	-19.88	-45.02	-40.43	-28.96	-1.28	-18.95	-44.87
Historical Stdev.	3.75	2.48	1.52	2.08	3.75	2.32	2.22	1.66	2.11	2.33
2050s Diff. (RCP 4.5)	5.22	4.38	<i>2.09</i>	4.81	5.29	6.32	4.35	2.12	7.56	5.6
2050s Stdev. (RCP 4.5)	1.76	1.77	0.97	1.15	1.45	1.94	1.56	0.76	1.87	1.7
2050s Diff. (RCP 8.5)	7.52	5.39	2.8	6.12	7.62	9.49	5.71	2.67	9.02	8.21
2050s Stdev. (RCP 8.5)	1.85	2.08	1.14	1.17	2.03	2.32	1.88	0.71	1.82	1.91
2080s Diff. (RCP 4.5)	6.9	5.91	2.52	5.89	6.51	8.32	5.24	<i>2.63</i>	8.61	7.01
2080s Stdev. (RCP 4.5)	1.69	1.48	1.06	1.06	1.64	1.88	1.48	0.78	1.54	1.54
2080s Diff. (RCP 8.5)	12.81	10.29	4.67	9.36	13.39	17.38	11	4.65	12.6	15.24
2080s Stdev. (RCP 8.5)	2.8	2.81	1.34	1.25	2.94	4.09	2.58	1.27	2.06	3.19

Table 2.4 Average seasonal maximum seasonal and annual daily maximum temperature (TNn, °C) for (DJF=December, January, February, MAM=March, April, May, JJA=June, July, August, SON=September, October, November) and annual (ANN) results for Alaska, Anchorage (ANC), Fairbanks (FAI) and Barrow (BAR) for RCP 4.5 and RCP 8.5. The station average historical (1971-2000) is shown for ANC, FAI and BAR; statewide station values are not available (NA).. Historical mean from the Reanalysis and the mean and standard deviation (Stdev.) for the GCM is shown below. The 2050s and 2080s for both RCP 4.5 and RCP 8.5 is shown below, with the value as the difference (Diff.) from the 1971-2000 period shown first, followed by the standard deviation (Stdev.) from all GCMs. Italicized results indicate significance at the 90% confidence interval, while bold italicized values indicate 95% confidence intervals.

TXx	Alaska					Anchorage (ANC)				
	DJF	MAM	JJA	SON	ANN	DJF	MAM	JJA	SON	ANN
Station	NA	NA	NA	NA	NA	5.05	12.84	23.3	11.61	25.02
Historical (Reanalysis)	-2.56	6.55	20.13	5.99	22.3	1.49	8.51	20.1	8.24	22.2
Historical (GCMs)	-2.34	4.51	19.38	5.32	22.28	0.12	3.95	19.35	6.82	22.5
Historical Stdev.	2.28	2.28	2.38	1.26	2.54	1.26	2.04	2.07	1.89	2.1
2050s Diff. (RCP 4.5)	2.29	2.47	2.17	2.24	2.05	1.65	2.82	2.37	2.12	1.95
2050s Stdev. (RCP 4.5)	1	0.71	1.23	0.72	1.2	0.59	1.12	1.23	0.81	1.3
2050s Diff. (RCP 8.5)	2.78	3.22	2.78	2.88	2.75	2.18	3.74	3.26	2.9	2.91
2050s Stdev. (RCP 8.5)	0.81	0.89	1.43	1	1.59	0.78	1.36	1.46	1.21	1.61
2080s Diff. (RCP 4.5)	2.67	3.02	2.74	2.45	2.49	2.07	3.56	3.13	2.55	2.69
2080s Stdev. (RCP 4.5)	0.63	0.94	1.55	0.77	1.48	0.7	1.12	1.5	0.92	1.4
2080s Diff. (RCP 8.5)	4.47	5.57	4.5	4.6	4.38	3.78	6.64	5.1	4.57	4.62
2080s Stdev. (RCP 8.5)	1.38	1.59	2.23	1.32	2.27	1.11	1.81	1.95	1.57	1.83
	Fairbanks (FAI)					Barrow (BRW)				
Station	-0.16	15.69	28.66	10.39	31.03	-8.16	-3.49	16.08	2.13	19.35
Historical (Reanalysis)	-2.69	10.73	24.02	7.1	26.27	-8.86	-0.94	17.63	1.84	19.84
Historical (GCMs)	-2.39	7.12	21.88	5.89	24.73	-6.34	0.37	17.12	2.65	20.06
Historical Stdev.	3.01	3.13	3.16	1.58	3.62	4.27	2.33	3.8	1.49	4.17
2050s Diff. (RCP 4.5)	2.21	2.46	1.74	2.2	1.59	2.95	2.3	2.45	2.86	2.43
2050s Stdev. (RCP 4.5)	1.06	0.78	1.22	0.7	1.14	2	0.34	1.34	0.74	1.51
2050s Diff. (RCP 8.5)	2.5	3.12	2.34	2.83	2.33	3.95	3.09	2.97	3.43	2.99
2050s Stdev. (RCP 8.5)	0.93	1.03	1.6	1.08	1.91	1.82	0.76	1.53	0.81	1.74
2080s Diff. (RCP 4.5)	2.45	2.91	2.24	2.34	1.99	3.71	2.81	2.96	3.02	2.73
2080s Stdev. (RCP 4.5)	0.71	1.18	1.64	0.74	1.72	1.58	1.06	1.81	0.71	1.97
2080s Diff. (RCP 8.5)	4.21	5.21	3.9	4.42	3.71	6.08	5.33	4.86	5.3	4.79
2080s Stdev. (RCP 8.5)	1.47	2.13	2.53	1.36	2.87	3	1.15	2.57	1.26	2.78

Table 2.5 Average seasonal and annual five-day maximum precipitation (Rx5, mm).for (DJF=December, January, February, MAM=March, April, May, JJA=June, July, August, SON=September, October, November) and annual (ANN) results for Alaska, Anchorage (ANC), Fairbanks (FAI) and Barrow (BAR) for RCP 4.5 and RCP 8.5 for The station average historical (1971-2000) is shown for ANC, FAI and BAR; statewide station values are not available (NA). Historical mean from the Reanalysis and the mean and standard deviation (Stdev.) for the GCM is shown below. The 2050s and 2080s for both RCP 4.5 and RCP 8.5 is shown below, with the value as the difference (Diff.) from the 1971-2000 period shown first, followed by the standard deviation (Stdev.) from all GCMs. Italicized results indicate significance at the 90% confidence interval, while bold italicized values indicate 95% confidence intervals.

Rx5	Alaska					Anchorage (ANC)				
Station	DJF	MAM	JJA	SON	ANN	DJF	MAM	JJA	SON	ANN
Historical (Reanalysis)	19	16	25	24	42	46	34	37	51	77
Historical (GCMs)	22	18	32	30	51	45	37	48	59	88
Historical Stdev.	4	3	2	2	2	10	7	5	11	11
2050s Diff. (RCP 4.5)	3	2	<i>4</i>	<i>5</i>	<i>7</i>	8	5	5	8	11
2050s Stdev. (RCP 4.5)	1	1	1	1	2	3	1	4	5	8
2050s Diff. (RCP 8.5)	4	3	<i>6</i>	<i>6</i>	<i>10</i>	9	6	<i>8</i>	10	16
2050s Stdev. (RCP 8.5)	1	1	1	3	4	4	1	4	8	9
2080s Diff. (RCP 4.5)	3	3	<i>5</i>	<i>5</i>	<i>8</i>	8	6	<i>7</i>	8	12
2080s Stdev. (RCP 4.5)	1	1	1	2	3	4	2	3	6	8
2080s Diff. (RCP 8.5)	<i>6</i>	<i>5</i>	<i>9</i>	<i>10</i>	<i>16</i>	<i>15</i>	11	<i>11</i>	<i>17</i>	<i>25</i>
2080s Stdev. (RCP 8.5)	2	1	3	4	5	4	3	5	7	9
	Fairbanks (FAI)					Barrow (BRW)				
Station	9	6	22	13	35	2	2	12	6	19
Historical (Reanalysis)	11	9	21	15	30	7	6	13	11	21
Historical (GCMs)	13	12	29	19	41	9	8	16	15	28
Historical Stdev.	3	2	4	2	5	2	2	4	1	3
2050s Diff. (RCP 4.5)	1	2	4	<i>4</i>	<i>6</i>	2	1	3	<i>2</i>	<i>6</i>
2050s Stdev. (RCP 4.5)	1	0	2	1	3	1	0	1	2	2
2050s Diff. (RCP 8.5)	2	3	<i>6</i>	<i>6</i>	<i>9</i>	2	1	5	<i>4</i>	<i>9</i>
2050s Stdev. (RCP 8.5)	2	1	2	3	4	1	0	2	2	3
2080s Diff. (RCP 4.5)	2	2	<i>4</i>	5	<i>8</i>	2	1	4	<i>3</i>	<i>7</i>
2080s Stdev. (RCP 4.5)	1	1	1	2	4	1	0	2	1	2
2080s Diff. (RCP 8.5)	2	<i>4</i>	<i>8</i>	<i>8</i>	<i>12</i>	<i>3</i>	3	<i>8</i>	<i>7</i>	<i>13</i>
2080s Stdev. (RCP 8.5)	2	2	3	3	5	1	1	3	3	5

Table 2.6 Comparison of changes in extreme values (ClimDEX indices) and mean values averaged over six models and the 30 years, annually, centered on the 2080s, from the RCP 8.5 simulations. Results are shown for TNn (°C), TXx (°C), and Rx5 (%).

ΔTNn vs. ΔTmean (°C)				
	Alaska	ANC	FAI	BRW
DJF	14.0 vs. 10.6	12.8 vs. 8.5	12.8 vs. 8.5	17.4 vs. 13.6
MAM	11.1 vs. 6.4	11.9 vs. 5.7	10.3 vs. 5.7	11.0 vs. 7.1
JJA	5.0 vs. 5.0	6.0 vs. 5.0	4.7 vs. 4.5	4.6 vs. 4.3
SON	9.7 vs. 7.8	8.5 vs. 6.4	9.4 vs. 6.4	12.6 vs. 11.6
Ann	14.3 vs. 7.4	13.1 vs. 6.4	13.4 vs. 6.4	15.9 vs. 9.1
ΔTXx vs. ΔTmean (°C)				
DJF	4.5 vs. 10.6	3.8 vs. 8.5	4.2 vs. 8.5	6.1 vs. 13.5
MAM	5.8 vs. 6.4	6.6 vs. 5.7	5.2 vs. 6.4	5.3 vs. 7.1
JJA	4.5 vs. 5.0	5.1 vs. 5.0	3.9 vs. 4.5	4.9 vs. 4.3
SON	4.6 vs. 7.8	4.6 vs. 6.4	4.4 vs. 6.4	5.3 vs. 11.6
Ann	4.4 vs. 7.4	4.6 vs. 6.4	3.7 vs. 6.4	4.8 vs. 9.1
ΔR5x vs. ΔPrec (mean, %)				
DJF	27 vs. 13	33 vs. 13	15 vs. 10	33 vs. 16
MAM	28 vs. 12	30 vs. 10	33 vs. 13	38 vs. 13
JJA	28 vs. 19	23 vs. 21	28 vs. 12	50 vs. 22
SON	33 vs. 16	29 vs. 14	42 vs. 16	47 vs. 18
Ann	31 vs. 15	28 vs. 14	29 vs. 13	46 vs. 18

2.9 References

- Alexander L, Zhang X, Peterson T, Caesar J, Gleason B, Klein Tank A, Haylock M, Collins D, Trewin B, Rahimzadeh F. 2006. Global observed changes in daily climate extremes of temperature and precipitation. *J. Geophys. Res. Atmos.* (1984–2012) **111**: D05109, DOI:10.1029/2005JD006290.
- Arora VK, Scinocca JF, Boer GJ, Christian JR, Denman KL, Flato GM, Kharin VV, Lee WG, Merryfield WJ. 2011. Carbon emission limits required to satisfy future representative concentration pathways of greenhouse gases. *Geophys. Res. Lett.* **38**: L05805, DOI:10.1029/2010gl046270.
- Bieniek PA, Bhatt US, Thoman RL, Angeloff H, Partain J, Papineau J, Fritsch F, Holloway E, Walsh JE, Daly C. 2012. Climate divisions for Alaska based on objective methods. *J. Appl. Meteorol. Climatol.* **51**: 1276–1289.
- Bieniek PA, Walsh JE, Thoman R, Bhatt US. 2014. Using climate divisions to analyze variations and trends in Alaska temperature and precipitation. *J. Clim.* **27**: 2800–2818, DOI:10.1175/JCLI-D-13-00342.1
- Bromwich, D. H., R. L. Fogt, K. I. Hodges, and J. E. Walsh, 2007: A tropospheric assessment of the ERA-40, NCEP, and JRA-25 global reanalyses in the polar regions. *J. of Geophysical Research: Atmospheres (1984–2012)*, **112**.
- Bronaugh, D., 2012: Package ‘climdex.psic’. *CRAN Repository*.
- Cassano, E. N., and J. J. Cassano, 2010: Synoptic forcing of precipitation in the Mackenzie and Yukon River basins. *International Journal of Climatology*, **30**, 658-674.10.1002/joc.1926.
- CCSP. 2008. Weather and Climate Extremes in a Changing Climate. Regions of Focus: North America, Hawaii, Caribbean, and U.S. Pacific Islands. A Report by the U.S. Climate Change Science Program and the Subcommittee on Global Change Research, Thomas RK, Gerald AM, Christopher DM, Susan JH, Anne MW, William LM (eds). Department of Commerce, NOAA’s National Climatic Data Center: Washington, DC, 164 pp.
- Chylek, P., J. Li, M. Dubey, M. Wang, and G. Lesins, 2011: Observed and model simulated 20th century Arctic temperature variability: Canadian earth system model CanESM2. *Atmos Chem Phys*, **11**, 22893-22907.
- Deser, C., A. Phillips, V. Bourdette, and H. Teng, 2012: Uncertainty in climate change projections: the role of internal variability. *Clim. Dyn.*, **38**, 527-546.
- Dufresne J, Foujols M, Denvil S, Caubel A, Marti O, Aumont O, Balkanski Y, Bekki S, Bellenger H, Benschila R. 2012. Climate change projections using the IPSL-CM5 Earth System Model: from CMIP3 to CMIP5. *Clim. Dyn.* **40**: 2123–2165

- Frich, P., L. Alexander, P. Della-Marta, B. Gleason, M. Haylock, A. Klein Tank, and T. Peterson, 2002: Observed coherent changes in climatic extremes during the second half of the twentieth century. *Climate Research*, **19**, 193-212.
- Gent PR, Danabasoglu G, Donner LJ, Holland MM, Hunke EC, Jayne SR, Lawrence DM, Neale RB, Rasch PJ, Vertenstein M. 2011. The community climate system model version 4. *J. Clim.* **24**: 4973–4991.
- Giorgetta, M., 2012: Climate change from 1850 to 2100 in MPI-ESM CMIP5 simulations. *J. Adv. Model. Earth Syst.* **5**(3): 572–597
- Goodison, B. E., 1978: Accuracy of Canadian snow gauge measurements. *Journal of Applied Meteorology*, **17**, 1542-1548.
- Groisman, P. Y., R. W. Knight, D. R. Easterling, T. R. Karl, G. C. Hegerl, and V. N. Razuvaev, 2005: Trends in intense precipitation in the climate record. *Journal of Climate*, **18**, 1326-1350.
- Hayhoe K. 2010. A Standardized Framework for Evaluating the Skill of Regional Climate Downscaling Techniques, PhD thesis, Atmospheric Sciences, University of Illinois, Urbana-Champaign, IL, 153 pp.
- Helsel, D. R., and R. M. Hirsch, 2002: *Statistical methods in water resources*. Vol. 323, US Geological survey Reston, VA.
- IPCC, 2007: Climate Change 2007: The Physical Science Basis. Contribution of Working Group I to the Fourth Assessment Report of the Intergovernmental Panel on Climate Change. Cambridge University Press, 996 pp.
- Karl TR, Melillo JM, Peterson TC. 2009. Global Climate Change Impacts in the United States. Cambridge University Press: Cambridge, UK, 188 pp.
- Katz, R. W., and B. G. Brown, 1992: Extreme events in a changing climate: variability is more important than averages. *Climatic Change*, **21**, 289-302.
- Kharin, V., F. Zwiers, X. Zhang, and M. Wehner, 2013: Changes in temperature and precipitation extremes in the CMIP5 ensemble. *Climatic Change*, **119**(2): 345–357.
- Klein Tank, A., F. Zwiers, and X. Zhang, 2009: Guidelines on analysis of extremes in a changing climate in support of informed decisions for adaptation. Climate Data and Monitoring WCDMP-No. 72. World Meteorological Organization: Geneva, Switzerland, 52 pp.
- Liepert BG, Lo F. 2013. CMIP5 update of ‘Inter-model variability and biases of the global water cycle in CMIP3 coupled climate models’. *Environ. Res. Lett.* **8**, DOI: 10.1088/1748-9326/8/2/029401.
- Massonnet, F., T. Fichefet, H. Goosse, C. M. Bitz, G. Philippon-Berthier, M. M. Holland, and P.-Y. Barriat, 2012: Constraining projections of summer Arctic sea ice. *The Cryosphere Discussions*, **6**, 2931-2959.

- Moss RH, Edmonds JA, Hibbard KA, Manning MR, Rose SK, van Vuuren DP, Carter TR, Emori S, Kainuma M, Kram T. 2010. The next generation of scenarios for climate change research and assessment. *Nature* **463**(7282): 747–756.
- Overland, J. E., M. Wang, N. A. Bond, J. E. Walsh, V. M. Kattsov, and W. L. Chapman, 2011: Considerations in the Selection of Global Climate Models for Regional Climate Projections: The Arctic as a Case Study. *Journal of Climate*, **24**, 1583-1597.
- Peterson TC, Heim RR, Hirsch R, Kaiser DP, Brooks H, Diffenbaugh NS, Dole RM, Giovannetone JP, Guirguis K, Karl TR, Katz RW, Kunkel K, Lettenmaier D, McCabe GJ, Paciorek CJ, Ryberg KR, Schubert S, Silva VBS, Stewart BC, Vecchia AV, Villarini G, Vose RS, Walsh J, Wehner M, Wolock D, Wolter K, Woodhouse CA, Wuebbles D. 2013. Monitoring and understanding changes in heat waves, cold waves, floods, and droughts in the United States: state of knowledge. *Bull. Am. Meteorol. Soc.* **94**: 821–834, DOI: 10.1175/bams-d-12-00066.1.
- Rawlins MA, Steele M, Holland MM, Adam JC, Cherry JE, Francis JA, Groisman PY, Hinzman LD, Huntington TG, Kane DL. 2010. Analysis of the arctic system for freshwater cycle intensification: observations and expectations. *J. Clim.* **23**: 5715–5737, DOI:10.1175/2010jcli3421.1.
- Reichler, T., and J. Kim, 2008: How Well Do Coupled Models Simulate Today's Climate? *Bulletin of the American Meteorological Society*, **89**, 303-311.10.1175/bams-89-3-303.
- Serreze, M. C., A. P. Barrett, and F. Lo, 2005: Northern high-latitude precipitation as depicted by atmospheric reanalyses and satellite retrievals. *Monthly Weather Review*, **133**(12):3407–3430, DOI: 10.1175/MWR3047.1
- Sillmann, J., V. Kharin, F. Zwiers, X. Zhang, and D. Bronaugh, 2013a: Climate extreme indices in the CMIP5 multi-model ensemble. Part 2: Future climate projections. *Journal of Geophysical Research: Atmospheres*. **118**(6): 2473-2493.
- Sillmann, J., V. Kharin, X. Zhang, F. Zwiers, and D. Bronaugh, 2013b: Climate extremes indices in the CMIP5 multi-model ensemble. Part 1: Model evaluation in the present climate. *Journal of Geophysical Research: Atmospheres*. **118**(4): 1716-1733.
- Stoner, A. M., K. Hayhoe, X. Yang, and D. J. Wuebbles, 2012: An asynchronous regional regression model for statistical downscaling of daily climate variables. *International Journal of Climatology*. **33**(11): 2473–2494, DOI:10.1002/joc.3603
- Trenberth KE, Jones P. 2007. Observations: surface and atmospheric climate change. In *Climate Change 2007: The Physical Science Basis. Contribution of Working Group I to the Fourth Assessment Report of the Intergovernmental Panel on Climate Change*, Solomon S, Qin D, Manning M, Chen

- Z, Marquis M, Averyt KB, Tignor M, Miller HL (eds). Cambridge University Press: Cambridge, UK and New York, NY, 235–336.
- Uppala SM, Kållberg PW, Simmons AJ, Andrae U, Bechtold VDC, Fiorino M, Gibson JK, Haseler J, Hernandez A, Kelly GA, Li X, Onogi K, Saarinen S, Sokka N, Allan RP, Andersson E, Arpe K, Balmaseda MA, Beljaars ACM, Berg LVD, Bidlot J, Bormann N, Caires S, Chevallier F, Dethof A, Dragosavac M, Fisher M, Fuentes M, Hagemann S, Hólm E, Hoskins BJ, Isaksen L, Janssen PAEM, Jenne R, McNally AP, Mahfouf JF, Morcrette JJ, Rayner NA, Saunders RW, Simon P, Sterl A, Trenberth KE, Untch A, Vasiljevic D, Viterbo P, Woollen J. 2005. The ERA-40 re-analysis. *Q. J. R. Meteorol. Soc.* **131**:2961–3012, DOI: 10.1256/qj.04.176.
- Vincent, L. A., and E. Mekis, 2006: Changes in daily and extreme temperature and precipitation indices for Canada over the 20th Century. *Atmosphere-Ocean*, **44**, 177-193.
- Voldoire A, Sanchez-Gomez E, y Méliá DS, Decharme B, Cassou C, Sénési S, Valcke S, Beau I, Alias A, Chevallier M. 2011. The CNRM-CM5.1 global climate model: description and basic evaluation. *Clim. Dyn.* **40**(9-10): 2091–2121.
- Walsh, J. E., W. L. Chapman, V. Romanovsky, J. H. Christensen, and M. Stendel, 2008: Global climate model performance over Alaska and Greenland. *Journal of Climate*, **21**, 6156-6174.
- Westra S, Alexander LV, Zwiers FW. 2012. Global increasing trends in annual maximum daily precipitation. *J. Clim.* **26**(11): 3904–3918, DOI: 10.1175/JCLI-D-12-00502.1
- Yukimoto, S., Y. Adachi, and M. Hosaka, 2012: A New Global Climate Model of the Meteorological Research Institute: MRI-CGCM3: Model Description and Basic Performance (Special Issue on Recent Development on Climate Models and Future Climate Projections). *Journal of the Meteorological Society of Japan*, **90**, 23-64.
- Zhang X, Zwiers FW. 2013. Statistical indices for the diagnosing and detecting changes in extremes. In *Extremes in a Changing Climate*. Aghakouchak A, Easterling D, Hsu K, Schubert S, Sorooshian S (eds). Springer: Netherlands, 1–14.
- Zhang, X., W. D. Hogg, and É. Mekis, 2001: Spatial and temporal characteristics of heavy precipitation events over Canada. *Journal of Climate*, **2001**, 1923-1936.
- Zhang, X., L. A. Vincent, W. D. Hogg, and A. Niitsoo, 2000: Temperature and precipitation trends in Canada during the 20th century. *Atmosphere-Ocean.*, **38**, 395-429.
- Zhang X, Alexander L, Hegerl GC, Jones P, Klein Tank A, Peterson RC, Trewin B, Zwiers FW. 2011. Indices for monitoring changes in extremes based on daily temperature and precipitation data. *Wiley Interdiscip. Rev. Clim. Change* **2**: 851–870.

CHAPTER 3: HISTORICAL TRENDS AND EXTREMES IN REGIONAL SCALE INTERIOR AND WESTERN ALASKA RIVER BASINS¹

Abstract

Climate change will shift the frequency, intensity, duration and persistence of extreme hydroclimate events and have particularly disastrous consequences in vulnerable systems such as the warm permafrost-dominated Interior region of boreal Alaska. This work focuses on recent research results from nonparametric trends and nonstationary generalized extreme value (GEV) analyses at eight Interior Alaskan river basins for the past 50/60 years (1954/64-2013). Trends analysis of maximum and minimum streamflow indicates a strong (> +50%) and statistically significant increase in 11-day flow events during the late fall/winter and during the snowmelt period (late April/mid-May), followed by a significant decrease in the 11-day flow events during the post-snowmelt period (late May and into the summer). The April-May-June seasonal trends show significant decreases in maximum streamflow for snowmelt dominated systems (<-50%) and glacially influenced basins (-24 to -33%). Annual maximum streamflow trends indicate that most systems are experiencing declines, while minimum flow trends are largely increasing. Nonstationary GEV analysis identifies time-dependent changes in the distribution of spring extremes for snowmelt dominated and glacially dominated systems. Temperature in spring influences the glacial and high elevation snowmelt systems and winter precipitation drives changes in the snowmelt dominated basins. The Pacific Decadal Oscillation was associated with changes occurring in snowmelt dominated systems, and the Arctic Oscillation was linked to one lake dominated basin, with half of the basins exhibiting no change in response to climate variability. The work indicates that broad scale studies examining trend and direction of change should employ multiple methods across various scales and consider regime dependent shifts to identify and understand changes in extreme streamflow within boreal forested watersheds of Alaska.

¹ K.E. Bennett, A. J. Cannon and L. Hinzman. In prep for the Journal of Hydrology. Historical Trends and Extremes in Regional Scale Interior and Western Alaska River Basins.

3.1 Introduction

Extreme hydroclimatic responses in regional-scale Alaskan watersheds are influenced by both climate change and natural climate variability, which lead to shifts in water storages that impact fresh water resource availability and quality. The signal of mean change in hydrologic systems has been well documented in previous work (ACIA, 2005; Hinzman et al., 2005) and include shifts in: snow cover extent (Brown, 2010); permafrost distribution (Osterkamp, 2005); lake and river freeze up and breakup (Magnuson et al., 2000); glacial mass-balance (Moore et al., 2009); and regional synoptic river discharge (Déry and Wood, 2005). Much of the work to-date focuses on climate change impacts in Arctic runoff in large river systems (Forbes and Lamoureux, 2005; Peterson et al., 2002b; Yang et al., 2002; Yang et al., 2003), or small watersheds (Kane et al., 2008; Kane et al., 2003) but analysis of changing streamflow extremes that are occurring in regional-scale watersheds is lacking.

Observed changes in mean streamflow indicates that the tails of the streamflow distributions are also likely to be changing and this could have an impact on human and ecologic systems at a regional-scale in the Arctic and subarctic (Zhang and Zwiers, 2013). Extreme events in critical watersheds such as those being considered for future power and hydro-electric resources (i.e. Susitna), or rivers such as the Yukon that are utilized for food and transport by numerous villages throughout Alaska (Alaska Energy Authority, 2014; Brabets et al., 2000) have the potential to put both industries and resources at risk. Flooding and low flows will have a great effect on mining, infrastructure, ecology, and society in all parts of the state of Alaska. Understanding these changes allows for comprehensive review of existing planning measures, including tailing ponds and spillway allowances, bridge maintenance, and flood evacuation protocols in regions and basins where changes are occurring or have occurred in the historical record.

Comprehensive extreme event analysis of changes in streamflow in the subarctic region of Alaska has been limited. This is because the building blocks for hydrologic models, such as a comprehensive understanding of hydro-climatologic regimes, snowmelt and freeze-thaw dynamics and antecedent moisture storage conditions driving events at the regional-scale in Alaskan watersheds remain unclear (Woo et al., 2008b). However, the lack of long term, high-quality, continuous records of streamflow available for comprehensive study, and for model calibration and validation also plays a large role in the paucity of research. Previous work on changes in extreme streamflow for Interior Alaskan boreal forest basins is also sparse. Major papers have looked at streamflow hydrology in the Kuparuk River basin, a high latitude watershed located on the North Slope of Alaska, adjacent to the Arctic Ocean (Kane et al., 2008; Kane et al., 2000; Kane et al., 2003; McNamara et al., 1998). Jones and Rinehart (2010) examined small watersheds located in the Caribou-Poker Creek to relate storm flow to permafrost and precipitation. Changes in streamflow attributable to the Pacific Decadal Oscillation (PDO) were presented in Neal et al.

(2002) for southeast Alaska, for the Yukon River by Brabets and Walvoord (2009), and for a broad range of coastal to interior sites for Alaska by Hodgkins (2009).

Large scale Arctic river networks have also been analyzed in a number of seminal research papers (Peterson et al., 2002b; Serreze et al., 2006; Serreze et al., 2002; Slater et al., 2006; Yang et al., 2002). Some of this work highlights the changing nature of hydrologic regimes with shifts in climate, namely the acceleration of the hydrologic cycle in northern regions, which is a major hypothesis for the change in extreme events within the Arctic (Rawlins et al., 2010; Serreze et al., 2009; Serreze et al., 2000). However, the direction of change and the proposed mechanisms driving streamflow changes is not agreed upon in the literature. Declining flow trends have been observed across northern, coastal Canadian rivers and rivers flowing into the Ungava, James and Hudson Bays (Déry et al., 2005; Déry and Wood, 2005). An updated paper in 2009 revealed a trend reversal towards increasing flows and flow variability for rivers in northern Canada when the time series was extended by four years (1964-2007, Déry et al., 2009). Increasing low flows have been reported in Interior river networks of the Northwest Territories (St. Jacques and Sauchyn, 2009) and the Yukon River (Walvoord and Striegl, 2007), attributable to enhanced infiltration due to permafrost thawing (Smith et al., 2007). In the Mackenzie River basin, no trends were found in flow magnitudes from 1973-1999, although variability was noted to be increasing (Woo and Thorne, 2003; Zhang et al., 2001). Janowicz (2011), focusing on the Yukon River region, associated streamflow declines with regions of thawing permafrost, owing to deeper infiltration and removal of runoff from the subsurface. Spence et al. (2011) documented increased winter baseflow to greater fall precipitation leading to a switch in systems from a purely snowmelt dominated system to a snowmelt-rainfall regime, a change that is most apparent at small systems not dominated by lakes.

The detection of long term trends is confounded by low-frequency climate variability, time scale of analysis, and the time period considered. A connection between process shifts in basins and across regions is possible by placing the nature of climate variability within the context of streamflow regimes. For example, Moore and Demuth (2001) examined streamflow at Place Glacier and found it to be declining. The basis for this was a correlation between winter and net glacier mass balance with the PDO, while summer glacier balance was negatively correlated with summer temperature, and showed a positive correlation with preceding winter balance. Fleming et al. (2006) distinctly different responses in snowmelt systems compared to glacier basins, where streamflow was moderated by the Arctic Oscillation (AO). Déry and Wood (2004) examined the impact of the AO on declining streamflow into Hudson Bay; isolating changes and linking those changes to streamflow regimes particular to the region. While annual trends in streamflow have been broadly considered (Déry et al., 2009; Peterson et al., 2002a; St. Jacques and Sauchyn, 2009), seasonal studies are less common, despite the fact that at finer scales of analysis

process shifts can be determined (Whitfield et al., 2002). Trends detection is also susceptible to time period which is not always recognized (Bone et al., 2010).

This paper seeks to expand our understanding of historical changes in hydroclimate extremes through the examination of trends in maximum and minimum flows, and through the use of nonstationary generalized extreme value theory (GEV) analysis to examine peak streamflow changes from comprehensive, long term records for regional scale Alaskan watersheds. The objective of this work is to document historical shifts in extreme streamflow and link observed changes associated with spring breakup peakflow with time, climate (temperature and precipitation) and/or climate variability by investigating the use of these variables as covariates in the GEV analysis of streamflow trends. The study is undertaken at eight watersheds across Interior and Western Alaska with variable hydrologic regimes – from glacial-snowmelt to snowmelt-rainfall. The paper outlines the study sites used in the analysis, and the methodology, including nonparametric trends and nonstationary GEV statistical approaches. Results are presented for trends and GEV, and results from each covariate analysis. The paper’s discussion focuses on a hypothesis-based presentation on the probable causes of changes observed to be occurring in these watersheds. The conclusion of the paper highlights the major points of the work and discusses implications.

3.2 Methods

3.2.1 Study Area

The streamflow stations considered for this analysis span a range of climate and topographic conditions (Table 3.1), extending from the central Interior region of Alaska near Fairbanks, southwest to the village of Dillingham, and east to the town of Eagle near the Yukon Territory, Canada (Figure 3.1). The sites are therefore a sample of Interior stations exhibiting both glacial and snowmelt influences (glacial-nival), and snowmelt and rainfall influences (nival-rainfall). Some stations gage very large river basins (i.e. the Yukon at Eagle), while others capture flow from smaller sub-watersheds of major basins (i.e. the Chena River, Table 3.1).

Historical streamflow in the Susitna and Talkeetna River (SUS, TAL, Figure 3.2) watersheds illustrates the characteristic glacial-nival shape of their hydrographs, with an initial snowmelt peak and a secondary peak in August associated with precipitation combined with glacial melt. The Kuskokwim River (KUS, Figure 3.2) is a complex system owing to its division between high elevation, mountainous and glacial headwater regions and its large low-elevation, boreal lowland/wetlands through which its extensive drainage flows. The Kuskokwim River therefore displays a subarctic nival-rainfall regime with some glacial influence. The Nuyakuk River (NUY, Figure 3.2) drains a large lake complex, glacial and

perennial snow and ice fields of the Aklun Mountains and lowland wetlands in the Bristol Bay region of Alaska, approximately 100 km north of the city of Dillingham (pop. ~2300). The Nuyakuk River is the most southern system analyzed. The lakes act to delay the snowmelt peak in this watershed into June. The Nuyakuk is hence classified as a prolacustrine-nival system.

The Yukon River watershed at Eagle drains a large expanse of Canadian landscape and has a sharp peak and a long recessional tail owing to snowmelt contributions located within high elevation regions of the watershed and glaciers of the White River basin in the Wrangell-St. Elias Mountain range (Table 3.1, Figure 3.2, Brabets et al. 2000). The glaciers in this area are receding and ablation is considered to dominate over changes in precipitation, based on a 30-year record from the Gulkana River glacier (Brabets et al., 2000). Permafrost is both continuous and discontinuous and vegetation is largely boreal black and white spruce, deciduous and tundra, with numerous high elevation rocky outcrops. The Tanana River basin, which has its headwaters in the Alaskan Range, has the second highest percentage of glacial coverage (5%) and exhibits peak flows during months where both melt from glaciers and summer precipitation maximums occur (TAN, Figure 3.2). The Salcha and Chena rivers, sub-watersheds to the Tanana, are dual nival-rainfall dominated systems (SAL, CHE, Figure 3.2). The snowmelt peak is the largest annual contribution to flow, followed by a secondary maximum peak in late June that is only apparent on the Salcha River (Figure 3.2). Salcha's June peak is indicative of late melt associated with high elevation snowpacks in the upper reaches of the watershed. The rainfall peak in both systems occurs in mid-August and is associated with frontal storms that results in widespread rainfall across the region. After a number of storm events, hillslopes become saturated and runoff occurs, which can generate peak flows and sometimes flooding.

3.2.2 Data Sources

All data were extracted from the United States Geological Survey's (USGS) daily historical streamflow database. Only the gages with more than 40 years of data were considered for inclusion in the work. From all gages in the region, only eight stations had sufficient data (> 70% complete) for the time period under study. Years analyzed range from 1954 to 2013 for six of the eight stations and 1964 to 2013 (Tanana/Talkeetna), see Table 3.1.

Winter streamflow at gages is generally assumed to begin in late October or early November and last until snowmelt in April/May. Stream flow records are continuous through the year for all stations, but when ice-affected conditions are present the rating curves is not valid and must be verified using additional measurements or information. Under-ice measurements are collected by the USGS technicians periodically (two to four times) through winter by cutting 20 holes in the ice and inserting a current meter into the holes to measure flow at the average of 0.2 and 0.8 depths, if the river is deeper than 2.5 ft

(Rantz, 1982). At times, acoustic doppler current profilers (ADCP) are used for flow measurement but only when conditions are adequate for ADCP (H. Best, pers. comm.). Slush, for example, prevents use of ADCP because it interferes with the flow measurements. Streamflow is interpolated between these under-ice readings to calculate daily flow values using additional information such as air temperature and precipitation data, knowledge of the river conditions by local USGS technicians and staff, and corrections against the index gages. The USGS demarcates the under-ice measurements with an ice flag in their database. For our analysis, we analyzed under-ice flows in the same manner as open water flows.

The Chena River basin is the USGS's index streamflow gage for northern Alaska because the Chena remains open (i.e. ice free) in one section through the winter. The Aurora Energy Coal Power Plant discharges steam and hot water into the Chena River from its outfall located at 64°50'54"N, 147°44'06"W (EPA, 2002) which results in warming and melting of a portion of the river downstream of the power plant (Ecology and Environment, 2012). Therefore the Chena can be gaged during the winter using standard gaging methods. Flows collected during winter months along the Chena are used to assess and correct flows at other Interior river sites where under ice measurements are undertaken. Most of the rivers in this study are proximal to the Chena index station which increases confidence in their winter streamflow measurements. The Kuskokwim and the Nuyakuk rivers do not have under-ice measurements observed during winter time and their winter flow curves are based on knowledge of the USGS technicians alone, so interpretation of these records must consider this assumption. It should be noted that the primary focus of this paper is on the AMJ and annual peak flows and therefore streamflow maximums for these systems occur outside of the time period that is ice-affected.

3.2.3 Analysis

Trends and nonstationary GEV analyzes were completed for all sites. Trends analysis was completed for 11-day, monthly, seasonal and annual periods. The daily streamflow records were pre-processed to select maximum and minimum flow values for the period of record. For the GEV analysis, only the seasonal and annual data were analyzed; in this case missing years were deleted and partial years were filled based on the mean value.

3.2.3.1 Trend Analysis

Nonparametric trend analysis was completed for the maximum and minimum 11-day, monthly, seasonal, and annual time series of the time periods. The 11-day periods were selected based on Whitfield et al.'s (2002) finding that shorter time periods (5 days, 12 days) yields improved separation of variability based on cluster analysis of precipitation and temperature data across Canada. Monthly values are calculated over the 12 months of the year, and seasonal values were calculated for January-February-

March (JFM), April-May-June (AMJ), July-August-September (JAS) and October-November-December (OND) seasons. Trends were only computed for records with greater than 70% complete time series. Trends were analyzed using an approach developed by Yue et al. (2002) as outlined in Wang and Swail (2001), where the trend magnitude is calculated using a Theil-Sen approach (Sen, 1968; Theil, 1950a; Theil, 1950b; Theil, 1950c). The nonparametric Mann-Kendall (Kendall, 1975; Mann, 1945) test for significance is used on this series. Prior to applying the Mann-Kendall test, a pre-whitening technique is applied to remove any serial correlation that may inflate the significance of the trend (Helsel and Hirsch, 2002). The analysis was carried out using the `zyp.R` trends package for R-project statistical software (Bronaugh and Werner, 2009).

3.2.3.2 Generalized Extreme Value Theorem Analysis

Trends analysis presented in the previous section is complementary to the generalized extreme value theory (GEV) as the approach relies on the nonparametric Mann-Kendall test to calculate the trend significance and does not make assumptions about the data distribution except that the data are independently distributed in time. The GEV approach, on the other hand, is grounded in the theory of extremal limits that states a sufficiently long time series of block maxima will approach the GEV distribution asymptotically at large sample sizes (Coles, 2001). This provides justification for making inferences about return periods of extremes. The GEV-based approach to streamflow extremes can easily incorporate nonstationarity, thus allowing inferences on the changes in the frequency and magnitude of floods and low flows (Milly et al., 2008). Specifically, the parameters in the GEV distribution can be allowed to change with time (or with covariates that are time-dependent), hence allowing the efficient detection of trends in extremes within this framework. The particular form of nonstationary GEV analysis used here allows us to determine the form of the nonstationarity (or, if there is indeed evidence of nonstationarity) that best fits the streamflow data. Each of these methods described above are univariate and thus are applied to each individual time series of maximum or minimum annual and seasonal time periods separately.

The GEV approach applied in this study utilizes the R-project's `GEVcdn` package as described in Cannon (2010; Cannon, 2011). The approach models the GEV distribution as a function of covariates using a conditional density network, which is a probabilistic extension of the multilayer perceptron (MLP) neural network. The cumulative distribution function (cdf) of a GEV is as follows,

$$F(y; \mu, \sigma, \kappa) = \exp \left[- \left\{ 1 - \kappa \frac{(y - \mu)}{\sigma} \right\}^{1/\kappa} \right], \kappa \neq 0, 1 - \kappa \frac{(y - \mu)}{\alpha} > 0 \quad (3-1)$$

$$F(y; \mu, \sigma) = \exp \left[-\exp \left\{ -\frac{(y-\mu)}{\sigma} \right\} \right], \kappa = 0 \quad (3-2)$$

$$F(y; \mu, \sigma, \kappa) = \exp \left[-\left\{ 1 - \kappa \frac{(y-\mu)}{\sigma} \right\}^{1/\kappa} \right], \kappa \neq 0, 1 - \kappa \frac{(y-\mu)}{\sigma} > 0 \quad (3-3)$$

$$F(y; \mu, \sigma) = \exp \left[-\exp \left\{ -\frac{(y-\mu)}{\sigma} \right\} \right], \kappa = 0 \quad (3-4)$$

where μ is the location parameter, which describes the distribution center; the scale parameter, σ , which determines the size of the deviations around μ ; and κ , which is the shape parameter that determines the tail behavior of the distribution (normally Fréchet, Weibull or Gumbel type, Katz, 2013). The probability density function (pdf) is given by

$$f(y; \mu, \sigma, \kappa) = \frac{1}{\sigma} \left\{ 1 - \kappa \frac{(y-\mu)}{\sigma} \right\}^{(1-\kappa)/\kappa} \exp \left[-\left\{ 1 - \kappa \frac{(y-\mu)}{\sigma} \right\}^{1/\kappa} \right], \kappa \neq 0 \quad (3-5)$$

$$f(y; \mu, \sigma, \kappa) = \exp \left[-\frac{(y-\mu)}{\sigma} \right] \exp \left[-\exp \left\{ \frac{(y-\mu)}{\sigma} \right\} \right], \kappa = 0 \quad (3-6)$$

To avoid problems with maximum likelihood (ML) estimation of the shape parameter, a penalized version of ML that applies a prior distribution to the shape parameter that is representative of natural processes (Cannon, 2010; Coles and Dixon, 1999; Martins and Stedinger, 2000) is used here. In addition, the shape parameter is kept constant in all candidate models.

The work presented herein details results from five different candidate models. The initial model is stationary (S), in which parameters are not allowed to vary with the covariate (time is used here as an example). In the remaining models, the location and scale parameters are allowed to vary in time by specifying either a linear or non-linear hidden-layer activation function in the conditional density network model architecture. In the linear GEV model, this is the identify function, whereas it is the hyperbolic tangent function in the non-linear models. A linear nonstationary (LNS) version of the GEV framework assumes that the location and scale parameters are allowed to vary linearly and log-linearly with time, respectively. For the non-linear models, the scale parameter was not allowed to fall below a minimum threshold (15% of the range of the streamflow series) to reduce over fitting to specific data points (Cannon, 2012).

This linear version of the nonstationary GEV essentially follows El Adlouni et al. (2007),

$$\mu(t) = \beta_1 + \beta_2 t \quad (3-7)$$

$$\log(\alpha(t)) = \delta_1 + \delta_2 t \quad (3-8)$$

where β_1 , β_2 , δ_1 and δ_2 are parameters estimated from data. In the non-linear models, the number of hidden-layer nodes controls the degree of non-linearity that can be represented (Cannon, 2010). Three non-linear nonstationary candidate models of increasing complexity are analyzed by changing the number of nodes from one to three (NLNS with one node, NLNS with two nodes, and NLNS with three nodes, respectively).

To determine which of the candidate model approaches is most applicable, a cost-complexity model selection criteria, the Akaike Information Criteria, corrected for small sample sizes (AICc), identified the best model when minimized (Burnham et al., 2011). To further prevent over fitting of the models, the model recommended by AICc was selected to run a bootstrapped version of the GEV analysis, which was iterated 100 times, and the mean value of the bootstrapped quantiles was used for plotting return values.

To test the goodness-of-fit of the distributions and determine if the GEV fit of the model candidates is appropriate and statistically significant, a Kolmogorov-Smirnov (K-S) test was applied. The K-S test is applied to the GEV cdf (Equation 1) values from each fitted candidate model, otherwise known as the probability integral transform (PIT) values. If the PIT values follow a uniform distribution then the models are calibrated appropriately to the particular distribution (Gneiting et al., 2007).

3.2.3.3 Covariate Analysis

As well as using time as a covariate, nonstationary GEV analysis was also conducted for climate variability of the spring time (AMJ) changes and maximum streamflow. Values of the Pacific North American (PNA) pattern, the Arctic Oscillation (AO), the Pacific Decadal Oscillation (PDO) and the El Nino Southern Oscillation (ENSO) index were examined as potential covariates. Monthly values for each index were obtained from online sources, as listed below, from 1954/1964-2013. Average values were generated for the months of November, December, January and February (NDJF) for the standardized PDO, PNA and AO indices and applied to the JFM season to represent the strength of the climate signal during Interior Alaska's winter (L'Heureux et al., 2004). October was included in the ENSO composite analysis to account for potential lags in tropical forcing and midlatitude response affecting the Alaskan climate (Bond and Harrison, 2006). A standardized ENSO value was generated by calculating the DJFM average value that was greater or less than the mean +/- half the standard deviation.

The PNA is an atmospheric teleconnection pattern that responds to warm sea surface temperature anomalies in the central equatorial Pacific, and impacts climate across the Northern Hemisphere. It

follows that the PNA pattern is linked with warm and cold ENSO events, with a widespread response of ENSO that has been shown to have a direct impact on winter time temperature and precipitation across the western US (Redmond and Koch, 1991) and in North America (Shabbar et al., 1997; Yarnal and Diaz, 1986). The PNA index was obtained from the National Weather Services' Climate Prediction Center's website (NWSCPC, CPC, Accessed Sep 2013).

AO is considered to be a dominant and persistent mode of atmospheric variability; it is one of two annular modes with its prime influence in the Northern Hemisphere. It is also referred to in the literature as the Northern Annual Mode (NAM). The AO has influence at the high latitudes and is associated with low pressure fields near the pole, and high pressure fields at mid-latitudes that are linked with strong westerly wind anomalies. Glacier streamflow has been positively correlated with the AO index by Fleming et al. (2006) for sites in the Yukon and north western British Columbia nearby the border of Alaska. It has also been investigated for regions of Northern Canada and is positively correlated with runoff to the Bering Strait, and anticorrelated to runoff to the Labrador Sea and the Hudson Bay (Déry and Wood, 2004). The monthly AO index was downloaded from the NWSCPC website (CPC, Accessed Sep 2014).

The PDO index is defined as the leading principal component of SST anomalies in the Pacific Ocean, poleward of 20°N. The PDO is an index of atmosphere and oceanic variability that encompasses both an interannual ENSO signal and a decadal ENSO-like mode (Bitz and Battisti, 1999; Mantua et al., 1997). Positive values of PDO indicate the 'warm phase', attributed by warmer than average water in the equatorial Pacific and colder than average in the central North Pacific; negative values indicate the opposite pattern. The PDO index was obtained from the Joint Institute for the Study of Atmosphere and Ocean (JIASO, Accessed Sep 2014).

ENSO represents the strength of the sea surface temperatures (SST) in the equatorial Pacific region. Warm SST anomalies lead to a weakening of easterly trade winds, and a reduction in the currents that contribute to upwelling along the eastern coast of the Pacific. A deepening of the thermocline thus develops and leads to enhanced precipitation along the equator, establishing a high pressure zone in the sub-tropics and strengthened low pressure in the Aleutians. The influence of ENSO is widespread and is linked in part to the strengthening of the jet stream northward, and the influence of the PNA in North America. The ENSO 3.4 index was downloaded from the ESRL NOAA site (ESRL NOAA, Accessed Sep 2014).

Precipitation and air temperature covariates were explored using the CRU TS 3.21 data set (Harris et al., 2014). The CRU TS 3.21 monthly temperature and precipitation data were clipped and averaged over each basin to generate seasonal composites. The data were corrected to adjust major biases using the Climate Western North America (ClimateWNA, Wang et al., 2012) average monthly

climatology (1971-2000) data. In all cases the tests were formalized such that the seasonal temperature and precipitation from the current season and the previous season were tested for minimization using the AICc statistic; minimized results are plotted in figures and tables.

3.3 Results

3.3.1 Trends

Trend results for each gage are presented for maximum and minimum streamflow in Table 3.2 (monthly, seasonal and annual) and in Figures 3.3-3.4 (11-day, seasonal and annual). These results are provided as a percentage difference from the normal, calculated based on the average maximum or minimum streamflow over the whole period of record. Changes in the annual maximum flow at these sites are due to decreases in the May and summer flows, while changes in minimum flows are reflective of the increasing fall/winter/spring baseflow values (Table 3.2). Annually, maximum flow values are declining particularly in the glacial-nival systems (Susitna and Talkeetna) and in the mid-elevation sites that are snowmelt dominated (i.e Chena). These declines dominate the annual flow regime as the bulk of the water passes through the system during these times (Table 3.2, Figure 3.2). On the other hand, minimum flows (baseflow) are increasing in October and/or May at most of the sites (Table 3.2) however these flows comprise a small percent of the total flow volume. These results are partially corroborated by Hinzman et al. (2005), although glacierized basins were reported to have increasing flow volumes. Annual flow declines noted in this work are most closely aligned with Déry and Wood's (2005) results of declining flow trends in rivers for Northern Canada.

April–May 11-day maximum flows across all systems are increasing, with statistically significant results in either the early April period, or late April-early May (Figure 3.3). The April-May 11-day flow increase is likely a sign of earlier snowmelt; flows are shifting from a normally low flow period where river is ice covered and winter base flow conditions are dominant, to a breakup period where the snow and ice begin to melt and rivers start to flow. However, the large 11-day trend illustrated in Figure 3.3 occurs early in the year when there is relatively low flows occurring, as opposed to the May flow decrease that is a smaller percentage change but represents a larger absolute difference in flow magnitude. Large declines are observed for May in the snowmelt dominated systems (Salcha and Chena), while the Talkeetna exhibits flow declines in June (Table 3.2). Summer maximum streamflow is largely characterized by declining flow trends, particularly in the largest glacierized basins such as the Susitna (July only) and the Talkeetna (JAS), but also at the snowmelt dominated Chena (JAS).

Overall, changes in maximum flow are more statistically significant than changes in minimum flows. Where changes in minimum flows are statistically significant, flows tend to be increasing, while

maximum flows are mixed. Annual minimum baseflows are significantly increasing on the Yukon, Tanana and the Nuyakuk rivers (Table 3.2). The Yukon and Tanana basins are permafrost dominated with glacial headwaters – these findings reflect Walvoord and Striegl (2007) and St. Jacques and Sauchyn (2009) research documenting winter baseflow increases in permafrost basins. The Nuyakuk system is a prolacustrine system where flow signals and particularly baseflow is likely influenced by lake storage (see discussion on Lockhart River, Woo et al., 2008a). The highest increase in minimum flows is offset from the maximum flow increase an observable 11-days later in all systems except the Kuskokwim (Figure 3.4, 3.5). This offset is likely due to the delay in baseflow response that occurs between recharge of snowmelt and runoff in these watersheds (Rouse et al., 1997).

3.3.2 Generalized Extreme Value Analysis

The local K-S tests results for the minimized models never rejected the global null hypothesis (the global null in the K-S test specifies that the values of the analysis variable are a random sample from the specified theoretical distribution) at the significance (0.05) level except for the annual and summer seasons for the Salcha, Chena and Tanana systems. The 1967 flood was identified as the cause for poor fits (K-S tests were rejected) in the Tanana, Salcha and Chena River basins (Rouse et al., 1997). The 1967 flow in the annual GEV analysis were therefore removed and replaced with the mean from the time series.

Overall, annual maximum flows are minimized by the stationary (S), followed by the linear nonstationary models (LNS) at three basins and simple nonlinear nonstationary models at Susitna (Figure 3.5). Stationary results are indicative of no trend in the system. When nonlinear models are recommended, simpler nonlinear architectures are more common (NLNS1) than the more complex models (NLNS3). Where declines are shown by the GEV, the nonparametric trend results support these reductions in annual flow (Table 3.2).

During the spring season, stationary and linear nonstationary models are more evenly split between the basins (Figure 3.6). The Talkeetna, Salcha and Chena River systems exhibit decreasing trends during this season (Table 3.2), and each system here is shown to decline via the GEV (Figure 3.6). All systems experience their peak flow during this time of the year with the exception of the Tanana River, which does not peak until late July (Figure 3.2).

It is interesting to note that although the Talkeetna and the Susitna River basins are adjacent to each other they appear to be responding differently. These differences are not attributable to the different trend period examined; over the 1964 period the Susitna has no significant shift in its AMJ flows and does not show a significant flow decline annually (results not shown). To investigate this matter, the average basin hypsometry (1780 m, Table 8 in Clarke et al., 1985) and a September, 2013 glacier inventory (Arendt et al., 2012) were examined. The Talkeetna glaciers are above the average ablation line

(1781 m) for the area as identified in Clarke et al. (1985), while Susitna River watershed has a higher percentage of its basin at lower elevations, including its glaciers (Figure 3.7). It is possible therefore that the Talkeetna is experiencing detectable shifts in its snowpack and glaciers, while the Susitna's glacial decline has been surpassed (Moore et al., 2009). A larger relative August decline in streamflow at Talkeetna also supports this, while the Susitna flows experience smaller declines over July and August that are non-significant (Table 3.2).

The Yukon River, Kuskokwim and Tanana River basins have no change in either annual or AMJ flow statistics with time, with the exception of increasing fall/winter baseflow on a monthly and seasonal time scale (Table 3.2), which is discussed above. The Nuyakuk, on the other hand, exhibits a slight increasing linear nonstationary pattern of flow in AMJ, likely owing to an earlier freshet in March and April that is not followed by strongly declining flows in May (Figure 3.3, Table 3.2).

Return periods (2, 5, 10, 20, 50 and 100 year) shown in Figure 3.5 and Figure 3.6 illustrate the magnitude of changes in extreme value statistics over time. For example, in the Salcha system (SAL) a winter time maximum streamflow of $\sim 25000 \text{ f}^3\text{s}^{-1}$ in the 1950s is recurrent at a 10% probability (10 year), but by 2013 the same flow volume is recurrent at a 98-99% probability (50-100 year return interval, Figure 3.6). Another way to think about this is that the 10 year winter time return flow value has decreased by approximately $5000 \text{ f}^3\text{s}^{-1}$ in the Salcha system over the 60 year period 1954-2013.

3.3.3 Covariates Analysis: Climate Variability

Results of the GEV analysis run using climate variability as a covariate indicate that decreasing maximum spring streamflow patterns are related to the occurrence of the positive PDO in snowmelt, and non-glacier/permafrost dominated systems (Figure 3.7g, h). The exception to this is the Nuyakuk River basin, where positive AO is associated with decreased maximum spring streamflow volumes (Figure 3.7c). This result is similar to findings of Déry and Wood (2004) where declining Hudson Bay River inflows were associated with a positive AO. Bond and Harrison (2006) discuss the impact of ENSO with AO on the Alaskan climate, documenting a higher precipitation rate with combined ENSO/AO- winters for southern Alaska. Fleming et al. (2006) examined the AO in the context of glacial rivers in southwest Yukon but found the opposite relationships – positive AO was associated with higher glacial outputs but these glacial responses were distinct from the nival streamflow systems.

In Alaska results the positive phase of the PDO generally leads to increased air temperature and decreased precipitation across interior regions of Alaska (Hartmann and Wendler, 2005). The negative PDO tends to bring about generally opposite changes in terms of direction although magnitudes can be considerably stronger (Brabets and Walvoord, 2009). Decreased maximum AMJ streamflow associated with positive PDO values is likely a result of the decreased precipitation and warmer temperatures

associated with positive phase of the PDO and leading to lower May runoff values overall. This decrease is most evident on the purely snowfall driven systems (Salcha, Chena), as opposed to the nival-glacial systems (Fleming et al. 2006), as discussed below (Figure 3.7). In the Kuskokwim River basin, which is comprised of mountainous, lowlands regions and soils with 50% discontinuous and 50% sporadic and isolated permafrost, streamflow is responding to PDO and associated shifts in year-to-year climate (Table 3.1).

The glacial/permafrost dominant basins Yukon, Tanana, Susitna and Talkeetna do not show a response to any of the climate variability indices for AMJ, indicative of their stationary responses (Figure 3.7), as in the previous analysis using time as a covariate (Figure 3.6). The lack of response to both time and climate variability as covariates indicates that maximum AMJ streamflow has an alternate mechanism that contributes to high and low streamflow responses. Because of the amount of high elevation areas, permafrost, bare ground/rock and glaciers in the Yukon basins, the lack of a response is not surprising given that glaciers, ice fields, frozen ground, and groundwater interaction in this basin may act in opposite directions to system drivers (i.e. climate variability) and complicate responses (Table 3.1, Woo et al. 2008). The Tanana system's peak flow response is not represented in the AMJ period, although no response to climate variability indices was observed during this peak flow season either (JAS, not shown).

3.3.4 Covariate Analysis: Precipitation and Temperature

Precipitation and temperature covariates had much stronger relationships than time or climate variability, which is not unexpected. Results for the spring season reveal the differences in the basins' response to changing conditions in the season analyzed, or the preceding season (JFM). Glacial and high elevation snowmelt systems respond most cohesively to temperature in the AMJ season, with all basins exhibiting smaller maximum streamflow with warmer conditions. The Kuskokwim, Tanana and Chena River basin respond most strongly to increasing precipitation in the JFM season, indicative of higher winter snowpacks. The Nuyakuk basin responds to temperature in JFM, with warmer winter temperatures resulting in larger streamflow maximums. The Salcha River basin has a unique step-change response that is represented by the nonlinear nonstationary model of AMJ temperatures. Lower streamflow maximums are observed with increased temperatures.

3.4 Discussion

Interior Alaska river basins respond to climate shifts across variable time scales (11-day, monthly, seasonal and annual). The glacier systems (Talkeetna and Susitna) respond to temperatures changes at an annual time scale (Figure 3.5, Table 3.2). Maximum streamflow declines were related to increase temperatures in the AMJ period in both the Talkeetna and the Susitna river basins. Flow

responses were primarily negative for the June, July and August months (Table 3.2), with shifts towards earlier snowmelt observed (Figure 3.3). Although volumetric accounting of glacier contributions to streamflow was not considered explicitly in this study, research by Arendt et al. (2002) on sixty seven glaciers in Alaska noted thinning and volume reductions between the 1950s and the 1990s, with the rate of change observed to be increasing since the 1990s. Thus, higher temperatures during the AMJ season are indicative of reduced snow packs, faster runoff, shifts in streamflow timing, and hence lower flows (Liston and Hiemstra, 2011; Stewart et al., 2005). On the other hand, no relationship was found between climate variability indices in these basins, indicating that maximum streamflows are not responding in the same manner as purely snowmelt dominated basins (Fleming et al. 2006). The Talkeetna River basin appears to be more sensitive than the Susitna, exhibiting primarily linear nonstationary responses to changes in temperatures noted for Alaska over the 1964-2013 period. The Talkeetna's response could be attributable to the percentage of glaciers located at high elevation compared to the Susitna which has a greater amount of its glaciers below the ablation line (Figure 3.7). Further research is required on these systems to determine the exact reason for the differences in response between these two adjacent basins.

Streamflow changes in snow dominated systems were the most detectable using trends analysis and GEV, responding to time and climate variability shifts (Table 3.2, Figure 3.6). The Salcha and Chena systems are both experiencing streamflow declines that can be related to changing spring streamflow associated with a loss of snowpack. The Chena responds to increased winter precipitation, higher flows occur with higher snowpacks - a clear result for a snowmelt dominated basin. However, the Salcha system with a much higher percentage of its basin at a higher elevation, is temperature modulated (Figure 3.9). Shifts in the Salcha AMJ streamflow peak have a nonlinearity, although the mechanism for this nonlinearity is unclear it does not seem to be directly traceable to the PDO (Figure 3.9). Both systems appear to be affected by PDO, with lower maximum streamflows associated with positive PDO. May and June streamflow was found to be lower on the Salcha River during warm PDO streamflow versus cold PDO (Table 3 in Brabets and Walvoord, 2009).

The Tanana does not experience detectable shifts in AMJ streamflow over the 1964-2013 period, nor does it response to climate variability but does respond in spring to winter precipitation. It should be noted that this response is not occurring at peak flow for the system (Figure 3.2). This is not unexpected given the Tanana's variable headwater influences, including high elevation mountain snowpacks and glaciers. Additionally, the Tanana basin has a combined total of 83% of its basin underlain by discontinuous or continuous permafrost, further complicating streamflow patterns. The Kuskokwim River has a much smaller percentage of glacier and a smaller fraction of discontinuous/continuous permafrost. This basin responds in a similar manner to the snowmelt dominated systems, with a detectable trend of lower spring streamflow maximums during the positive PDO (Figure 3.8).

Winter baseflow increases noted in this work have been related to thawing permafrost in the Northwest Territories of Canada (St. Jacques and Sauchyn, 2009) and in the Yukon River basin of Alaska and Canada (Walvoord and Striegl, 2007). Most of the eight watersheds, and in particular the Yukon, are experiencing higher October, November or December maximum flows and higher minimum flows in October or March (Table 3.2). Baseflow increases are hypothesized to be occurring in conjunction with climate change (Hinzman et al., 2005). Extensive/continuous permafrost dominated soils do not thaw until late summer and hence any snowmelt and precipitation runoff occurring during this time is delivered to the river systems as runoff. As temperatures warm, the active layer depths deepen and permafrost degrades, hence the land surface can act more as a storage reserve for runoff. The water will eventually work its way through the system and exit this groundwater storage in the fall or winter time as baseflow. Water storage in the active layer increases through summer, as noted by Bolton et al. (2000) for the Caribou Poker Creek watershed, but reaches a threshold when overland flow occurs off of the saturated active layer and into rivers as runoff. However, streamflow may also be responding to increased summer/fall precipitation inputs, supported by research documenting that summer precipitation exceeds evapotranspiration in recent years at these sites (Carey and Woo, 1999; Jones and Rinehart, 2010). Generally, this region of the world is thought to be dominated by positive net precipitation (Serreze et al., 2006).

The Nuyakuk River basin examined in this work is clearly a unique system and is operating often in an opposite direction to either the glacial systems or the snowmelt dominated streamflow regimes. The peak flow at this site is increasing in fall, and minimum flow magnitudes show an annual increase. The lake is drained by the Aklun Mountains that receive influences from the Bering Sea and the Gulf of Alaska that may be leading to increased snowpacks. However, the modulating effect of the lake confounds signals and more in-depth research of the patterns of change occurring at this site is needed, particularly in regards to its response to the Arctic Oscillation.

The Yukon River trends responded only to increased temperatures during the snowmelt season, similar to those of the glacially dominated Susitna and Talkeetna basins (Figure 3.9). Annual or spring streamflow changes were not observed to be occurring over time, or in response to climate variability and trends are not significant during either period. This watershed exhibits a plethora of landscape types, including glacier, high elevation snowpacks, and permafrost substrates, all of which could be changing but in opposite directions. However, if the basin's primary driver is temperature, the indication is that future increases in temperature within the region may eventually lead to lower streamflow that could outweigh the increases in either winter baseflow conditions, deepening active layers or alterations in summer or fall precipitation inputs. On the other hand, for the Tanana system, where winter precipitation inputs are a primary driver of spring streamflow, we could see a response to declining snowpacks at lower

elevations that may outweigh changes in permafrost and active layer shifts. However, changes in snowpacks at the high elevation aspects of the Tanana would also need to be considered.

3.5 Conclusions

Trends and nonstationary GEV analyses were applied to examine changes in maximum and minimum streamflow over a 50-60 year time period for eight Interior and Western Alaskan watersheds located in the discontinuous and continuous boreal permafrost zone. The observed trends indicate that regime shifts are occurring in Alaskan Interior snowmelt dominated systems that are indicative of nonstationary linear responses to climate variability and climate change. Glacial systems appear to have passed the stage of flow increases and are declining. For some systems, changes are non-significant or opposite in nature and therefore offset any detectable shifts in the system, as evidenced in the Yukon River basin.

Trends analysis indicated that streamflow is changing, as follows:

- Annually, maximum streamflow is decreasing, while minimum flows are increasing.
- Direction of changes is not always apparent when considering the seasonal or annual flows. In order to determine how streamflow systems are changing, a mixture of techniques is required to detect processes, differentiate changes and link to broader phenomena such as climate variability.
- Shifts in streamflow occur in different time periods depending on the physical processes that are changing. The Talkeetna river watershed has a delayed response in its flow changes associated with its high elevation snow and glacier complexes and results in a magnitude change in flow trend that is not comparable to an adjacent site (Susitna).
- Maximum streamflow is increasing in nival-dominated streamflow systems such as the Chena and Salcha River basins in spring indicative of a shift in snowmelt freshet; these systems have an associated decline in May flows that is indicative of a transfer of the pulse of flow from May to April. These systems are responding to changes in PDO, which could be included in modeling efforts or streamflow forecasting for ungaged Interior Alaskan snowmelt dominated systems.
- The Salcha River has a larger percentage of its basin at a high elevation, and hence it is more responsive to temperature shifts in the spring snowmelt season, with a nonlinear change associated with warming temperatures.
- Streamflow is declining in spring, summer and annually in glacial systems and this change results in reduced streamflow associated with warming temperatures and climate change accelerated melt.
- Large basins with developed rocky upland zones, mixed nival/glacier/pluvial regimes and where groundwater contributions could be changing, such as the Yukon, do not respond to climate variability, or climate change directly.

- Increasing winter baseflow is observed across many systems. These changes are reflected in minimum flow results as well but are more strong and significant in the maximum streamflow trends. These changes have been noted by other researchers but represent a small proportion of the overall streamflow volumes. This results in non-detectable annual change in the hydrology of systems such as the Yukon.
- Maximum streamflow responses were clearly linked to changes in climate, such as temperature or precipitation increases/decreases. This has implications for future climate change with regards to how (strongly) these systems may respond to shifts in either temperature or precipitation.
- The Tanana and Kuskokwim systems have the same response to climate drivers and climate variability (Kuskokwim only) to snowmelt dominated watersheds while the Yukon responds similarly to glacial basins.
- The Nuyakuk River, which drains a number of large lake complexes, has a very different hydrology compared to other sites, and requires more in-depth study.

3.5.1 Implications

Changes in extremes influence systems to a greater extent than mean change (Katz and Brown 1992). Extreme value theory offers an analytical means to present and understand changes that are occurring in response to nonstationary forcings (i.e. climate variability) and in non-linear manners. Not only is this important from a research standpoint, but it is also fundamental information for operational and resource management perspectives within governmental agencies and the Alaskan public, who rely on the development of frequency analysis of return levels to demarcate floods of major and minor impact (Ed Plumb, NWS, pers. comm.).

The results of this work demonstrate that analysis of peak flows within a regime-based framework can identify particular processes that are impacted by climate change or variability. Likewise, directional changes are not likely to be consistent across regions – rather they are more likely to be consistent between regimes. Complicated systems such as the Yukon may be experiencing multiple effects that cascade down the system and can result in opposing changes in the system – changes that could very well cancel out in terms of streamflow volume or timing changes. Systems must be examined very carefully and in a fashion that enables a clear separation of regimes operating across expansive basins of the north. However, there are identifiable limits of extrapolation of results from trends analysis, such as identifying the nature of processes such as permafrost degradation versus increased fall precipitation. For this research, a more fine scale, physical model of the basins is required.

3.6 Acknowledgements

The work conducted for this research project supported by Grant/Cooperative Agreement Number GIOAC00588 from the United States Geological Survey's Alaska Climate Science Center and the National Science and Engineering Council of Canada. Its contents are solely the responsibility of the authors and do not necessarily represent the official views of the USGS. This paper benefited greatly from the review of Markus Schnorbus at the Pacific Climate Impacts Consortium. The authors thank the Arctic Region Supercomputer Center for the use of their supercomputer PACMAN.

3.7 Figures

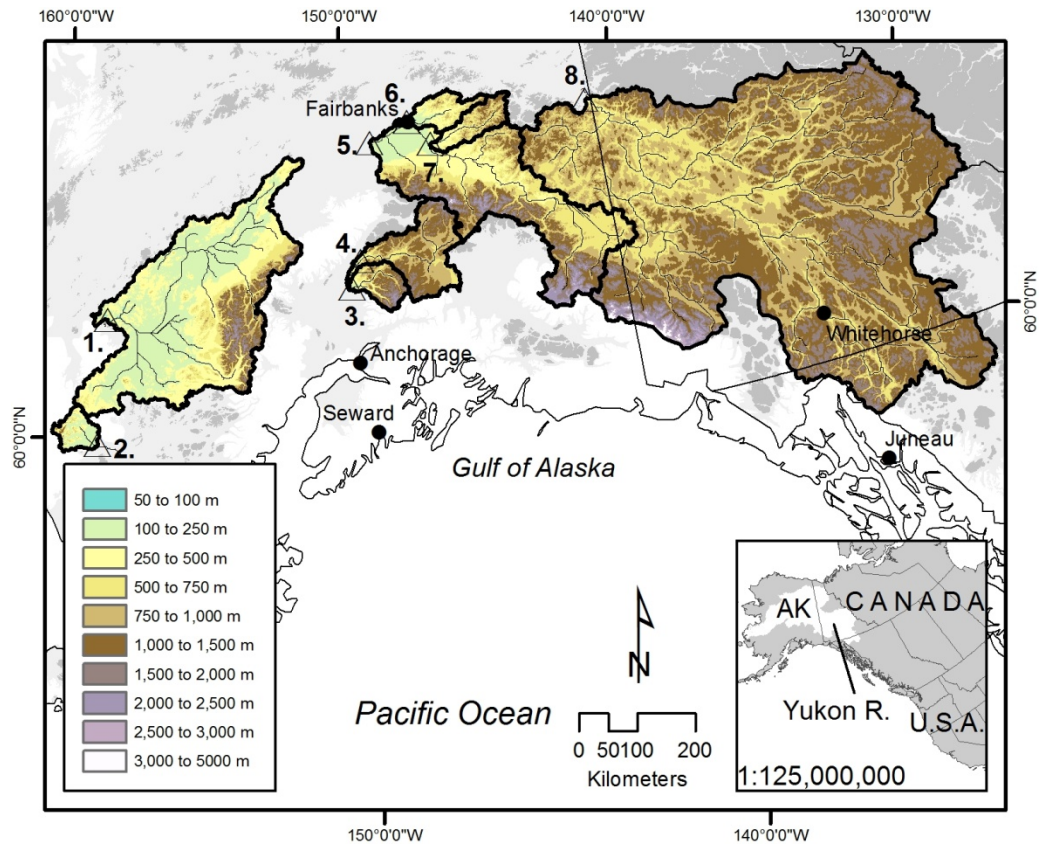


Figure 3.1. Stations analyzed in the study. Basins are identified by numbers at gages (open triangles), index provided in Table 3.1. The inset shows the basin set in the context of North America.

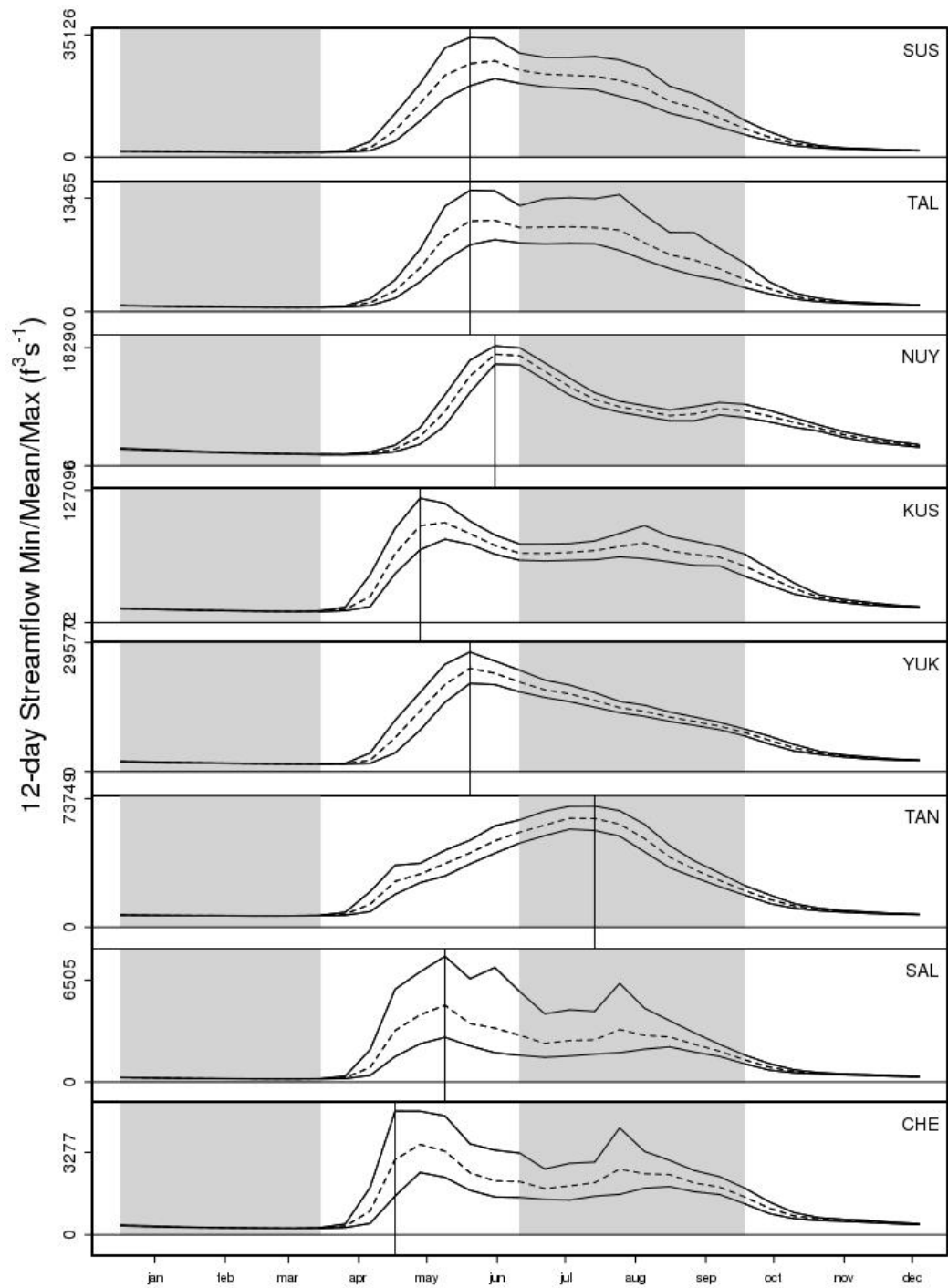


Figure 3.2 Streamflow hydrographs shown for 11-day composites for all eight stations, mean (dashed), maximum and minimum line are shown, with a horizontal line indicated the day of maximum flow. Seasons are greyed (JFM, JAS grey, AMJ and OND white) to illustrate the data ranges, and months of the year (representing the mid-month date) are on the x-axis. Abbreviations for basins are found in Table 3.1.

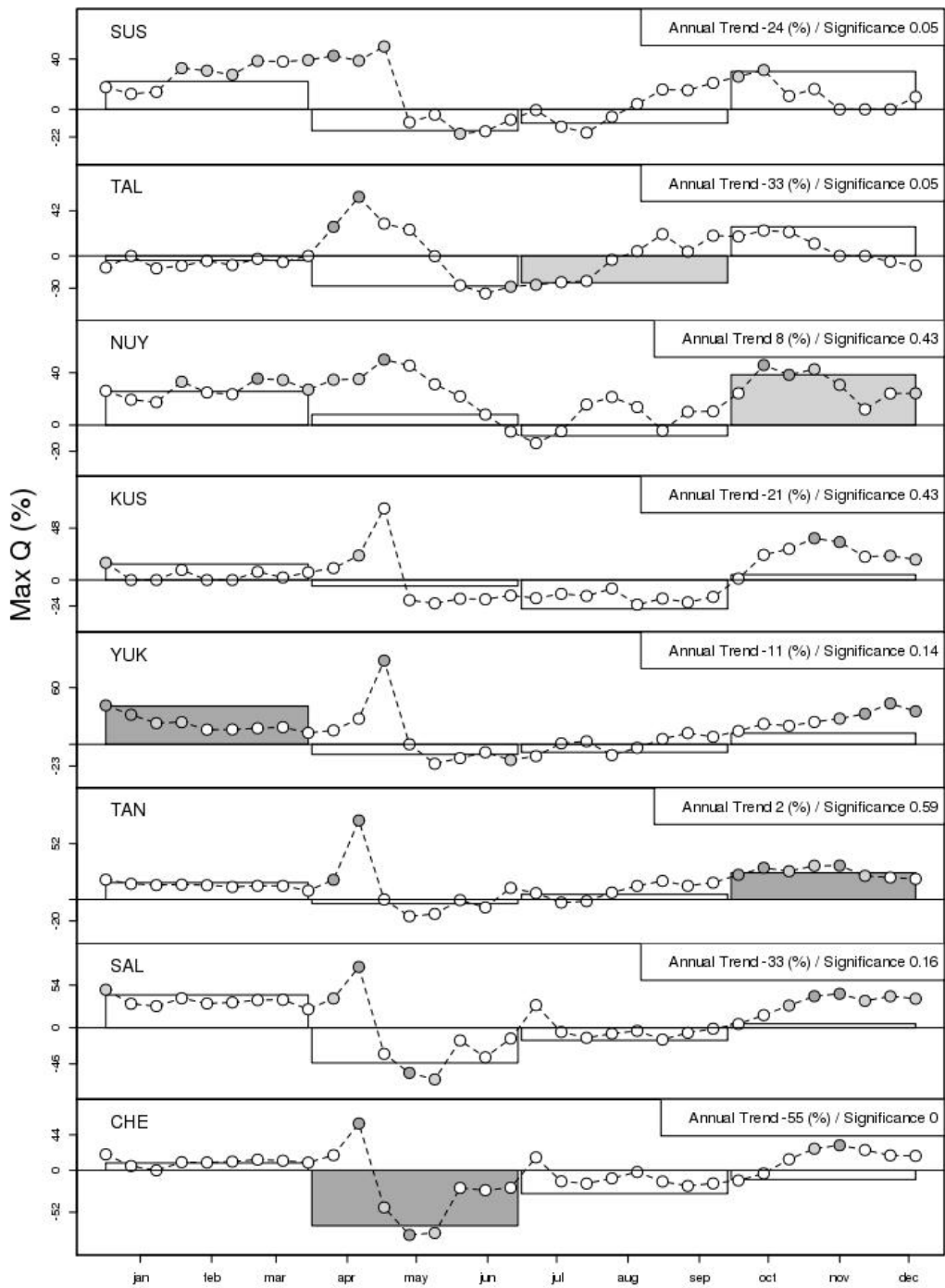


Figure 3.3 Maximum streamflow trends (%) for the period of record for all eight stations. Trends for 11-days are shown in circles, seasonal results are in boxes and annual trend is given in the upper right box. Statistical significance is shown as follows, dark grey is 99th confidence interval, light grey is the 95th confidence interval, and non-significant results are white. The y-axis indicates the trend magnitude, while the x-axis illustrates the months of the year (representing the mid-month date). Abbreviations for basins are found in Table 3.1.

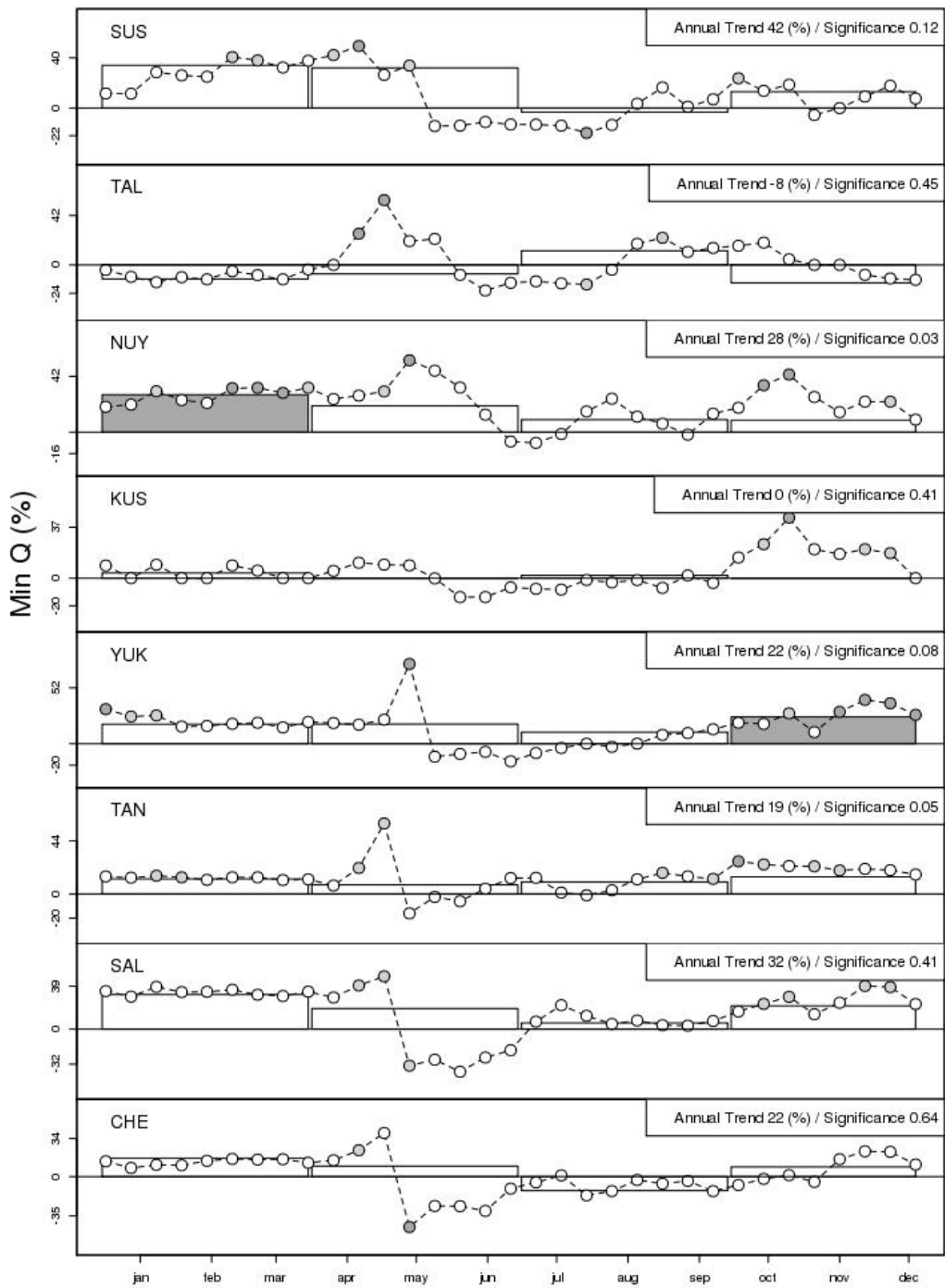


Figure 3.4 Minimum streamflow trends (%) for the period of record for all eight stations. Trends for 11-days are shown in circles, seasonal results are in boxes and annual trend is given in the upper right box. Statistical significance is shown as follows, dark grey is 99th confidence interval, light grey is the 95th confidence interval, and non-significant results are white. The y-axis indicates the trend magnitude, while the x-axis illustrates the months of the year (representing the mid-month date). Abbreviations for basins are found in Table 3.1.

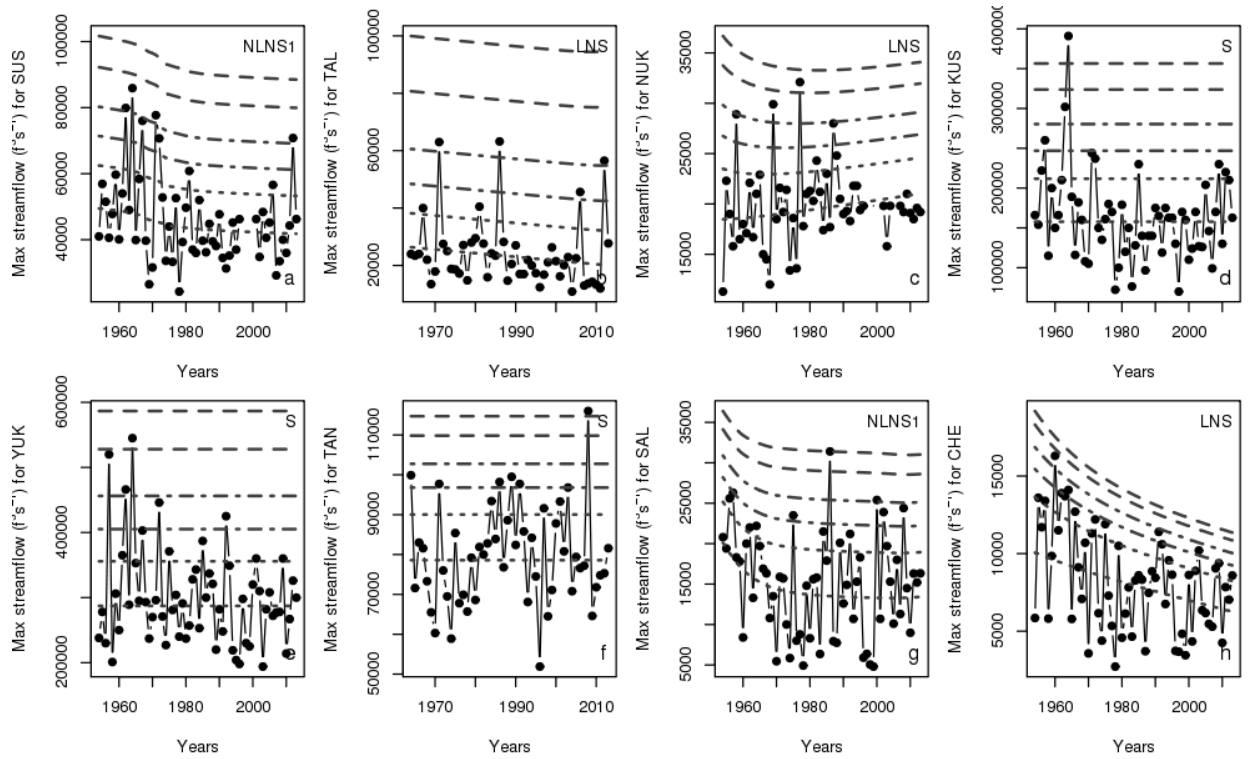


Figure 3.5 GEV results for maximum streamflow for the annual time period for the eight basins examined in this study. Black circles and lines illustrate the streamflow maximums for the season. Dashed lines show 2, 5, 10, 20, 50 and 100 year return intervals, based on the GEV fits. Time interval (x-axis) is relative to length of record.

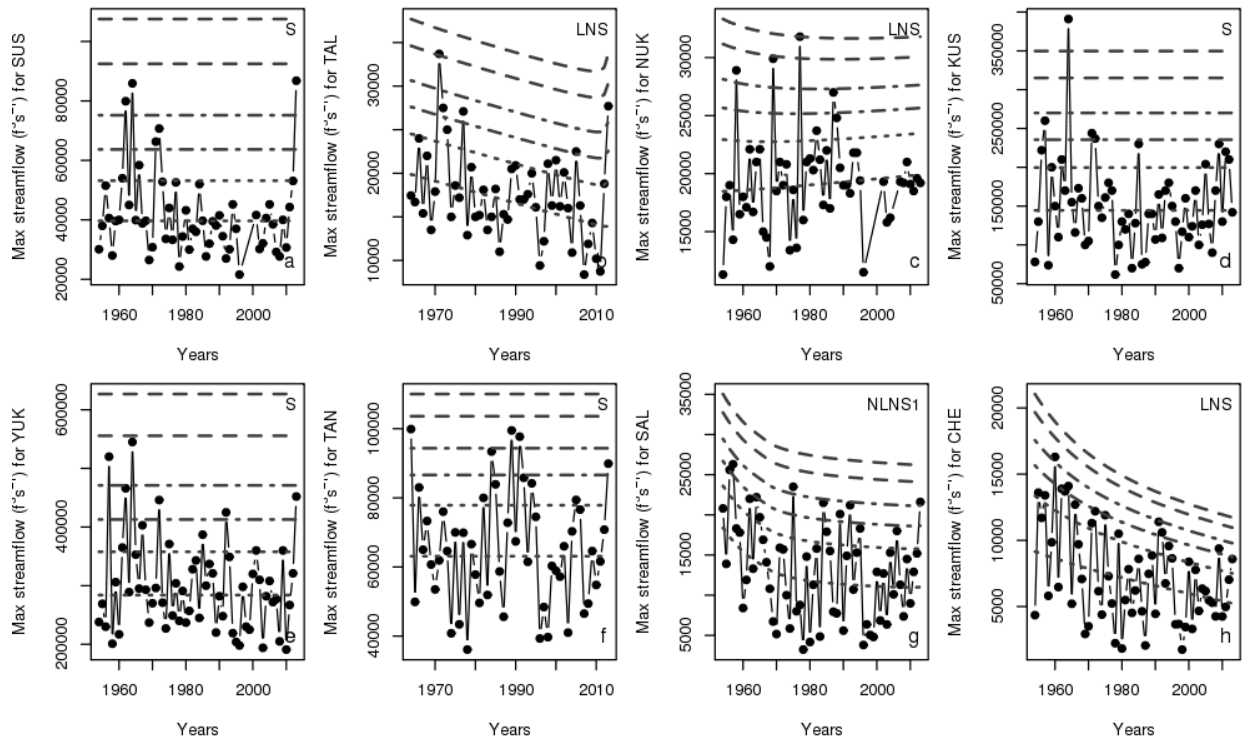


Figure 3.6 GEV results for maximum streamflow in AMJ for the eight basins examined in this study. Black circles and lines illustrate the streamflow maximums for the season. Dashed lines show 2, 5, 10, 20, 50 and 100 year return intervals, based on the GEV fits. Time interval (x-axis) is relative to length of record.

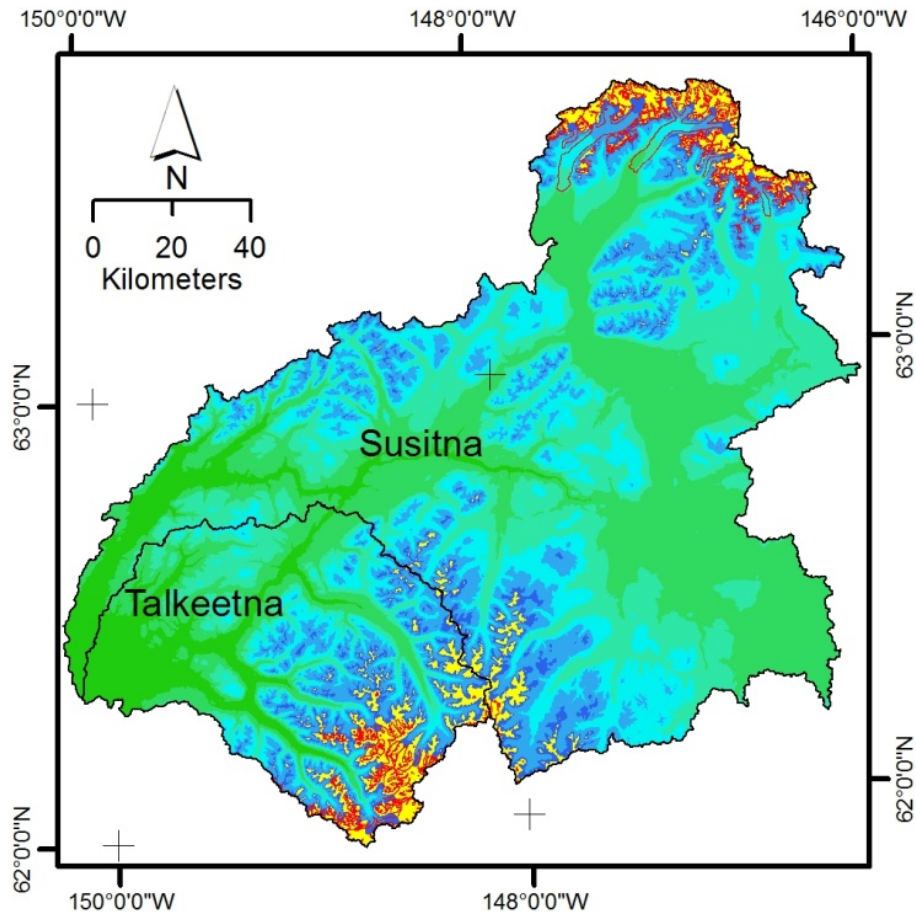


Figure 3.7 Susitna and Talkeetna river basins elevation ranges. Mapping based on the National Elevation Data (NED) are shown from green to light blue to dark blue. Regions above the average ablation line (1781 m) are shown in yellow. Glaciers are clipped to the watershed boundaries (Arendt et al. 2012) and illustrated with red outlines.

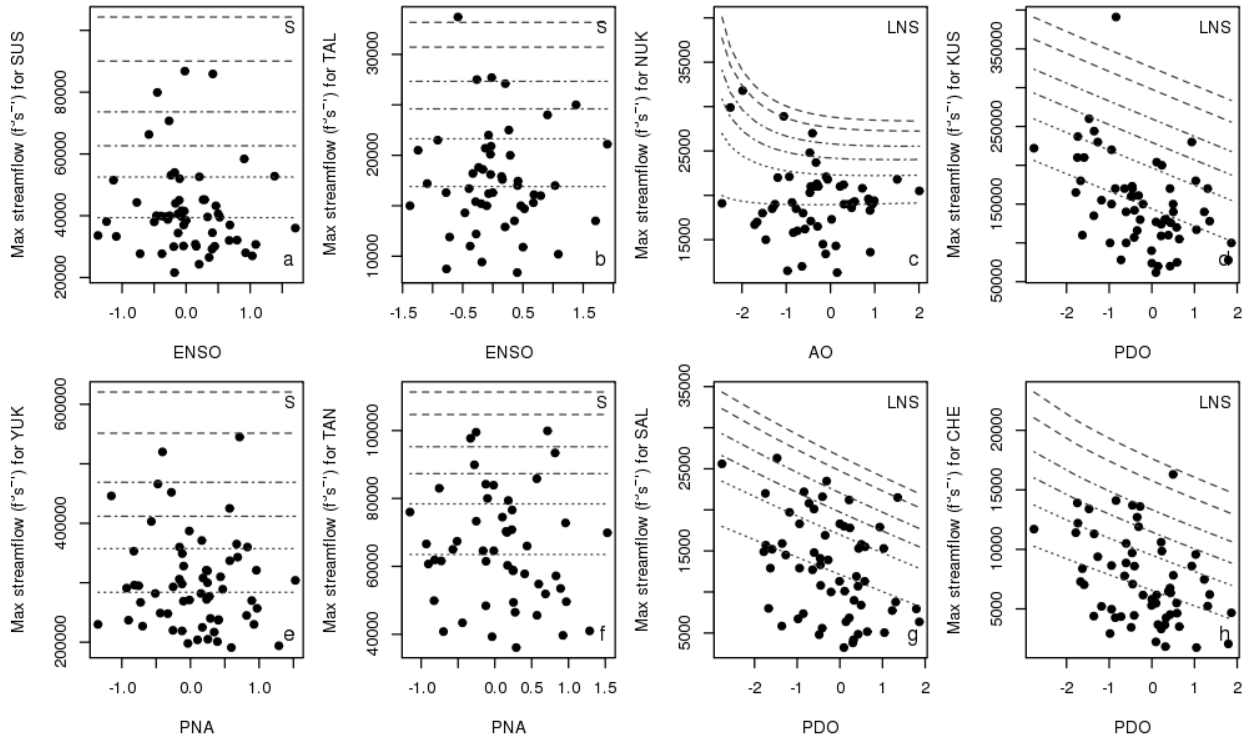


Figure 3.8 GEV climate variability results for maximum streamflow for AMJ. Black circles and lines illustrate the streamflow maximums for the season. Stationary results indicate no trend; and minimized climate variability indices are not meaningful. Dashed lines show 5, 20 and 100 year return intervals, based on the GEV fits. The x-axis shows the selected GEV index, as described in the text.

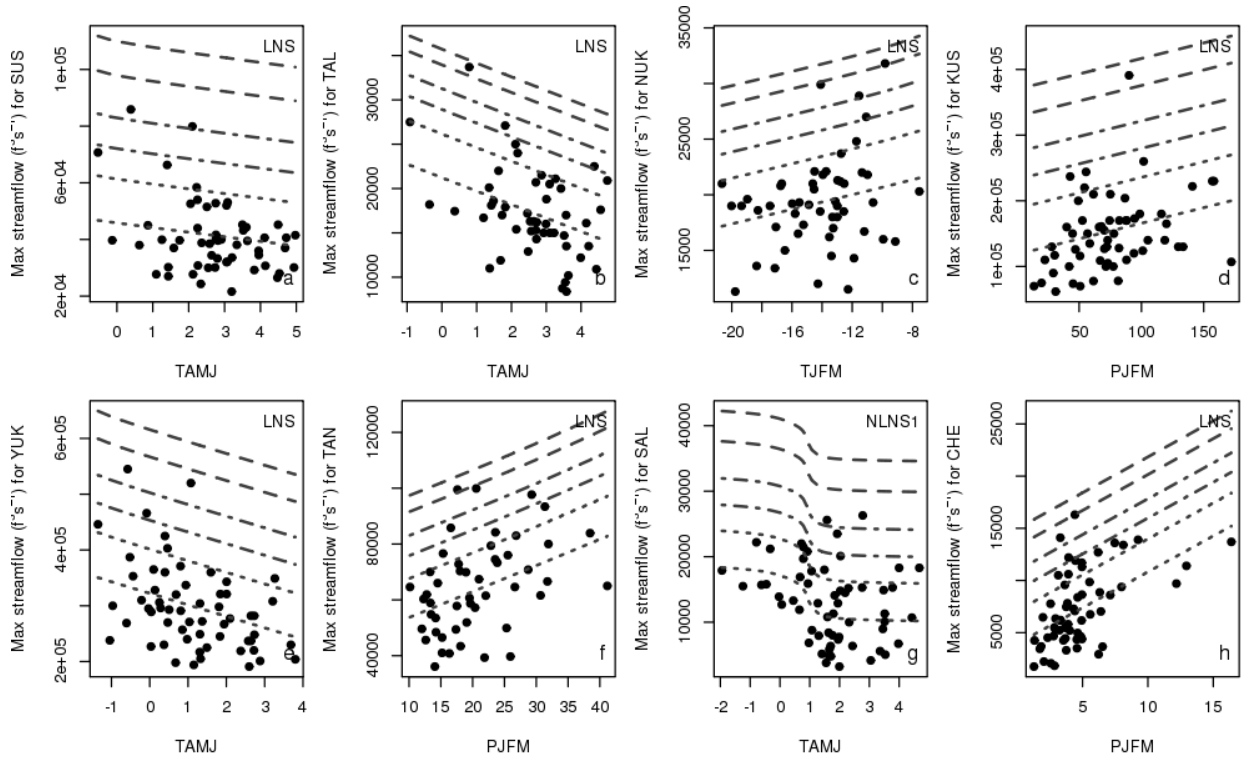


Figure 3.9 GEV results for maximum streamflow in MAM, temperature or precipitation covariates for the eight basins examined in this study. Black circles and lines illustrate the streamflow maximums for the season. Dashed lines show 2, 5, 10, 20, 50 and 100 year return intervals, based on the GEV fits. Temperature or precipitation (x-axis) is relative to values in record.

3.8 Tables

Table 3.1 Table of station information. Site/station names, station number, drainage basin size, elevation, length of record, and geographic setting/climatic setting. Permafrost results are provided for continuous, discontinuous, sporadic and isolated, respectively.

Site/Station Name	Station Number	Station Code (Map Number)	Basin Size (km ²)	Elevation at Gage (Mean) (m)	Time Period
Susitna R at Gold Creek	15292000	SUS (4)	16,350	676	1949-2012
Talkeetna R near Talkeetna	15292700	TAL (3)	5,270	400	1964-2012
Nuyakuk R near Dillingham	15302000	NUY (2)	3,910	325	1953-2012
Kuskokwim R at Crooked Creek	15304000	KUS (1)	81,415	150	1951-2012
Yukon R at Eagle	15356000	YUK (8)	287,690	850	1950-2012
Tanana R at Nenana	15515500	TAN (5)	66,205	338	1962-2012
Salcha R near Salchaket	15484000	SAL (7)	5,740	631	1948-2012
Chena R at Fairbanks	15514000	CHE (6)	5,350	422	1947-2012
	Snow + Ice (%)	Glaciers ⁺ (%)	Deciduous (%)	Coniferous (%)	Permafrost (%)
Susitna R at Gold Creek	4	4	1	16	69, 19, 4, 3
Talkeetna R near Talkeetna	14	5	5	6	68, 0, 24, 2
Nuyakuk R near Dillingham	5	1	1	7	2, 0, 45, 1
Kuskokwim R at Crooked Creek	1	1	4	33	46, 0, 29, 23
Yukon R at Eagle	5	2	1	64	73, 11, 15, 2
Tanana R at Nenana	10	5	11	39	67, 15, 5, 4
Salcha R near Salchaket	0	0	14	45	88, 12, 0, 0
Chena R at Fairbanks	0	0	22	47	97, 2, 0, 0

*interpolated from NED

⁺calculated based on Arendt et al. (2012)

Table 3.2 Monthly, seasonal and annual trends results for the period of records (1954/1964 -2013) for maximum and minimum flow statistics as a percent difference from the normal. Bolded, bracketed values illustrate statistically significant results > 90th percentile confidence interval.

Code	Jan (%)	Feb (%)	Mar (%)	Apr (%)	May (%)	Jun (%)	Jul (%)	Aug (%)	Sep (%)	Oct (%)	Nov (%)	Dec (%)	JFM (%)	AMJ (%)	JAS (%)	OND (%)	YR (%)
Maximum Streamflow																	
SUS	20 (0.32)	33 (0.03)	44 (0.01)	97 (0)	2 (0.81)	-12 (0.35)	-16 (0.05)	-10 (0.28)	11 (0.7)	29 (0.06)	25 (0.06)	12 (0.34)	22 (0.14)	-17 (0.34)	-11 (0.23)	30 (0.09)	-24 (0.05)
TAL	-7 (0.25)	-9 (0.27)	0 (0.62)	58 (0)	21 (0.16)	-41 (0.05)	-36 (0.1)	-19 (0.07)	6 (0.87)	27 (0.09)	14 (0.24)	0 (0.82)	-4 (0.32)	-28 (0.06)	-25 (0.03)	27 (0.09)	-33 (0.05)
NUY	27 (0.06)	34 (0.04)	38 (0.01)	58 (0.01)	36 (0.15)	8 (0.42)	-7 (0.28)	20 (0.24)	14 (0.55)	40 (0.02)	46 (0)	30 (0.03)	26 (0.11)	8 (0.39)	-8 (0.33)	38 (0.01)	8 (0.43)
KUS	16 (0.04)	10 (0.11)	14 (0.05)	49 (0)	13 (0.68)	-21 (0.22)	-16 (0.09)	-31 (0.04)	-29 (0.32)	12 (0.41)	53 (0)	32 (0)	15 (0.06)	-6 (0.5)	-27 (0.11)	5 (0.67)	-21 (0.43)
YKE	41 (0)	25 (0.02)	21 (0.1)	52 (0.38)	5 (0.89)	-13 (0.17)	-10 (0.29)	-3 (0.56)	7 (0.6)	14 (0.25)	38 (0.02)	46 (0)	40 (0)	-11 (0.2)	-8 (0.4)	12 (0.41)	-11 (0.14)
TAN	18 (0.04)	14 (0.14)	14 (0.12)	72 (0)	0 (0.76)	-4 (0.78)	2 (0.59)	6 (1)	26 (0)	22 (0.01)	33 (0.03)	22 (0.18)	16 (0.19)	-4 (0.82)	5 (0.58)	25 (0.01)	2 (0.59)
SAL	44 (0.04)	38 (0.11)	42 (0.23)	105 (0)	-59 (0.02)	-14 (0.91)	10 (0.97)	-21 (0.17)	-18 (0.69)	5 (0.74)	42 (0)	46 (0.01)	42 (0.05)	-45 (0.09)	-16 (0.37)	5 (0.74)	-33 (0.16)
CHE	15 (0.64)	10 (0.81)	11 (0.72)	71 (0.01)	-75 (0)	-13 (0.77)	0 (0.86)	-18 (0.2)	-30 (0.28)	-11 (0.58)	30 (0.05)	25 (0.08)	9 (0.92)	-69 (0)	-29 (0.05)	-11 (0.58)	-55 (0)
Minimum Streamflow																	
SUS	14 (0.38)	23 (0.16)	33 (0.08)	32 (0.06)	28 (0.17)	-9 (0.49)	-12 (0.14)	-3 (0.77)	-3 (0.69)	4 (0.62)	0 (0.99)	14 (0.29)	34 (0.08)	32 (0.06)	-3 (0.69)	13 (0.33)	42 (0.12)
TAL	-14 (0.17)	-11 (0.38)	-12 (0.33)	-8 (0.62)	58 (0.01)	-7 (0.98)	-14 (0.21)	10 (0.4)	12 (0.31)	0 (0.48)	-3 (0.79)	-15 (0.39)	-12 (0.33)	-8 (0.62)	12 (0.32)	-15 (0.36)	-8 (0.45)
NUY	14 (0.37)	20 (0.13)	28 (0)	20 (0.12)	31 (0.05)	27 (0.36)	3 (0.8)	14 (0.38)	1 (0.83)	21 (0.25)	10 (0.49)	9 (0.25)	28 (0)	20 (0.12)	9 (0.91)	9 (0.29)	28 (0.03)
KUS	0 (0.93)	0 (0.66)	0 (0.45)	0 (0.98)	8 (0.58)	-6 (0.43)	-8 (0.26)	-6 (0.5)	-5 (0.98)	23 (0.1)	14 (0.16)	0 (0.29)	4 (0.35)	0 (0.98)	2 (0.91)	0 (0.29)	0 (0.41)
YKE	21 (0.05)	13 (0.29)	16 (0.14)	17 (0.15)	20 (0.57)	-11 (0.31)	-2 (0.63)	0 (0.79)	11 (0.28)	23 (0.07)	25 (0.02)	27 (0.01)	18 (0.15)	18 (0.14)	11 (0.28)	25 (0.01)	22 (0.08)
TAN	11 (0.21)	13 (0.06)	12 (0.33)	8 (0.35)	62 (0.01)	-3 (0.87)	7 (0.34)	14 (0.13)	10 (0.1)	25 (0.03)	14 (0.21)	16 (0.12)	12 (0.11)	8 (0.35)	10 (0.1)	14 (0.27)	19 (0.05)
SAL	26 (0.28)	30 (0.4)	30 (0.47)	19 (0.63)	46 (0.03)	-35 (0.09)	8 (0.73)	-3 (0.7)	7 (0.52)	19 (0.11)	11 (0.64)	23 (0.23)	32 (0.38)	19 (0.63)	6 (0.84)	21 (0.27)	32 (0.41)
CHE	5 (0.88)	14 (0.64)	12 (0.64)	9 (0.71)	41 (0.06)	-37 (0.08)	-6 (0.4)	-15 (0.35)	-2 (0.98)	-4 (0.86)	-1 (0.96)	15 (0.24)	16 (0.51)	9 (0.71)	-12 (0.3)	9 (0.41)	22 (0.64)

3.9 References

- ACIA, 2005. Chapter 6: Cryosphere and Hydrology. In: Walsh, J.E. (Ed.), *The Arctic Climate Impact Assessment*. Cambridge University Press, pp. 1042.
- Alaska Energy Authority, 2014. *Susitna-Watana Hydroelectric Project (FERC No. 14241). Initial Study Report Overview*. pp. 24.
- Arendt, A.A., Echelmeyer, K.A., Harrison, W.D., Lingle, C.S., Valentine, V.B., 2002. Rapid wastage of Alaska glaciers and their contribution to rising sea level. *Science*, 297 (5580): 382-386.
- Arendt, A. et al., 2012. *Randolph Glacier Inventory [v1. 0]: A dataset of global glacier outlines*. Global Land Ice Measurements from Space, Boulder Colorado, USA. Digital Media.
- Bitz, C.M., Battisti, D.S., 1999. Interannual to decadal variability in climate and the glacier mass balance in Washington, Western Canada, and Alaska. *J. Clim.*, 12 (11): 3181-3196.
- Bolton, W.R., Hinzman, L.D., Yoshikawa, K., 2000. Stream flow studies in a watershed underlain by discontinuous permafrost. In: Kane, D.L. (Ed.), *Water Resources in Extreme Environments*. Am. Water Resour. Assoc., Middleburg, VA., pp. 31–36.
- Bond, N., Harrison, D., 2006. ENSO's effect on Alaska during opposite phases of the Arctic Oscillation. *Int. J. Climatol.*, 26(13): 1821-1841.
- Bone, C., Alessa, L., Kliskey, A., Altaweel, M., 2010. Influence of statistical methods and reference dates on describing temperature change in Alaska. *Journal of Geophysical Research: Atmospheres* (1984–2012), 115(D19).
- Brabets, T.P., Walvoord, M.A., 2009. Trends in streamflow in the Yukon River Basin from 1944 to 2005 and the influence of the Pacific Decadal Oscillation. *Journal of Hydrology*, 371(1): 108-119.
- Brabets, T.P., Wang, B., Meade, R.H., 2000. *Environmental and hydrologic overview of the Yukon River Basin, Alaska and Canada*. US Department of the Interior, US Geological Survey.
- Bronaugh, D., Werner, A., 2009. Package 'zyp'. CRAN Repository.
- Brown, R.D., 2010. Northern Hemisphere snow cover variability and change, 1915–97. *J. Clim.*, 13: 2339–2355.
- Burnham, K.P., Anderson, D.R., Huyvaert, K.P., 2011. AIC model selection and multimodel inference in behavioral ecology: some background, observations, and comparisons. *Behav. Ecol. Sociobiol.*, 65(1): 23-35.
- Cannon, A.J., 2010. A flexible nonlinear modelling framework for nonstationary generalized extreme value analysis in hydroclimatology. *Hydrol. Process.*, 24(6): 673-685.

- Cannon, A.J., 2011. GEVcdn: An R package for nonstationary extreme value analysis by generalized extreme value conditional density estimation network. *Computers & Geosciences*, 37(9): 1532-1533.
- Cannon, A.J., 2012. Neural networks for probabilistic environmental prediction: Conditional Density Estimation Network Creation and Evaluation (CaDENCE) in R. *Computers & Geosciences*, 41: 126-135.
- Carey, S.K., Woo, M.K., 1999. Hydrology of two slopes in subarctic Yukon, Canada. *Hydrol. Process.*, 13(16): 2549 - 2562.
- Clarke, T., Johnson, D., Harrison, W.D., 1985. Glacier Mass Balances and Runoff in the Upper Susitna and MacLaren River Basins, 1981 – 1983. Final Report. Available at: <http://www.arlis.org/docs/vol2/hydropower/SUS528.pdf>.
- Coles, S., 2001. An introduction to statistical modeling of extreme values. Springer Verlag, London, UK, 209 pp.
- Coles, S.G., Dixon, M.J., 1999. Likelihood-based inference for extreme value models. *Extremes*, 2(1): 5-23.
- CPC, Accessed Sep 2013. Pacific North American Pattern. <http://www.cpc.ncep.noaa.gov/products/precip/CWlink/pna/pna.shtml>.
- CPC, Accessed Sep 2014. Arctic Oscillation. http://www.cpc.ncep.noaa.gov/products/precip/CWlink/daily_ao_index/monthly.ao.index.b50.current.ascii.table.
- Déry, S.J., Hernández-Henríquez, M.A., Burford, J.E., Wood, E.F., 2009. Observational evidence of an intensifying hydrological cycle in northern Canada. *Geophys. Res. Lett.*, 36(13): L13402.
- Déry, S.J., Stieglitz, M., McKenna, E.C., Wood, E.F., 2005. Characteristics and trends of river discharge into Hudson, James, and Ungava Bays, 1964-2000. *J. Clim.*, 18(14): 2540-2557.
- Déry, S.J., Wood, E., 2005. Decreasing river discharge in northern Canada. *Geophys. Res. Lett.*, 32: L10401.
- Déry, S.J., Wood, E.F., 2004. Teleconnection between the Arctic Oscillation and Hudson Bay river discharge. *Geophys. Res. Lett.*, 31 (18): L18205.
- Ecology and Environment, 2012. Aurora Energy Coal Power Plant Preliminary Assessment, Fairbanks, AK. TDD: 11-06-0004, United States Environmental Protection Agency, Seattle. pp. 30.
- El Adlouni, S., Ouarda, T.B.M.J., Zhang, X., Roy, R., Bobée, B. 2007. Generalized maximum likelihood estimators of the non-stationary GEV model parameters, *Water Resour. Res.*, 43, W03410. doi:10.1029/2005WR004545.

- EPA, 2002. Fact Sheet for Wastewater Discharge Permit to Aurora Energy Chena Power Plant. AK-0053333-3, U.S. Environmental Protection Agency, Seattle. pp 20.
- ESRL NOAA, Accessed Sep 2014. East Central Tropical Pacific SST. Accessed September 2014. <http://www.esrl.noaa.gov/psd/data/correlation/nina34.data>.
- Fleming, S., Moore, R.D., Clarke, G.K.C., 2006. Glacier-mediated streamflow teleconnections to the Arctic Oscillation. *Int. J. Climatol.*, 26: 619–636.
- Forbes, A.C., Lamoureux, S.F., 2005. Climatic controls on streamflow and suspended sediment transport in three large Middle Arctic catchments, Boothia Peninsula, Nunavut, Canada. *Arct. Antarct. Alp. Res.*, 37(3): 304-315.
- Gneiting, T., Balabdaoui, F., Raftery, A.E., 2007. Probabilistic forecasts, calibration and sharpness. *J. Roy. Stat. Soc. Ser. B. (Stat. Method.)*, 69(2): 243-268.
- Harris, I., Jones, P., Osborn, T., Lister, D., 2014. Updated high-resolution grids of monthly climatic observations—the CRU TS3. 10 Dataset. *Int. J. Climatol.*, 34(3): 623-642.
- Hartmann, B., Wendler, G., 2005. The significance of the 1976 Pacific climate shift in the climatology of Alaska. *J. Clim.*, 18(22): 4824-4839.
- Helsel, D.R., Hirsch, R.M., 2002. *Statistical methods in water resources*, 323. US Geological survey Reston, VA.
- Hinzman, L.D., Bettez, N.D., Bolton, W.R., Chapin, F.S., Dyurgerov, M.B., Fastie, C.L., Griffith, B., Hollister, R.D., Hope, A., Hutton, H.P., Jensen, A.M., Jia, G.J., Jorgenson, T., Kane, D.L., Klein, D.R., Kofinas, G., Lynch, A.H., Lloyd, A.H., McGuire, A.D., Nelson, F.E., Oechel, W.C., Osterkamp, T.E., Racine, C.H., Romanovsky, V.E., Stone, R.S., Stow, D.A., Sturm, M.D., Walker, D.A., Webber, P.J., Welker, J.M., Winker, K.S., Yoshikawa, K., 2005. Evidence and implications of recent climate change in northern Alaska and other Arctic regions. *Clim. Change*, 72: 251-298.
- Hodgkins, G.A., 2009. Streamflow changes in Alaska between the cool phase (1947–1976) and the warm phase (1977–2006) of the Pacific Decadal Oscillation: The influence of glaciers. *Water Resour. Res.*, 45(6): W06502.
- Janowicz, J.R., 2011. Streamflow responses and trends between permafrost and glacierized regimes in northwestern Canada, International Union of Geodesy and Geophysics (IUGG): Symposium H02, Cold Region Hydrology in a Changing Climate, Melbourne, Australia.
- JIASO, Accessed Sep 2014. PDO Index. <http://jisao.washington.edu/pdo/>.
- Jones, J.B., Rinehart, A.J., 2010. The long-term response of stream flow to climatic warming in headwater streams of interior Alaska. *Canadian Journal of Forest Research-Revue Canadienne De Recherche Forestiere*, 40(7): 1210-1218.

- Kane, D.L., Hinzman, L.D., Gieck, R.E., McNamara, J.P., Youcha, E.K., Oatley, J.A., 2008. Contrasting extreme runoff events in areas of continuous permafrost, Arctic Alaska. *Hydrol Res*, 39 (4): 287-298.
- Kane, D.L., Hinzman, L.D., McNamara, J.P., Zhang, Z., Benson, C.S., 2000. An overview of a nested watershed study in Arctic Alaska. *Nordic Hydrology*, 31(4-5): 245-266.
- Kane, D.L., McNamara, J.P., Yang, D.Q., Olsson, P.Q., Gieck, R.E., 2003. An extreme rainfall/runoff event in Arctic Alaska. *J. Hydrometeorol.*, 4(6): 1220-1228.
- Katz, R.W., Brown, B.G., 1992. Extreme events in a changing climate: variability is more important than averages. *Clim. Change*, 21: 289-302.
- Katz, R.W., 2013. Statistical methods for nonstationary extremes, *Extremes in a Changing Climate*. Springer, pp. 15-37.
- Kendall, M.G., 1975. *Rank Correlation Methods*. Griffin, London.
- L'Heureux, M.L., Mann, M.E., Cook, B.I., Gleason, B.E., Vose, R.S., 2004. Atmospheric circulation influences on seasonal precipitation patterns in Alaska during the latter 20th century. *Journal of Geophysical Research: Atmospheres* (1984–2012), 109(D6).
- Liston, G.E., Hiemstra, C.A., 2011. The changing cryosphere: Pan-Arctic snow trends (1979-2009). *J. Clim.*, 24(21): 5691-5712.
- Magnuson, J.J., Robertson, D.M., Benson, B.J., Wynne, R.H., Livingstone, D.M., Arai, T., Assel, R.A., Barry, R.G., Card, V., Kuusisto, E., 2000. Historical trends in lake and river ice cover in the Northern Hemisphere. *Science*, 289 (5485): 1743.
- Mann, H.B., 1945. Nonparametric tests against trend. *Econometrica*, 13: 245-259.
- Mantua, N.J., Hare, S.R., Zhang, Y., Wallace, J.M., Francis, R.C., 1997. A Pacific interdecadal climate oscillation with impacts on salmon production. *B. Am. Meteorol. Soc.*, 78: 1069-1079.
- Martins, E.S., Stedinger, J.R., 2000. Generalized maximum-likelihood generalized extreme-value quantile estimators for hydrologic data. *Water Resour. Res.*, 36(3): 737-744.
- McNamara, J.P., Kane, D.L., Hinzman, L.D., 1998. An analysis of streamflow hydrology in the Kuparuk River Basin, Arctic Alaska: a nested watershed approach. *Journal of Hydrology*, 206(1): 39-57.
- Milly, P.C.D., Betancourt, J., Falkenmark, Hirsch, R.M., Kundzewicz, Z.W., Lettenmaier, D.P., Stouffer, R.J., 2008. Stationarity is dead: whither water management. *Science*, 319: 573-574.
- Moore, R., Fleming, S., Menounos, B., Wheate, R., Fountain, A., Stahl, K., Holm, K., Jakob, M., 2009. Glacier change in western North America: influences on hydrology, geomorphic hazards and water quality. *Hydrol. Process.*, 23 (1): 42-61.
- Moore, R.D., Demuth, M.N., 2001. Mass balance and streamflow variability at Place Glacier, Canada, in relation to recent climate fluctuations. *Hydrol. Process.*, 15: 3473-3486.

- Neal, E.G., Walter, M.T., Coffeen, C., 2002. Linking the pacific decadal oscillation to seasonal stream discharge patterns in Southeast Alaska. *Journal of Hydrology*, 263: 188-197.
- Osterkamp, T., 2005. The recent warming of permafrost in Alaska. *Global Planet. Change*, 49(3-4): 187-202.
- Peterson, B.J., Holmes, R.M., McClelland, J.W., Vörösmarty, C.J., Lammers, R.B., Shiklomanov, A.I., Shiklomanov, I.A., Rahmstorf, S., 2002a. Increasing river discharge to the Arctic Ocean. *Science*, 298 (5601): 2171-2173.
- Peterson, B.J., Holmes, R.M., McClelland, J.W., Vorosmarty, C.J., Lammers, R.B., Shiklomanov, A.I., Shiklomanov, I.A., Rahmstorf, S., 2002b. Increasing river discharge to the Arctic Ocean. *Science*, 298.
- Rantz, S.E., 1982. Chapter 5. Measurement of Discharge by Conventional Measurement and Computation of Streamflow. Volume 1. Measurement of Stage and Discharge. Water Supply Paper 2175. U.S. Geological Survey, pp. 79-183.
- Rawlins, M.A., Steele, M., Holland, M.M., Adam, J.C., Cherry, J.E., Francis, J.A., Groisman, P.Y., Hinzman, L.D., Huntington, T.G., Kane, D.L., Kimball, J.S., Kwok, R., Lammers, R.B., Lee, C.M., Lettenmaier, D.P., McDonald, K.C., Podest, E., Pundsack, J.W., Rudels, B., Serreze, M.C., Shiklomanov, A., Skagseth, O., Troy, T.J., Vorosmarty, C.J., Wensnahan, M., Wood, E.F., Woodgate, R., Yang, D.Q., Zhang, K., Zhang, T.J., 2010. Analysis of the Arctic System for Freshwater Cycle Intensification: Observations and Expectations. *J. Clim.*, 23 (21): 5715-5737.
- Redmond, K.T., Koch, R.W., 1991. Surface climate and streamflow variability in the Western United States and their relationship to large-scale circulation indices. *Water Resour. Res.*, 27(9): 2381-2399.
- Rouse, W.R., Douglas, M.S.V., Hecky, R.E., Hershey, A.E., Kling, G.W., Lesack, L., Marsh, P., McDonald, M., Nicholson, B.J., Roulet, N.T., Smol, J.P., 1997. Effects of climate change on the freshwaters of arctic and subarctic North America. *Hydrol. Process.*, 11 (8): 873-902.
- Sen, P.K., 1968. Estimates of the regression coefficient based on Kendall's tau. *J. Amer. Statistical Assoc.*, 63: 1379-1389.
- Serreze, M., Barrett, A., Stroeve, J., Kindig, D., Holland, M., 2009. The emergence of surface-based Arctic amplification. *Cryosphere*, 3(1): 11-19.
- Serreze, M.C., Barrett, A.P., Slater, A.G., Woodgate, R.A., Aagaard, K., Lammers, R.B., Steele, M., Moritz, R., Meredith, M., Lee, C.M., 2006. The large-scale freshwater cycle of the Arctic. *Journal of Geophysical Research: Oceans* (1978–2012), 111 (C11).
- Serreze, M.C., Bromwich, D.H., Clark, M.P., Etringer, A.J., Zhang, T.J., Lammers, R., 2002. Large-scale hydro-climatology of the terrestrial Arctic drainage system. *J. Geophys. Res.: Atmos.*, 108 (D2).

- Serreze, M.C., Walsh, J.E., Chapin, F.S., Osterkamp, T., Dyurgerov, M., Romanovsky, V., Oechel, W.C., Morison, J., Zhang, T., Barry, R.G., 2000. Observational evidence of recent change in the northern high-latitude environment. *Clim. Change*, 46 (1-2): 159-207.
- Shabbar, A., Bonsal, B., Khandekar, M., 1997. Canadian precipitation patterns associated with the Southern Oscillation. *J. Clim.*, 10: 3016 - 3026.
- Slater, A.G., Bohn, T.J., McCreight, J.L., Serreze, M.C., Lettenmaier, D.P., 2006. A multi-model simulation of pan-arctic hydrology, *J. Geophys. Res.*
- Smith, L.C., Pavelsky, T.M., MacDonald, G.M., Shiklomanov, A.I., Lammers, R.B., 2007. Rising minimum daily flows in northern Eurasian rivers: A growing influence of groundwater in the high-latitude hydrologic cycle. *Journal of Geophysical Research: Biogeosciences*, 112(G4): G04S47.
- Spence, C., Kokelj, S.V., Ehsanzadeh, E., 2011. Precipitation trends contribute to streamflow regime shifts in northern Canada, International Union of Geodesy and Geophysics (IUGG): Symposium H02, Cold Region Hydrology in a Changing Climate. IASH, Melbourne, Australia.
- St. Jacques, J.-M., Sauchyn, D.J., 2009. Increasing winter baseflow and mean annual streamflow from possible permafrost thawing in the Northwest Territories, Canada. *Geophys. Res. Lett.*, 36(1): L01401.
- Stewart, I.T., Cayan, D.R., Dettinger, M.D., 2005. Changes toward earlier streamflow timing across Western North America. *J. Clim.*, 18: 1136-1155.
- Theil, H., 1950a. A rank-invariant method of linear and polynomial regression analysis, I. *Nederlands Akad. Wetensch. Proc.*, 53: 386-392.
- Theil, H., 1950b. A rank-invariant method of linear and polynomial regression analysis, II. *Nederlands Akad. Wetensch. Proc.*, 53: 521-525.
- Theil, H., 1950c. A rank-invariant method of linear and polynomial regression analysis, III. *Nederlands Akad. Wetensch. Proc.*, 53: 1397-1412.
- Walvoord, M.A., Striegl, R.G., 2007. Increased groundwater to stream discharge from permafrost thawing in the Yukon River basin: Potential impacts on lateral export of carbon and nitrogen. *Geophys. Res. Lett.*, 34(12): L12402.
- Wang, T., Hamann, A., Spittlehouse, D.L., Murdock, T.Q., 2012. ClimateWNA-high-resolution spatial climate data for western North America. *J. Appl. Meteorol. Clim.*, 51(1): 16-29.
- Wang, X.L., Swail, V.R., 2001. Changes in extreme wave heights in northern hemisphere oceans and related atmospheric circulation regimes. *J. Clim.*, 14: 2204-2221.
- Whitfield, P.H., Bodtker, K., Cannon, A.J., 2002. Recent variations in seasonality of temperature and precipitation in Canada, 1976-1995. *Int. J. Climatol.*, 22: 1617-1644.

- Woo, M.-k., Thorne, R., Szeto, K., Yang, D., 2008a. Streamflow hydrology in the boreal region under the influences of climate and human interference. *Philosophical Transactions of the Royal Society B: Biological Sciences*, 363(1501): 2249-2258.
- Woo, M.K., Kane, D.L., Carey, S.K., Yang, D.Q., 2008b. Progress in permafrost hydrology in the new millennium. *Permafrost and Periglacial Processes*, 19(2): 237-254.
- Woo, M.K., Thorne, R., 2003. Streamflow in the Mackenzie Basin, Canada. *Arctic*, 56 (4): 328-340.
- Yang, D. et al., 2002. Siberian Lena River hydrologic regime and recent change. *J. Geophys. Res.*, 107(D23): 4.
- Yang, D., Robinson, D., Zhao, Y., Estilow, T., Ye, B., 2003. Streamflow response to seasonal snow cover extent changes in large Siberian watersheds. *J. Geophys. Res.*, 108(D18): 4578.
- Yarnal, B., Diaz, H.F., 1986. Relationships between extremes of the Southern Oscillation and the winter climate of the Anglo-American Pacific coast. *Journal of Climatology*, 6: 197-219.
- Zhang, X., Harvey, D.K., Hogg, W.D., Yuzyk, T.D., 2001. Trends in Canadian streamflow. *Water Resour. Res.*, 37 (4): 987–998.
- Zhang, X., Zwiers, F.W., 2013. Statistical Indices for the Diagnosing and Detecting Changes in Extremes. In: AghaKouchak, A., Easterling, D., Kuolin, H., Siegfried, S., Soroosh, S. (Eds.), *Extremes in a Changing Climate*. Springer, Dordrecht Heidelberg New York London, pp. 1-14.

CHAPTER 4: ESTIMATING, VERIFYING AND PREDICTING SNOW COVER DEPLETION IN BOREAL WATERSHEDS OF INTERIOR ALASKA FROM REMOTE SENSING, *IN SITU* MEASUREMENTS AND STATISTICAL MODELING¹

Abstract

Snow cover depletion timing in subarctic Interior Alaska is a fundamental process that affects multiple climatic, human, and ecological systems and is known to be changing in response to amplified climate warming. The lack of a high quality, spatially and temporally dense meteorological network in Alaska for use in basin scale snowpack modeling necessitates alternative methods to estimate characteristics of melt timing. This work provides an estimate of melt timing characteristics for 38 stations across Interior Alaska using the Moderate Resolution Imaging Spectroradiometer (MODIS) remote sensing snow cover extent (SCE) products and a nonlinear regression approach for 2000-2012. The nonlinear model replicates the MODIS depletion curve with accuracy compared to observed data, and shows promise as a statistical tool to represent snow depletion timing features. One index, the date of maximum snow depletion initiation, closely correlated with snow depth observed at climate stations (average $\rho=0.57$, p -values < 0.001). The peak SCE, midpoint of melt and relative slope can be predicted using tree regression techniques based on statistical climate and physiographic indices and used to provide a prediction of the year-to-year snow depletion timing. The most important climate and physiographic variables used for prediction are temperature, albedo, wind speeds combined with topographic features (slope and aspect). Together, these models can be used to recreate the SCE curve and estimate it over a longer duration of time (1979-2012), allowing for further analysis of melt metrics over time (trends), and greater understanding of relationships between SCE and observable but sparsely monitored climate features (i.e. SWE and snow depth) for boreal Interior subarctic systems. The methods here can also be used in a prognostic manner to predict the pattern of snow cover depletion for river forecasting and water resource management.

¹ K.E. Bennett, J.E. Cherry, C.A. Hiemstra, L. Hinzman, M. Leonawicz. In prep for Water Resources Research. Estimating, verifying and predicting snow cover depletion in boreal watersheds of Interior Alaska from remote sensing, *in situ* measurements, and statistical modeling.

4.1 Introduction

Spring snowmelt in the Alaskan Interior is the dominant driver of watershed hydrology and the timing and characteristics of the melt can amplify or mitigate flood events, sedimentation patterns, forest fires, and drought. Defining the variability of snow cover extent (SCE) and identifying the main hydroclimate drivers of spring snow cover depletion is useful in identifying linkages among climate and hydrologic impacts at local-and watershed-scales in the warm-permafrost dominated boreal regions of the subarctic [Hinzman *et al.*, 2005; Serreze *et al.*, 2002]. This work is particularly important in vast Alaskan Interior boreal watersheds that remain under-monitored, despite a heightened interest in climate change in the Arctic and subarctic.

Changes in spring SCE duration and depletion timing associated with shifts in climate may lead to earlier snowmelt that could increase the length of the snow-free season and has been linked to numerous ecologic and physiological indicators of change [Chapin III *et al.*, 2005; Trujillo *et al.*, 2012; Wipf *et al.*, 2009] such as growing season length [McDonald *et al.*, 2004], tree growth in Siberia [Kirilyanov *et al.*, 2003], CO₂ fluxes [Aurela *et al.*, 2004], and active-layer thaw rates [Oelke *et al.*, 2004]. There is also a correlation between the length of the snow-free season and forest fires in the Yukon River basin, which is corroborated with results from studies in the Western US [Hess *et al.*, 2001; Semmens and Ramage, 2012; Westerling *et al.*, 2006], but remains an open research question in boreal Alaska [Duffy *et al.*, 2005]. Increased fires could result in subsequent effects such as permafrost thawing [Kasischke *et al.*, 2010; Yoshikawa *et al.*, 2002] that may lead to a major shift for the boreal forest, the world's largest biome, and hence a fundamental alteration in a major ecosystem of the Northern Hemisphere. Thus, developing a clear understanding of snow ablation timing is important for modeling the effects of a changing melt regime in Alaska.

Modeling of snow disappearance timing in Alaskan watersheds has been primarily limited to the treeless, high northern sub-basins that have available, accurate observational data, with few exceptions [Kane *et al.*, 1997; Liston and Hiemstra, 2011; Ramage and Semmens, 2012; Woo and Thorne, 2006]. Where no *in situ* observational data exists, satellite imagery can be used to infill gaps. The satellite records information across a swath of the landscape, as opposed to a single point, which can be advantageous when considering heterogeneous snow conditions. Additionally, satellite imagery is often available on a routine (i.e. daily or weekly) basis, thus the temporal records for these data are continuous.

However, work using remote satellite data for snow depletion analysis has been limited in large part because of the challenges associated with capturing meso-scale snow conditions obscured under the boreal canopy [Hall and Riggs, 2007; Klein *et al.*, 1998]. Vegetation, topography, cloud cover, scaling issues, and shading effects can reduce the quality of remote sensing tools to capture on-the-ground

observations of SCE [Simic *et al.*, 2004]. Because of these errors, the information must be thoroughly tested to ensure it is providing an accurate picture of the boreal North. Comparison at the watershed scale is paramount prior to using these data to inform models such that both spatial and temporal biases may be identified and removed if necessary.

An additional concern with remotely sensed information is the lack of a long record for both the satellites themselves and the observations to validate them. Satellite sensors tend to have a short life, on the order of 5-10 years. In order to construct a useful, long-term record using this information, methods must be developed to be able to link longer-term surveys of remotely sensed information such as SCE [Brown *et al.*, 2010]. In addition, new sensors such as Visible Infrared Imaging Radiometer Suite (VIIRS) onboard the Suomi National Polar-orbiting, which retrieves daily remotely sensed information and has recently come online, requires testing to determine improvement compared to the current generation of products (i.e. MODIS). The station network that would allow validation of snow depletion studies in Alaska is also a major limitation. Station observations tend to be shorter than 30 years (the climatologic standard), operate intermittently, and have quality issues related both to systematic (i.e. human or instrumental bias, or a lack of metadata) and random (i.e. mechanical failure) effects.

Work-to-date on SCE timing has focused on characterizing data from the high Arctic and/or on fine and very coarse scales (i.e. pan-Arctic). Research has widely applied binary response data, utilizing remote satellite sensors operating in the visible range [Dye, 2002]. Much of this work relies on the National Oceanic and Atmospheric Administration's National Ice Center (NOAA/NIC) SCE charts and their associated uncertainties [Wang *et al.*, 2005] to measure the weekly change in SCE and examine melt timing as anomalies of the mean day of snow disappearance across the Arctic [Brodzik and Armstrong, 2013; Derksen and Brown, 2012; Foster *et al.*, 2008]. The Moderate Resolution Imaging Spectroradiometer (MODIS) satellite imagery has been used to estimate percentage SCE change in studies focusing on high Arctic basins [Déry *et al.*, 2005; Liston, 1999]. A body of work also focuses on utilizing the passive microwave satellite remote sensors for small scale and broad scale studies of SCE, at coarse resolutions [Ramage and Isacks, 2003; Tedesco *et al.*, 2009]. More recently, Ramage and Semmens [2012], Ramage *et al.* [2007], and Yan *et al.* [2009] detailed their work utilizing the Advanced Microwave Scanning Radiometer – Earth Observing System (AMSR-E) and SSM/I brightness temperatures coupled with the SWEHydro model to estimate changes in SWE timing and runoff in the upper Yukon River basins of the Stewart and Pelly rivers. Studies are also ongoing to map melt onset using the brightness temperature over a long time scale utilizing several different passive microwave sensors [Wang *et al.*, 2013] across the pan-Arctic.

Combined approaches to examine changes in SCE are also being developed for the Arctic region as a whole, either through multi-sensor averaging or data assimilation, using two or more sensors and

imaging types [Brown *et al.*, 2010]. A new, coarse scale (25 km) global snow product has been developed by the US Air Force Weather Agency (AFWA) and the Hydrospheric and Biospheric Sciences Laboratory at NASA/Goddard Space Flight Center. Referred to as the AFWA–NASA Snow Algorithm (ANSA), the product is a blend of MODIS, AMSR-E [AMSR-E, Kawanishi *et al.*, 2003] and the Quick Scatterometer [QuikSCAT, Nghiem and Tsai, 2001] sensors [Foster *et al.*, 2011]. ANSA is currently being evaluated in the Great Lakes region, Finland, and Turkey [Akyurek *et al.*, 2010; Hall *et al.*, 2012] and was recently analyzed for Alaska [Liu *et al.*, 2013].

Examples from other forested regions of the world highlight the issues in obtaining an accurate metric of snow disappearance timing. Several studies have analyzed snow ablation based on changes in center of mass of streamflow [Stewart *et al.*, 2005; Westerling *et al.*, 2006]. However, the center of mass approach has been shown to be a weak indicator of changes in snowmelt timing [Whitfield, 2013]. To estimate snow disappearance, some satellite studies utilize a binary snow on/snow off within a cell over a region (i.e. Arctic) that may be based on the full snow season or a shorter duration, as such, results for these various estimates may differ [Choi *et al.*, 2010]. Binary, lumped responses across regions cannot be related specifically to site conditions such as elevation, slope or vegetation patterns that exhibit control over snowmelt [Blöschl *et al.*, 1991; Sturm and Wagner, 2010].

Landsat has been widely applied to capture SCE from visible imagery using several different approaches [Rosenthal and Dozier, 1996]. The goal of much of this work is obtain SCE estimates from remote sensing for estimate of snow water equivalent (SWE) [Cline *et al.*, 1998; Molotch, 2009; Rango and Martinec, 1979] via the processing of depletion curves or modified depletion curves [e.g. Anderson, 1976; Buttle and McDonnell, 1987; Liston, 1999; Luce *et al.*, 1999]. But, many of the studies inherently require an accurate assessment of SCE through time and also require selection of imagery not obscured by clouds [Gao *et al.*, 2010; Molotch *et al.*, 2004]. This is where uncertainties can be introduced into the calculation of SWE should the underlying SCE depletion curve estimate be erroneous [Parajka and Blöschl, 2008]. These techniques can also be complex, computationally prohibitive and require *in situ* measurements which are all subject to error, and do not necessary capture inter-annual variability in snow depletion [Shamir and Georgakakos, 2007]. However, the remotely sensed SCE time series itself offers a tool that can be mined to understand regional variation in snow depletion timing. If these SCE data are properly validated, it can be used to guide resource managers, forecasters and hydrologists towards focused selection of more complex modeling approaches. Subsequent processing may follow based on this initial study of the depletion curve and its variability through time and space.

The outline of the paper are as follows: 1) define a nonlinear regression curve that replicates the MODIS remotely sensed SCE data through the melt season for 38 sites in Alaska's boreal Interior region and create a continuous time series of SCE data 2) use this data to validate the MODIS SCE data and

characterize the snow cover depletion properties at each site in terms of the dates of maximum, mid-melt and melt termination, melt duration and melt rates 3) estimate the logistic parameters of the nonlinear snow cover depletion curve using tree regression and a combination of uncorrelated climate and physiographic indices to reconstruct the depletion curve, 4) illustrate the use of this tool by reconstructing snow cover depletion at one site from 1979-2012. The objectives of the work are as follows;

- validate the MODIS SCE data in subarctic boreal Interior watersheds,
- illustrate how a quantifiable, repeatable nonlinear modeling approach can be used to generate multiple metrics of snow cover depletion to characterize temporal and spatial variability of snow depletion at site-specific, basin-wide, or pan-Arctic scales, for improved understanding of process shifts in melt depletion timing,
- identify relationships between melt cover depletion timing metrics and provide a tool that can be used to a) examine relationships between melt depletion timing and other indicators to better understand these relationships in boreal Arctic ecosystems, and b) reconstruct these curves over a longer duration of time using available climate reanalysis products for other types of analysis such as the trends example illustrated in this paper or c) predict patterns of snow depletion used for agencies monitoring flooding hazards or water resources.

The method will also be useful to compare specific snow depletion timing characteristics across remote sensing data products as sensors experience phase out and researchers advance towards improved and/or new snow cover fractional extent algorithm development [i.e. *Painter et al.*, 2009].

4.2 Methods

4.2.1 Study Area

The boreal interior of Alaska includes the southeast, northeast and central regions as indicated in Bieniek et al. [2012]. Stations are situated north of the Chugach mountain range in southern Alaska; north to the Brooks Range; west to the village of Galena in the Yukon-Koyukuk region; and east to the Canadian border at Eagle (Figure 4.1). Five index sites from the region were selected to highlight study results. The most northern index site is the Bettles Airport Global Historical Climate Network (GHCN) station (USW00026533, 66.92°N, 151.51°W, 205 m), which began operating on May 1st, 1951. The Fairbanks International Airport GHCN site (USW00026411) is located in the central interior Yukon-Tanana Upland regions of the Fairbanks North Star Borough at 64.80°N 147.89°W at an elevation of 135 m; the site has been operational since July 1st, 1948. The Fairbanks Airport site is proximal to the city of Fairbanks North Star Borough, Alaska, population ~100,000 [*Parnell et al.*, 2012], and thus is generally considered to be affected by urbanization, particularly in the estimation of the lowest temperature records.

Despite this, the Fairbanks station was included as an index site because of its long period of record and central location. The nearby Mt. Ryan SNow TELEmetry (SNOTEL) site (Centralized Database System record id 46Q01, SNOTEL id 948) is located in the Yukon-Tanana Upland regions of the Fairbanks North Star Borough at 65.25°N, 146.15°W, at an elevation of 853 m, and has been operating since 1981. The McGrath GHCN climate station (USW00026510) is located Western Alaska's Tanana-Kuskokwim lowlands outside the village of McGrath at 62.96°N, 155.61°W, and has been operational since April 1st, 1939. The site is situated on the alluvial floodplain of a meander bend of the Kuskokwim River. The Eagle GHCN site (USW00026422) is the most easterly location (64.79N, 141.20W) on the banks of the Yukon River in the village of Eagle. The Eagle station has been operational since September 1st, 1949.

4.2.2 Data Sources

Fractional SCE imagery was extracted from the MODIS/Terra Snow Cover Daily L3 Global Version 5 (MOD10A1) 500 m gridded data set available from the National Snow and Ice Data Center [Hall and Riggs, 2007; Hall *et al.*, 2006]. MOD10A1 SCE is estimated using the Normalized Difference Snow Index (NDSI) to calculate the difference between MODIS band 4 (0.555 μm) and MODIS band 6 (1.6 μm), divided by the sum of the two reflectance values. The resulting NDSI value is then subject to several conditions that determine if a cell is snow covered [Hall *et al.*, 2001]. If the cell is found to be snow covered, the snow cover fraction is calculated as outlined by Salomonson and Appel [2004]. The MODIS Re-projection Tool was used to pre-process imagery into an Alaska Equal Area Conic projected GeoTIFF of fractional SCE [USGS, 2011].

The MOD10A fractional SCE data does not contain the tree cover correction described by Klein *et al.* [Klein *et al.*, 1998] therefore SCE was adjusted to remove the effects of screening by the forest cover that would result in underestimated SCE values in the product. For this work, an approach to inflate the MOD10A SCE on the viewable gap fraction, or the amount of snow covered ground between trees that the sensor can see [Liu *et al.*, 2004] was applied. This technique, while widely applied, assumes that the viewable gap fraction remains constant through the snowmelt season, which is incorrect as we know that the viewable gap fraction can vary based on a complex number of factors, including forest canopy density, age and class, zenith angle of the sensor, solar zenith angles, topography and snow loading [Kane *et al.*, 2008; Liu *et al.*, 2008; Molotch and Margulis, 2008; Raleigh *et al.*, 2013; Rittger *et al.*, 2013]. To account for these issues, rather than applying a forest cover product to correct the product itself, the MOD10A1 data were applied [Durand *et al.*, 2008]. All 2000-2013 March 1-March 15th MOD10A1 pixels across Interior Alaska were differenced from 100 and then a composite average of all days (n=207) was calculated. While in southeast Alaska some melt may have occurred during this time, the Interior SCE should still be at 100% across most of the region. To account for bare ground regions such as open,

wind-blown rocky faces values less than 20% SCE were removed from the correction. The standard division by viewable gap fraction, or $SCE/(1-F)$ where F is the tree cover percentage was then applied to each SCE pixel in all days and years. The results were constrained to 100% when exceeded.

R (R-Project, <http://www.r-project.org>) was used to analyze the corrected SCE images and extract grid cell results for a 10 km circular buffer zone around each site for the period of time March 1st through July 31st, 2000-2012. The snow cover fraction information (i.e. the grid cell values equaling 100% or less) was averaged across cells in the buffer zone to create a single daily fractional SCE for each site and time step; this average value is referred to when discussing SCE. Missing data, cloud cover, or cells where the target was obscured from view were not included in the SCE fraction calculation.

SNOTEL [SNOTEL, NRCS, 2013; Serreze *et al.*, 1999] snow water equivalent (SWE, mm) was downloaded from the National Resource Conservation Service (NRCS) snow pillow data repository (<http://www.wcc.nrcs.usda.gov/ftpref/data/snow/snotel/cards/alaska/>). The snow course data (SWE measurements of snow on the first-of-the-month) were downloaded from the same repository (http://www.wcc.nrcs.usda.gov/ftpref/data/snow/snow_course/table/history/). GHCN [Menne *et al.*, 2012; Williams *et al.*, 2006] snow depth on-the-ground (mm) data were downloaded from the National Climatic Data Center's Climate Data Online repository (<http://www.ncdc.noaa.gov/cdo-web/>). Sites with greater than 20 years of data and five contiguous years of record were selected from the broader network; to avoid spatial co-linearity proximal stations were removed, prioritizing record lengths. A total of 38 sites with continuous records of observational data for the period under study were chosen for in-depth analysis.

The North American Regional Reanalysis (NARR) data were used to represent climate information not readily or consistently spatially or temporally available from the SNOTEL and GHCN networks including: precipitation, temperature, albedo, relative humidity, radiation, and wind speeds [Mesinger *et al.*, 2006]. NARR (~32 km in latitude and longitude) was downloaded from NOAA's Earth System Research Laboratory Physical Sciences Division site (<ftp.cdc.noaa.gov/pub/Datasets/NARR/Dailies/monolevel/>) and pre-processed to extract the time series from the NARR grid cell closest to the climate stations [Mesinger *et al.*, 2006]. NARR wind magnitudes were calculated using the square-root of the squared u - and v -wind components.

NARR data were compared with a station in the Caribou-Poker Creek research watershed (CPCRW) to illustrate the reliability of the reanalysis product in this area. NARR climate data used in Figure 4.2 is compared with the station observations at a site located in the Caribou-Poker Research Watershed (CPCRW, Figure 4.3). Six panels illustrate air temperature ($^{\circ}\text{C}$), precipitation (mm), snow depth (mm), relative humidity (%), wind speed (m/s), downwelling shortwave (W/m^2) and longwave

radiation (W/m²) at CPCRW compared to the NARR data. Data are only available for two years; 2007-2008, and 2010-2011.

Topographic data (elevation, slope, aspect) used in the study were derived from the 60 m National Elevation Dataset (NED) [Gesch *et al.*, 2002] digital elevation model (DEM), updated for Alaska in 2012. Data were averaged from the 10 km buffer zone around each climate station.

4.2.3 Analysis

Simple models of snow depletion timing based on measured change in MODIS fractional SCE were developed using a log-logistic nonlinear regression function available via R's "drc" package [Bates and Watts, 1988; Ritz, 2010; Ritz and Streibig, 2008]. The function (Equation 1) utilizes three main parameters and has a lower limit of zero; the maximum extent of snow cover occurring before the melt begins, the asymptote (*asym*) of maximum fractional SCE; the midpoint of the snow cover depletion melt in terms of date (*midpt*); and the relative slope of the depletion curve around *asym* (*rslop*, Figure 4.4),

$$f(x, (a, s, m)) = \frac{a}{1 + e^{s(\log x - \log m)}} \quad (4-1)$$

where *a* is the asymptote, *m* is the midpoint, *s* is the relative slope around *a* and *x* is the time sequence [Pinheiro and Bates, 2000; Streibig *et al.*, 1993]. The nonlinear function is constrained to values lesser than one (or 100% SCE), and values approximating zero are considered to be zero (i.e. 0% SCE). These parameters are ideal in that they both define the snow depletion curve and have a physical meaning representative of the MODIS SCE depletion through time.

The first derivative of the nonlinear function was used to estimate the remaining SCE depletion statistics, including the initiation of the depletion (the point at which the upper asymptote starts its downward trajectory) and the termination (the starting point at which the lower asymptote levels off). The maximum depletion, or the point in time at which the snow depletion rate is at a maximum value, was defined from the maximum value of the curvature (κ), formulated as,

$$\kappa = \frac{|f'(x)|}{\left(1 + f'(x)^2\right)^{\frac{3}{2}}} \quad (4-2)$$

The minimum values of the curvature defined the termination of the maximum snow depletion period.

Regression models to estimate the logistic parameters of the nonlinear function (*asym*, *midpt*, *rslop*) were developed using ensemble machine learning techniques designed to overcome issues related to weak predictors [Hancock *et al.*, 2005] common in climate analysis using R's "caret" [classification and regression training, Kuhn, 2008; Kuhn *et al.*, 2013] package. Machine learning is the application of

algorithms that are utilized in order to extract information from data. Ensemble approaches are defined by the use of multiple modeling tools run iteratively upon multiple composites of predictors. Together, they are used in this work to determine a) the best model from a suite of models, and b) the best set of model predictors from a set of multiple predictors. The aim was to find a statistically significant, parsimonious regression model to represent the logistic parameters of the MODIS SCE nonlinear function that would identify or rank the importance of the features (variables and indices). The independent variables or predictors in the regression models are the climate/physiographic variables and indices (i.e. maximum seasonal temperature), and the dependent variable is *asym*, *midpt*, or *rslop*; separate models were developed for each logistic parameter.

Eight different climate (NARR) and physiographic *variables* (derived from the NED DEM) were considered in the initial regression models; temperature (°C), precipitation (mm), albedo (%), sea level pressure (Pa), wind speed (m/s), relative humidity (%), radiation (W/m²) and topography (Table 4.2). NARR mean sea level pressure was selected as a variable to represent broad scale pressure variations associated with changes in temperatures that is not susceptible to local variability effects [Compo *et al.*, 2011]. Within these main variables, approximately 70 different *indices* were generated. A major challenge in model development is that climate indices tend to display a high amount of multi-collinearity, which invalidates modeling techniques that do not address these issues. A process was therefore utilized that focused first on reducing climate indices to only those with weak and non-significant correlations, calculated using a nonparametric Spearman's rank measure of dependence (*rho*), and analyzed for significant and strong correlations (*rho* > 30%, p-value ≤ 0.05). This reduced the input indices to 19 (Table 4.2). A framework was developed to test all possible combinations of the non-correlated climate indices using all eight variables which resulted in 432 different formulations, which were analyzed in four different models for each parameter at the 38 sites and all years (2000-2012, n=494, Table 4.3). Cumulative freezing (thawing) days were calculated as the minimum (maximum) cumulative sum of temperature on the days for which the minimum (maximum) daily temperatures were below (above) zero °C, respectively. The maximum cumulative freezing degree days was calculated as the maximum value of the cumulated degree-day value from October to April 15th. The date of maximum change in downward shortwave radiation is the first day of the year on which the cumulative flux (difference day-to-day) in radiation increases above 100 W/m² (henceforth referred to as CSWR). For example, this occurs on average at the Mt. Ryan site on Julian Day 91 (April 1st).

Regression models included random forest [RF, Breiman, 2001] and generalized boosted regression modeling [GBM, Friedman, 2001; 2002; Ridgeway, 1999; 2012]. RF is a tree-based regression selects random sub-samples of data to calculate predictor space into rectangles, using rule based selection of regions with the best mean response to predictors; normal distribution errors are assumed [Elith *et al.*,

2008]. Bootstrapping approaches are used to select samples from the sub-subsets for each split in each classification tree [Strobl *et al.*, 2009; Strobl *et al.*, 2008]. RF just has one meta-parameter in caret (mtry, the number of parameters in the model, Table 4.3). GBM is a modeling approach that uses stage-wise processing to build progressively improved models while minimize a loss function with each new tree to form a generalized ensemble of prediction models [Elith *et al.*, 2008; Ridgeway, 1999]. These models can be thought of as numerous regression trees that are developed from random sub-samples of the training data set using the residuals of the previous tree to improve response variation not explained by the model [Friedman, 2001; 2002]. The GBM model used herein utilized three meta-parameters, shrinkage (which was kept constant at 0.1), number of trees (1500) and interaction depth (number of parameters utilized, 5, Table 4.3). Both techniques (RF and GBM) protect against model overfitting and minimize the effect of outliers by building recursive trees but the models must be run to allow the appropriate (large, but to a threshold) number of trees to be built. The additional application of cross-fold validation (see below), split-sample processing and removal of correlated parameters reduces model overfitting.

The data set was divided by random selection training (50%) and validation (50%) data partitions, preserving the representative sample distribution in each. To retain consistency in the randomization between model runs, a specific random seed was used [Kuhn, 2008] although not for partitioning. All models were run with k-fold cross-valuation (k=10), repeated 25 times, to iteratively select the model's ensemble meta-parameters (i.e. mtry in the case of RF). This technique splits the sample into k partitions and all but one of these partitions is used for model training, while predictions are made on the withheld observations. This process is repeated 25 times and the results are averaged. RMSE was used to evaluate model performance, along with R² and p-value summaries, with Bonferroni adjustment to inflate p-values according to the number of models that were explored [Dunn, 1961].

Variable importance measures were calculated and used to create parsimonious models. Variable importance is calculated in GBM and RF using similar methods. For RF, a “permutation” approach is used to calculate the mean standard error (MSE) of the prediction for the out-of-bag observations in each tree and recalculated iteratively and compared with the initial error after all predictors have been added to the tree to determine if the order of the predictors affects the MSE result [Breiman and Cutler, 2014]. Normalization of the MSE differences is not performed when the standard error is zero [Breiman and Cutler, 2014]. A “relative influence” variable importance calculation is used in GBM. It is a similar approach to Breiman's random forests, but GBM computes variable importance using the entire training dataset (not the out-of-bag observations) [Ridgeway, 2012]. For this work, top models and parameterizations that result in the lowest RMSE and highest R² were selected. These top models were further reduced by iteratively removing the lowest ranked variable based on the variable importance measures. Results of the top performing combination of non-correlated climate indices for the four

models are illustrated for the training data set (Figure 4.5a), and the test data set (Figure 4.5b). Values for RMSE, R^2 and p-value statistics are given in Table 4.3.

Utility of the method is illustrated by recreating SCE data for all index sites and making predictions using the models described above and NARR from 1979-2012. Trends were analyzed using an approach developed by Yue et al. [2002] as outlined in Wang and Swail [2001], where the trend magnitude is calculated using Theil-Sen approach [Sen, 1968; Theil, 1950a; b; c]. The trend slope, as long as it is not close to zero, is assumed to be linear and the time series is pre-whitened and the trend and the residuals are combined. The effect of this pre-whitening is to remove any serial correlation that may inflate the significance of the trend. The nonparametric Mann-Kendal [Kendall, 1975; Mann, 1945] test for significance is used on this series. The analysis was carried out using the “zyp” R trends package for R-project statistical software [Bronaugh and Werner, 2009].

4.3 Results

In the following text, the three logistic parameters used in the nonlinear regression are referred to as ‘logistic parameters’. The eight main climate and physiographic classes used to predict logistic parameters are referred to as ‘variables’, while the specific climate and topographic statistics (i.e. minimum elevation or maximum temperature in October to March) are referred to as ‘indices’.

Validation of the MODIS data were undertaken in part by comparing plots of SWE/snow depth and MODIS SCE depletion. Peak SWE/snow depth occurs on or just after April 1st, and plateaus until mid-April to late-April (based on SWE captured at the SNOTEL pillow/snow course or snow depth at the GHCN station) with the melt beginning shortly after this point (Figure 4.2). At some sites, MODIS observations match closely with the SWE captured over the period by the snow course recordings (red circles, Mt. Ryan in Figure 4.2). The MODIS SCE data match with the station snow depletion timing at the Fairbanks and Mt. Ryan sites. At Eagle, Bettles and McGrath, the MODIS SCE does not detect the same melt depletion dates (Figure 4.2c, d). The grey envelope around the MODIS data illustrates the range of the MODIS SCE (based on the 25 and 75th quartile) from year-to-year; showing the continuity of the depletion patterns and the range from year-to-year at each site (i.e. Figure 4.2). This is not a surprising finding given that the stations tend to be located in open clearings that may have higher exposure to radiation and wind effects, causing them to melt out earlier than the surrounding region [Molotch and Bales, 2006]. However, the Mt. Ryan and Fairbanks sites are located within regions that contain urban developments (i.e. airport, roads) and Mt. Ryan is an alpine treed site. Note that in these figures the snowpack volume is not being considered; only the timing is compared. Thus, where Mt. Ryan SNOTEL and the MODIS regression lines differ from each other on the y-axis, this is occurring because SWE (mm) is accumulating, while SCE stays the same (95-100%, Figure 4.2).

Inter-comparison of the NARR data with the CPRW site specific meteorological data collected over two years shows that NARR provides a good approximation of almost all climate variables considered in this study (Figure 4.3) with a couple of exceptions. NARR has been noted to out-perform other reanalysis products for monthly temperature in Alaska [Lader, 2014] although some issues with the precipitation assimilation are apparent (Figure 4.3). NARR also seems to have limited ability to characterize winds in CPRW. It is common, however, for models to under predict the low wind speeds experienced in the interior of Alaska [Mölders and Kramm, 2010]. Radiation data appears to match closely in year 2010-2011, but NARR over predicts the SR in 2007-2008 during the latter half of the year, which is consistent with the findings of Markovic et al. [2009]. However, NARR also appears to overestimate longwave radiation in 2007-2008, which was not corroborated in the Markovic et al. (2009) study. It is unclear if this is due to under prediction of cloud cover, as suggested by Markovic [2009], or if there are other factors leading to the under estimate (i.e. station quality). NARR data has been utilized in previous hydrologic modeling studies to estimate snowmelt contributions in northern latitude basins [Choi et al., 2009; Woo and Thorne, 2006].

4.3.1 Nonlinear Model

SCE observations (MODIS), nonlinear modeling simulations and derived timing characteristics are illustrated in Figure 4.6, and described in Table 4.4 to characterize the 38 sites examined herein. MODIS SCE is illustrated for each year 2000-2012 along with the SNOTEL SWE or GHCN snow depth, depending on the site. Generally, the nonlinear model was successful at fitting the snow depletion curve for most sites and years, with the exception of situations when there was too much cloud cover or erroneous sensor retrievals in the time series during the early or late part of the melt season. The five different index stations have variable melt timing statistics (Table 4.4, bold) based on physiography, illustrating different processes involved in snowmelt across sites. Year-to-year variation is apparent but sites maintain similar melt patterns across the years (Figure 4.6). The earliest melt initiation dates of JD 101/107 occur at Fairbanks' and Eagle's airport stations (Table 4.4). The latest melt initiation date is the most northern station, Bettles. Eagle (furthest east) and Mt. Ryan (highest elevation) are the last stations to melt out, with the lowest melt rates. Bettles has the fastest melt rate and the shortest melt duration, while McGrath and Fairbanks (the lowest elevation sites) have similar melt rates although they have different melt initiation dates by 12 days. Eagle and Fairbanks have the lowest SCE at the beginning of melt, on average over the study period, with 92% and 93% respectively, with the rest of the stations having 95-97%.

The MODIS SCE and the SNOTEL SWE year-to-year timing are quite similar for most years and stations, however for some years they do not correspond as well, namely 2001/2006 at the Fairbanks

Airport station (Figure 4.6), 2003 at Bettles (not shown), 2003/2009 for Mt. Ryan (not shown), 2003/2009/2012 at McGrath (not shown). The timing between SNOTEL SWE and MODIS SCE at Eagle are quite different (not shown). Reasoning for why these years in particular were not well matched is based on analysis of the climate and MODIS data. Some of these mismatched years had warmer winter temperatures and more precipitation, but this was not consistent across the sites. Cloud cover (based on a count of the cells designated as clouds in the MOD10A1 data set) was sometimes higher but not anomalously high compared to other years. For example, Fairbanks and Mt. Ryan experienced higher cloud cover days ($> 40\%$ of the buffer cells contained clouds) during these years, but other years had similarly high values when there was no noted difference between the station and the MODIS snow depletion timing. The Eagle site represents an interesting case, as it appears that the GHCN site has a very different melt timing signature from the MODIS estimates.

The snow depletion timing metrics were examined in relation to snow data observed across the sites. The snow depletion indices were correlated with snow depth (GHCN stations) over the season revealing a strong and significant positive relationship between the mean snow depth in February, March, DJF and over the Oct to mid-April season, including the date of snow depletion initiation (average $\rho=0.52$ p-values < 0.001) for 2000-2012. Other snow depletion timing indices were significantly correlated with mean snow depth in February and March, max and mean winter snow depth (DJF) and max and mean snow depth over the Oct to mid-April season, including the midpoint of the melt (average $\rho=0.53$, p-values < 0.001), date of maximum snow depletion initiation (average $\rho=0.57$ p-values < 0.001), and SCE % at the beginning of the season (*asym*, average $\rho=0.53$, p-values < 0.001).

4.3.2 Nonlinear Logistic Parameters Regression Models

The boosted trees [GBM, *Ridgeway*, 1999] provides the best observed to predicted correlation value for the midpoint and relative slope logistic parameters [*Breiman*, 2001; *Breiman and Cutler*, 1993], while random forest (RF) model provides the best results for the asymptote logistic parameter (Table 4.3). The final RF model predicts *asym* (maximum SCE 2000-2012) for $n=494$ with a root mean squared error (RMSE) of 2.50 and an adjusted R^2 value of 81% (significant at the 99% confidence interval). GBM provided estimates of *midp* with an RMSE of 3.90 and an adjusted R^2 value of 88% (significant at the 99% confidence interval). GBM predicted the *rslop* parameter for $n=494$ with RMSE of 17.25 and adjusted R^2 of 82% (p-value < 0.001). Table 4.3 lists the training statistics for the models; note that these statistics change slightly depending on the seed used to generate the split sample data. The model predictions for the Fairbanks site are shown with a red line in Figure 4.6.

Models to estimate the logistic parameters indicated the importance of broad scale climate features, namely on temperature, albedo, wind speeds combined with topographic features (slope and

aspect) to identify melt characteristics. Of less importance were precipitation, radiation and relative humidity. Indices used for modeling the *asym* parameters included the mean temperature in winter, range in slope, CSWR, average March sea level pressure, and average March wind speeds. The indices used in the *midp* model included the mean temperature in winter, mean albedo in February, change in relative humidity from February to March, and mean daily March sea level pressure. The *midp* parameter did not use a topographic index. The *rslop* parameter was modeled by the RF using indices of the mean temperature in winter, mean wind speed in March, mean albedo in February, the total number of precipitation days for October to April 15th, and the standard deviation of aspect.

The utility of the estimated nonlinear regression tool is introduced by applying the tool to produce the long term (1979-2012) climatic trends in snow timing indices. The availability of more than just one indicator allows for a more in-depth analysis of changes in snow metrics. Trends results indicate that the Fairbanks, Mt. Ryan McGrath, and Eagle stations are experiencing changes in snow timing that are significant at an 80% confidence interval, while only Eagle snow depth exhibits change at this significance level. Fairbanks shows a decline in four of its melt timing indices of more than 3 days over a standardized 30 year period. At McGrath, a 5% increase in maximum SCE occurs while at Eagle site, there is a decrease in the average maximum SCE (6%) at the beginning of the season.

4.4 Discussion

Due to the availability of remote sensing products across the entire state of Alaska, characterizing snow depletion timing characteristics for watersheds and regions where station data do not exist is of great value. Forecasters, researchers, modelers, engineers and resource managers who require intra-year and multi-year estimates of snow depletion patterns can use the characteristics for a plethora of information needs. The tools illustrated in this paper allow for generation of a continuous estimate of SCE through melt season based on existing data sources, and also allow for reconstruction of the SCE over longer durations that are suitable for climate change studies. This data may be useful in tracking longer-term changes of snow depletion properties, or when examined across different sites, can point to coherence or variability in conditions between different sites or at one site over several years. Utilizing the SCE depletion results in this way can highlight locations and regions where the greatest change is occurring and further field studies are needed. This type of prioritization of focal studies is required in the vast, understudied remote regions of the globe such as the boreal forest.

The work presented in this study serves to validate the MODIS SCE data for subarctic boreal Interior watersheds. While capturing snow conditions at different scales, the MODIS 500m products relate well to the snow pillow and snow depth sensors at SNOTEL and GHCN observations across the Interior (~ 3m scale), provided the 500 m MODIS cell is averaged for a 10 km buffer zone around the

observed station. The averaging technique overcomes the issue of a paucity of information at small (i.e. one grid cell) scales due to cloud cover or other issues with MODIS data on specific days throughout the year and minimizes the inherent bias that results when one specific cell is chosen to represent sites. Differences found between the stations and MODIS melt depictions are likely complex and dependent on many factors, including observed data quality and the nature of the average 10 km MODIS to represent the surrounding region and/or the station. Better understanding will require a more thorough analysis to compare the anomalies between the station melt to the MODIS data, and other remotely sensed satellite information, which is beyond the scope of the current work.

Quantifiable metrics of snow cover depletion can be used to characterize temporal and spatial variability of snow depletion at site-specific, basin-wide, or pan-Arctic scales. The snow depletion timing examined in this study varies between proximal locations experiencing similar broad scale climate conditions due to differences in physiographic setting (i.e. elevation, aspect) or vegetation patterns. For instance, Mt. Ryan, an alpine treed site, begins to melt later (13 days) and with a more protracted melt on average compared to the lower elevation Fairbanks Airport site that is reflected both in duration of melt and the melt rate [Table 4.4, *Storck et al.*, 2002]. Fairbanks Airport is open and susceptible to changing weather conditions during the melt period, exhibited by its fast melt rate and shorter duration of melt. Increased melt rates at the Fairbanks site also occur due to a thinner snowpack, increased radiation exposure during March and April, and emergence of vegetation leading to decreased albedo. Mt. Ryan, in comparison, has increased interception and shading associated with its thin but present canopy cover, and its high elevation dictates that it would have deeper, more persistent snow cover compared to the open Fairbanks sites where snow can be easily re-distributed by wind and humans [*Pomeroy and Granger*, 1997; *Storck et al.*, 2002]. Increased melt rates for open areas compared to forested stands have also been observed by *Faria et al.* [2000] and by *Pomeroy and Granger* [1997].

SCE timing values are corroborated with other work on melting timing characteristics at nearby sites. *Carey and Woo* [2001] noted a snow free date for a headwater basin to the Yukon River located in the Yukon (Wolf Creek) on April 26th (116) for a south-facing slope, and May 19th (139) for a north-facing slope, but melt onset was not noted. A proximal site at a similar elevation to Wolf Creek (1175 m) is the Nabesna (863 m), which has a termination date of ~May 25th (143). Nabesna is located further west than the Wolf Creek site, and slightly further north. Snow depletion timing noted in other studies includes a melt date of ~120 for a high elevation site southeast of the extent of this study [*Ramage and Isacks*, 2003].

The tools provided in this work are helpful for identifying relationships between melt cover depletion timing metrics through the melt season which allow for analysis pointing to shifts in processes that may not otherwise be identifiable from a single melt statistic. The strong and significant relationship

found between melt timing indices and total seasonal snow depth for GHCN sites is an example. The date of melt is aligned with the snow pack characteristics, despite the variability in both melt dates and snow depths, allowing for identification of patterns in the snow timing and snow characteristics. These findings suggest that statistics, such as melt start date, initiation maximum date, and midpoint of melt may capture more information in regards to snow pack characteristics. Meanwhile, the overall duration of the melt period was not as strongly correlated with the snow depth indices examined.

The NARR-based nonlinear model reconstruction shows good coherence to the MODIS SCE nonlinear regression (illustrated in Figure 4.6). At times, the reconstruction matches more closely with the station results, particularly in the timing of the melt termination. This can be observed for the Fairbanks station in years 2001 and 2006 (Figure 4.6). Although *asym* and *midp* test data set results were successful, the *infl* parameter was challenging to model in general (Table 4.3). This could be due to the fact that melt rate (*rslop*) may be largely determined by the canopy conditions, as suggested by Metcalfe and Buttle [1998], which is why it is difficult to estimate based on available and largely coarse-scale climate and topographic data used in this study. Outliers in the data set were also difficult to capture accurately – very fast or slow melt timing is not always replicated well in this approach (Eagle). Therefore, this technique may not be applicable in coastal regions or low elevation sites.

Important climate variables and indices used to estimate the logistic model parameters highlighted the utility the nonlinear model reconstruction. Statistical models used to estimate parameters do not imply causation however some of the variables used in these models were ranked consistently, between different models (RF and GBM) and between the logistic parameters. The consistency in some of the model variable importance rankings suggests that they have meaning and can be discussed. However, a note of caution is required as indices and rankings will shift depending upon the input data, station mixes and periods of record therefore the results are discussed in regards to the broader scale variable groups rather than focusing on specific climate indices and their importance ranking.

Important model variables included climate factors with an emphasis on temperature, albedo, wind speeds combined with topographic features (slope and aspect). This finding is similar to that presented in Gelfan et al. [2004], which suggests that snow depletion is driven largely by the interaction between topographic and climate conditions. Slope in this work is indicative of elevation and was strongly, positively correlated with maximum elevation. Elevation driven increases in snow pack caused by orographic uplift and cooling mechanisms are well known causes of increases in snow and snow cover. The standard deviation of aspect was negatively correlated with mean slope ($\rho=-0.41$), elevation and latitude (average $\rho=-0.38$). Thus, the variation in aspect may be representative of combined factors found in the more southern portions of the study region at moderate elevations, such as the north and south facing slopes that are a dominant factor for melt timing in the Fairbanks region. North versus south

facing slopes are noted to melt five days to a week apart even in the same watershed (S. Lindsey, pers. comm.).

Analysis of sea level pressure revealed that sea level pressure and temperature variables were related in this study (although indices used in the models were not correlated as noted previously). Temperature is known to be an important influence on the snowmelt and is often used as the single factor in modeling melt [Anderson, 2006; Hock, 2003]. Increased sea level pressure was indicative of declines in air temperature at the sites. This was found to be related to stability of air masses during the winter that favored cold, clear days where insolation is low, and gradients between pressure cells allowed for transport of cold, dry air from the Eastern Arctic (results not shown). However, the values of sea level pressure are less susceptible to local variations that may be exhibited in temperature data from stations records [Compo *et al.*, 2011]. Sea level pressure in February was representative of the broad scale temperature regimes occurring across the sites.

Albedo is known to play an important role in snowpack melt timing and rates of melt associated with snow ripening and declines in albedo [Blöschl, 1991]. In this work, albedo was used in two models and tended to be ranked higher in variable importance when used. Albedo was positively correlated with topographic parameters (elevation and slope, average $\rho=0.55$) and negatively correlated with thawing degree days – when the temperatures were greater than 0°C, the albedo values were low. Albedo conditions in the boreal forest are strongly tied to absorption of radiative energy, and are typically higher in the winter and decrease in value as the melt progresses, shrubs and trees emerge and snow cover declines [Warren and Wiscombe, 1980]. Wind speed was an important factor in the models when considering the maximum SCE for the season and the relative slope. Wind speed was negatively correlated with relative humidity ($\rho=-0.35$) and topography ($\rho=-0.34$) in the work, indicating the combined effect of these parameters on melt conditions. Wind speed, radiation and relative humidity, when combined, is considered to be just as important as temperature in melt for prediction of snow depletion [Zuzel and Cox, 1975]. Interestingly, the (maximum) count of precipitation days through the season was the only time precipitation was utilized to estimate the *rslop* logistic parameter. It is possible that precipitation does not play a strong role in the modeling the logistic parameters because it is poorly measured in NARR (Figure 4.3).

The reconstruction was used to estimate trends, highlighting how the SCE climatology may be applied to glean useful information regarding snow fractional depletion metrics. Three of the five index stations showed changes in their melt depletion metrics, although not all findings were statistically significant (90% confidence interval). Most stations showed declining initial melt date and melt termination dates, resulting in slightly faster melt rates but no change in duration of melt. However, the Mt. Ryan station illustrated an increased duration and a decline in melt rates that were significant. At

Bettles, the melt initiation did not change but the termination was reduced and thus the slope has declined (increased melt rate), although only the slope change was significant (p -value=0.01). At Eagle, all melt timing indices changed by about five days. Although declines in SWE and snow depth were noted for all stations, none of these declines were statistically significant. Eagle was the only site where the snow depth declined over the period at an 85% confidence interval. None of the timing changes associated with start and end dates of melt may be understood from looking at the declines in SWE/SD alone.

4.5 Conclusions

The paper describes a technique to utilize MODIS SCE data to capture key characteristics of melt timing and use this information to identify relationships between snow depletion, climate and topographic variables in subarctic Interior Alaskan systems. Nonlinear estimates of MODIS SCE data were representative of site-specific snow depletion timing, although some years were challenging to replicate and the reasons behind these poorly matched years are still under investigation. The approach was applied to estimate specific properties of the melt timing, such as maximum melt and date of snow off. The relationship between the melt timing indices and the snow cover depth was strong and provides an example of how a complete suite of snowmelt timing characteristics can be useful to define the nature of melt timing in relationship to snow cover properties. This is anticipated to be valuable in calculating timing characteristics required for estimates of SWE that are widely used in modeling approaches, and also for regional characterization of snow depletion timing that can inform modeling approaches or more complex data assimilation techniques.

The methods described in this paper will be particularly useful at a broad scale across ungaged basins of the north. These regions have little information on snow depletion timing other than models (i.e. reanalysis tools) and thus a data base to identify regional variations and patterns in snow depletion timing is needed. Additionally, the MODIS Terra and Aqua Earth-observing mission is planned to go offline in the coming years and will be replaced by newer platforms such as the Suomi National Polar-orbiting Partnership (NPP) and its VIIRS sensor. Defining snow depletion characteristics during this overlap period can assist to identify and determine if algorithms in the new sensors are operating at the same level as the previous sensors to replicate snow depletion patterns on a local and a broad scale.

Modeling to estimate the logistic parameters of the nonlinear regression function was successful based on training data sets, and these estimates were used to replicate the snow depletion regression. The climate variables had consistency between the types of models utilized and the estimated parameters. The main drivers of the logistic parameters of are climate indices relating to temperature, albedo and wind speed, along with topographic variables related to slope and aspect. Precipitation and relative humidity

were not as useful in estimating the logistic parameters, although this doesn't negate their importance in energy balance and snowmelt models outside of this application.

The utility of this work is shown by reconstructing the SCE depletion curve and calculating all metrics of snow timing, and then running a trends analysis over the long term (1979-2012) for the five index sites. The results indicate that changes in the sites can be observed in the melt timing that are distinct from trends in the snow depth or SWE alone. Plots of snow depth (Figure 4.7) exemplify as well the exploration of relationships between important parameters that are sparsely observed in the region. If a clear relationship can be understood between the long term reconstructed SCE data and these parameters, attempts can be made to calculate these based on SCE.

It is important to note that the ensemble machine learning tools determined to most successfully estimate relationships between the climate variables and snow depletion indices may fluctuate depending on the region under examination, data sets and also depending on the time interval that is used. However the process of model exploration and development described in this work may be useful in attempts to estimate relationships between snow depletion and weak predictors such as climate and other physiographic drivers.

The next steps in this research are to input the MODIS data into the Sacramento [Burnash *et al.*, 1973] rainfall-runoff model to estimate the changes to snow depletion patterns within meso-scale watersheds in the interior of Alaska. The work is part of a larger project to estimate changes in historical and future extreme hydroclimate events in watersheds in Interior Alaska.

4.6 Acknowledgements

The co-authors of this work wish to acknowledge the collaborative support of the National Weather Services' Alaska Pacific River Forecast Center, particularly Scott Lindsey, Ben Balk and Dave Streubel. The authors are grateful for internal review and valuable commentary provided by Dr. John Walsh. MODIS data processing tools were originally developed with assistance from staff at the Geographic Information Network for Alaska, located at the University of Alaska Fairbanks. Funding for this project was provided by the NOAA NESDIS Proving Ground project (NA08OAR432075), Alaska Climate Science Center and Natural Science Research Council of Canada.

4.7 Figures

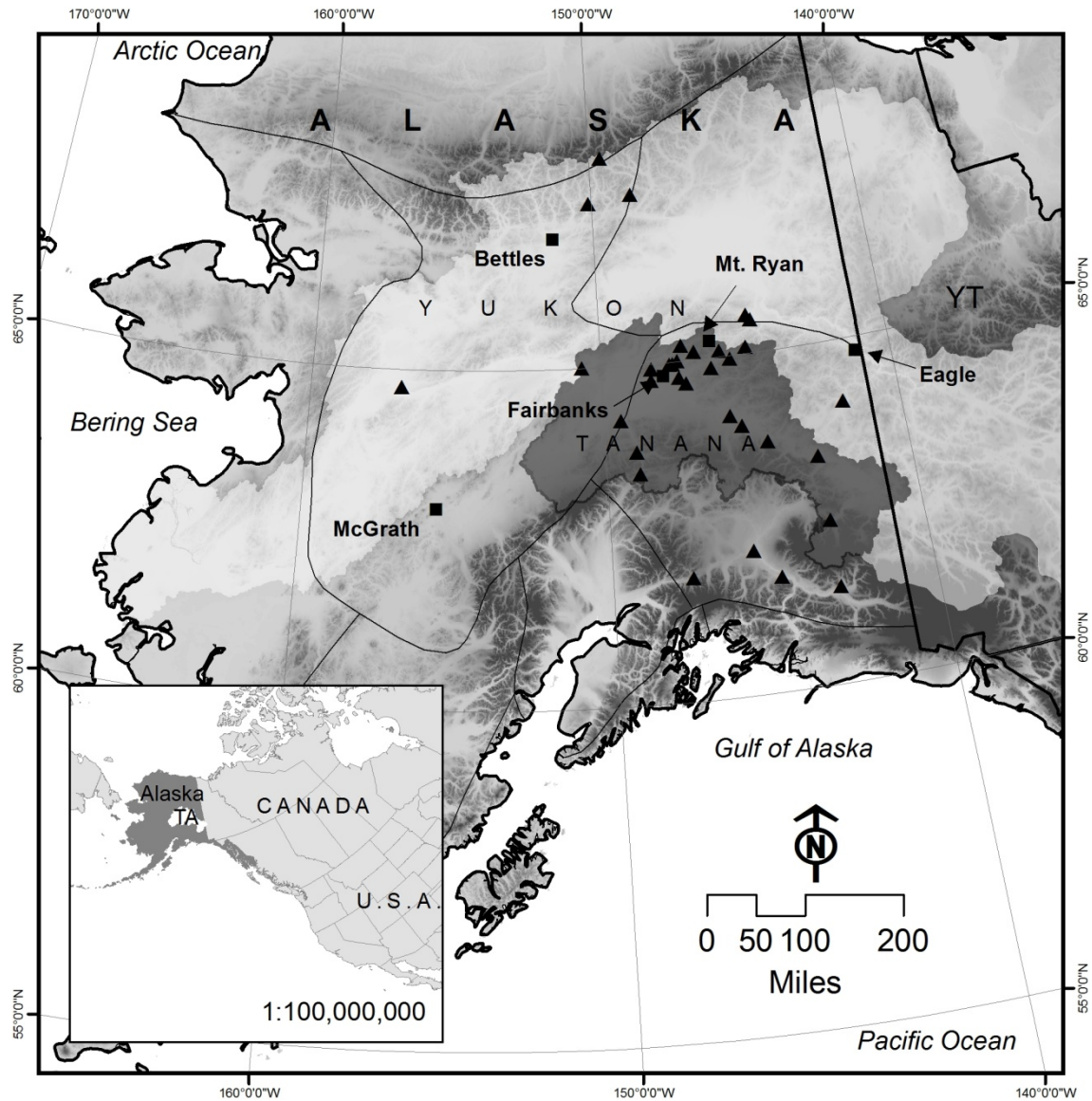


Figure 4.1 Study sites and their geographic location in Alaska. The 38 sites SNOTEL and GHCN sites (triangles) in the Interior regions of Alaska. The Alaska climate divisions are shown in black lines (Bieniek et al. 2012). Index sites are labeled on the map and shown with square boxes. The Tanana River basin is illustrated in transparent gray. The Yukon River basin is shown in transparent white.

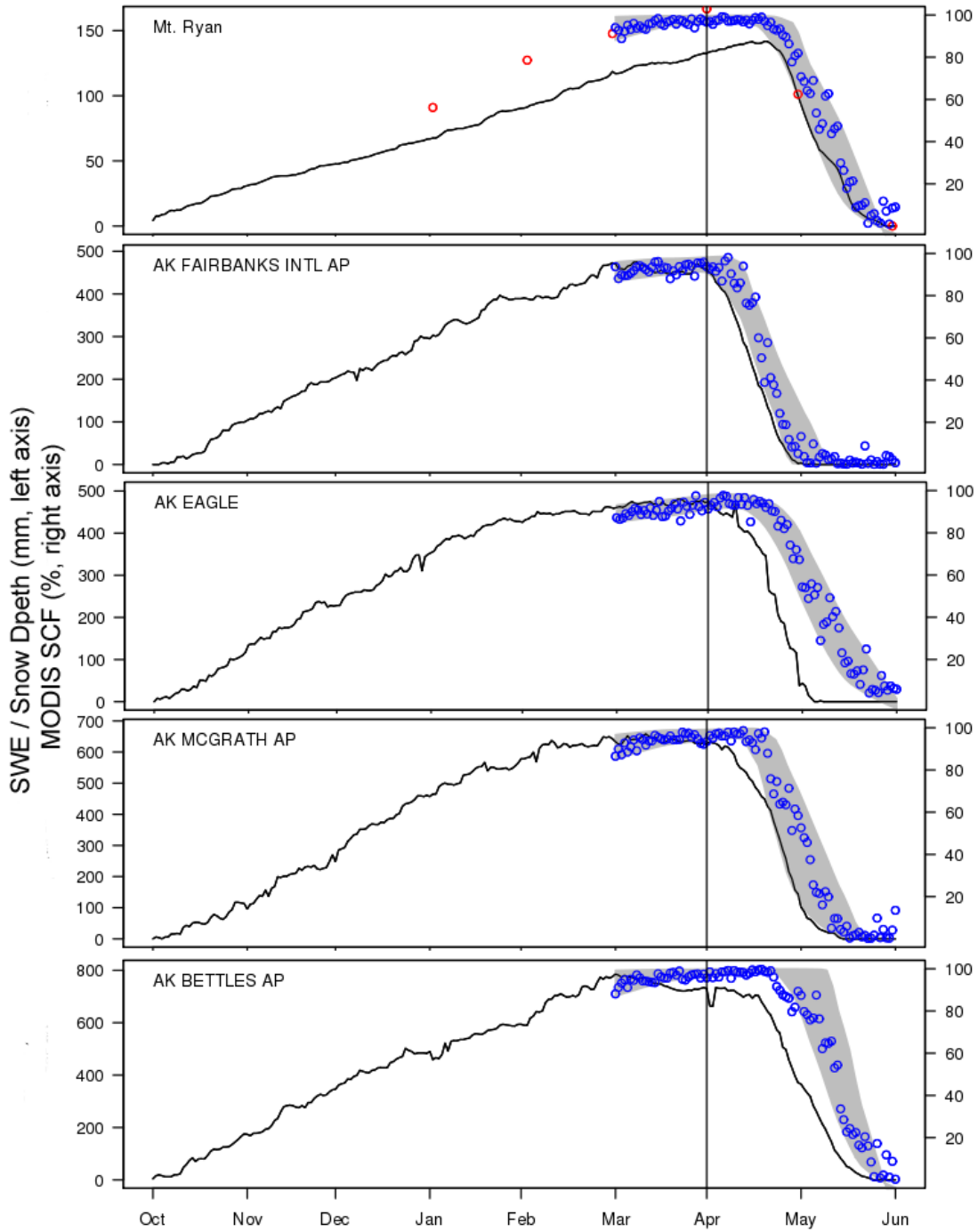


Figure 4.2 SNOTEL, NARR, snow course, and MODIS data for all index stations a) Mt.Ryan, b) Fairbanks Airport, c) Eagle, d) McGrath, and e) Bettles. Plots illustrate snow accumulation from SNOTEL SWE at the pillow or GHCN snow depth (black line, mm on left axis), SWE at the snow course (red open circles, mm on left axis, SNOTEL only), and MODIS SCE (blue circles, % on right axis), with the grey illustrating the MODIS SCE variability over the time period. The x-axis indicates months from October 1st through May 31st. The data are calculated as averages from 2000-2012.

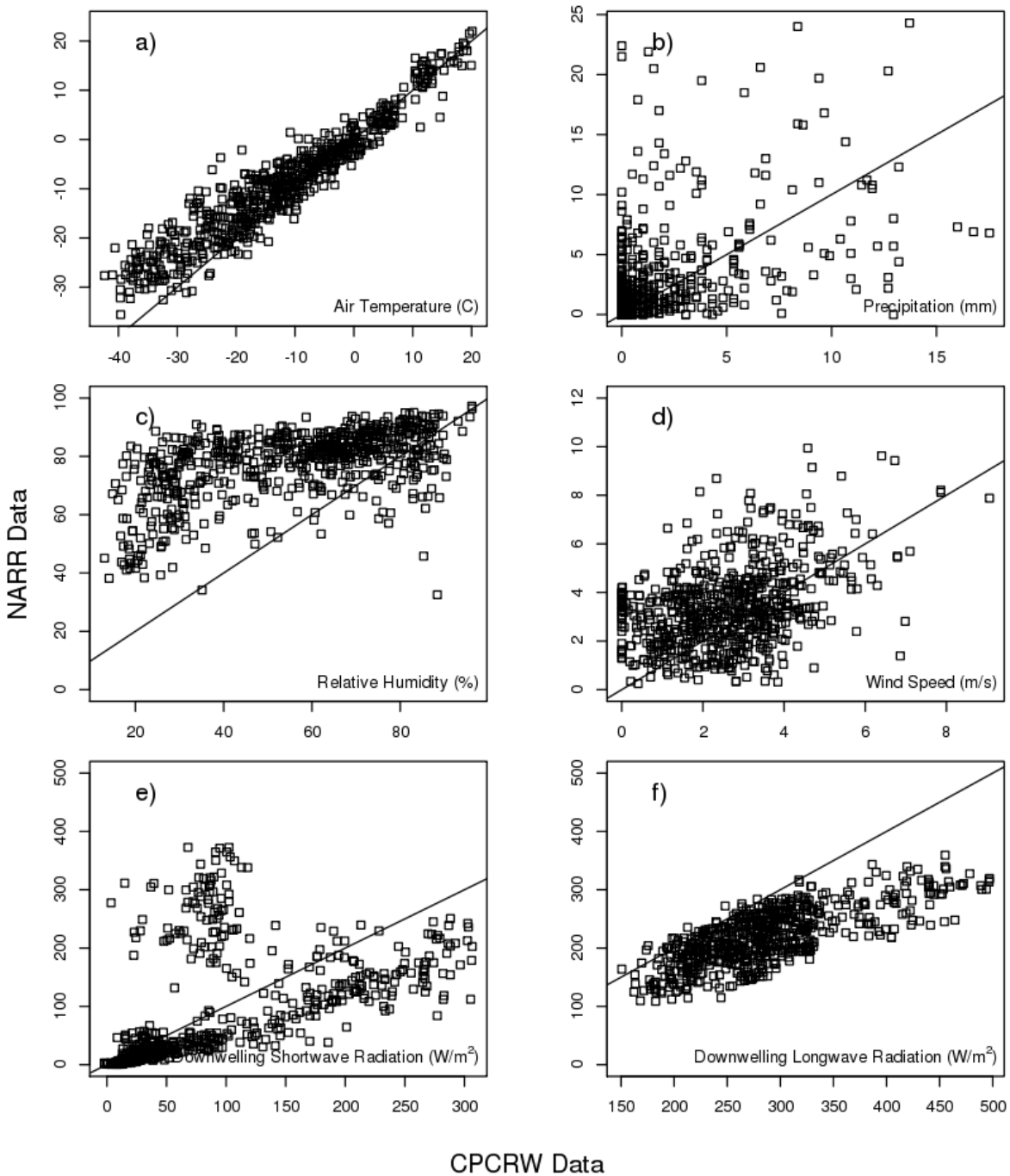


Figure 4.3 Inter-comparison with NARR data at the Caribou Poker Creek Research Watershed, located nearby Fairbanks, Alaska. CPRW data shown on x-axis, NARR data shown on y-axis. Data Source: CPRW database, 2007-2008, 2010-2011. Air temperature (a), precipitation (b), relative humidity (c), wind speed (d), downwelling shortwave (e) and longwave radiation (f).

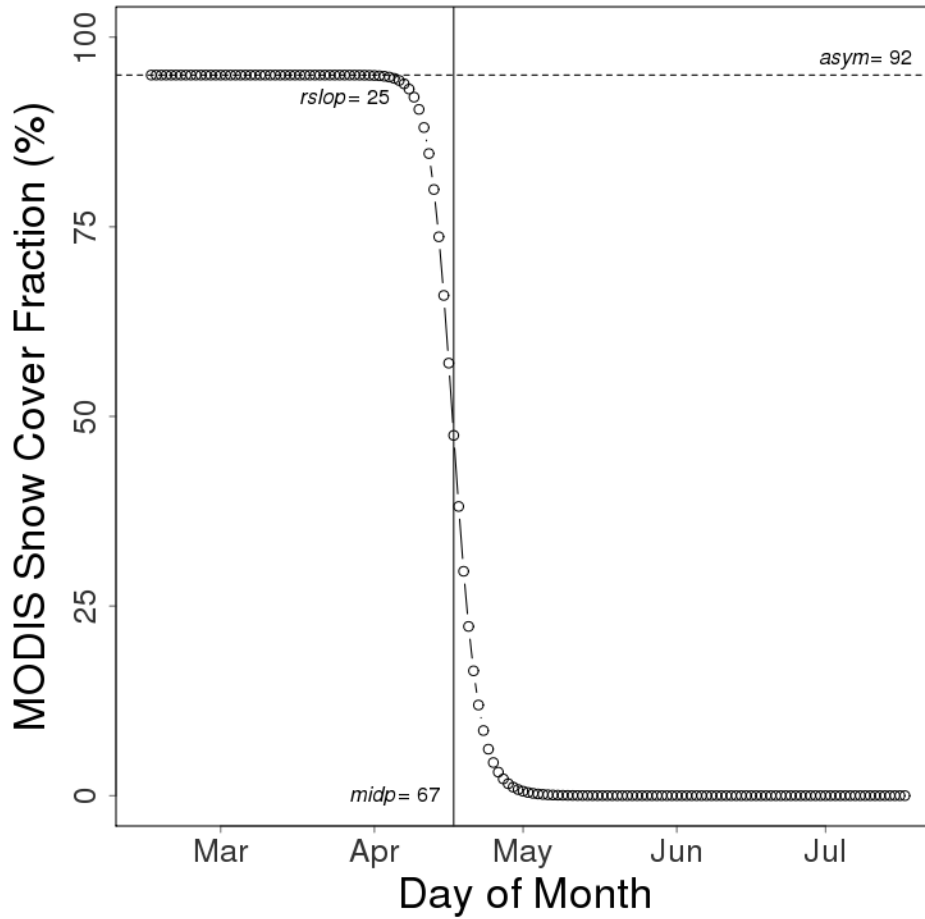


Figure 4.4 Example of the nonlinear regression function with sample values illustrated for *asym*, *midp* and *rslop*.

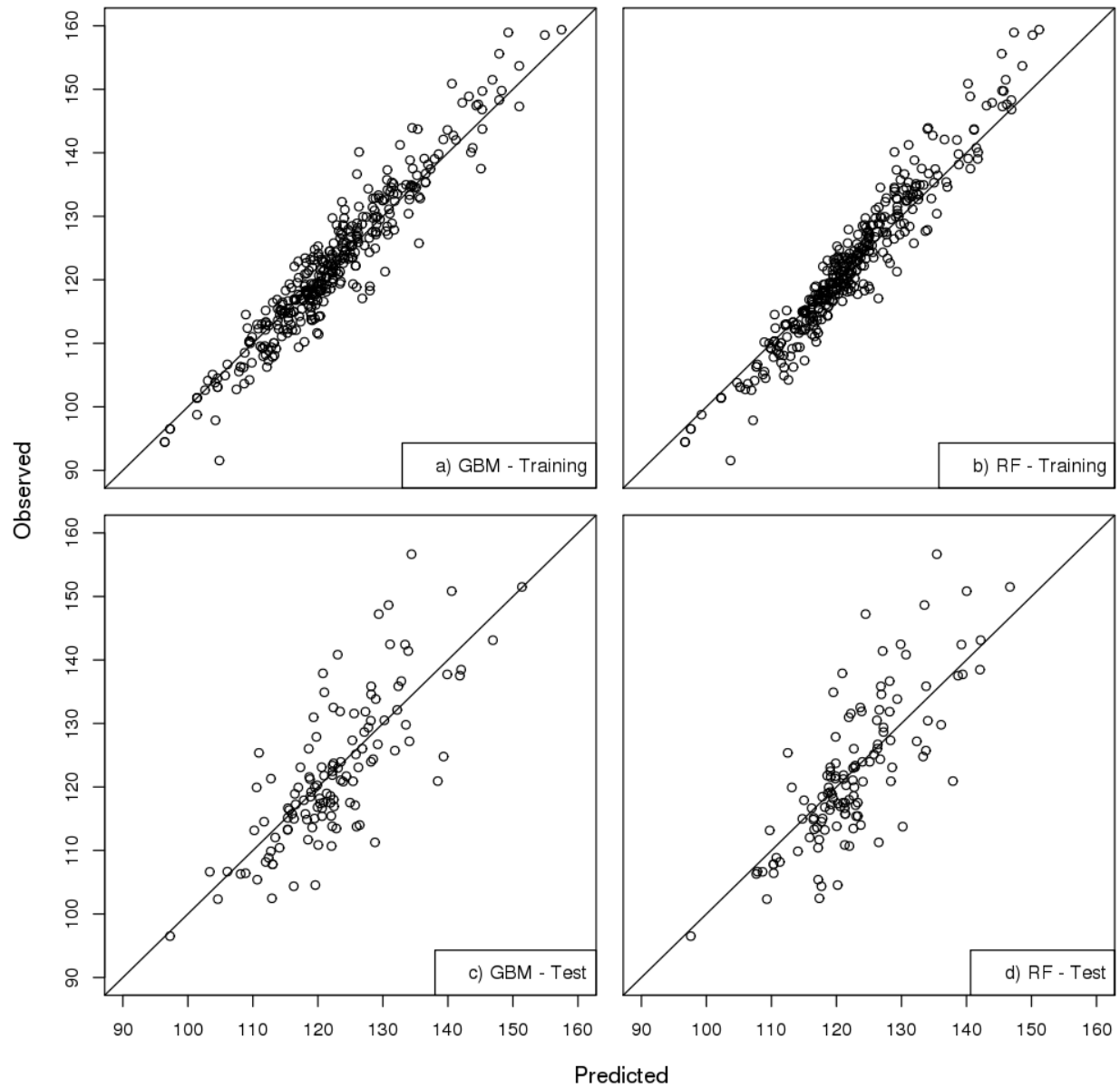


Figure 4.5 Model fits for the midpoint logistic parameter, predicted versus observed, for the a) GBM for the training data set and b) RF for the training data set, and c) GBM for the test data set and d) RF for the test data set. See Table 4.3 for model codes.

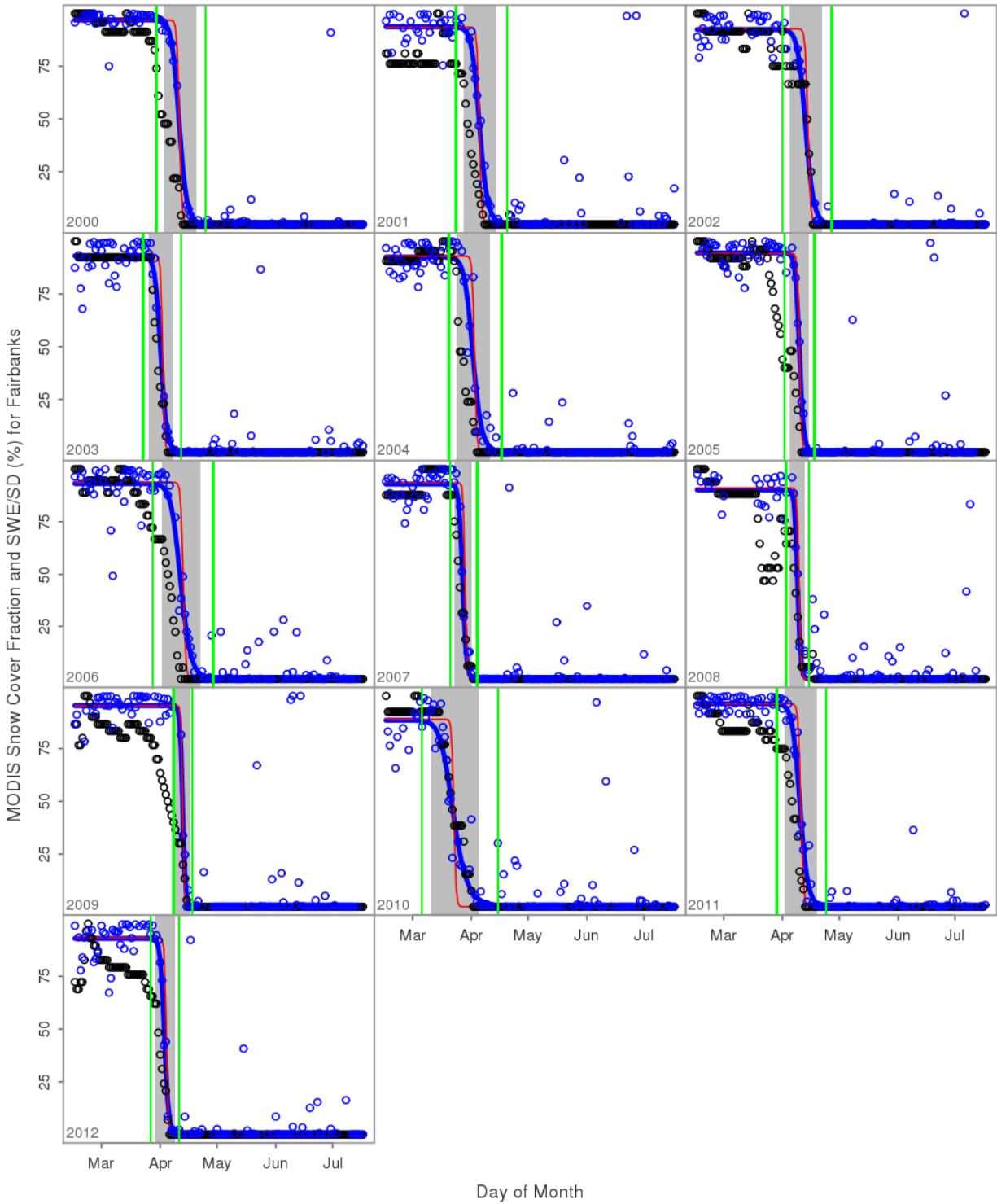


Figure 4.6 The Fairbanks GCHN climate station MODIS SCE observed and estimated. (USW00026411) Each panel represents a year from 2000-2012, dates are mid-month. The blue circles indicate the MODIS SCE, the black circles indicate the GHCN snow depth (mm), the blue line is the nonlinear regression model based on the MODIS snowmelt curves, and the red line is the recreated nonlinear regression model. Green straight lines illustrate the dates of snowmelt initiation/termination and the grey bar indicates the period of maximum melt.

4.8 Tables

Table 4.1 Stations used in the study with physiographic information (2000-2012). Index sites discussed in the text are bolded.

Station ID	Station Name	Elev (m)	Lat (dd)	Long (dd)	PC	AJMT (°C)	ATWP (mm)	ASWE /ASD (mm)
<i>SNOTEL</i>								
44Q07	Upper Chena	869	65.10	-144.93	C	-16.3	136	59
45O04	Granite Crk	378	63.95	-145.40	D	-19.8	87	33
45P03	Teuchet Creek	500	64.95	-145.52	D	-20.6	96	35
45Q02	Monument Creek	564	65.08	-145.87	D	-20.9	123	44
46P01	Munson Ridge	945	64.85	-146.20	D	-17.2	165	78
46Q01	Mt. Ryan	853	65.25	-146.15	D	-17.6	106	47
46Q02	Little Chena Ridge	610	65.12	-146.73	D	-15.5	110	40
48P01	Bonanza Creek	351	64.75	-148.30	D	-18.3	47	31
<i>GHCN</i>								
USC00501243	Cantwell 2E	656	63.40	-148.90	D	-17.2	114	281
USC00501466	Central #2	293	65.57	-144.77	D	-26	60	201
USC00501492	Chandalar Lake	556	67.51	-148.49	C	-27.1	26	456
USC00501497	Chandalar Shelt.	991	68.08	-149.56	C	-20.6	103	468
USC00501684	Chicken	415	64.09	-141.92	D	-29.5	54	156
USC00501987	Circle Hot Springs	285	65.49	-144.64	D	-27.5	60	209
USC00502339	Delta 6N	320	64.12	-145.75	D	-20.7	65	100
USC00502568	Dry Creek	412	63.68	-144.60	D	-22.4	92	177
USC00502707	Eielson Fld.	167	64.67	-147.10	D	-21.8	68	161
USC00503160	Ft Knox Mine	494	65.00	-147.34	D	-17.8	103	151
USC00503181	Fox 2 SE	358	64.96	-147.63	D	-18.5	40	210
USC00503212	Galena	46	64.74	-156.88	S	-23.9	125	261
USC00503275	Gilmore Creek	292	64.97	-147.51	D	-20.9	73	175
USC00503304	Glennallen	445	62.11	-145.53	D	-19.5	73	123
USC00504567	Kenny Lake 7SE	378	61.68	-144.76	D	-18.1	128	136
USC00504621	Keystone Ridge	488	64.92	-148.27	D	-16.2	98	231
USC00504971	Kobe Hill	244	64.19	-149.43	D	-21.3	90	245
USC00505644	Manley Hot Springs	99	65.00	-150.65	S/D	-28.3	73	118
USC00505778	McKinley Park	638	63.72	-148.97	D	-17.1	84	199
USC00505880	Mile 42 Steese	284	65.22	-147.17	D	-19.9	79	221
USC00506147	Nabesna	863	62.40	-143.00	D	-19.7	60	226
USC00506581	North Pole	146	64.76	-147.33	D	-24.1	79	195
USC00507513	Port Alcan	589				-26.2	36	90
USC00508409	Sheep Mtn Lodge	853	61.81	-147.50	D	-15.7	70	215
USC00509313	Tok	497	63.35	-143.04	D	-24.6	62	197
USC00509869	Wiseman	393	67.42	-150.11	C	-24.9	90	237
USW00026411	Fairbanks⁺	135	64.80	-147.88	D	-23.1	73	163
USW00026422	Eagle	245	64.79	-141.20	D	-23.2	93	188
USW00026510	McGrath*	104	62.96	-155.61	I	-22.3	166	257
USW00026533	Bettles*	205	66.92	-151.51	C	-24.7	142	309

Station identification code (ID); Elev, elevation; Lat, latitude (dd, decimal degrees); Long, longitude (dd, decimal degrees), PC, permafrost condition (C=continuous, D=discontinuous, S=sporadic, I=isolated); AJMT, average January mean temperature (°C); ATP, average total Oct-Mar precipitation (mm); and ASWE/SD, average winter snow water equivalent or average snow depth (mm).

⁺ Intl Airport

* Airport

Table 4.2 Climate variables and climate indices used to estimate asym, midpt and slope for the RF and GBM models.

Variables	Indices (Units)	Logistic Parameter
Temperature	Mean daily temperature for October to April 15 th (days)	
	Minimum daily temperature for October to April 15 th (days)	
	Mean daily temperature for December, January, February (degree)	<i>a, m, i</i>
	Maximum daily temperature for December, January, February (degree)	
	Count of freezing degree days for October to April 15 th (days)	
	Maximum cumulative sum of freezing degree days October to April 15 th (days)	
Precipitation	Maximum precipitation October to March (mm)	
	Precipitation days from October to March (days)	<i>i</i>
Albedo	Mean albedo for October to April 15 th (%)	
	Change in mean albedo from February to March (%)	
	Mean albedo in February (%)	<i>m, i</i>
	Mean albedo in March (%)	
Sea Level Pressure	Maximum daily average sea level pressure for December to February (Pa)	
	Mean daily average sea level pressure for February (Pa)	
	Mean daily average sea level pressure for March (Pa)	<i>a, m</i>
Relative humidity	Change in maximum relative humidity from February to March (%)	<i>m</i>
	Maximum relative humidity in March (%)	
Wind Speed	Mean wind speed for October to April 15 th (m/s)	
	Maximum wind speed in February (m/s)	
	Mean wind speed in March (m/s)	<i>a, i</i>
	Maximum wind speed in March (m/s)	
Radiation	Mean downward shortwave radiation for October to November (W/m ²)	
	Mean downward shortwave radiation for March (W/m ²)	
	Date of daily cumulative downward shortwave radiation change > 100 W/m ² (day)	<i>a</i>
Physiography	Mean aspect (degree)	
	Standard deviation aspect (degree)	<i>i</i>
	Range slope (degree)	<i>a</i>
	Longitude (decimal degrees)	

Table 4.3 Training and testing results for RF and GBM for all stations.

Logistic Params	Model	Method/Base Package	Model Params	RMSE	R²	P- value*
				Training		
<i>asym</i>	RF	rf/ randomForest	mtry	3.41	0.40	< 0.001
<i>midp</i>				7.82	0.48	< 0.001
<i>rslop</i>				30.80	0.27	< 0.001
<i>asym</i>	GBM	gbm/gbm	n.trees, shrinkage, interaction depth	3.51	0.34	< 0.001
<i>midp</i>				7.92	0.49	< 0.001
<i>rslop</i>				30.82	0.32	< 0.001

Params, Parameters; RMSE, root mean square error; R², r-squared; RF is random forest; GBM is gradient boosting

*with Bonferroni adjustment

Table 4.4 Snowmelt timing statistics for all sites based on the MODIS SCE nonlinear regression analysis as averages for the 2000-2012. The five index stations used to illustrate results are in bold.

Station ID	Station Name	Init. Date (Jday)	Term. Date (Jday)	Max. Melt (Jday)	Min. Melt (Jday)	Middle of Melt (Jday)	Dur. (days)	Rate
44Q07	Upper Chena	110	141	115	134	124	31	-7.3
45O04	Granite Crk	93	153	102	135	118	60	-3.4
45P03	Teuchet Creek	105	148	111	137	124	43	-3.9
45Q02	Monument Creek	106	151	113	140	126	46	-3.9
46P01	Munson Ridge	103	138	108	130	119	35	-5.5
46Q01	Mt. Ryan	114	148	120	141	130	34	-5.0
46Q02	Little Chena Ridge	106	146	112	137	124	40	-4.5
48P01	Bonanza Creek	102	125	106	121	113	23	-7.1
USC00501243	Cantwell 2E	99	177	111	153	132	77	-2.4
USC00501466	Central #2	114	128	116	126	121	14	-12.5
USC00501492	Chandalar Lake	121	172	129	159	144	50	-3.6
USC00501497	AK Chandalar Shelt.	129	172	136	162	149	43	-4.3
USC00501684	Chicken	111	128	113	125	119	18	-9.7
USC00501987	Circle Hot Springs	110	141	115	135	124	31	-6.0
USC00502339	Delta 6N	88	133	94	120	106	45	-4.0
USC00502568	Dry Creek	93	155	102	137	119	62	-2.7
USC00502707	Eielson Fld.	104	120	106	117	111	16	-11.7
USC00503160	Ft Knox Mine	101	136	107	128	117	35	-5.2
USC00503181	Fox 2 SE	101	123	104	119	111	22	-7.2
USC00503212	Galena	118	140	122	136	129	21	-8.0
USC00503275	Gilmore Creek	101	123	104	119	111	22	-7.2
USC00503304	Glennallen	101	136	106	128	117	35	-4.6
USC00504567	Kenny Lake 7SE	93	167	104	144	124	73	-2.5
USC00504621	Keystone Ridge	99	138	105	128	116	39	-4.5
USC00504971	Kobe Hill	102	132	107	125	116	29	-8.9
USC00505644	Manley Hot Springs	108	130	111	126	118	23	-8.5
USC00505778	McKinley Park	95	153	103	134	118	58	-3.8
USC00505880	Mile 42 Steese	113	140	117	134	125	27	-6.5
USC00506147	Nabesna	92	171	103	144	124	79	-2.9
USC00506581	North Pole	104	120	106	117	111	16	-11.7
USC00507513	Port Alcan	107	132	111	127	119	25	-7.1
USC00508409	Sheep Mtn Lodge	112	165	120	151	135	52	-3.9
USC00509313	Tok	103	133	108	127	117	30	-5.6
USC00509869	Wiseman	119	154	125	147	135	35	-4.9
USW00026411	Fairbanks⁺	101	123	104	119	111	22	-7.2
USW00026422	Eagle	107	154	114	143	128	47	-3.5
USW00026510	McGrath*	113	132	116	129	122	19	-8.4
USW00026533	Bettles*	125	140	128	137	132	15	-12.4

Init., Initiation of melt depletion; Term., termination of melt depletion; Max. Melt, maximum melt depletion; Min. Melt, minimum melt depletion; Middle of melt, midpoint of melt; Dur., duration of melt in days; Rate, rate of melt duration; Jday, Julian Date of year

⁺International Airport

* Airport

4.9 References

- Akyurek, Z., D. K. Hall, G. A. Riggs, and A. Sensoy (2010), Evaluating the utility of the ANSA blended snow cover product in the mountains of eastern Turkey, *Int. J. Remote Sens.*, 31(14), 3727-3744.
- Anderson, E. (2006), Snow Accumulation and Ablation Model - SNOW17. http://www.nws.noaa.gov/oh/hrl/nwsrfs/users_manual/part2/_pdf/22snow17.pdf.
- Anderson, E. A. (1976), A point energy and mass balance model of a snow cover.
- Aurela, M., T. Laurila, and J.-P. Tuovinen (2004), The timing of snow melt controls the annual CO₂ balance in a subarctic fen, *Geophys. Res. Lett.*, 31(16), L16119.
- Bates, D. M., and D. G. Watts (1988), Nonlinear Regression Analysis and Its Applications, *Analysis*, 60(4), 856865.
- Bieniek, P. A., U. S. Bhatt, R. L. Thoman, H. Angeloff, J. Partain, J. Papineau, F. Fritsch, E. Holloway, J. E. Walsh, and C. Daly (2012), Climate Divisions for Alaska Based on Objective Methods, *J. Appl. Meteorol. Clim.*, 51(7), 1276-1289.
- Blöschl, G. (1991), The influence of uncertainty in air temperature and albedo on snowmelt, *Nord. Hydrol.*, 22(2), 95-108.
- Blöschl, G., D. Gutknecht, and R. Kirnbauer (1991), Distributed Snowmelt Simulations in an Alpine Catchment: 2. Parameter Study and Model Predictions, *Water Resour. Res.*, 27(12), 3181-3188.
- Breiman, L. (2001), Random forests, *Mach. Learn.*, 45(1), 5-32.
- Breiman, L., and A. Cutler (1993), A deterministic algorithm for global optimization, *Math. Prog.*, 58(1), 179-199.
- Breiman, L., and A. Cutler (2014), Random forests – Classification manual. http://www.stat.berkeley.edu/~breiman/RandomForests/cc_manual.htm.
- Brodzik, M., and R. Armstrong (2013), Northern Hemisphere EASE-Grid 2.0 Weekly Snow Cover and Sea Ice Extent. Version 4., edited, National Snow and Ice Data Center, Boulder, Colorado USA.
- Bronaugh, D., and A. Werner (2009), Package ‘zyp’. *CRAN Repository*.
- Brown, R., C. Derksen, and L. Wang (2010), A multi-data set analysis of variability and change in Arctic spring snow cover extent, 1967–2008, *J. Geophys. Res.: Atmos.*, 115(D16), D16111.
- Burnash, R. J. E., R. L. Ferral, and R. A. McGuire (1973), A generalized streamflow simulation system. Rep, 204 pp., Joint Federal-State River Forecast Center, Sacramento, CA.
- Buttle, J., and J. McDonnell (1987), Modelling the areal depletion of snowcover in a forested catchment, *Journal of Hydrology*, 90(1), 43-60.
- Carey, S. K., and M. Woo (2001), Spatial variability of hillslope water balance, Wolf Creek basin, subarctic Yukon, *Hydrol. Process.*, 15, 3113-3132.

- Chapin III, F. S., et al. (2005), Role of land-surface changes in arctic summer warming, *Science*, 310(5748), 657-660.
- Choi, G., D. A. Robinson, and S. Kang (2010), Changing Northern Hemisphere Snow Seasons, *J. Clim.*, 23, 5305-5310.
- Choi, W., S. J. Kim, P. F. Rasmussen, and A. R. Moore (2009), Use of the North American Regional Reanalysis for hydrological modelling in Manitoba, *Can. Water Resour. J.*, 34(1), 17-36.
- Cline, D. W., R. C. Bales, and J. Dozier (1998), Estimating the spatial distribution of snow in mountain basins using remote sensing and energy balance modeling, *Water Resour. Res.*, 34(5), 1275-1285.
- Compo, G. P., J. S. Whitaker, P. D. Sardeshmukh, N. Matsui, R. Allan, X. Yin, B. Gleason, R. Vose, G. Rutledge, and P. Bessemoulin (2011), The twentieth century reanalysis project, *Q. J. Roy. Meteor. Soc.*, 137(654), 1-28.
- Derksen, C., and R. Brown (2012), Spring snow cover extent reductions in the 2008–2012 period exceeding climate model projections, *Geophys. Res. Lett.*, 39(19), L19504.
- Déry, S. J., V. V. Salomonson, M. Stieglitz, D. K. Hall, and I. Appel (2005), An approach to using snow areal depletion curves inferred from MODIS and its application to land surface modelling in Alaska, *Hydrol. Process.*, 19(14), 2755-2774.
- Duffy, P. A., J. E. Walsh, J. M. Graham, D. H. Mann, and T. S. Rupp (2005), Impacts of large-scale atmospheric-ocean variability on Alaskan fire season severity., *Ecol. Appl.*, 15(4), 1317-1330.
- Dunn, O. J. (1961), Multiple comparisons among means, *J. Amer. Statistical Assoc.*, 56(293), 52-64.
- Durand, M., N. P. Molotch, and S. A. Margulis (2008), Merging complementary remote sensing datasets in the context of snow water equivalent reconstruction, *Remote Sens. Environ.*, 112(3), 1212-1225.
- Dye, D. G. (2002), Variability and trends in the annual snow-cover cycle in Northern Hemisphere land areas, 1972-2000, *Hydrol. Process.*, 16, 3065-3077.
- Elith, J., J. R. Leathwick, and T. Hastie (2008), A working guide to boosted regression trees, *J. Anim. Ecol.*, 77(4), 802-813.
- Faria, D., J. Pomeroy, and R. Essery (2000), Effect of covariance between ablation and snow water equivalent on depletion of snow-covered area in a forest, *Hydrol. Process.*, 14(15), 2683-2695.
- Foster, J. L., D. A. Robinson, D. K. Hall, and T. W. Estilow (2008), Spring snow melt timing and changes over Arctic lands, *Polar Geogr.*, 31(3-4), 145-157.
- Foster, J. L., D. K. Hall, J. B. Eylander, G. A. Riggs, S. V. Nghiem, M. Tedesco, E. Kim, P. M. Montesano, R. E. Kelly, and K. A. Casey (2011), A blended global snow product using visible, passive microwave and scatterometer satellite data, *Int. J. Remote Sens.*, 32(5), 1371-1395.

- Friedman, J. H. (2001), Greedy function approximation: a gradient boosting machine.(English summary), *Ann. Statist.*, 29(5), 1189-1232.
- Friedman, J. H. (2002), Stochastic gradient boosting, *Comput. Stat. Data Anal.*, 38(4), 367-378.
- Gao, Y., H. Xie, N. Lu, T. Yao, and T. Liang (2010), Toward advanced daily cloud-free snow cover and snow water equivalent products from Terra–Aqua MODIS and Aqua AMSR-E measurements, *Journal of Hydrology*, 385(1–4), 23-35.
- Gelfan, A., J. Pomeroy, and L. Kuchment (2004), Modeling forest cover influences on snow accumulation, sublimation, and melt, *J. Hydrometeorol.*, 5(5), 785-803.
- Gesch, D., M. Oimoen, S. Greenlee, C. Nelson, M. Steuck, and D. Tyler (2002), The National Elevation Dataset: Photogrammetric Engineering and Remote Sensing, 68(1), 5-11.
- Hall, D. K., and G. A. Riggs (2007), Accuracy assessment of the MODIS snow products, *Hydrological Processes*, 21(12), 1534-1547.
- Hall, D. K., G. A. Riggs, and V. V. Salomonson (2006), MODIS/Terra Snow Cover Daily L3 Global 500m Grid V005, 2000-Daily Updates., edited, National Snow and Ice Data Center, Boulder, Colorado USA.
- Hall, D. K., J. L. Foster, S. Kumar, J. Y. Chien, and G. A. Riggs (2012), Improving the accuracy of the AFWA-NASA (ANSA) blended snow-cover product over the Lower Great Lakes region, *Hydrol. Earth Syst. Sci. Discuss*, 9, 1141-1161.
- Hall, D. K., G. A. Riggs, V. V. Salomonson, J. Barton, K. Casey, J. Chien, N. DiGirolamo, A. Klein, H. Powell, and A. Tait (2001), Algorithm theoretical basis document (ATBD) for the MODIS snow and sea ice-mapping algorithms. Rep.
- Hancock, T., R. Put, D. Coomans, Y. Vander Heyden, and Y. Everingham (2005), A performance comparison of modern statistical techniques for molecular descriptor selection and retention prediction in chromatographic QSRR studies, *Chemometrics Intellig. Lab. Syst.*, 76(2), 185-196.
- Hess, J. C., C. A. Scott, G. L. Hufford, and M. D. Fleming (2001), El Niño and its impact on fire weather conditions in Alaska, *Int. J. Wildland Fire*, 10(1), 1-13.
- Hinzman, L. D., et al. (2005), Evidence and implications of recent climate change in northern Alaska and other Arctic regions, *Clim. Change*, 72, 251-298.
- Hock, R. (2003), Temperature index melt modelling in mountain areas, *Journal of Hydrology*, 282, 104-115.
- Kane, D. L., R. E. Gieck, and L. D. Hinzman (1997), Snowmelt Modeling at Small Alaskan Arctic Watershed, *J. Hydrolog. Eng.*, 2(4), 204-210.

- Kane, V. R., A. R. Gillespie, R. McGaughey, J. A. Lutz, K. Ceder, and J. F. Franklin (2008), Interpretation and topographic compensation of conifer canopy self-shadowing, *Remote Sens. Environ.*, *112*(10), 3820-3832.
- Kasischke, E. S., et al. (2010), Alaska's changing fire regime - implications for the vulnerability of its boreal forests This article is one of a selection of papers from The Dynamics of Change in Alaska's Boreal Forests: Resilience and Vulnerability in Response to Climate Warming, *Can. J. For. Res.*, *40*(7), 1313-1324.
- Kawanishi, T., T. Sezai, Y. Ito, K. Imaoka, T. Takeshima, Y. Ishido, A. Shibata, M. Miura, H. Inahata, and R. W. Spencer (2003), The Advanced Microwave Scanning Radiometer for the Earth Observing System (AMSR-E), NASDA's contribution to the EOS for global energy and water cycle studies, *IEEE Trans. Geosci. Remote*, *41*(2), 184-194.
- Kendall, M. G. (1975), *Rank Correlation Methods*, Griffin, London.
- Kirdyanov, A., M. Hughes, E. Vaganov, F. Schweingruber, and P. Silkin (2003), The importance of early summer temperature and date of snow melt for tree growth in the Siberian Subarctic, *Trees-Struct. Funct.*, *17*(1), 61-69.
- Klein, A. G., D. K. Hall, and G. A. Riggs (1998), Improving snow cover mapping in forests through the use of a canopy reflectance model, *Hydrol. Process.*, *12*(10-11), 1723-1744.
- Kuhn, M. (2008), Building predictive models in R using the caret package, *J. Stat. Softw.*, *28*(5), 1-26.
- Kuhn, M., J. Wing, S. Weston, A. Williams, C. Keefer, A. Engelhardt, and T. Cooper (2013), *Caret: Classification and Regression Training*. R package version 5.15-052, edited.
- Lader, R. (2014), *A users guide to reanalysis products in Alaska*, University of Alaska Fairbanks, Fairbanks, Alaska.
- Liston, G. E. (1999), Interrelationships among snow distribution, snowmelt, and snow cover depletion: Implications for atmospheric, hydrologic, and ecologic modeling, *J. Appl. Meteor.*, *38*(10), 1474-1487.
- Liston, G. E., and C. A. Hiemstra (2011), The changing cryosphere: Pan-Arctic snow trends (1979-2009), *J. Clim.*, *24*(21), 5691-5712.
- Liu, J., R. A. Melloh, C. E. Woodcock, R. E. Davis, and E. S. Ochs (2004), The effect of viewing geometry and topography on viewable gap fractions through forest canopies, *Hydrol. Process.*, *18*(18), 3595-3607.
- Liu, J., C. E. Woodcock, R. A. Melloh, R. E. Davis, C. McKenzie, and T. H. Painter (2008), Modeling the view angle dependence of gap fractions in forest canopies: Implications for mapping fractional snow cover using optical remote sensing, *J. Hydrometeorol.*, *9*(5), 1005-1019.

- Liu, Y., C. D. Peters-Lidard, S. Kumar, J. L. Foster, M. Shaw, Y. Tian, and G. M. Fall (2013), Assimilating satellite-based snow depth and snow cover products for improving snow predictions in Alaska, *Advances in Water Resources*, 54, 208-227.
- Luce, C. H., D. G. Tarboton, and K. R. Cooley (1999), Sub-grid parameterization of snow distribution for an energy and mass balance snow cover model, *Hydrol. Process.*, 13(12), 1921-1933.
- Mann, H. B. (1945), Nonparametric tests against trend, *Econometrica*, 13, 245-259.
- Markovic, M., C. G. Jones, K. Winger, and D. Paquin (2009), The surface radiation budget over North America: gridded data assessment and evaluation of regional climate models, *Int. J. Climatol.*, 29(15), 2226-2240.
- McDonald, K. C., J. S. Kimball, E. Njoku, R. Zimmermann, and M. Zhao (2004), Variability in Springtime Thaw in the Terrestrial High Latitudes: Monitoring a Major Control on the Biospheric Assimilation of Atmospheric CO₂ with Spaceborne Microwave Remote Sensing, *Earth Interact.*, 8(20), 1-23.
- Menne, M. J., I. Durre, R. S. Vose, B. E. Gleason, and T. G. Houston (2012), An overview of the global historical climatology network-daily database, *J. Atmos. Ocean. Tech.*, 29(7), 897-910.
- Mesinger, F., et al. (2006), North American Regional Reanalysis, *B. Am. Meteorol. Soc.*, 87(3), 343-360.
- Metcalfe, R., and J. Buttle (1998), A statistical model of spatially distributed snowmelt rates in a boreal forest basin, *Hydrol. Process.*, 12(1011), 1701-1722.
- Mölders, N., and G. Kramm (2010), A case study on wintertime inversions in Interior Alaska with WRF, *Atmos. Res.*, 95(2), 314-332.
- Molotch, N., S. Fassnacht, R. Bales, and S. Helfrich (2004), Estimating the distribution of snow water equivalent and snow extent beneath cloud cover in the Salt–Verde River basin, Arizona, *Hydrol. Process.*, 18(9), 1595-1611.
- Molotch, N. P. (2009), Reconstructing snow water equivalent in the Rio Grande headwaters using remotely sensed snow cover data and a spatially distributed snowmelt model, *Hydrol. Process.*, 23(7), 1076-1089.
- Molotch, N. P., and R. C. Bales (2006), SNOTEL representativeness in the Rio Grande headwaters on the basis of physiographics and remotely sensed snow cover persistence, *Hydrol. Process.*, 20(4), 723-739.
- Molotch, N. P., and S. A. Margulis (2008), Estimating the distribution of snow water equivalent using remotely sensed snow cover data and a spatially distributed snowmelt model: A multi-resolution, multi-sensor comparison, *Advances in Water Resources*, 31(11), 1503-1514.
- Nghiem, S. V., and W.-Y. Tsai (2001), Global snow cover monitoring with spaceborne Ku-band scatterometer, *IEEE Trans. Geosci. Remote*, 39(10), 2118-2134.

- NRCS (2013), SNOTEL Data & Products. Alaska Region. Updated Daily. <http://www.wcc.nrcs.usda.gov/snotel/Alaska/alaska.html>, edited.
- Oelke, C., T. J. Zhang, and M. C. Serreze (2004), Modeling evidence for recent warming of the Arctic soil thermal regime, *Geophys. Res. Lett.*, *31*(7), -.
- Painter, T. H., K. Rittger, C. McKenzie, P. Slaughter, R. E. Davis, and J. Dozier (2009), Retrieval of subpixel snow covered area, grain size, and albedo from MODIS, *Remote Sens. Environ.*, *113*(4), 868-879.
- Parajka, J., and G. Blöschl (2008), Spatio-temporal combination of MODIS images – potential for snow cover mapping, *Water Resour. Res.*, *44*(3), W03406.
- Parnell, S., D. Blumer, B. Keith, D. Robinson, E. Hunsinger, D. Howell, and E. Sandberg (2012), US Census 2012 - Alaska Population Overview, edited, Department of Labor and Workforce Development, Research and Analysis Section. US Federal Government.
- Pinheiro, J. C., and D. M. Bates (2000), *Mixed effects models in S and S-PLUS*, Springer Verlag.
- Pomeroy, J. W., and R. J. Granger (1997), Sustainability of the western Canadian boreal forest under changing hydrological conditions. I. Snow accumulation and ablation, *IAHS Pub.*, *240*, 237-242.
- Raleigh, M. S., K. Rittger, C. E. Moore, B. Henn, J. A. Lutz, and J. D. Lundquist (2013), Ground-based testing of MODIS fractional snow cover in subalpine meadows and forests of the Sierra Nevada, *Remote Sens. Environ.*, *128*(0), 44-57.
- Ramage, J., and K. A. Semmens (2012), Reconstructing snowmelt runoff in the Yukon River basin using the SWEHydro model and AMSR-E observations, *Hydrol. Process.*
- Ramage, J. M., and B. L. Isacks (2003), Interannual variations of snowmelt and refreeze timing on southeast-Alaskan icefields, USA, *J. of Glaciolo.*, *49*(164), 102-116.
- Ramage, J. M., J. D. Apgar, R. A. McKenney, and W. Hanna (2007), Spatial variability of snowmelt timing from AMSR-E and SSM/I passive microwave sensors, Pelly River, Yukon Territory, Canada, *Hydrol. Process.*, *21*(12), 1548-1560.
- Rango, A., and J. Martinec (1979), Application of a snowmelt-runoff model using Landsat data, *Nordic Hydrology*, *10*(4), 225-238.
- Ridgeway, G. (1999), The state of boosting, *Comput. Sci. Stat.*, 172-181.
- Ridgeway, G. (2012), Generalized Boosted Models: A guide to the gbm package, *Update*.
- Rittger, K., T. H. Painter, and J. Dozier (2013), Assessment of methods for mapping snow cover from MODIS, *Advances in Water Resources*, *51*, 367-380.
- Ritz, C. (2010), Toward a unified approach to dose–response modeling in ecotoxicology, *Environ. Toxicol. Chem.*, *29*(1), 220-229.
- Ritz, C., and J. C. Streibig (2008), *Nonlinear regression with R*, Springer, New York, NY.

- Rosenthal, W., and J. Dozier (1996), Automated mapping of montane snow cover at subpixel resolution from the Landsat Thematic Mapper, *Water Resour. Res.*, 32(1), 115-130.
- Salomonson, V., and I. Appel (2004), Estimating fractional snow cover from MODIS using the normalized difference snow index, *Remote Sens. Environ.*, 89(3), 351-360.
- Semmens, K. A., and J. Ramage (2012), Investigating correlations between snowmelt and forest fires in a high latitude snowmelt dominated drainage basin, *Hydrol. Process.*, 26, 2608-2617.
- Sen, P. K. (1968), Estimates of the regression coefficient based on Kendall's tau., *J. Amer. Statistical Assoc.*, 63, 1379-1389.
- Serreze, M. C., M. P. Clark, R. L. Armstrong, D. A. McGinnis, and R. S. Pulwarty (1999), Characteristics of the western United States snowpack from snowpack telemetry(SNOTEL) data, *Water Resour. Res.*, 35(7), 2145-2160.
- Serreze, M. C., D. H. Bromwich, M. P. Clark, A. J. Etringer, T. J. Zhang, and R. Lammers (2002), Large-scale hydro-climatology of the terrestrial Arctic drainage system, *J. Geophys. Res.: Atmos.*, 108(D2).
- Shamir, E., and K. P. Georgakakos (2007), Estimating snow depletion curves for American River basins using distributed snow modeling, *Journal of Hydrology*, 334(1-2), 162-173.
- Simic, A., R. Fernandes, R. Brown, P. Romanov, and W. Park (2004), Validation of VEGETATION, MODIS, and GOES + SSM/I snow-cover products over Canada based on surface snow depth observations, *Hydrol. Process.*, 18(6), 1089-1104.
- Stewart, I. T., D. R. Cayan, and M. D. Dettinger (2005), Changes toward earlier streamflow timing across Western North America, *J. Clim.*, 18, 1136-1155.
- Storck, P., D. P. Lettenmaier, and S. M. Bolton (2002), Measurement of snow interception and canopy effects on snow accumulation and melt in a mountainous maritime climate, Oregon, United States, *Water Resour. Res.*, 38(11), 1223.
- Streibig, J. C., M. Rudemo, and J. E. Jensen (1993), Dose-Response Curves and Statistical Models., in *Herbicide Bioassays*, edited by P. Kudsk and J. C. Streibig, pp. 29-55, CRC Press, Boca Raton.
- Strobl, C., J. Malley, and G. Tutz (2009), An introduction to recursive partitioning: rationale, application, and characteristics of classification and regression trees, bagging, and random forests, *Psychol. Methods*, 14(4), 323.
- Strobl, C., A.-L. Boulesteix, T. Kneib, T. Augustin, and A. Zeileis (2008), Conditional variable importance for random forests, *BMC Bioinformatics*, 9(1), 307.
- Sturm, M., and A. M. Wagner (2010), Using repeated patterns in snow distribution modeling: An Arctic example, *Water Resour. Res.*, 46(12), W12549.

- Tedesco, M., M. Brodzik, R. Armstrong, M. Savoie, and J. Ramage (2009), Pan arctic terrestrial snowmelt trends (1979–2008) from spaceborne passive microwave data and correlation with the Arctic Oscillation, *Geophys. Res. Lett.*, *36*(21).
- Theil, H. (1950a), A rank-invariant method of linear and polynomial regression analysis, I., *Nederlands Akad. Wetensch. Proc.*, *53*, 386-392.
- Theil, H. (1950b), A rank-invariant method of linear and polynomial regression analysis, II., *Nederlands Akad. Wetensch. Proc.*, *53*, 521-525.
- Theil, H. (1950c), A rank-invariant method of linear and polynomial regression analysis, III., *Nederlands Akad. Wetensch. Proc.*, *53*, 1397-1412.
- Trujillo, E., N. P. Molotch, M. L. Goulden, A. E. Kelly, and R. C. Bales (2012), Elevation-dependent influence of snow accumulation on forest greening, *Nature Geosci.*, *5*(10), 705-709.
- USGS (2011), MODIS Reprojection Tool User's Manual, Release 4.1 (https://lpdaac.usgs.gov/tools/modis_reprojection_tool), edited, Land Processes DAAC. USGS Earth Resources Observation and Science (EROS) Center.
- Wang, L., C. Derksen, R. Brown, and T. Markus (2013), Recent changes in pan-Arctic melt onset from satellite passive microwave measurements, *Geophys. Res. Lett.*, *40*(3), 522-528.
- Wang, L., M. Sharp, R. Brown, C. Derksen, and B. Rivard (2005), Evaluation of spring snow covered area depletion in the Canadian Arctic from NOAA snow charts, *Remote Sens. Environ.*, *95*(4), 453-463.
- Wang, X. L., and V. R. Swail (2001), Changes in extreme wave heights in northern hemisphere oceans and related atmospheric circulation regimes, *J. Clim.*, *14*, 2204-2221.
- Warren, S. G. and Wiscombe, W. J. 1980. A model for the spectral albedo of snow-II: snow containing atmospheric aerosols, *J. Atmos. Sci.*, *37*, 2734–2745.
- Westerling, A. L., H. G. Hidalgo, D. R. Cayan, and T. W. Swetnam (2006), Warming and earlier spring increase Western U.S. forest wildfire activity, *Science*, *313*, 940-943.
- Whitfield, P. H. (2013), Is ‘Centre of Volume’ a robust indicator of changes in snowmelt timing?, *Hydrol. Process.*
- Williams, C., R. Vose, D. Easterling, and M. Menne (2006), United States historical climatology network daily temperature, precipitation, and snow data, in *ORNL/CDIAC-118, NDP-070. Available on-line [http://cdiac.ornl.gov/epubs/ndp/ushcn/usa.html]*. edited, Carbon Dioxide Information Analysis Center, Oak Ridge National Laboratory, US Department of Energy, Oak Ridge, Tennessee.
- Wipf, S., V. Stoeckli, and P. Bebi (2009), Winter climate change in alpine tundra: plant responses to changes in snow depth and snowmelt timing, *Clim. Change*, *94*(1), 105-121.

- Woo, M. K., and R. Thorne (2006), Snowmelt contribution to discharge from a large mountainous catchment in subarctic Canada, *Hydrol. Process.*, 20(10), 2129-2139.
- Yan, F., J. Ramage, and R. McKenney (2009), Modeling of high-latitude spring freshet from AMSR-E passive microwave observations, *Water Resour. Res.*, 45(11), n/a-n/a.
- Yoshikawa, K., W. R. Bolton, V. E. Romanovsky, M. Fukuda, and L. D. Hinzman (2002), Impacts of wildfire on the permafrost in the boreal forests of Interior Alaska, *J. Geophys. Res.: Atmos.*, 107(D1), 8148.
- Zuzel, J. F., and L. M. Cox (1975), Relative importance of meteorological variables in snowmelt, *Water Resour. Res.*, 11(1), 174-176.

CHAPTER 5: USING MODIS ESTIMATES OF FRACTIONAL SNOW COVER EXTENT TO IMPROVE RIVER FORECASTING MODELS IN INTERIOR ALASKA¹

Abstract

Remotely sensed snow cover observations provide an opportunity to improve snowmelt and streamflow prediction in remote regions. This is particularly true in Alaska, where remote basins and a spatially and temporally sparse gaging network plague efforts to understand and forecast the hydrology of subarctic boreal watersheds. In this study, the operational framework employed by the United States National Weather Service (NWS), including the Alaska Pacific River Forecast Center (APRFC) is adapted to integrate Moderate Resolution Imaging Spectroradiometer (MODIS) remotely sensed observations of snow cover extent (SCE) to determine if these data improve forecasting of streamflow in Interior Alaskan river basins. Two versions of the MODIS fractional SCE are tested in this study, the MOD10A1 product and the newly available MODSCAG data. Observed runoff is compared to simulated runoff to calibrate both iterations of the model. MODIS forced runs have improved snow depletion timing compared with snow telemetry sites in the basins, and discernable increases in skill are obtained for the streamflow simulations. The MODSCAG SCE version appears to provide some moderate increases in skill but is similar to the MOD10A1 results in these watersheds. The basins with the greatest improvement in streamflow simulations have the sparsest observations of streamflow, suggesting the utility of these corrections in basins with low quality gaging records. Basins with higher quality streamflow records (better spatial and temporal coverage) show less improvement from assimilation of the SCE products. These findings indicate that although improvements in predicted discharge values are subtle, the snow model is better constrained to physical conditions of the snow pack, suggesting a more robust method under possible future climate change scenarios. This work provides direction for both the APRFC and other RFCs across the US to implement remote sensing observations within their operational framework, to refine the representation of snow, and to improve the skill in forecasting streamflow within basins of low or poor quality observations.

¹ Bennett, K.E., Cherry, J.E., Balk, B., Lindsey, S. In Prep for Journal of Hydrology. Using MODIS estimates of fractional snow cover extent to improve river forecasting models in Interior Alaska.

5.1 Introduction

Skillful hydrological models are useful for a number of different applications, including the analysis of extreme events and to study future climate change, particularly in the high latitude regions where shifts in the hydrosphere are anticipated to cause disruptions to hydrological and ecological realms (Dowdeswell et al., 1997; Euskirchen et al., 2009; Hinzman et al., 2005; Overpeck et al., 1997; Serreze et al., 2000). The observations of rapid change and climate projections highlight alterations to the subarctic Interior boreal forest, and indicate increasing risk associated with these changes, not only to the local and state resources but also regionally and globally. This multi-scale risk introduces a pressing need in Alaska to further understand the anticipated changes through modeling of major climate drivers of streamflow (Bennett and Walsh, 2014).

However, Alaska's vast territory, complex landscape and sparse observational network represent an enormous challenge for scientists attempting to develop and accurately calibrate streamflow models. An approach to dealing with the lack of stream gages and *in situ* snow observations is to use remotely sensed snow cover areal extent (SCE) to supplement point observations such as temperature, precipitation and streamflow commonly used as the main inputs to models and for calibration and validation (Parajka and Blöschl, 2008). There are two main ways that this data has been used, either to directly insert a time series of SCE data into the model (McGuire et al., 2006; Rodell et al., 2004) or to use complex assimilation procedures to filter the snow series and merge it with observational data (Andreadis and Lettenmaier, 2006; Sun et al., 2004). However, assimilation approaches have yet to be integrated into operational models, in part due to multi-step processing that has not been streamlined for the operational user community. There is a concern that direct insertion methods are ineffective at improving streamflow models and do not perform better than uninformed models because melt can happen before reductions in snow cover below 100% occur (Clark et al. 2006). In addition, the melt season duration can often be short, transitioning rapidly from snow covered to snow free, although this is considered to be basin-dependent (Clark et al., 2006). Another study found calibrating models based solely on SCE values may not improve skill in estimating discharge, and the improvements for in-catchment distributed SCE estimates does not always result in improved discharge simulation (Franz and Karsten 2013).

Alaskan hydrologic systems suffer from large uncertainties in various data inputs, and thus require great care when attempting to simulate hydrologic water balance components with skill. Reducing these uncertainties is of utmost importance, as they will overwhelm model output (Slater et al. 2013) and generate results that are non-transferable to problems such as future changes in snow cover extents that are anticipated as a result of climate change (Stocker et al., 2013). In addition, the variability in landscape (i.e. forest cover, topography, discontinuous permafrost) and climate across Alaska and amplification of

changes (Serreze and Barry, 2011; Serreze and Francis, 2006; Serreze et al., 2000) requires robust modeling techniques to account for these shifts. Temperature index models, based on the most reliable climate forcing, are therefore presumed to perform better in regions with highly variable landscapes and a sparse network (Hock, 2003; Stahl et al., 2006). Additionally, a skillfully calibrated conceptual model may provide a better representation of hydrologic responses because the underlying model is reliant upon parameterizations rather than observations that lack spatial and temporal consistency (Franz et al., 2008; Reed et al., 2004).

One approach is to utilize newly developed forecasting frameworks to integrate remotely sensed data on snow cover extent for calibration of streamflow models. These newer tools have been recently adopted by the National Weather Services' (NWS) River Forecast Centers (RFCs) and offer an opportunity for more advanced forecasting techniques, including ensemble prediction using variable input and/or forcing data. The Community Hydrologic Prediction System (CHPS), brought online in 2012 by the Alaska Pacific River Forecast Center (APRFC), is a test case for this approach. The modeling framework, developed on the Delft-FEWS software platform, can run many different types of models, but in its current state implements the conceptual Sacramento Soil Moisture Accounting System (SAC-SMA) rainfall-runoff model (Burnash et al., 1973), with snowpack input from the SNOW17 snow model (Anderson, 2006).

The objectives of this work are to adapt the CHPS operational forecasting modeling framework to ingest the Moderate Resolution Imaging Spectroradiometer (MODIS) remotely sensed SCE data for streamflow modeling in the Interior boreal forest region of Alaska. A simple procedure is undertaken to replace the standard areal depletion curve used in SNOW17 with pre-processed MODIS SCE grids for snow depletion. Two different versions of MODIS are applied, the MOD10A1 fractional SCE product (Hall et al., 2002), and the MOD-Snow Covered Area and Grain size (MODSCAG) fractional SCE product (Painter et al., 2009). The SNOW17 manual calibration with evaluation by two criteria is described. A detailed consideration of all model parameters, including a tolerance parameter controlling snow cover updates (snow cover tolerance, SCTOL), is investigated to simulate a mixed method between direct insertion and more complex data assimilation. Pre-processing, model frameworks and use of existing parameterization structures are thus offered as a means of employing remotely sensed information into operational models that can be utilized out-of-the box by the NWS RFCs. The work also offers insight on several previously unknown components of the research, including the use of the MODIS SCE product in high latitude boreal forest basins, interpolation of missing data, and how to improve discharge estimates using calibration of model parameters.

5.2 Methods

5.2.1 Study Area

This study is carried out in five adjoining headwater sub-basins of the Tanana River, which is a sub-basin of the Yukon River basin (Figure 5.1). The Chatanika River basin above the Steese Highway (64°50'37"N, 147°43'23"W, Figure 5.1) is approximately 950 km² in size and runs predominantly east to west. Only the area upstream of the Caribou-Poker Creek confluence is considered in this study. The Chatanika was gaged from 1987 to 2007 but the records are highly discontinuous. The Upper Chena River basin is approximately 2440 km² and has gage records from 1967 onward. This portion of the basin contains high elevation peaks and rocky outcrops where snow can persist late into the melt season. The Little Chena is 1030 km² and has the highest proportion of lowlands located within it, relative to the others; it has been gaged since 1966.

The Salcha River watershed is a large 5740 km² basin with its gage at the Salchaket Bridge; Salcha has the longest historical record of all rivers in this region (1948 onward). The Goodpaster basin is located east of the Salcha and is 1770 km² in size. It has the highest proportion of its basin above 600 m elevation. The Goodpaster basin has been gaged since 1997. There are minor urban and agriculture developments throughout the region, including the town of Fairbanks, which is located downstream of the Little Chena gage on the main stem of the Chena River. These minor developments have little or no bearing on the hydrologic response of the headwater systems of Chena basins we examine here. More information on the watersheds and basin units is provided in Table 5.1.

5.2.2 Data

The MODIS satellite product (Terra MOD10A1, version 5) daily, 500 m resolution snow cover fractional areal extent (SCE) data are downloaded from the National Snow and Ice Data Center (Hall and Riggs, 2007; Hall et al., 2006) for 2000-2010 and preprocessed into a projected GeoTIFFs (North Pole Stereographic). The MOD10A1 fractional SCE data are developed based on the normalized difference snow index (NDSI), which is calculated as a ratio of band 4 and band 6 on Terra:

$$\text{NDSI} = \frac{b_4 - b_6}{b_4 + b_6} \quad (5-1)$$

Snow is mapped when NDSI is greater than 0.4 (Hall et al., 2002) and where reflectance in MODIS band 2 is >11% and MODIS band 4 is >10%. The fractional product is then calculated based on an empirical algorithm generated from a linear regression developed from analysis of binary Landsat Thematic Mapper scenes and applied to MODIS NDSI (Salomonson and Appel, 2004).

MODSCAG data products are obtained from the NASA Jet Propulsion Laboratory’s Snow Data System Portal (<http://snow.jpl.nasa.gov/>) for the area of interest and preprocessed as described above. MODSCAG is a spectral mixing model that utilizes end member analysis to identify the best fit of linear end members that has the strongest relationship to surface spectral reflectance in the Terra MOD09GA product (Painter et al., 2009). Operating under the assumption that spectral reflectance viewed by the MODIS sensor varies based on grain size of the snow, MODSCAG utilizes a radiative transfer model to calculate reflectance across different snow grain sizes. A look up table is used to store and retrieve the spectral reflectance end member formulations. From this look up table, all the end members are permuted to generate multiple models and the algorithm selects the minimized model solution (i.e. low error and minimum number of end members). When a pixel is identified as containing snow, then the fraction of the pixel containing snow is calculated in relation to other end members (soil, rock, ice, vegetation), normalized by the shading geometry (Rittger et al., 2013). Both MODIS products are initially screened to remove any values that are classified as cloud cover; only SCE data from 0-100% for March 1st to June 30th are ingested into CHPS.

Both MOD10A1 and MODSCAG fractional products require correction to adjust the values of SCE estimates (Raleigh et al., 2013; Rittger et al., 2013), which do not account for the snow that is blocked from the sensor view. For the MOD10A1 SCE product, this calculation is based on the viewable gap fraction, or the amount of snow covered ground between trees that the sensor can see (Liu et al., 2004). This technique, while widely applied, assumes that the viewable gap fraction remains constant through the snowmelt season, which is incorrect as the viewable gap fraction can vary based on a complex number of factors, including forest canopy density, age and class, zenith angle of the sensor, solar zenith angles, topography and snow loading (Kane et al., 2008; Liu et al., 2008; Molotch and Margulis, 2008; Raleigh et al., 2013; Rittger et al., 2013). To account for some of these issues, rather than applying a forest cover product to correct the product itself, the MOD10A1 data are used (Durand et al., 2008). All 2000-2013 March 1-March 15th MOD10A1 pixels across Interior Alaska are differenced from 100 and then a composite average of all days (n=207) is calculated. While in southeast Alaska some melt may have occurred during this time, the Interior SCE should still be at 100% across most of the region. To account for bare ground regions such as open, wind-blown rocky faces, values less than 20% SCE are removed from the correction. The standard division by viewable gap fraction,

$$SCE_{fadj} = \frac{SCE_f}{1-F_{veg}} \quad (5-2)$$

where F_{veg} is the tree cover percentage, SCE_{fadj} (henceforth referred to simply as SCE) is the fractional SCE adjusted for canopy cover, and SCE_f is the unadjusted SCE data. This formulation is applied as a

static adjustment to each SCE pixel in all days and years. For MODSCAG, the daily vegetation fractional product provided with the data product is utilized, resulting in a dynamic adjustment for each SCE pixel in all days and years. In both cases the results are constrained to 100% SCE when exceeded.

Mean areal values of temperature and precipitation at 6 hour increments are obtained for each sub-watershed from the APRFC for the time period 1969 to 2012; only the 1999-2010 data are utilized in this study. River discharge at each gage is based on the United States Geological Survey (USGS) gaging record database. The exception to this is the Chatanika River at the Steese Highway site, where observed discharge is generated based on once-a-day stage readings from a Cooperative Network observer. These daily stages are converted to mean daily discharge using the APRFC's rating curve for the river. To calculate north and south facing slopes and elevation criteria, the 30 m US Geological Survey's National Elevation Dataset (NED), updated for the region in 2012, is applied (Gesch et al., 2002). Seven snow telemetry (SNOTEL) sites are utilized to compare results of modeled simulated SWE with observed data (Table 5.2, NRCS 2013). SNOTEL snow water equivalent (SWE, mm) is downloaded from the National Resource Conservation Service (NRCS) snow pillow data repository (<http://www.wcc.nrcs.usda.gov/ftpref/data/snow/snotel/cards/alaska/>).

Potential evapotranspiration (PE) estimates are provided by the APRFC based on an assessment of historical PE from pan evaporation data and in some cases Thornthwaite estimates (Anderson 2006). These data are used to develop a general linear relationship between PE and elevation to estimate average monthly PE values for a generic low-elevation site. The APRFC uses the low elevation PE values to derive monthly PE estimates for the mean elevations of the sub-basins as a coefficient. The coefficient, C , is derived using the equation,

$$C = 0.9 - [(e - 1000) \cdot 0.00011] \quad (5-3)$$

where e represents elevation in feet. For example, if the catchment mean elevation is 2350 ft, the coefficient is 0.75. Finally, a monthly PE adjustment factor is applied to account for vegetation changes during the year. The result is an evapotranspiration demand estimate that is used in the SAC-SMA model, described in the proceeding section.

5.2.3 Models

5.2.3.1 SNOW17

The SNOW17 snow model is a single layer snow model that calculates snow accumulation and ablation using empirical formulae to estimate heat and liquid water storage, liquid water throughflow and snowmelt (Anderson, 1976). The model is designed for river forecasting and has been used operationally by the NWS RFCs since the mid-1970s. The only input requirements for SNOW17 are temperature and

precipitation, at the time step of the model (6 hrs). There are 12 parameters in the SNOW17 model, including the areal depletion curve; sensitive or ‘major’ parameters control the model while less sensitive or ‘minor’ parameters have little impact (Table 5.3, He et al., 2011).

SNOW17 determines the division between rain and snow using the rain-snow elevation (RSNWELEV) module. RSNWELEV uses a defined lapse rate ($6\text{ }^{\circ}\text{C}/100\text{m}$) to determine the elevation of the threshold temperature (PXTEMP). The elevation is passed to SNOW17 where the percent area above and below is determined from a defined area elevation curve. Multiplying these percentages by the precipitation will distinguish the proportion of precipitation that is falling as snow or rain in the basin. Non-rain snowmelt (mm) is determined from air temperature minus the value MBASE, or the baseline for which melt occurs (set to 0°C), weighted by a seasonably variable melt factor that is calculated using an oscillating sine curve that varies between parameters MFMIN and MFMAX, representing the minimum and maximum melt factors for December 21st and Jun 21st ($\text{mm}/^{\circ}\text{C}/6\text{ hrs}$). These values are adjusted for northern latitudes above 54°N to account for low radiation input, a paucity of days when temperatures rise above freezing, and rapid changes in melt rates during spring and fall (Anderson, 2006). The TAELEV parameter, when it differs from basin mean elevation, is used to lapse mean air temperature within the lumped basins by a standard value. This fixed lapse rate can be configured in the SNOW17 model using TALMIN and TALMAX parameters; set to $0.6^{\circ}\text{C}/100\text{m}$ in this study.

A simplified energy balance method is used to calculate melt from rain-on-snow, making assumptions about the meteorology, including the use of the Stefan-Boltzman constant for incoming longwave radiation, negligible shortwave radiation, 90% relative humidity, and accounting for wind speed ($\text{mm}/\text{mb}/6\text{hrs}$) using the parameter UADJ. In-pack heat content is calculated based on the difference between air temperature and the antecedent temperature index, scaled using the TIPM parameter, which determines the time interval length for weighting. Heat deficit in the snow is either negative or positive and the rate of loss or gain is based on the negative melt factor (NMF) weighted by MFMAX to account for seasonal variations in pack heat translation. Heat can also be translated from the ground to the snow in SNOW17 using the DAYGM parameter and is assumed to occur constantly through the snow season. When the capacity of the snow to hold water (PLWHC) is filled and the pack is isothermal at 0°C , the snow is ripe and any excess water entering the snow will flow through it as outflow. As water passes through a ripe pack, it is attenuated or lagged based on empirical formula derived from lysimeter studies (Anderson 2006).

SNOW17 uses an areal depletion curve (ADC) to calculate the extent of the snow cover, which is used in the model for calculating the percentage of area over which surface melt, changes in heat storage, ground melt, and rainfall on bare ground occurs. The ADC not only represents areal extent of snow cover, but also accounts for slope, aspect and differences in vegetative cover (i.e. open versus closed sites). In

this study, the ADC is replaced by the observed areal extent of snow cover, thus the description that follows only pertains to the APRFC baseline run. The areal extent of snow cover is calculated from a lookup table that defines the depletion curve and relates the curve to the ratio of SWE to the areal index. The areal index is either the maximum value of SWE that occurred during snow accumulation or a parameter SI that represents the areal SWE at which 100% snow cover exists. The curve is applied as follows; when snow accumulates, the snow cover is set to 100%, and it stays at this value until it falls below SI or the maximum SWE value, whichever is smaller. If new snow totaling greater than 0.2 mm/hr falls onto bare ground, 100% snow cover is assumed until 25% of the new snow has melted. In Alaska, there are several different ADC configurations used depending on whether slopes are south versus north facing, or upper versus lower elevation basins. Basins examined in this study use the same ADC for upper south, upper north and lower units since they have similar orientation in a similar geographic region. The Little Chena uses a different ADC for its upper basin since no north/south aspect split is used in this basin.

A tolerance parameter is available in the SNOW17 model that can be used to alter the impact of the observed SCE data. The tolerance setting for snow cover (SCTOL) can be altered from 0 to 1 to adjust the use of observed data when there are differences in the simulated versus observed areal extents. When the areal extent of snow cover subtracted from the observed (in absolute terms) is greater than the tolerance multiplied times the observed, the snow cover is updated. Otherwise it is left the same. The effect of this parameter is to rely solely on the observed data value (SCTOL=0), rely partially on observed only when there are large differences (0.1-0.9), or to rely wholly on the simulated data (SCTOL=1).

5.2.3.2 SAC-SMA

A conceptual rainfall-runoff model can be used to produce a streamflow simulation from observed input precipitation and PE (Burnash et al., 1973). The SAC-SMA model has been widely applied by the NWS to estimate streamflow runoff in basins across the United States. The model moves water into either an upper or lower storage zones that conceptually represent soil interception or deep groundwater storage. Interception water in the upper zone flows to the lower zones via downward percolation or can run off directly or via interflow when the upper zone layers become saturated and precipitation rate exceeds downward percolation. Lower zone water can be held in tension storage and contributes to baseflow runoff slowly over time or can run off more quickly over shorter durations. Drainage from the upper and lower zones follows gravity drainage and is governed in part by both water delivery from the upper zone and soil moisture in the lower zone. Tension water is driven by potential evapotranspiration (PE) and diffusion; with a fraction of the lower zone unavailable for potential PE as it is considered below the rooting zone.

5.2.3.3 Community Hydrologic Prediction System

The Community Hydrologic Prediction System (CHPS) was implemented at River Forecast Centers across the United States in 2012 and builds on the Delft-FEWS model framework, developed by Deltares. The system allows for integration and ensemble forecasting of multiple models under a single synchronous system. The framework can be run in live mode for forecasting purposes or in an offline standalone mode for testing and development purposes (Werner et al., 2013). The offline model is implemented for this study at the University of Alaska Fairbanks using the calibration capabilities introduced to the NWS with the FEWS 2013.01 build in November, 2013.

The CHPS framework is modified to allow for the ingestion of the MODIS SCE data to replace the SNOW17 snow cover areal depletion curve, or to update the curve in the case of $SCTOL > 0$. The MODIS SCE grids are read in using an import function, and then clipped and averaged over each sub-watershed area using a preprocessing module. The SCE grids are imported as special forms of ArcInfo ASCII files in a Stereographic projection (this projection, which is generally inappropriate for Alaska, is used due to the limitations of CHPS projection parameters). Calibration modules are configured for peakflow, discharge statistics and water balance for each sub-watershed. We developed a parallel configuration to allow simultaneous display of MODIS and non-MODIS-forced model output. Statistics are generated for calibration, validation and for the entire time period by altering the initial conditions appropriately for each run using the input MOD10A1 data.

The framework is set up to run on semi-lumped upper and lower sub-basins with additional designations (referred to as units) for north and south facing slopes in the Chena, Chatanika, Salcha and Goodpaster basins. The model runs at a six-hourly timestep, and is run continuously from 2000 to September 2010, with initial conditions starting in October, 1999. Updates to the model framework included the basin area, and north/south facing slope delineation with new information from the 2012 NED digital elevation model (Gesch et al., 2002). This also formed the basis of updates to the model's area elevation curves and unit hydrographs.

Linear interpolation is used to estimate snow cover over periods when no MODIS SCE data are available. An optional element in FEWS, `maxGapLength`, can be configured to define the maximum length of gaps that should be filled. Gaps equal to or smaller than `maxGapLength` will be filled with interpolated values. Gaps larger than `maxGapLength` will not be filled. A `maxGapLength` of 11 days is used; gaps greater than 11 days are not interpolated. This ensured that periods with extensive cloud cover obscuring the MODIS SCE data are interpolated but long periods with no data, such as the summer period, are not interpolated. Testing of a shorter interpolation time steps resulted in lower streamflow simulation skill, thus the 11-day length is applied.

A unit hydrograph model is used to time distribute the runoff produced by the SAC-SMA model. Each sub-watershed has its own unit hydrograph to translate the runoff through the channel system to the gage location. Simple routines sum the unit hydrograph outputs to calculate simulated streamflow at the basin outlet. While downstream basins incorporate routing models, e.g. Lag/K, this study focuses on headwater basins so no routing models are needed.

5.2.4 Calibration and Validation

Several calibration procedures are undertaken for this project. The first calibration effort updated the SAC-SMA/SNOW17 model parameters previously adjusted by APRFC to 1970-2003 historical data to the 2000-2010 study years used in this study. This provided a baseline calibration for the APRFC runs. The MODIS manual calibrations are undertaken using this baseline, utilizing the features of the APRFC CHPS calibration version to adjust parameters and then generate statistics for the 11 years of the study. Visualizations of streamflow hydrographs from 2006-2010 are used for calibration; however statistics from the entire period of record are generated for ultimate parameters selection. For validation purposes, statistics from 2000-2005 are provided for all watersheds except the Chatanika. The Chatanika basin is calibrated on 2000-2004, and validated from 2005-2010 to make use of improved data quality and availability during the first five years of the study.

To calibrate the MODIS model output, a simple approach is taken to minimize the terms required for calibration. This simple approach ensures that it is easy to replicate the model adjustments to the MODIS SCE data and focused solely on the snow parameterization. An attempt to adjust the SAC-SMA parameters resulted in only minor improvements to statistics during the breakup period, therefore only the SNOW17 parameters are considered. A priority is placed on adjusting the empirical parameters towards a physically-based realization using sub-unit properties, including the topographic aspects and the observed melt trajectory impacted by the MODIS SCE data. To complete this simple, physically realistic calibration approach only the parameters MFMAX and TAELEV are adjusted.

The goal of the physically realistic calibration is one that focuses only on the empirical parameters that have physically based schemes associated with them. For example, the maximum melt factor for non-rain melt periods (MFMAX, specified for June 21st) represents the melt rate; increasing this parameter is indicative of increasing melt responses towards an earlier date in the season and changing melt timing. The MFMAX value incorporates slope, aspect, forest cover and meteorological conditions; it is generally considered to be higher for open regions with predominantly deciduous tree covers, higher wind speeds and mountainous terrain. The TAELEV parameter is used to warm or cool the MATs without recompiling the historical data. ELEV is the mean elevation of the catchment and the elevation at which the MAT is applied in the snow model. TAELEV is the elevation associated with the historical

MAT time series. Using a standard lapse rate of 0.6°C per km, if ELEV is 1000m and TAELEV is set to 1200m, then the MAT that is applied in the SNOW17 model is effectively warmed by 1.2°C. Since MAT is generated for the entire upper zone, we used TAELEV to "warm" the temps for the southern basin units and "cool" the temps for the northern basin units. Slight adjustments to the NMF parameter are made across all basins and sub-basin units to correct a small over estimate of the values; this is anticipated to have little impact on the overall results but is undertaken to ensure representativeness of the north, south and lower basins.

5.2.5 Analysis

Statistics used to evaluate model success are based on five main objective functions. The first two of these criteria are standard in NWS RFC calibration approaches and are provided in the CHPS statistical output. These statistics are used for evaluation during the calibration; total volume bias as a percent (PBIAS, %) and the correlation coefficient (R, unitless). An additional three objectives are added for further validation of the results, Nash Sutcliff efficiency (NSE, unitless) and the mean absolute error (MAE, m³/sec) and the root mean squared error (RMSE, m³/sec). Statistics are run for April, May and June only to focus on the changes to the snowmelt season; March is not included because breakup in Interior Alaska occurs after March and thus any differences in statistics would be indicative of changing winter conditions rather than changes in spring snowmelt timing or volume. The equations are calculated as follows:

$$PBIAS = \left[\frac{\sum_{i=1}^N (S_i - Q_i)}{\sum_{i=1}^N Q_i} \right] * 100 \quad (5-4)$$

$$R = \frac{N \cdot \sum_{i=1}^N S_i \cdot Q_i - \sum_{i=1}^N S_i \cdot \sum_{i=1}^N Q_i}{\left[\left(N \cdot \sum_{i=1}^N S_i^2 - \left(\sum_{i=1}^N S_i \right)^2 \right) \left(N \cdot \sum_{i=1}^N Q_i^2 - \left(\sum_{i=1}^N Q_i \right)^2 \right) \right]^{0.5}} \quad (5-5)$$

$$NSE = 1 - \left(\frac{\sum_{i=1}^N (S_i - Q_i)^2}{\sum_{i=1}^N (\bar{Q} - Q_i)^2} \right) \quad (5-6)$$

$$MAE = \sum_{i=1}^N |S_i - Q_i| \quad (5-7)$$

$$RMSE = \left[\frac{\sum_{i=1}^N (S_i - Q_i)^2}{N} \right]^{0.5} \quad (5-8)$$

where N is equal to the number of data points (i.e. sub-daily streamflow realizations), i is the time step (days), S is the simulated streamflow (m³/s), and Q is the observed streamflow (m²/sec).

5.3 Results

5.3.1 Model Results

The APRFC SAC-SMA/SNOW17 model estimates of streamflow in Interior Alaskan river basins for the 11-year period of record indicate that these watersheds are captured with skill. The Chatanika basin is problematic given the limited quality and quantity of the observed streamflow data, as noted in the below statistics for each objective function. For all of the five basins analyzed, the daily average bias for the period of record is $\pm 3\%$ or less. Daily correlation coefficients (R) are equal to or greater than 0.84 (unitless) and higher for the four watersheds with quality observed data, while the Chatanika basin is 0.70 (unitless). NSE daily values are also above 0.60 (unitless) for all basins except the Chatanika (which is 0.18 due to the noise in the observed data values). Daily mean absolute error statistics are below 10 m^3/sec for all basins except the Salcha, which is 15.89 m^3/s (owing to its large discharge record). RMSE is between 3.5 m^3/s (Chatanika) to 33 m^3/s (Salcha). Across all basins, SCE are variable by elevation zones and years (Figure 5.2). Upper elevation areas tend to have 100% SCE, while mid-to-lower areas often begin the year with 75% SCE or less. The very lowest elevation zone appears to have a slightly higher SCE values than the next two bins (Figure 5.2). Some years have a markedly late melt out, with high variability across the elevation bins. Lower elevation zones tend to melt out in early April, while the upper regions of the watersheds hold snowpack weeks or months into the subarctic spring (Figure 5.2).

5.3.2 Parameters

Calibrated SNOW17 parameters for the APRFC and MOD10A1 runs illustrate increases to MFMAX for north facing aspect in two sub-basins and increases in TAELEV for the northern slopes (Table 5.4). In some systems, TAELEV is set to be equal for the north and south basins, for reasons that are discussed in the following section. MFMAX for the Chatanika's lowland sub-basin is increased and TAELEV at the north sub-basin is increased, while TAELEV is decreased for the south unit. MFMAX in the Upper Chena north unchanged and TAELEV is equalized for both south and north units. The Little Chena sub-basin is altered by setting MFMAX equal to its maximum recommended value (1.4) for the upper and lower sub-basins and by increasing TAELEV 100 m greater than the elevation for both sub-basins. TAELEV for Salcha and the Goodpaster are differenced by 100 m for the north and south units and the northern sub-basin MFMAX for Goodpaster is increased slightly. Goodpaster's lower basin MFMAX is reduced by a small amount. Although these changes may appear minor, because MFMAX is a very sensitive parameter during the melt season, the changes have a substantial effect on the MODIS SCE forced snowmelt trajectory at these sites (Anderson, 2006).

In the MODSCAG runs, the values for MFMAX are increased slightly for the northern units for all basins. The TAELEV values are adjusted slightly in Upper Chena, Salcha and Little Chena basins (Table 5.5), and they are not altered from the baseline run in Chatanika. In the Goodpaster basin, the TAELEV value for the south unit is decreased. For this version of MODIS, it appears that a slightly more rigorous calibration is required.

NMF is altered slightly to account for different snow densities and thermal conductivities of snow on south and lowland sites versus north aspects. Snow density is generally low in Interior Alaskan watersheds; based on analysis of field data from the Caribou Poker Creek watershed, snow density on the sites is approximately 0.20 and is slightly higher on the southern sites compared to the north site. The northern facing slopes are therefore given the NMF value of 0.15 mm/°C/6hr, which Anderson (2002) indicates is the 'reasonable' value of NMF. The south and lowland sites, which have generally warmer temperatures and more dense snow, are assigned the NMF value of 0.2. For these runs, SCTOL is set to 0 for all basins to ensure that the MODIS data are utilized 100% of the time.

5.3.3 SASC and SWE

Compared to the APRFC runs, the MODIS runs have less snow cover on the north facing slopes and more on the south facing slopes (Figure 5.3, Upper Chena River basin results for 2001 is shown as an example). Differences between the two runs become discernable in late January as a result of the different calibrations of the SNOW17 model in the watersheds (Figure 5.3), with larger differences at the north units compared to the south unit. As soon as the MODIS SCE begins to alter the weighting factors for outflow from the snow, differences between the SWE generated by APRFC and MODIS runs are observed (after March 1st). The greatest differences between the model runs occur during the melt season. All model runs peak in early April and start the downward melt trajectory from this point, and reflect the melt patterns of the upper elevation SNOTEL sites, Mt. Ryan, Munson, and Upper Chena. The MODSCAG SCE north unit estimates are closer to the APRFC runs in volume, and melt out more slowly than both the MOD10A1 and the APRFC run, although all runs terminate on the same approximate day for the northern sub-basins. The SNOTEL sites are mostly located at upper elevations (Mt. Ryan, 850m and Munson, 940 m) compared to the SNOW17s ~800 m for the upper basin and thus illustrate conditions exhibited at high elevation northern sites in the basin. Mt. Ryan, in particular, does not build a snow pack early in the season, perhaps owing to its open, mountainous and presumably windy environment. The SNOW17 model is run over a lumped area so there is a mix of site conditions that act to smooth the model responses; hence these comparisons are inherently qualitative as opposed to quantitative (Molotch and Bales, 2005). Lower elevation sites such as Teuchet and Little Chena melt out significantly earlier than the model and remote sensing estimates. There is stronger coherence in the response of the northern sites

as opposed to the southern sites. At the southern sub-basins, the MODIS runs melt out later, with MODSCAG again having the latest melt, similar in timing to the high elevation stations.

The areal extent of snow cover varies from basin to basin across the watersheds in both runs. The preprocessed gridded MOD10A1 SCE illustrated for May 15th, 2001 for the watersheds is shown in Figure 5.4a and the MODSCAG SCE is shown in Figure 5.4b. The high elevation snow pack (blue) is present within the upper watershed regions but the pack is largely gone in the valleys and lower basin reaches. This translates into the lumped average SCE estimates as shown in Figure 5.4c and 5.4d, which illustrates the way that CHPS ingests and converts the gridded MODIS SCE for the sub-basins and units. North and south units are differentiated in the upper basin units but not other locations because both aspects have begun to melt by this date (as opposed to early in the melt period when the south slopes would have comparatively less SCE than the north slopes). MODSCAG has less cloud cover interaction in this scene (Figure 5.4b) and this results in slightly higher values of SCE (Figure 5.4d). Basin SWE estimates for MOD10A1 (Figure 5.5a), MODSCAG (Figure 5.5b), and the difference between the MODIS (both versions) and APRFC run (Figure 5.5c and 5.5d) is shown for May 15th, 2001. Basin units can be clearly differentiated in these plots, which illustrate the range of SWE values from 0-0.5 inches in the lowland regions to 5 inches remaining in the upper headwater zones. The MODSCAG data has an average SCE value of 0.5 and SWE is 1.7 inches, whereas the MOD10A1 has an average of 0.45 SCE, has an average of 2.1 inches SWE, very small differences overall although basin-to-basin the variation between the products is notable. The difference plots highlight the fact that MODIS tends to have lower SWE values compared to the APRFC SNOW17 model runs on the north facing slopes and higher values on the south facing slopes. The APRFC tends to have lower SWE estimates for the lowland regions, although this is more true for MOD10A1 versus MODSCAG (Figure 5.4c, d).

5.3.4 Streamflow Estimates

Calibration and validation results are provided for April-May-June (Table 5.6) for the MODIS and APRFC runs. The calibration, validation and whole period of record results based on observed discharge are provided for all watersheds for MAE, NSE, PBias, R and RMSE, boxplots illustrate the range of all basins exhibited for the each run of the model and the SCTOL results which are discussed in the preceding section (Figure 5.6). The boxplots, whiskers and outliers indicate the range in results across basins. The results show moderate improvements; model improvements are observed for the MODSCAG run during the calibration periods in the Chatanika, Salcha and Goodpaster basins. The validation period statistics showed improvement for the Chatanika, Little Chena, and Upper Chena basins. Many statistics are similar or nearly identical to the APRFC run with slight declines in model performance and some gains (Chatanika, Little Chena), particularly for the analysis focused on the whole period of record. The

MOD10A1 is improved for the Chatanika and Goodpaster systems during the calibration period, while it performs similarly or slightly worse during the validation and period of record in most of the basins except the Chatanika. NSE statistics are particularly poor for all runs in the Chatanika basin, where the lack of continuous and high quality observations hamper calibration efforts. The boxplots illustrate a reduction in volume biases (PBIAS) for MOD10A1 during the calibration period however PBIAS remains below 10% for almost all cases for the ten year period with the exception of Chatanika. Over the period of record there is almost no difference in statistics across all the model runs (Figure 5.6). Overall, the greatest improvements in skill are observed for the MODIS runs in the Chatanika and Goodpaster basins, the validation period for Upper Chena and the calibration period for Goodpaster (Table 5.6). Volume biases are improved in most of the basins as well. MODSCAG tends to do slightly better where improvements are made compared to the MOD10A1, while all runs perform nearly identically over the 11-year period.

Cumulative streamflow for each basin illustrate the differences between simulated discharges plotted against observed discharge at the streamflow gage (Upper Chena, Figure 5.7-5.11). Plots illustrate all years of the study with the mean value provided in the last panel. Only March to June results are shown; in March the basins have not begun to melt and hydrograph depicts baseflow contributions in the systems. The active period begins in late March, early April and the differences between the two estimates of streamflow persist until June, after which point streamflow responses to rainfall input are essentially the same. Statistics for the April-May-June calibration, validation and the period of record are also provided in Table 5.6. The Upper Chena River basin (Figure 5.7) shows improvement for some years (2000, 2006- 2008) compared to the APRFC run, while some years have poor fits between both simulations (2002-2004, 2009). For Chatanika, the simulated MODIS runs are of greater magnitude (Figure 5.8) and have earlier timing compared to the observed flows (not shown), which are sparse as noted earlier. In the Little Chena river basin, MODIS simulated discharge overall fits better than the model, which over simulates streamflow on average; the MOD10A1 provides slightly higher streamflow simulations at peak flow values (Figure 5.9). Streamflow simulations for the Salcha and Goodpaster systems capture the observed flows well on average, with some years improved upon by the MODSCAG runs and for other years by the MOD10A1 (Figure 5.10, 5.11).

5.3.5 Sensitivity to Parameter SCTOL

The sensitivity of model parameter SCTOL represents a way to partially integrate the MODIS data into CHPS as a means for forecasters to combine the strength of the areal depletion curve and the MODIS data together. Table 5.7 and boxplots 4-6 in Figure 5.6 illustrates the results of setting the SCTOL parameter to 0.25, 0.50, and 0.75 for the MODSCAG run, while holding the rest of the

parameters constant. No recalibration is performed. The boxplots illustrate the advantage of using this parameter. NSE and R statistics increase during the calibration period, MAE and RMSE remain similar on average but the interquartile range decreases for the SCTOL=0.50. The basin with the greatest improvement based on differences between APRFC and MODIS runs (Chatanika) does not benefit from model integration, owing to the low skill performance of APRFC model version (Table 5.7). However, for the remaining basins strong improvements are apparent for the increase values of SCTOL during the calibration period (Upper Chena, Little Chena and Salcha), validation and period of record (Upper Chena, Little Chena). Diminishing returns occurring at a threshold between 0.25 and 0.50 SCTOL for most basins, however the Goodpaster improves at 0.50 but not 0.75. This suggests that the SCTOL parameter should be uniquely applied dependent upon the basin.

5.4 Discussion

Results for the study illustrate how basins in interior Alaska can be captured with skill using conceptual, semi-lumped hydrologic models. Using gridded observations of MODIS SCE in the models generates streamflow estimates as good or better than estimates based on SNOW17s areal depletion curve, particularly if the initial streamflow observations are of poor quality (i.e. Chatanika River basin). However, there are challenges in obtaining improved estimates in streamflow discharge values when introducing additional observed data sets and their associated uncertainties into models. These results are similar to work performed in the American River basin where the California Nevada RFC (CNRFC) lumped model provided the most accurate representation of snow cover area (Franz and Karsten 2013). As indicated by Franz and Karsten (2013), although the gridded representation of SCE is improved in their distributed version of SNOW17, the streamflow simulations and associated statistics did not reflect this improvement. In addition, they found that discharge values had lower skill when estimates of snow cover are included in the calibration even though it is hypothesized that the process representation is improved, which is a finding of a number of other research studies focusing on this topic (Parajka and Blöschl, 2008; Udnæs et al., 2007). These findings are also true for Alaskan interior boreal watersheds, highlighting the importance of performing this work in remote and under monitored systems that are changing quickly due to climate shifts and increased occurrences of extreme events (Bennett and Walsh, 2014; Sillmann et al., 2013).

The goal of this work is, in part, to undertake a simple application of inserting preprocessed MODIS SCE into the CHPS operational framework to simulate streamflow across basins in Interior Alaska. The preprocessing of MODIS data for insertion into the model, which included the MOD10A1 and MODSCAG data products, along with the CHPS areal averaging eliminated some of the issues related to cloud cover and missing data given the comparison between the results provided in Lui et al.

(2013) for similar stations in the region. For example, the findings in Lui et al. (2013) for the best case (assimilated Air Force Weather Agency–National Aeronautics and Space Administration Snow Algorithm or (ANSA) SCE data) indicate NSE improvement for Salcha, Little Chena and Chena at Fairbanks of 0.30, 0.31, and 0.06. Our study reports comparable NSE improvement values for some stations (Chatanika and Goodpaster) for the months impacted by the adjustments although the Salcha and Little Chena system differences are closer to those values reported for the raw MODIS data in Lui et al.'s (2013) study. The averaging approach and use of a newly developed tools (ANSA, MODSCAG) applied in both studies appear to produce slightly superior results from that of MOD10A1. Further analysis is required to determine if cloud correction processes, such as those applied in the ANSA study, would act to reduce the impact of pixel shifting that is likely a major problem in Alaska (Arsenault et al. 2014) and improve streamflow estimates further. Both studies indicate improved representation of internal snow pack and improvements in streamflow estimates for some basins, but not all, for these new iterations of the MODIS data.

Differences in the improvements provided by Lui et al. (2013) for the Salcha and Little Chena highlight some important variations between the two studies that should be considered. The first is that, as noted by the authors, the model simulated streamflow estimates are biased and thus the improvements reported in the paper are still poor representations of the streamflow (Lui et al. 2013). The question then remains that if a model result without updated observations is already skillful, how much better or improved can the model be by added information (which carries its own uncertainty with it)? Perhaps the differences between the distributed model in Lui et al. (2013) versus the lumped models used in this study is also adding a buffer to the data improvements in the case of this study, and limiting the amount of difference or improvement that MODIS SCE insertion can provide. Snow cover data appears to be improved at Interior locations within the model when compared to five different SNOTEL stations (Figure 5.4), particularly for the melt timing. However, the discharge values improved moderately given either MODIS input over the different periods analyzed, and in particular smaller changes are noted over the entire period of record (Table 5.6). For the Chatanika basins with limited observed data and poorer streamflow simulations however, the improvements are closer to the values shown in the Lui study. These results suggest that skill can be added by introducing new observations when the models are performing poorly due to inadequate or low quality records. Considering that there are numerous incomplete and low-quality gages throughout the high latitudes, this result is of great value and indicates the utility of the MODIS SCE data in this regard. Another obvious difference is that this study did not run the accumulation season with MODIS inputs, which explains the focus on statistics in the melt season (April-May-June).

Calibrations performed are limited in nature and targeted specifically at two parameters that had the most influence on improving discharge estimates during the melt season. MFMAX and TAELEV control the air temperature and impact the snow cover depletion to speed or retain melt. Previously, the APRFC parameters are set to lower MFMAX values. The TAELEV parameter was not equal to ELEV and set to different values for north and south aspects. For north-facing upper elevations, $TAELEV < ELEV$ so temperatures were lapsed upward to simulate the slower melt rates and cooler conditions. For south-facing aspects, $TAELEV > ELEV$ so temperatures were lapsed downward to simulate increased melt from solar influence. The updated parameterization where the MODIS data are employed requires an upward adjustment of these values because the areal depletion curve is no longer controlling the melt rate; thus SCE present on northern, upper elevation slopes in the late spring must have higher melt rates applied to melt the snow with the correct timing. The primary reason that the areal depletion curves in SNOW17 differs from one that would be derived from actual measurements of SCE is that melt rates decline as SCE declines because the remaining snow is usually found in locations where snow melts at a slower rate, such as under canopies or on north facing slopes (Anderson, 2006).

Adjustments to MFMAX across the northern units represented the underestimation of the modified areal depletion curves within SNOW17 to accurately capture snow covered area. At many of the sites, particularly for the MODSCAG product, the MFMAX for the northern sites required adjustment upwards; indicating a lower setting in the APRFC run that is attempting to account for cooler temperatures on the northern slopes by retaining the snow on these slopes for longer and hence slowing runoff (Franz and Karsten 2013). By more accurately representing the conditions on the northern units of the watersheds, the MODIS runs required an increase in the snowmelt factor that would allow for initiation of the melt on these slopes. The MFMAX represents the dependency between the melt factor to account for a constant SCE curve used in the model; and the ability of the 'standard' SCE curves used in the APRFC SNOW17 to replicate the conditions of the melt properties within the basins (Shamir and Georgakakos 2007). As noted in Shamir and Georgakakos (2007), there is considerable inter-annual variability in snow cover depletion and this variability is not represented when the standard APRFC model is applied. Thus by improving the internal physical processes in the model, the snowmelt timing should improve. However, this still may not translate into improved discharge estimates because precipitation and temperature inputs may still be incorrect, and errors in forcing data that generates incorrect water equivalents for snow carry larger uncertainty bounds than that which can be impacted by changing the weighting factors and timing of snowmelt by adjusting SCE, as undertaken here.

For the MOD10A1 calibration, fewer parameters were adjusted compared to the MODSCAG runs. The end result is that the MODSCAG data has improvements that are slightly greater than the MOD10A1 result. The model parameters require greater adjustment for MODSCAG runs as a result of

the variability between the two data sets compared to the baseline runs of the model. As shown in Figure 5.3, the MODSCAG data have a different melt trajectory for northern slopes, and holds snow for longer on the south facing slopes of the Upper Chena River basin while the MOD10A1 acts similarly to the APRFC melt trajectory for SWE data. Whether this is more correct or not is difficult to say. This region is known to have variable melt timing based on south-facing slopes therefore the north and south slopes should be differentiated to reflect the physical processes occurring on the warmer south facing slopes compared to the cold, and often permafrost dominated north facing slopes (Jones and Rinehart, 2010). Although MODSCAG improvement is noted for Chatanika and Goodpaster basins in the streamflow statistics, the results for both MODIS versions are overall very similar in this region. This may be due to the different canopy adjustments applied to the data sets, or because of the lack of a spectral end member for the boreal forest. Regardless, it is not clear that one of these data sets is markedly improving streamflow estimates and it is possible that both approaches could be considerably useful as additional observations of SCE estimates for the region.

Two other means by which the CHPS framework can be altered to improve streamflow estimates are explored in this work. The interpolation between missing data values is altered from 1 day to 11 days to determine how changing the value impacted model results. Generally, the number of days of interpolation had little impact on the results, but the longer interpolation period results produced slightly higher correlations and improved streamflow estimation. The SCTOL parameter in the SNOW17 model indicates a means by which a partial rule-based direct insertion approach can be simulated without any additional change to the CHPS model framework. Because this allows for interaction between the model and the observed MODIS SCE data, it may be a useful technique for the RFCs to apply during recalibration efforts to observed snow cover data. An advantage is noted between the MODSCAG with an SCTOL setting greater than to 0.25. However, the basins with the strongest improvement (Chatanika) over the APRFC run did not improve using an SCTOL greater than zero because the baseline model performed so poorly given the weakness of the underlying observed discharge data. Therefore the RFCs may wish to selectively apply this parameter when basins have reliable observed information and the MODIS data can be utilized partially in conjunction with the model ADC and partially on the MODIS SCE observations.

5.5 Conclusions

Although complex tools and distributed models are available in the CHPS system, the RFCs across the US are not currently using these features in their river forecasting to estimate flooding and droughts. This study focuses on developing tools that can, with a minor amount of testing, be brought into the RFC's CHPS modeling framework and used to improve physical estimates of SCE across watersheds

of interest. The method integrates information such as the MODIS remotely sensed snow cover into the model framework using a simple calibration approach for the SNOW17 model, and also provides some input regarding expected improvements and other possible parameters that can be introduced to improve forecasting and simulation of streamflow. These interim modes of research and operations are badly needed until a point at which the RFCs are prepared to transition to more complex modeling and data assimilation tools. Several outstanding questions are answered regarding the application of this data in the RFC models, mainly the limited impact of changing the interpolation length between missing days, and also the new algorithms for estimating SCE based on MODIS remotely sensed data. Basins with poor quality streamflow observations benefited from the use of the MODIS SCE but improvements are also made to the internal snow timing estimates, observed in both the validation against SNOTEL data and also through the calibration that corrected the model parameters to better reflect the physical differences altering processes occurring on north and south facing slopes. Although marginal differences were observed between MOD10A1 and MODSCAG data, the MODSCAG data provided a slight improvement over MOD10A1 when improvements to streamflow simulations were observed for both data sets. The utility of the MODIS data in CHPS also goes beyond improvements to the streamflow; these tools can be used for a number of internal checks for SWE and SCE that are currently under way, such as the ingestion of data for multi-model ensemble forecasts (HEFS) (Lindsey, pers. comm). This study opens the door for insertion of parameters via assimilation alongside developments such as physically based model usage.

5.6 Acknowledgements

Bennett acknowledges support for this work from the Alaska Climate Science Center and the National Science and Engineering Research Council of Canada. Bennett, Balk, and Cherry acknowledge support from the GOES-R High Latitude Proving Ground award NA08OAR432075. The authors thank the Alaska Pacific River Forecast Center staff for their collaborative efforts and the Arctic Region Supercomputer Center for the use of their supercomputer PACMAN.

5.7 Figures

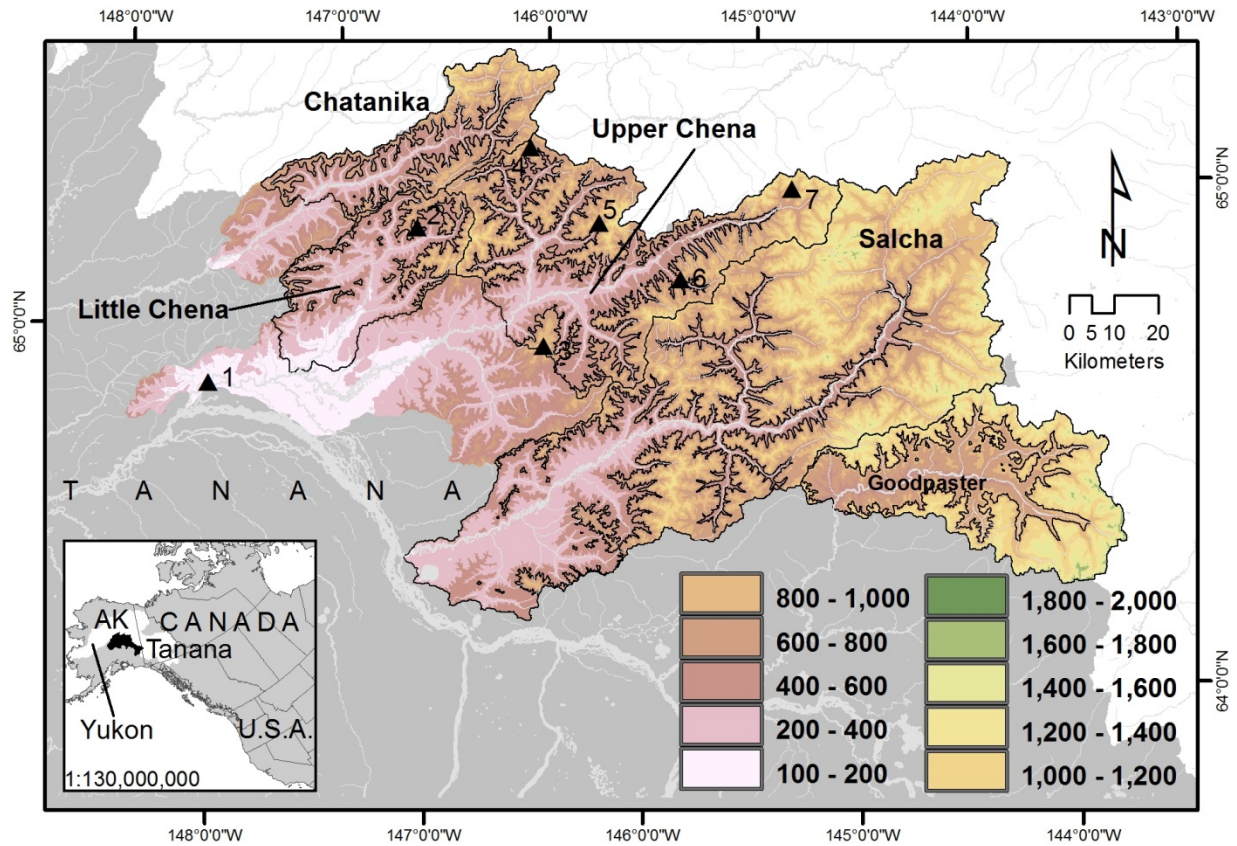


Figure 5.1 Map of the four study basins with upper and lower divisions shown. Alaska SNOTEL sites are shown with black triangles, number indicate SNOTEL sites; 1), Fairbanks International Airport 2) Little Chena Ridge, 3), Munson Ridge, 4) Mt. Ryan, 5), Monument Creek, 6) Teuchet Creek, 7) Upper Chena (Table 5.2). Legend illustrates topographic variation throughout the basins. Inset shows the Tanana River basins location in the Yukon watershed in proximity to Canada and the USA.

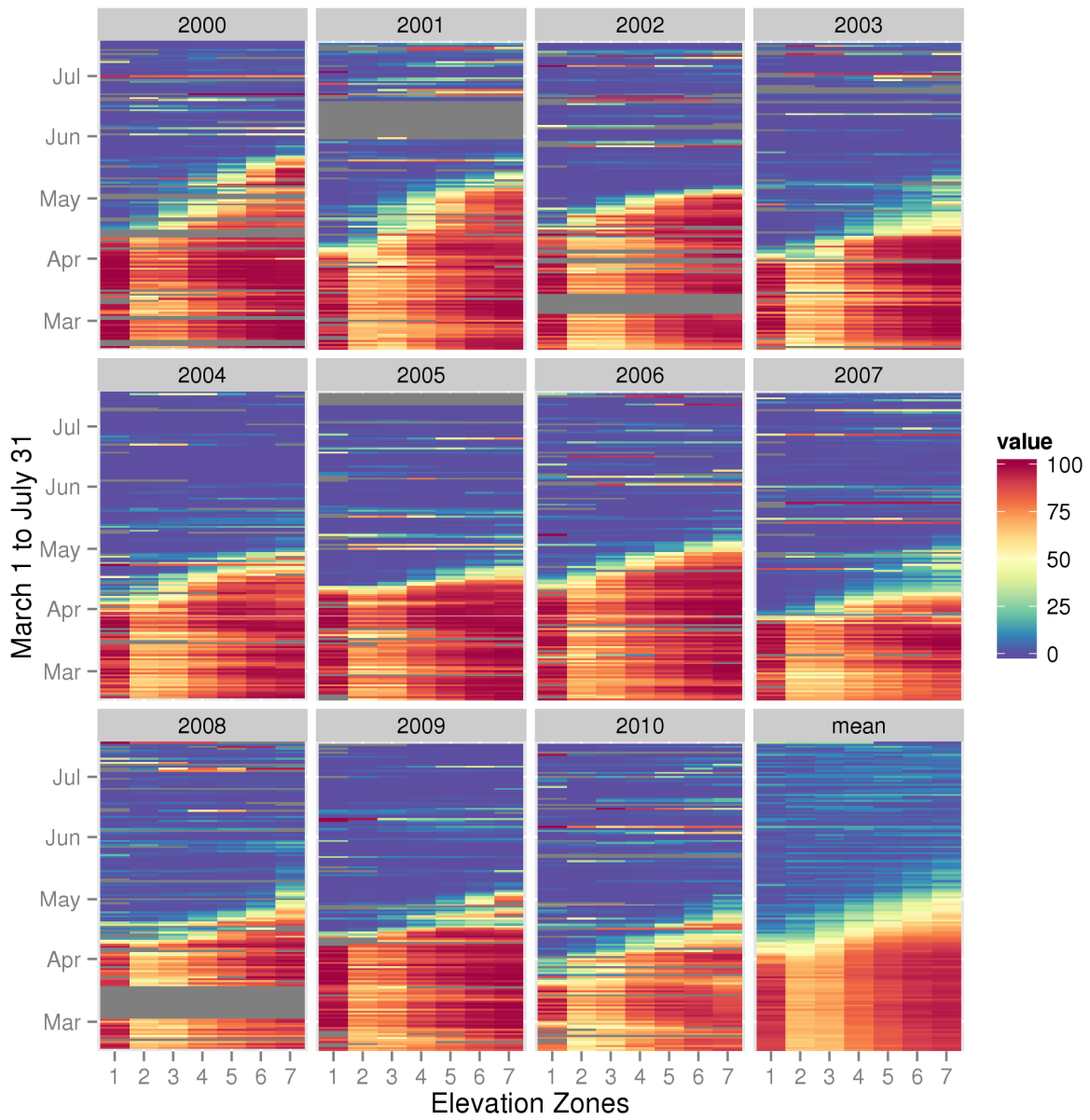


Figure 5.2 Snow cover fractional extents based on MOD10A1 for the entire region divided into elevation zones. The years 2000 to 2010 are shown, with the mean of all years in the final panel. Grey areas indicate dates when there is no SCE information (i.e. cloud cover, sensor error).

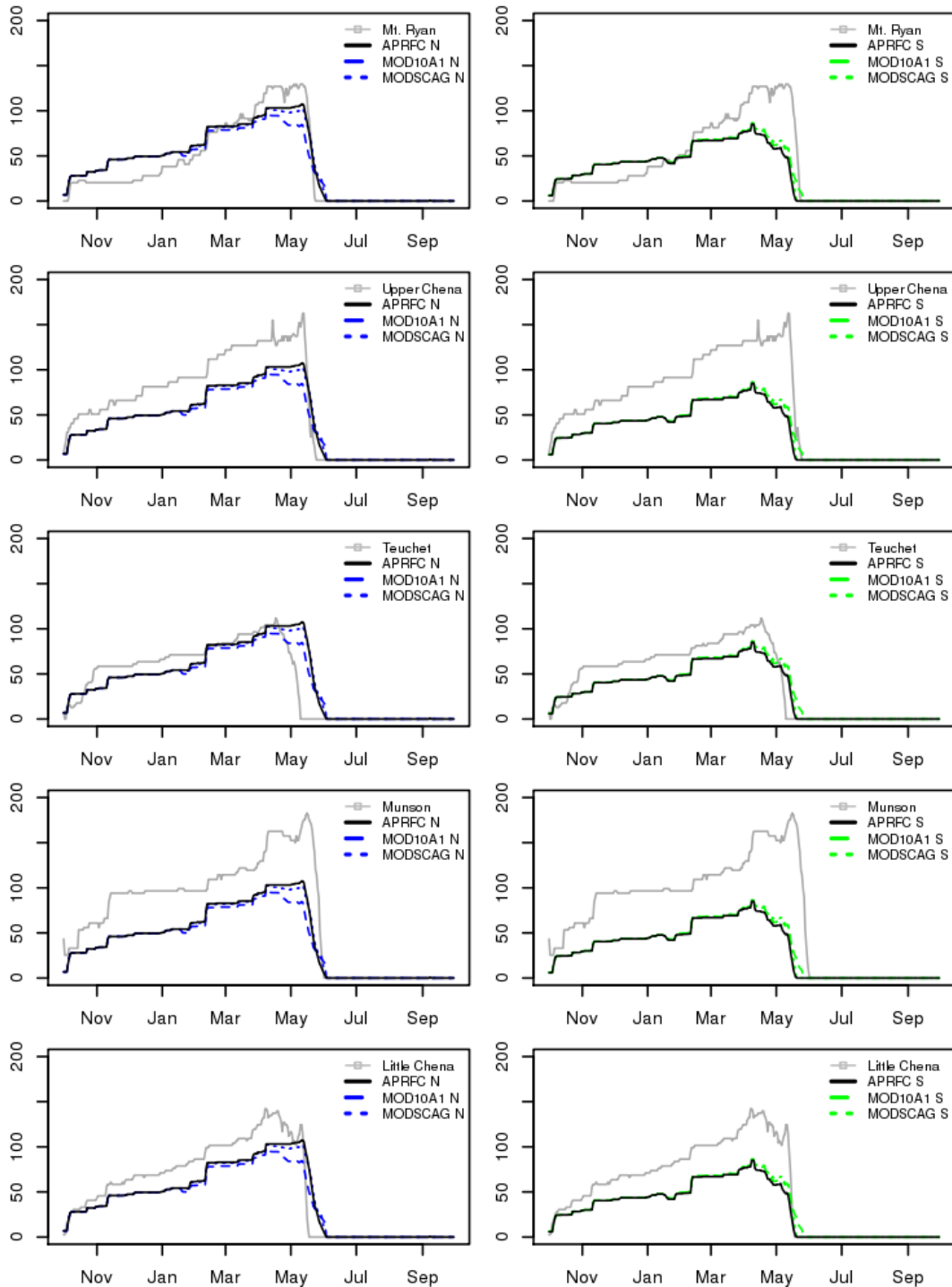


Figure 5.3 Simulated model output for SWE (mm) versus SNOTEL SWE (mm) for APRFC (solid black), MOD10A1 (dashed), MODSCAG (dotted) for October 2000 to June 30th, 2001. The north slope of the Upper Chena River basin is shown in blue in left panels, and the south slope is shown in green on right panel.

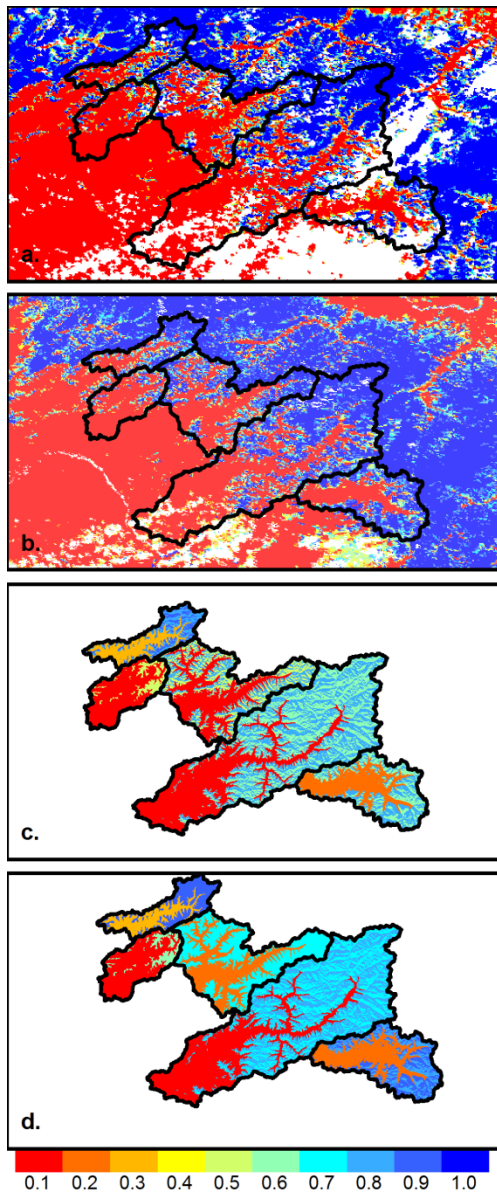


Figure 5.4 Study area areal extent of snow cover in the CHPS model framework for a) MOD10A1, b) MODSCAG, where white is either missing or cloud covered, and the lumped snow cover extent based on c) MOD10A1, and d) MODSCAG for all basins for May 15th, 2001. Values range from 0.1 to 1, or 10% to 100% snow cover.

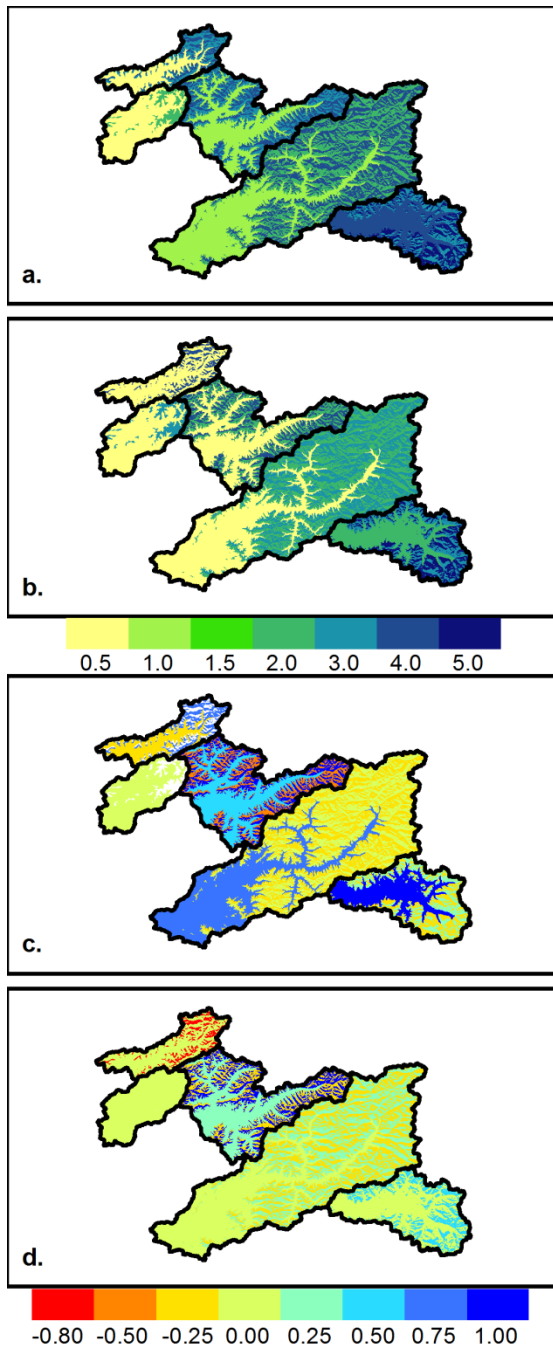


Figure 5.5 Study area basin SWE (in) estimates in CHPS model framework for a) MOD10A1, b) MODSCAG, and the difference between the both SWE estimates and the APRFC run (positive values are higher MODIS, and negative values are higher APRFC estimates, Figure c and d) for May 15th, 2001.

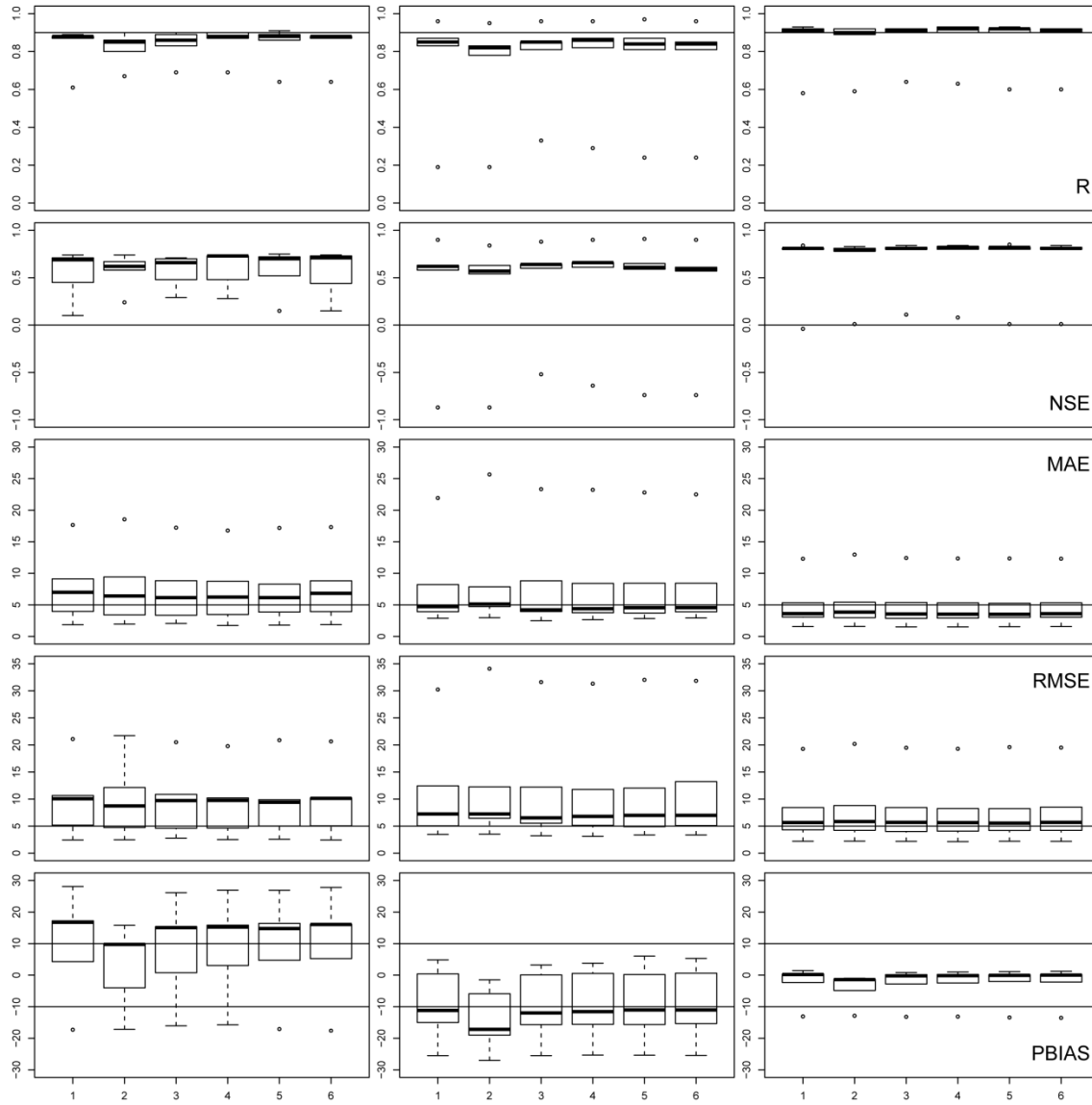


Figure 5.6 Streamflow evaluation and validation statistics for R, NSE, MAE, RMSE and PBAIS for calibration (first column), validation (second column) and third row (period of record). Values given for all five basins within boxplots, 1=APRFC, 2=MOD10A1, 3=MODSCAG, 4= MODSCAG with SCTOL=0.25, 5= MODSCAG with SCTOL=0.50, 6= MODSCAG with SCTOL=0.75).

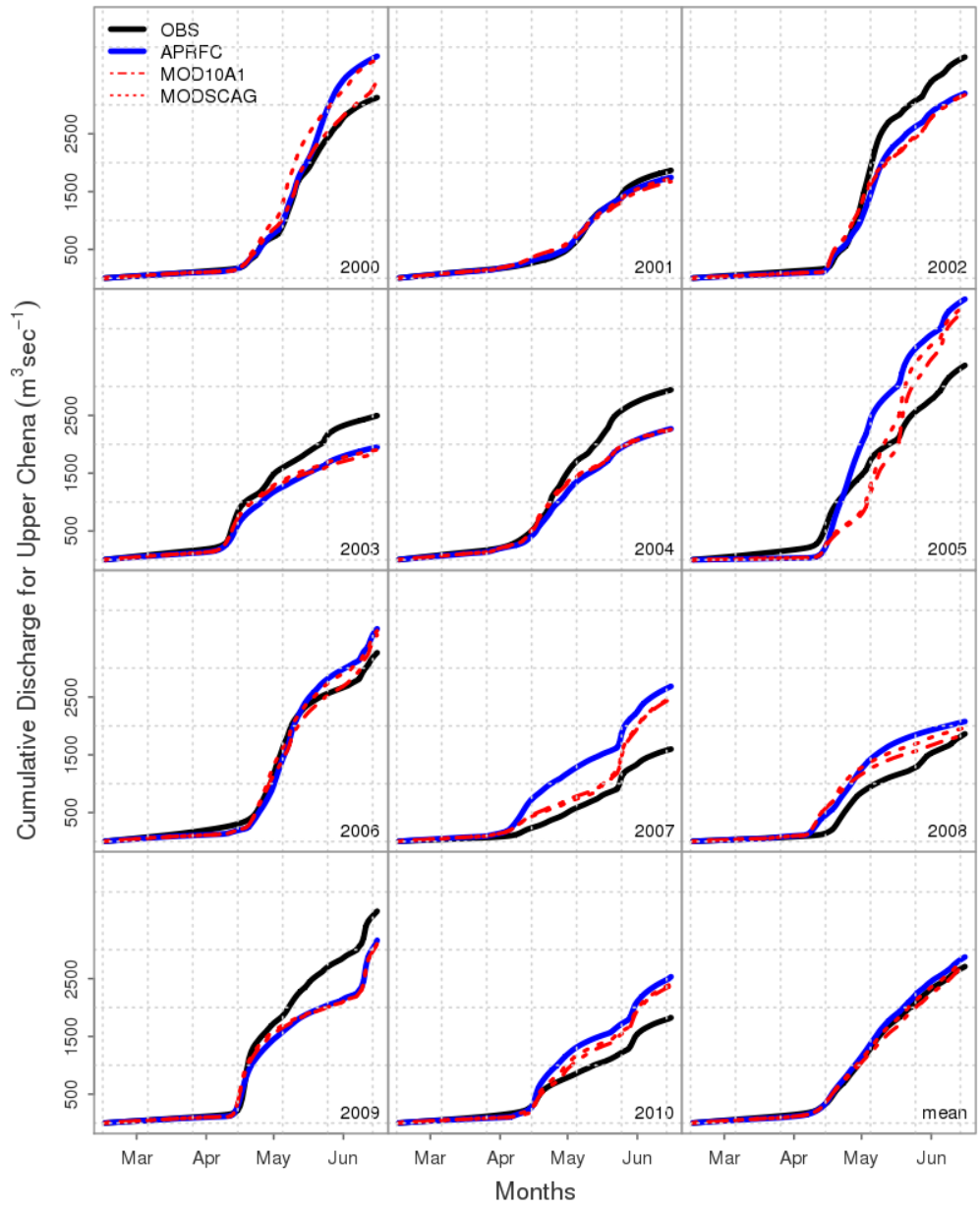


Figure 5.7 Upper Chena River basin simulated versus observed flows. Observed (black line), simulated APRFC (blue) simulated MOD10A1 (red dash-dot line) and MODSCAG (red dotted line) as the cumulative flow distribution for all years 2000-2010. The mean of all years is shown in the final panel.

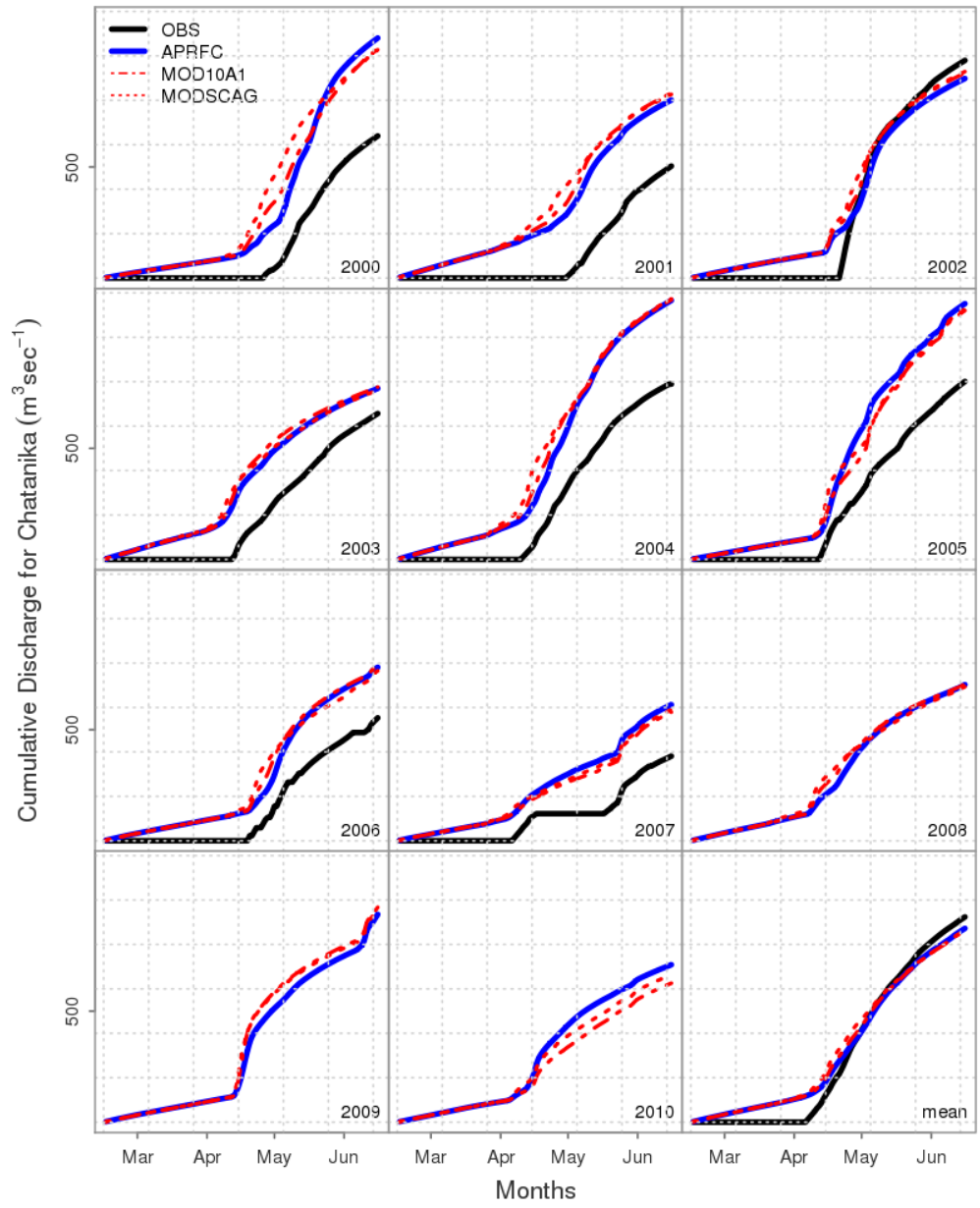


Figure 5.8 Chatanika River basin simulated versus observed flows. Observed (black line), simulated APRFC (blue) simulated MOD10A1 (red dash-dot line) and MODSCAG (red dotted line) as the cumulative flow distribution. The mean of all years is shown in the final panel.

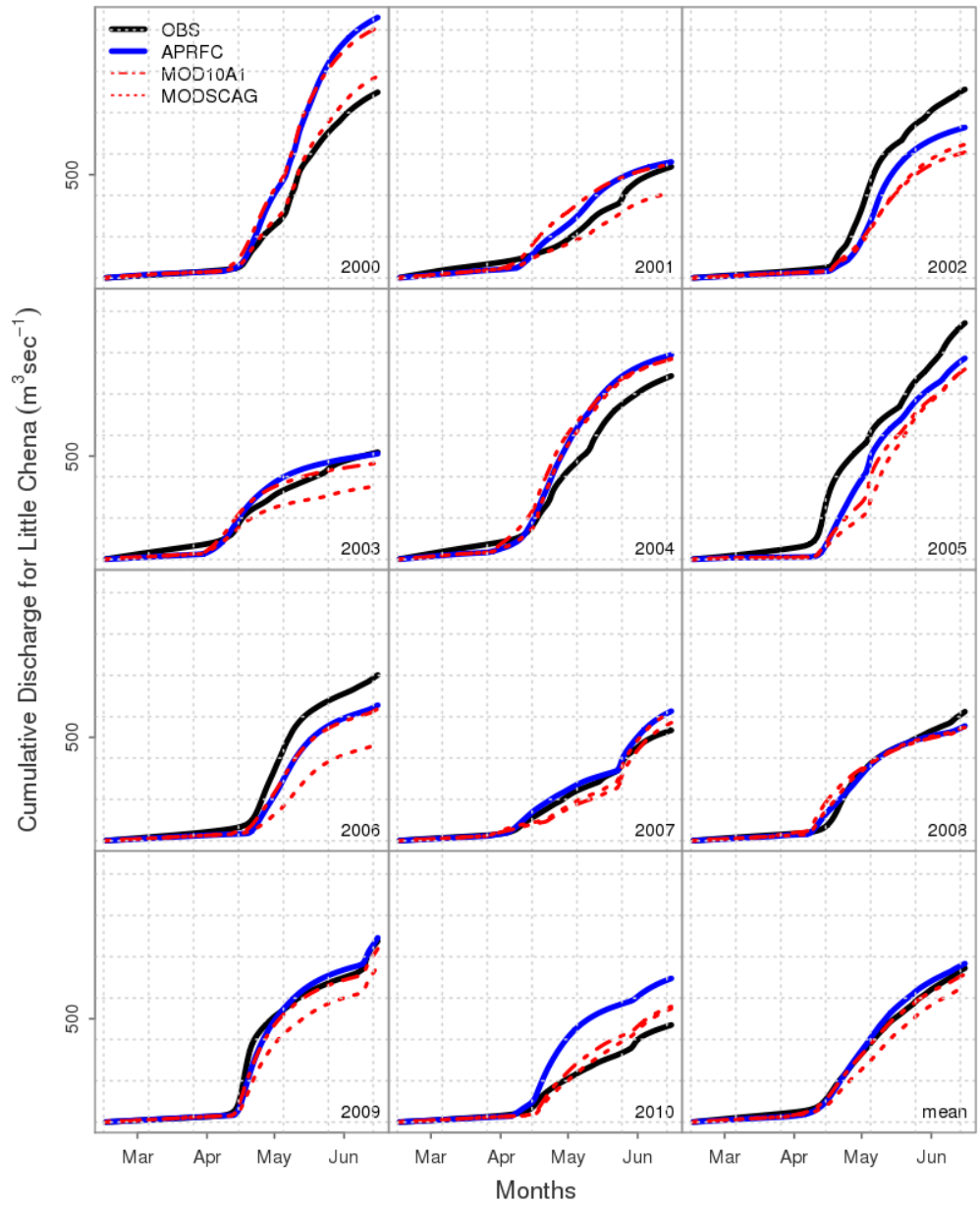


Figure 5.9 Little Chena River basin simulated versus observed flows. Observed (black line), simulated APRFC (blue) simulated MOD10A1 (red dash-dot line) and MODSCAG (red dotted line) as the cumulative flow distribution. The mean of all years is shown in the final panel.

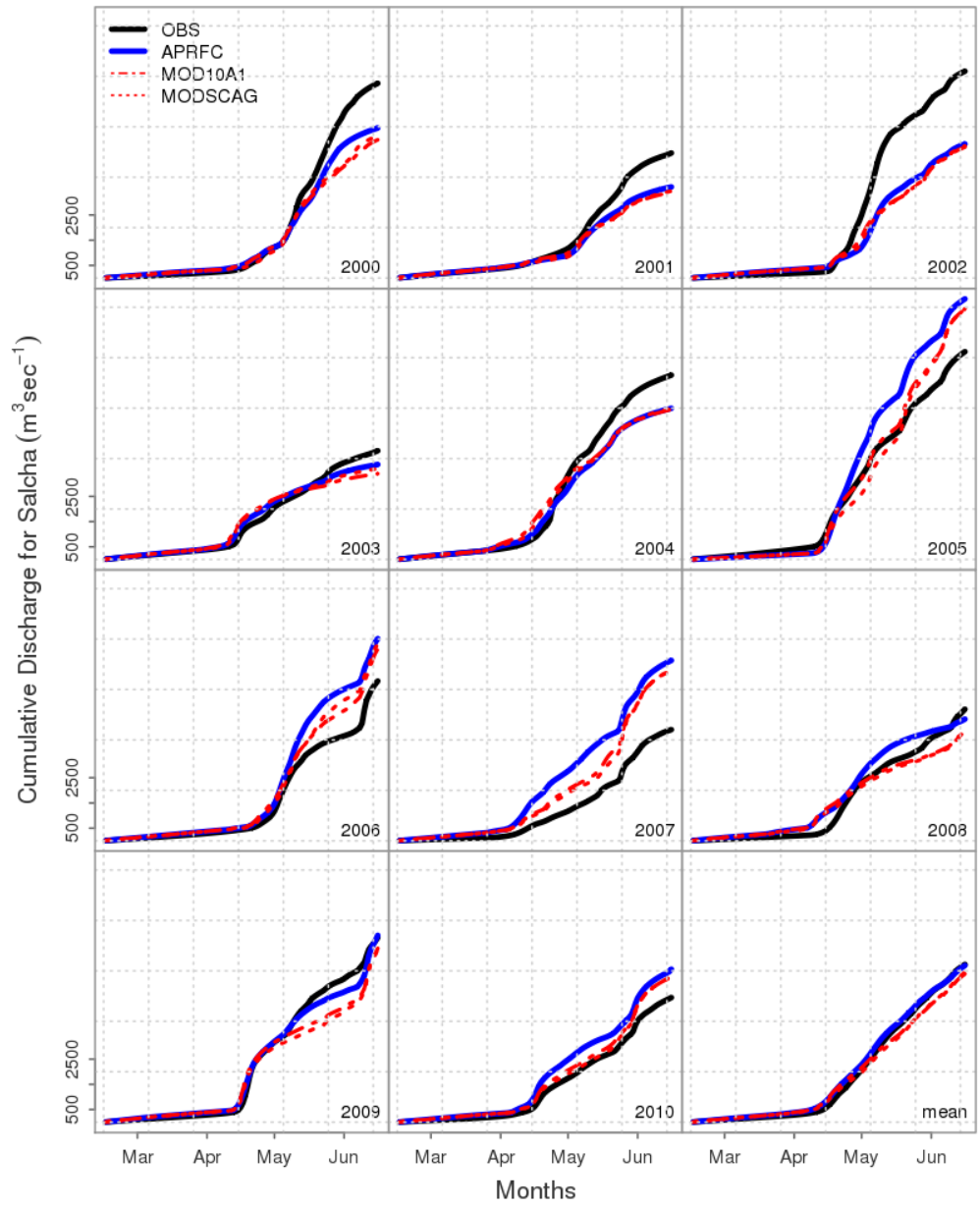


Figure 5.10 Salcha River basin simulated versus observed flows. Observed (black line), simulated APRFC (blue) simulated MOD10A1 (red dash-dot line) and MODSCAG (red dotted line) as the cumulative flow distribution. The mean of all years is shown in the final panel.

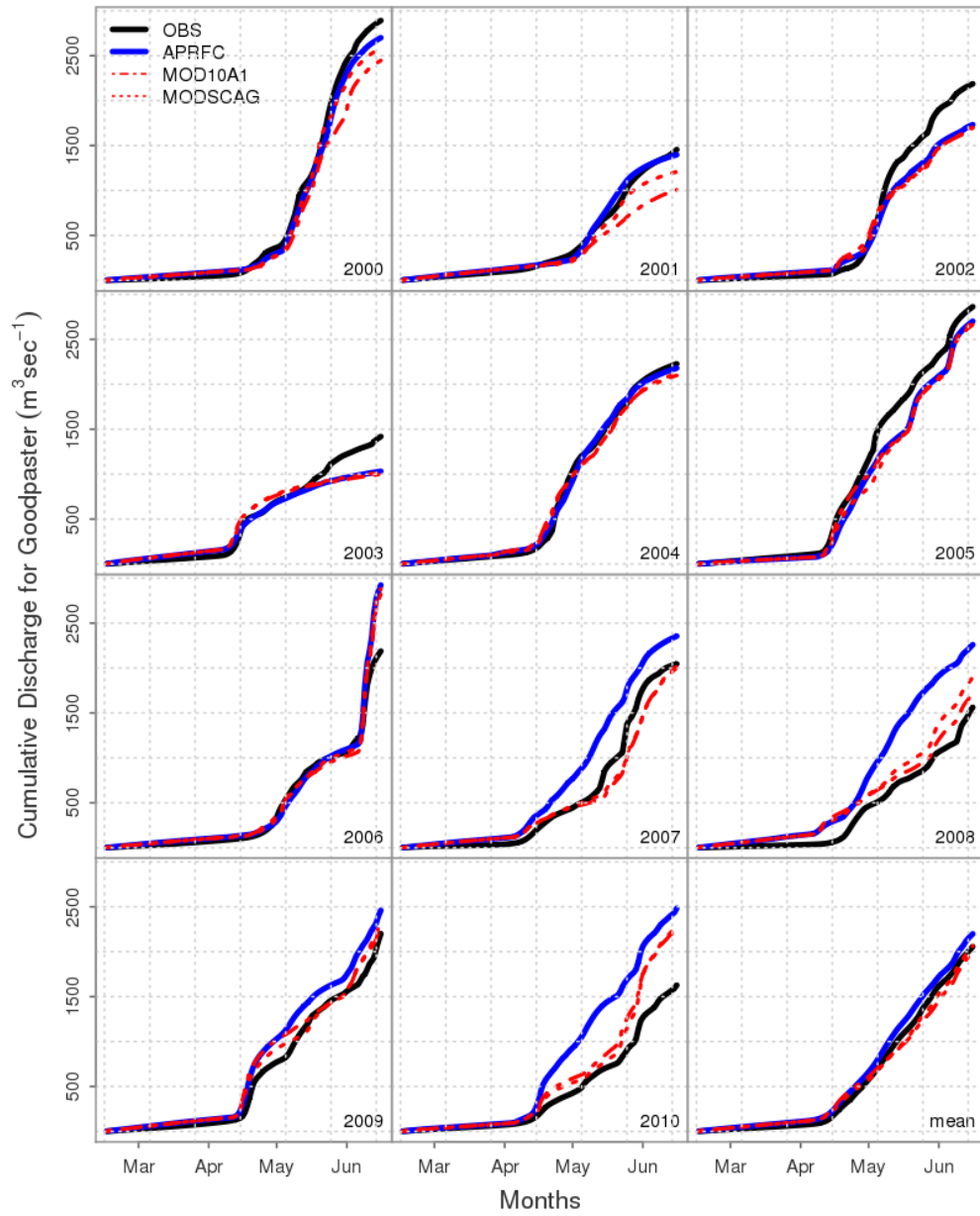


Figure 5.11 Goodpaster River basin simulated versus observed flows. Observed (black line), simulated APRFC (blue) simulated MOD10A1 (red dash-dot line) and MODSCAG (red dotted line) as the cumulative flow distribution. The mean of all years is shown in the final panel.

5.8 Tables

Table 5.1 Sub-basin characteristics, including name, sub-basin ID, area, elev (elevation, mean and range below in brackets), T (temperature, January and July), P (precipitation, winter October-March and summer April-September in brackets), Q (annual average daily discharge), % basin units (lower, N=north and S=south), % land cover (based on majority cover values*). T, P, and Q calculated for the 2000-2010 water year.

Name	Sub-basin ID	Sub-basin Unit	Area (km ²)	Elev (m)	T (°C)	P (mm)	Q (m ³ /s/d)	% Units (N/S ⁺)	% Land cover
Chatanika at the Steese	CRSA2	Lower	395	475 (228 – 625)	-22.5 (12.6)	96 (393)	11	42	9 D, 83 C, 4S
		Upper	558	780 (548 – 1513)	-18.5 (11.9)	116 (441)		25/33	0 D 76 C, 15 S / 2 D, 47 C, 39 S
Little Chena	CHLA2	Lower	802	380 (141 – 617)	-24.4 (13.7)	97 (385)	6	78	16 D, 78 C, 5 S
		Upper	225	721 (584 – 1230)	-21 (11.5)	116 (464)		10/12	2 D, 80 C, 13 S / 8 D, 63 C, 26 S
Upper Chena	UCHA2	Lower	973	466 (223 – 626)	-22.5 (12.7)	75 (370)	20	40	9 D, 84 C, 5 S
		Upper	1462	806 (553 – 1584)	-18.2 (11.6)	103 (426)		29/31	2 D, 74 C, 17 S / 10 D, 54 C, 33 S
Salcha	SALA2	Lower	1838	421 (194 – 624)	-23.9 (13.8)	74 (364)	44	32	18 D, 69 C, 10 S
		Upper	3900	924 (581 – 1768)	-19.3 (10.6)	111 (475)		33/35	2 D, 63 C, 20 S / 7 D, 50 C, 31 S
Goodpaster	GBDA2	Lower	737	734 (411 – 967)	-20.6 (11.8)	83 (389)	14	42	2 D, 84 C, 12 S
		Upper	1036	1166 (873 – 1961)	-19.3 (10.1)	104 (465)		29/29	5 C, 33 D 45 S / 2 D, 24 C, 56 S

+denoted for upper units only

Table 5.2 SNOTEL stations, map identification, length of record, and average snow water equivalent (SWE) used to compare model SWE results. Average SWE is based on the average over the entire period of record, and summed over the snow season.

SNOTEL Station	Map ID	Record Length	Average SWE (mm)
Fairbanks F.O. (47P03)	1	1983-current	446
Little Chena Ridge (46Q02)	2	1981-current	595
Munson Ridge (46P01)	3	1980-current	1016
Mt. Ryan (46Q01)	4	1981-current	639
Monument Creek (45Q02)	5	1980-current	554
Teuchet Creek (45P03)	6	1981-current	461
Upper Chena (44Q07)	7	1985-current	792

Table 5.3 Range of parameter values in the SNOW17 model for APRFC and MODIS runs. Sensitivity indicates whether a parameter is major or minor influence in the model. Minimum (Min) and maximum (Max) ranges are provided.

Parameter	Sensitivity	Description	Min	Max
SCF	Major	Snow correction factor that adjusts precipitation for gage deficiencies and processes not explicitly represented in the model (dimensionless)	0.65	0.95
MFMAX	Major	Maximum melt factor during non-rain periods occurring on June 21 (mm/°C/6 hrs)	0.9	1.4
MFMIN	Major	Minimum melt factor during non-rain periods occurring on December 21(mm/°C/6 hrs)	0.2	0.2
UADJ	Major	Average wind function during rain-on-snow periods (mm/mb)	0.03	0.03
SI	Major	Mean areal snow water equivalent below which there is less than 100% snow cover and the areal depletion curve is applied (mm)	500	500
NMF	Minor	Maximum negative melt factor (mm/°C/6 hrs)	0.15	0.3
DAYGM	Minor	Constant melt rate at the snow/soil interface (mm)	0	0
MBASE	Minor	Base air temperature for non-rain melt computations (°C)	0	0
PXTEMP	Minor	Air temperature threshold determining precipitation as rain or snow (°C)	1.7	1.7
PLWHC	Minor	Maximum liquid water holding capacity of the snowpack (decimal fraction)	0.05	0.05
TIPM	Minor	Antecedent temperature index (dimensionless)	0.1	0.1
PXADJ	Minor	Adjustment factor for precipitation, must be between 0.0 and 1.0 (dimensionless)	0.97	1.21
TAELEV	Minor	Elevation associated with the air temperature time series (m)	380	1267
ELEV	Minor	Average sub-basin elevation (m)	380	1167
SCTOL	Minor	Tolerance used when updating water-equivalent or areal extent of snow cover with observed data. Range is 0.0 to 1.0. Updates when Simulated-Observed > tolerance *Observed (dimensionless)	0	0.05

Table 5.4 Parameters for the MOD10A1 calibration. North (N), south (S) and lower (L) sub-basins are described. The first column indicates the parameter value in the APRFC calibration; the second parameter provides the value for the MODIS calibration. Bolded values indicate change.

Parameters	Sensitivity	N		S		L		N		S		L		U	L		
		CRSA2						UCHA2						CHLA2			
MFMAX	Major	1.00	1.00	1.40	1.40	1.00	1.40	0.90	0.90	1.40	1.40	1.00	1.00	0.90	1.40	1.30	1.40
NMF	Minor	0.30	0.15	0.30	0.20	0.30	0.20	0.30	0.15	0.30	0.20	0.30	0.20	0.20	0.20	0.20	0.20
TAELEV	Minor	665	865	1088	988	474	474	708	908	1002	908	465	465	720	820	380	480
SCTOL	Minor	0.05	0.00	0.05	0.00	0.05	0.00	0.05	0.00	0.05	0.00	0.05	0.00	0.05	0.00	0.05	0.00
		SALA2						GBDA2									
MFMAX	Major	0.90	0.90	1.40	1.40	1.00	1.00	0.90	1.00	1.40	1.40	1.00	0.90				
NMF	Minor	0.30	0.15	0.30	0.20	0.30	0.20	0.30	0.15	0.30	0.20	0.30	0.20				
TAELEV	Minor	823	1023	1123	1123	420	420	863	1167	1267	1267	734	734				
SCTOL	Minor	0.05	0.00	0.05	0.00	0.05	0.00	0.05	0.00	0.05	0.00	0.05	0.00				

Table 5.5 Parameters employed in the MODSCAG calibration. North (N), south (S) and lower (L) sub-basins are described. The first column indicates the parameter value in the APRFC calibration; the second parameter provides the value for the calibration. Bolded values indicate changes were made.

Parameters	Sensitivity	N	S	L	N	S	L	U	L								
				CRSA2				UCHA2				CHLA2					
MFMAX	Major	1.00	1.20	1.40	1.40	1.00	1.2	0.90	1.00	1.40	1.40	1.00	0.90	0.90	0.90	1.30	1.20
NMF	Minor	0.30	0.15	0.30	0.20	0.30	0.2	0.30	0.15	0.30	0.20	0.30	0.20	0.30	0.20	0.30	0.20
TAELEV	Minor	665	665	1088	1088	474	474	708	702	1002	902	465	465	720	720	380	580
SCTOL	Minor	0.05	0.00	0.05	0.00	0.05	0.00	0.05	0.00	0.05	0.00	0.05	0.00	0.05	0.00	0.05	0.00
				SALA2				GBDA2									
MFMAX	Major	0.90	1.00	1.40	1.40	1.00	1.10	0.90	1.00	1.40	1.40	1.00	0.90				
NMF	Minor	0.30	0.15	0.30	0.20	0.30	0.20	0.30	0.15	0.30	0.20	0.30	0.20				
TAELEV	Minor	823	923	1123	1023	420	420	863	863	1267	1163	734	734				
SCTOL	Minor	0.05	0.00	0.05	0.00	0.05	0.00	0.05	0.00	0.05	0.00	0.05	0.00				

Table 5.6 April-May-June monthly calibration statistics (Cal), validation (Val) and the period of record (Per., 1999-2010) statistics (MAE=mean absolute error (m3/sec), NSE=Nash Sutcliff efficiency (unitless), PBIAS=flow bias (%), R=correlation coefficient (unitless), and RMSE=root mean squared error (m3/sec) for APRFC, and MOD10A1, and MODSCAG modeled discharge for all basins.

	Stat	Cal.	Val.	Per.	Cal.	Val.	Per.	Cal.	Val.	Per.
		APRFC			MOD10A1			MODSCAG		
CRSA2	MAE	3.96	4.73	3.07	3.45	4.64	2.96	3.26	4.17	2.85
	NSE	0.10	-0.87	-0.04	0.27	-0.81	0.03	0.30	-0.40	0.14
	PBias	-17.28	-25.48	-13.08	-16.68	-26.74	-13.01	-18.34	-27.26	-13.53
	R	0.61	0.19	0.58	0.69	0.21	0.61	0.72	0.37	0.64
	RMSE	5.17	7.24	4.31	4.65	7.12	4.16	4.57	6.27	3.94
CHLA2	MAE	1.85	2.88	1.57	1.95	2.97	1.59	2.28	1.98	1.51
	NSE	0.74	0.58	0.81	0.74	0.57	0.81	0.59	0.73	0.81
	PBias	4.29	4.84	-2.32	-4.01	-1.48	-4.87	-10.27	-10.98	-7.24
	Corr.	0.88	0.87	0.93	0.86	0.82	0.92	0.78	0.89	0.92
	RMSE	2.44	3.46	2.20	2.47	3.51	2.22	3.09	2.80	2.21
UCHA2	MAE	9.12	8.22	5.34	9.06	8.02	5.39	8.77	8.45	5.32
	NSE	0.71	0.62	0.81	0.64	0.65	0.80	0.65	0.68	0.81
	PBias	16.76	0.39	0.21	10.63	-4.49	-0.87	12.66	-0.96	-0.51
	Corr.	0.87	0.85	0.91	0.81	0.84	0.91	0.83	0.86	0.91
	RMSE	10.64	12.43	8.43	11.85	11.95	8.66	11.70	11.51	8.40
SALA2	MAE	17.66	21.93	12.31	19.36	25.13	13.02	20.21	23.59	12.81
	NSE	0.69	0.63	0.80	0.62	0.53	0.78	0.55	0.53	0.77
	PBias	17.21	-14.98	0.35	9.90	-18.98	-1.13	10.53	-17.64	-0.85
	Corr.	0.89	0.83	0.90	0.82	0.78	0.88	0.81	0.78	0.88
	RMSE	21.1	30.24	19.27	23.54	34.42	20.6	25.53	34.17	20.79
GBDA2	MAE	7.00	3.91	3.62	6.55	5.37	3.93	6.46	4.62	3.81
	NSE	0.45	0.90	0.84	0.56	0.83	0.82	0.52	0.86	0.83
	PBias	28.1	-11.17	1.46	14.29	-17.61	-1.31	17.65	-14.41	-0.37
	Corr.	0.88	0.96	0.92	0.89	0.95	0.91	0.90	0.95	0.92
	RMSE	10.05	5.05	5.66	8.92	6.77	6.01	9.40	6.08	5.93

Table 5.7 Comparison between RMSE (%) and NSE (in brackets) based on AMJ using SCTOL values of 0.25, 0.50 and 0.75. Differences are calculated as percent and absolute differences from the MODSCAG base run.

SCTOL		CRSA2	UCHA2	CHLA2	SALA2	GBDA2
0.25	Cal.	-2 (-0.02)	19 (0.14)	11 (0.07)	23 (0.18)	-4 (-0.04)
0.50		-8 (-0.24)	-11 (-0.07)	-1 (-0.01)	8 (0.08)	17 (0.04)
0.75		-3 (-0.06)	4 (0.02)	2 (0.01)	7 (0.03)	5 (0.01)
0.25	Val.	-10 (-0.15)	17 (0.13)	15 (0.1)	18 (0.15)	0 (-0.01)
0.50		-11 (-0.34)	-20 (-0.12)	-2 (-0.02)	6 (0.06)	22 (0.05)
0.75		-7 (-0.13)	1 (0.01)	3 (0.01)	6 (0.03)	6 (0.02)
0.25	Per.	-10 (-0.15)	21 (0.15)	12 (0.08)	19 (0.16)	-7 (-0.08)
0.50		-11 (-0.34)	-20 (-0.12)	-12 (-0.09)	7 (0.06)	17 (0.04)
0.75		-7 (-0.13)	1 (0.01)	-1 (0)	6 (0.03)	4 (0.01)

5.9 References

- Anderson, E., 2006. Snow Accumulation and Ablation Model - SNOW-17. http://www.nws.noaa.gov/oh/hrl/nwsrfs/users_manual/part2/_pdf/22snow17.pdf, NWS NOAA, pp. 44.
- Anderson, E.A., 1976. A point energy and mass balance model of a snow cover.
- Andreadis, K.M., Lettenmaier, D.P., 2006. Assimilating remotely sensed snow observations into a macroscale hydrology model. *Advances in Water Resources*, 29 (6): 872-886.
- Bennett, K.E., Walsh, J., 2014. Spatial and temporal changes in indices of extreme precipitation and temperature for Alaska. *International Journal of Climatology*. DOI: 10.1002/joc.4067.
- Burnash, R.J.E., Ferral, R.L., McGuire, R.A., 1973. A generalized streamflow simulation system, Joint Federal-State River Forecast Center, Sacramento, CA, pp. 204.
- Clark, M.P., Slater, A.G., Barrett, A.P., Hay, L.E., McCabe, G.J., Rajagopalan, B., Leavesley, G.H., 2006. Assimilation of snow covered area information into hydrologic and land-surface models. *Advances in water resources*, 29 (8): 1209-1221.
- Dowdeswell, J.A., Hagen, J.O., Björnsson, H., Glazovsky, A.F., Harrison, W.D., Holmlund, P., Jania, J., Koerner, R.M., Lefauconnier, B., Ommanney, C.S.L., 1997. The mass balance of circum-Arctic glaciers and recent climate change. *Quatern. Res.*, 48 (1): 1-14.
- Durand, M., Molotch, N.P., Margulis, S.A., 2008. Merging complementary remote sensing datasets in the context of snow water equivalent reconstruction. *Remote Sens. Environ.*, 112 (3): 1212-1225.
- Euskirchen, E., McGuire, A., Chapin III, F., Yi, S., Thompson, C., 2009. Changes in vegetation in northern Alaska under scenarios of climate change, 2003-2100: implications for climate feedbacks. *Ecol. Appl.*, 19 (4): 1022-1043.
- Franz, K.J., Hogue, T.S., Sorooshian, S., 2008. Operational snow modeling: Addressing the challenges of an energy balance model for National Weather Service forecasts. *Journal of Hydrology*, 360 (1-4): 48-66.
- Hall, D.K., Riggs, G.A., 2007. Accuracy assessment of the MODIS snow products. *Hydrol. Process.*, 21 (12): 1534-1547.
- Hall, D.K., Riggs, G.A., Salomonson, V.V., 2006. MODIS/Terra Snow Cover Daily L3 Global 500m Grid V005, 2000-Daily Updates. National Snow and Ice Data Center, Boulder, Colorado USA.
- Hall, D.K., Riggs, G.A., Salomonson, V.V., DiGirolamo, N.E., Bayr, K.J., 2002. MODIS snow-cover products. *Remote Sens. Environ.*, 83 (1): 181-194.

- He, M., Hogue, T.S., Franz, K.J., Margulis, S.A., Vrugt, J.A., 2011. Characterizing parameter sensitivity and uncertainty for a snow model across hydroclimatic regimes. *Advances in Water Resources*, 34 (1): 114-127.
- Hinzman, L.D., Bettez, N.D., Bolton, W.R., Chapin, F.S., Dyrgerov, M.B., Fastie, C.L., Griffith, B., Hollister, R.D., Hope, A., Hurlbert, H.P., Jensen, A.M., Jia, G.J., Jorgenson, T., Kane, D.L., Klein, D.R., Kofinas, G., Lynch, A.H., Lloyd, A.H., McGuire, A.D., Nelson, F.E., Oechel, W.C., Osterkamp, T.E., Racine, C.H., Romanovsky, V.E., Stone, R.S., Stow, D.A., Sturm, M.D., Walker, D.A., Webber, P.J., Welker, J.M., Winker, K.S., Yoshikawa, K., 2005. Evidence and implications of recent climate change in northern Alaska and other Arctic regions. *Clim. Change*, 72: 251-298.
- Hock, R., 2003. Temperature index melt modelling in mountain areas. *Journal of Hydrology*, 282: 104-115.
- Jones, J.B., Rinehart, A.J., 2010. The long-term response of stream flow to climatic warming in headwater streams of interior Alaska. *Canadian Journal of Forest Research-Revue Canadienne De Recherche Forestiere*, 40 (7): 1210-1218.
- Kane, V.R., Gillespie, A.R., McGaughey, R., Lutz, J.A., Ceder, K., Franklin, J.F., 2008. Interpretation and topographic compensation of conifer canopy self-shadowing. *Remote Sens. Environ.*, 112 (10): 3820-3832.
- Liu, J., Melloh, R.A., Woodcock, C.E., Davis, R.E., Ochs, E.S., 2004. The effect of viewing geometry and topography on viewable gap fractions through forest canopies. *Hydrol. Process.*, 18 (18): 3595-3607.
- Liu, J., Woodcock, C.E., Melloh, R.A., Davis, R.E., McKenzie, C., Painter, T.H., 2008. Modeling the view angle dependence of gap fractions in forest canopies: Implications for mapping fractional snow cover using optical remote sensing. *J. Hydrometeorol.*, 9 (5): 1005-1019.
- McGuire, M., Wood, A.W., Hamlet, A.F., Lettenmaier, D.P., 2006. Use of satellite data for streamflow and reservoir storage forecasts in the Snake River Basin. *Journal of Water Resources Planning and Management*, 132: 97.
- Molotch, N.P., Bales, R.C., 2005. Scaling snow observation from the point to the grid element: Implications for observation network design *Water Resour. Res.*, 41: 1-16.
- Molotch, N.P., Margulis, S.A., 2008. Estimating the distribution of snow water equivalent using remotely sensed snow cover data and a spatially distributed snowmelt model: A multi-resolution, multi-sensor comparison. *Advances in Water Resources*, 31 (11): 1503-1514.

- Overpeck, J., Hughen, K., Hardy, D., Bradley, R., Case, R., Douglas, M., Finney, B., Gajewski, K., Jacoby, G., Jennings, A., 1997. Arctic environmental change of the last four centuries. *Science*, 278 (5341): 1251-1256.
- Painter, T.H., Rittger, K., McKenzie, C., Slaughter, P., Davis, R.E., Dozier, J., 2009. Retrieval of subpixel snow covered area, grain size, and albedo from MODIS. *Remote Sens. Environ.*, 113 (4): 868-879.
- Parajka, J., Blöschl, G., 2008. The value of MODIS snow cover data in validating and calibrating conceptual hydrologic models. *Journal of Hydrology*, 358 (3): 240-258.
- Raleigh, M.S., Rittger, K., Moore, C.E., Henn, B., Lutz, J.A., Lundquist, J.D., 2013. Ground-based testing of MODIS fractional snow cover in subalpine meadows and forests of the Sierra Nevada. *Remote Sens. Environ.*, 128 (0): 44-57.
- Reed, S., Koren, V., Smith, M., Zhang, Z., Moreda, F., Seo, D.-J., 2004. Overall distributed model intercomparison project results. *Journal of Hydrology*, 298: 27-60.
- Rittger, K., Painter, T.H., Dozier, J., 2013. Assessment of methods for mapping snow cover from MODIS. *Advances in Water Resources*, 51: 367-380.
- Rodell, M., Houser, P., Jambor, U.e.a., Gottschalck, J., Mitchell, K., Meng, C.-J., Arsenault, K., Cosgrove, B., Radakovich, J., Bosilovich, M., 2004. The global land data assimilation system. *B. Am. Meteorol. Soc.*, 85 (3).
- Salomonson, V., Appel, I., 2004. Estimating fractional snow cover from MODIS using the normalized difference snow index. *Remote Sens. Environ.*, 89 (3): 351-360.
- Serreze, M.C., Barry, R.G., 2011. Processes and impacts of Arctic amplification: A research synthesis. *Global Planet. Change*, 77 (1-2): 85-96.
- Serreze, M.C., Francis, J.A., 2006. The Arctic amplification debate. *Clim. Change*, 76 (3-4): 241-264.
- Serreze, M.C., Walsh, J.E., Chapin, F.S., Osterkamp, T., Dyurgerov, M., Romanovsky, V., Oechel, W.C., Morison, J., Zhang, T., Barry, R.G., 2000. Observational evidence of recent change in the northern high-latitude environment. *Clim. Change*, 46 (1-2): 159-207.
- Sillmann, J., Kharin, V., Zhang, X., Zwiers, F., Bronaugh, D., 2013. Climate extremes indices in the CMIP5 multi-model ensemble. Part 1: Model evaluation in the present climate. *J. Geophys. Res.: Atmos.*
- Stahl, K., Moore, R.D., Floyer, J.A., Asplin, M.G., McKendry, I.G., 2006. Comparison of approaches for spatial interpolation of daily air temperature in a large region with complex topography and highly variable station density. *Agricultural and Forest Meteorology*, 139: 224-236.
- Stocker, T.F., Qin, D., Plattner, G.-K., Tignor, M., Allen, S.K., Boschung, J., Nauels, A., Xia, Y., Bex, V., Midgley, P.M., 2013. *Climate change 2013: The physical science basis*. Intergovernmental

Panel on Climate Change, Working Group I Contribution to the IPCC Fifth Assessment Report (AR5)(Cambridge Univ Press, New York).

Sun, C., Walker, J.P., Houser, P.R., 2004. A methodology for snow data assimilation in a land surface model. *J. Geophys. Res.: Atmos.*, 109 (D8): D08108.

Udnæs, H., Alfnes, E., Andreassen, L.M., 2007. Improving runoff modelling using satellite-derived snow covered area? *Nordic hydrology*, 38 (1): 21-32.

Werner, M., Schellekens, J., Gijssbers, P., Van Dijk, M., Van den Akker, O., Heynert, K., 2013. The Delft-FEWS flow forecasting system. *Environ. Model. Software*, 40: 65-77.

CHAPTER 6: CLIMATE CHANGE IMPACTS ON EXTREME EVENTS IN A SNOW DOMINATED WATERSHED OF BOREAL INTERIOR ALASKA¹

Abstract

The Interior discontinuous permafrost zone of the boreal subarctic represents one of the largest ecosystems on earth and is vastly understudied with respect to changing hydrologic extreme events. This work focuses on an analysis of extreme events in Interior Alaskan watersheds using six global climate models, two emission scenarios, two hydrologic models and two different time periods to project changes in a snowmelt dominated basin of the Tanana River, a sub-watershed to the Yukon River system. Increases for minimum and maximum temperature and changes in the distribution of annual precipitation result in large shifts within these watersheds. Minimum temperature, maximum temperature and five-day precipitation are captured well by the downscaled GCMs, with expected underestimation in the variability around maximum temperature and precipitation, based on the 1971-2000 time period at the Fairbanks Airport Global Historical Climate Network first order climate station. Future extreme peak flow events become increasingly large and associated with rainfall induced peak flow events, as the dominant driver of streamflow shifts from snowmelt to a snowmelt-rainfall mixed system by the 2050s and a rainfall driven system by the 2080s. Analysis of changing return intervals based on generalized extreme value theorem approaches indicate that 5, 10 and 20 year peak flows will increase by 1.6 times in flow volume and the 100-year flow event will double by the 2080s. Percentile flow exceedances were five times greater for maximum (99th) percentile flood events than the median (50th) percentile flood events, indicating great underestimation of risk if return interval analysis is based on median (mean) condition. Given the large changes projected by GCMs and hydrologic models for maximum flow events, analysis of projected changes in streamflow should focus on maximum distributions in order to fully evaluate the potential for flooding and associated impacts in regional studies.

¹ K.E. Bennett, Cherry, J.E., Hinzman, L, Walsh, J.E. Climate change impacts on extreme events in a snow dominated watershed of boreal Interior Alaska.

6.1 Introduction

The discontinuous permafrost zone of the boreal subarctic represents one of the largest ecosystems on earth and is vastly understudied with respect to changing hydrologic extreme events. Extreme hydrologic events in Alaska's Interior boreal forest may be exasperated by climate shifts linked to the warming of the hydroclimate system in the Arctic (Stocker et al., 2013). These events have the propensity to impact ecosystems and infrastructure services in severe and possibly irreversible ways. The occurrence, duration, frequency, and timing of extreme events may change, such that existing modeling, forecasting and management tools and/or rule based infrastructure designs may be ineffective in the face of such changes. As such, it is important for both scientists and managers to understand the risks associated with changing streamflow extremes, where vulnerability exist in the context of these changes and how to best plan for changes in the face of uncertainties around specific numbers.

At the global level, Working Groups I (WGI) and II (WGII) of the IPCC's Special Report on Managing the Risks of Extreme Events and Disasters to Advance Climate Change Adaptation (SREX) was released in 2012 (IPCC, 2012). Chapter three of this report specifically details how extremes are changing, with emphasis on shifts in temperature, precipitation, droughts and floods. Temperature extremes have changed - cold days and nights have decreased while warm days and nights have increased and the length of warm spells or heat waves has increased in many regions and in particular in the high latitude Northern Hemisphere region (Alexander et al., 2006; Trenberth et al., 2007). Brown et al. (2008) found extreme trends in land area annual daily maximum temperature maximums and minimums to be increasing across most of the Arctic (1.64-1.95°C), with annual daily minimum temperature maximums and minimums exhibiting the greatest change over the largest percentage of the area (1.98-2.49°C) based on gridded data from 1950-2004.

Trends in the number of days above the 90th percentile of minimum temperature for Alaska are for 1-3 more days per decade, with the southern region around Anchorage exhibiting the greatest trends (>2.7 days/decade, Peterson et al., 2008). Extreme temperatures were found to be changing at all stations analyzed in Interior Alaska, with the greatest increases (decreases) occurring in the frequency of warm (cold) extremes occurring in spring and winter (Stewart et al., 2013). Future projected extreme temperature examined globally, including results for Alaska, indicates that most GCMs agree that the fraction of warm days and warm nights will increase, and the fraction of cool days and cool nights will decrease, with the strongest changes projected for the cool indicators annually and for the summer (Orlowsky and Seneviratne, 2012). Kharin et al. (2007) also noted increases in annual daily maximum temperature maximums under different emission scenarios on the order of 2-4°C by the 2090s based on results of 12 CMIP3 GCMs.

Globally, heavy precipitation events have strong regional variation although statistically significant increases are more common than statistically significant decreases (Alexander et al., 2006). In Alaska, heavy precipitation extremes have been increasing south of 62°N, based on the 99.7th percentile of daily precipitation (37%) since the 1950s although the results were not statistically significant (Groisman et al., 2005). The 95th percentile threshold was noted to be increasing by 18%, and total precipitation increased by 10.3%, both statistically significant results. The Canadian Arctic as a whole was analyzed by Stone et al. (2000), measuring large changes (increases) in precipitation events over the region from 1950 onward. Peterson et al. (2008) documented slight decreases in precipitation intensity based on the Simple Daily Intensity Index (an index of heavy precipitation) for parts of southern Interior Alaska to the coast, with increases in the rest of the state, although these results were not statistically significant. Extreme precipitation was noted by Stewart et al. (2013) to be highly variable in Alaska, with only 50% (33%) of stations in Interior Alaska showing increasing trends of heaviest 1% of 3-day precipitation for spring, summer and fall (winter). Model projections of daily precipitation for indicate that wet day intensity, percentage of days with precipitation greater than the 95th quantile, and fraction of days greater than 10 mm are all increasing in Alaska, with 90% of the 12 CMIP3 GCMs analyzed agreeing on the results (Orlowsky and Seneviratne 2011). Kharin et al. (2007) provided projections of return intervals for daily maximum precipitation rates, and presented results indicating that Alaska and Western Canada are projected to experience between 10-30 % increases in return values by the 2080s. One study used downscaled precipitation data to examine extremes, finding a lowered chance of extreme precipitation over Alaska; however the author's suggest that their findings are not robust due to the lack of climate stations in the region (Wang and Zhang, 2008).

Extreme streamflow events have been analyzed across the globe, with no evidence supporting a world-wide or a US/Canada increase in flooding, with most of the changes occurring in low flows or baseflow values (Lins and Slack, 1999; McCabe and Wolock, 1999; McCabe and Wolock, 2002). On the other hand, streamflow peaks in snow-dominated and glacially-fed systems are occurring earlier (Regonda et al., 2005; Rosenzweig et al., 2007; Stewart et al., 2005) and earlier breakup is occurring with respect to river ice (Beltaos and Prowse, 2009; Smith, 2000; Zhang et al., 2001). Burn (2008) examined multiple timing measures for changes in peak streamflow in the Mackenzie River basin and found the strongest trends in spring freshet towards an earlier peak across most of the stations for all three time periods analyzed (between 1961-2005). Peak flow studies from small scale basins in the Kuparuk River watershed in northern Alaska describe two extreme streamflow events that occurred due to high amounts of rainfall falling across the entire river basin (Kane et al., 2008; Kane et al., 2003). Due to the rainfall amount and intensity, coupled with continuous permafrost conditions which retard infiltration, Kane

argues that the largest floods will occur during summer while peak snowmelt events are more common on average.

Extreme events are considered to be changing more than mean events due to the capacity of the atmosphere to hold exponentially greater amounts of moisture as temperatures increase, as governed by the Clausius-Clapeyron theory (Trenberth, 1999). Due to the constraints on relative humidity, the moisture content of saturated air has 6.5% more water vapor for every 1°C rise in temperature, although due to energy limitations it is possible that this could be much closer to 3.4% °C⁻¹ lower (Allen and Ingram, 2002). Therefore, when precipitation occurs it is more likely to be heavier due to the larger amounts of water in the air parcel, and the intensity is expected to increase as more moisture comes available. The latent heat of moisture also adds energy to the atmosphere, which must be balanced by increased evaporation at the surface, leading to an intensification feedback cycle towards increased extremes that is particularly relevant in the hydrologic cycle (Arnell, 2001; Huntington, 2006; Rawlins et al., 2010). However, as noted by Pall et al. (2007) an overall increase in the upper 50th percentile of total precipitation (mm/day) at high latitudes (65°N) did not follow the Clausius-Clapeyron relation and was indicative of changing dynamics across high latitudes that could be related to sea-ice distributions or other feedbacks and associated amplifications of the climate occurring in these regions (Serreze et al., 2009; Serreze and Barry, 2011). However the extreme changes were larger on the order of 20-30% when compared to changes in the mean at high latitudes (Pall et al., 2007).

The main goal of this work is to provide a local scale understanding of projected changes extreme hydrological events in the subarctic domain, specifically focusing on the Chena River basin near Fairbanks, Alaska. The primary objectives are to examine changes in temperature, precipitation and streamflow (runoff) extremes and to answer the questions 1) are the projected changes in streamflow detectable 2) are the maximum streamflow changes projected greater than the mean changes and 3) what are the greatest indicators on changing extreme streamflow based on indices of extreme temperature and precipitation. The work employed two streamflow models, one semi-lumped model used by the Alaska Pacific River Forecast Center (APRFC) to forecast streamflow in Alaska and the other a semi-distributed land surface scheme, six downscaled GCMs, two emissions scenarios and two future time periods (2050s, 2080s). We focus on understanding changes in temperature and precipitation through the use of the ClimDEX suite of indices (Alexander et al., 2011), and Generalized Extreme Value theorem to consider shifts in streamflow return intervals. The study area, models used, downscaling techniques and analytical approaches are described in the Methods sections. The results and discussion present the major findings of the paper and the implications for subarctic basins, and the paper concludes with a summary of work and future directions.

6.2 Methods

6.2.1 Study Area

The Chena River basin is situated in the Yukon-Tanana Uplands, within the discontinuous permafrost region of the subarctic Alaskan Interior Boreal forest (Figure 6.1). The watershed (5350 km²) is a meso-scale headwater system to the Tanana River basin, which drains eventually into the Yukon River, entering the Bering Sea via Norton Sound (Figure 6.1). The Chena runs through the town of Fairbanks, Alaska and is proximal to long term climate, snowpack and river gaging sites used to develop streamflow simulations and for verification of the modeling tools used in this study. Table 6.1 lists the main properties of the basin, and Figure 6.2 illustrated the mean annual minimum temperature and monthly precipitation totals. The system is snowmelt-dominated with rainfall peaks occurring in August corresponding to frontal systems that are common in Interior Alaska. The climate ranges from cold, dry winters with average January temperatures of approximately -21°C, and July average temperatures 10-14°C with periodic warm (>20 °C) and cold spells (-40°C, Shulski and Wendler, 2007). The region is considered to be semi-arid due to low annual precipitation totals (approximately 270 mm, Fairbanks International Airport climate station, 1970-2000), with higher precipitation in the hills (Table 6.1, Figure 6.2). Vegetative cover in the Chena consists largely of black spruce (60%), deciduous (15%), and shrubs (12%, Table 6.1). Because of the relationship of tree cover to discontinuous permafrost, the ratio of deciduous to coniferous forest cover is indicative of permafrost located under black spruce stands found on north facing slopes and low slope/elevations within the basin (Haugen et al., 1982). Due to this fact the Chena is hypothesized to have slightly greater amounts of permafrost owing to larger amounts of its basin at low elevation while other more upland basins adjacent the Chena (i.e. the Salcha River basin) have more shrub upland and white spruce conifers. Soils in the Chena consists of loess at depth of Aeolian origin with organic horizons overtop moisture rich permafrost soils on north slopes and moderately well-draining silt loams under birch and aspen stands on south facing slopes (Haugen et al. 1982).

6.2.2 Climate and Topographic Data

Climate data to run both hydrologic models were generated by the Alaska Pacific River Forecast Center (APRFC) for use in this project. A technique referred to as Mountain Mapper was applied to generate historical gridded forcing data for the region for the time period with 1970-2010 (Schaake et al., 2004). An inverse distance weighting function was used to convert point station data to gridded fields, and then corrects these against the Parameter-elevation Regressions on Independent Slopes Model (PRISM) climatology for Alaska (Daly et al., 2002). Only the US National Climate Data Center Cooperative daily climate stations were used to generate the gridded fields. The data set, which extended

from Anchorage to Fairbanks, was comprised of 82 minimum and maximum temperature stations and 180 precipitation stations. A variable mix of these stations was combined for each day to form complete records at each grid cell over the entire time series, dependent upon the record availability and grid cell proximity to the station. The updated PRISM climatology data at 800 m (monthly average temperature and total precipitation, 1971-2000) was used for monthly correction (Gibson, 2009). The final 800 m cells were resampled by mean condition to 3.2 km by 3.2 km and values were extracted to a 1/16th grid (approximately 4 km by 7 km in Interior Alaska). This gridded data set was then preprocessed specifically for each hydrological model accordingly, described below. Topographic information required for estimating elevation was derived using the 60m National Elevation Dataset (NED) digital elevation model (DEM) updated for Alaska in 2012 by the US Geological Survey (Gesch et al., 2002).

6.2.3 Models

6.2.3.1 SAC-SMA

The Sacramento Soil Moisture and Accounting Model (SAC-SMA), coupled with SNOW17, is the model used in Alaskan river basins by the APRFC to forecast streamflow conditions across the state of Alaska (Burnash et al., 1973; Peck, 1976). SAC-SMA is run in a semi-lumped mode, and was applied to basin divisions for upper and lower sub-basins and for north and south facing slopes for snow and rainfall-runoff accounting. The model ingests average areal mean temperature (°F, Mean Areal Temperature, MAT) and precipitation (in, Mean Areal Precipitation, MAP) on a six-hourly time scale for the period of interest for each lumped sub-basin. For historical data analysis and calibration in Alaska, the APRFC runs these models using the MAT/MAP data. However, for this work a gridded data set was required for downscaling of the GCM data to generate the future projections of temperature and precipitation in both hydrologic models. To generate lumped MAT/MAPs from the gridded climate data, all grid cells in each sub-basins were averaged and then converted from daily to six-hourly format using seasonally weighted diurnal fluctuations adapted specifically for Alaska (http://www.nws.noaa.gov/oh/hrl/nwsrfs/users_manual/part2/_pdf/27ofs_mat.pdf), as follows,

$$12Z-18Z=WN_1 * TN_{d-1} + WX_1 * TX_d \quad (6-1)$$

$$18Z-0Z=WN_{2a} * TN_{d-1} + WX_2 * TX_d + WN_{2b} * TN_d \quad (6-2)$$

$$0Z-6Z=WX_3 * TN_d + WN_3 * TN_d \quad (6-3)$$

$$6Z-18Z=WN_1 * TN_{d-1} + WX_1 * TX_d \quad (6-4)$$

Where d is the current hydrologic day, time is in Zulu hours and WX_n and WN_n are weighting factors for Alaskan river basins, listed for each season in Table 6.2 (NWSRFC, 2005). Hours were adjusted accordingly to match with CHPS local timing (+9 hrs GMT). The monthly climatological (1970-2010) MATs provided by APRFC were used to bias correct the gridded temperature data developed using the Mountain Mapper technique (Schaake et al., 2004). This step was included because the gridded temperature derived from COOP stations and PRISM data were too cool and delayed snowmelt in the SAC-SMA/SNOW17 models (unpublished results).

The SAC-SMA model has been widely applied to estimate streamflow runoff in basins across the United States (Boyle et al., 2001; Gan and Burges, 2006; Gupta et al., 1998) and globally (e.g. Vaze et al., 2011). The model moves water into either upper or lower storage zones that conceptually represent soil interception or deep groundwater storage. Interception water in the upper zone flows to the lower zones via downward percolation or can run off directly via interflow when the upper zone layers become saturated and precipitation rate exceeds infiltration. Lower zone water can be held in tension storage and either may contribute to baseflow runoff slowly over time, or can run off more quickly over shorter durations. Drainage from the upper and lower zones follows gravity drainage and is governed in part by both water delivery from the upper zone and soil moisture in the lower zone. Tension water is driven by potential evapotranspiration (PE) and diffusion; with a fraction of the lower zone unavailable for PE as it is considered below the rooting zone. PE estimates are provided by the APRFC based on an assessment of historical PE from pan evaporation data and in some cases Thornthwaite estimates (Anderson, 2002). These data are used to develop a general linear relationship between PE and elevation to estimate average monthly PE values for a generic low-elevation site. The APRFC calculates a coefficient to apply the low elevation PE values to monthly PE estimates for the mean elevations of the sub-basins. The coefficient, C , is derived using the equation

$$C = 0.9 - [(e - 1000) \cdot 0.00011] \quad (6-5)$$

where e represents elevation in feet. For example, if the catchment mean elevation is 2350 ft, the coefficient is 0.75. Finally, a monthly PE adjustment factor is applied to account for vegetation changes during the year. The result is an evapotranspiration demand estimate that is used in the Sacramento model, described in the proceeding section.

The SNOW17 snow model is a single layer temperature index based snow model that calculates snow accumulation and ablation using empirical formulas to estimate heat and liquid water storage, liquid water throughflow and snowmelt (Anderson, 1976). The model is designed for river forecasting and has been used operationally by the NWS RFCs since the mid-1970s. The only input requirements for SNOW17 are temperature and precipitation, at the time step of the model (6 hrs). There are 12 parameters

in the SNOW17 model, including the areal depletion curve; sensitive or ‘major’ parameters control the model while less sensitive or ‘minor’ parameters have little impact (Table 6.3, He et al., 2011).

A unit hydrograph model is used to distribute the runoff produced by the SAC-SMA model. Each sub-watershed has its own unit hydrograph, calculated based on basin elevation, to translate the runoff through the channel system to the gage location. Simple routines sum the unit hydrograph outputs to calculate simulated streamflow at the basin outlet. While downstream basins incorporate routing models, e.g. Lag/K, this study focuses on headwater basins so no routing models are needed.

Parameterizations for the SAC-SMA and SNOW17 models were adopted from the APRFC modeling system used to forecast river flows in Alaska. These parameterizations were adjusted based on the MAT/MAP 1970-2010 lumped forcing data during calibration, which was run from 1970-2010 following the normal protocol for calibration adopted by the APRFC. Following this, the gridded, bias corrected MAT/MAPs were used to calibrate SNOW17 values to address any outstanding snowmelt issues arising from slightly different climate data. Results are provided in Table 6.3 in comparison with VIC calibration and validation time periods, along with the period of record.

6.2.3.2 VIC

The Variable Infiltration Capacity (VIC) hydrologic model is a distributed model that was originally developed as a land surface scheme (Liang et al., 1994; Liang et al., 1996). VIC contains explicit formulations for snow accumulation, snow ablation, evapotranspiration, and frozen soils and solves the full energy balance at a sub-daily time scale to simulate daily baseflow and runoff for individual grid cells. These fluxes are then collected and routed downstream using an offline routing model to simulate streamflow (Lohmann et al., 1996; Lohmann et al., 1998).

VIC was implemented at a 1/16th degree grid scale (4 by 7 km) in four Interior Alaskan watersheds, the Chatanika, Chena, Salcha and Goodpaster systems, although results are only presented herein for the Chena River basin. Methods to set up VIC generally followed the approach described in Bennett et al. (2012) and Schnorbus et al. (2014). VIC was run on a 3 hourly basis using energy balance and frozen ground modules and results were output at a daily time scale. VIC’s primary input requirements are daily minimum and maximum temperature (°C), precipitation (mm) and wind speed (m/s). To generate the VIC gridded climate data, the minimum and maximum temperature and precipitation data were extracted from the Mountain Mapper upscaled grids for each 1/16th grid cell for 1970-2010. To correct the APRFC MAT data, the same climatological bias correction approach was applied to the VIC temperature grids to maintain consistency between the two data sets. Daily wind speeds were generated by resampling the National Centers for Environmental Prediction-National Center for Atmospheric Research (NCEP-NCAR) reanalysis (Kalnay et al., 1996) 10-m wind speed for all 1/16th

degree grid cell. To account for overly high estimates of wind speeds for this region, values > 4 m/s were adjusted (-1.3 m/s) based on analysis of local data from the Bonanza Creek watershed (<http://www.lter.uaf.edu/>, results not shown, Mölders and Kramm, 2010).

VIC's fluxes are generated based on distinct parameterizations for soils, vegetation, and topographic information, which are generally prepared using available local data, or when no local information is available, using regional or global scale data. Due to a lack of available soils data for the entire region, a global soils classification was implemented using a soil pedon database created by the International Soil Reference and Information Centre (Batjes, 1995) and merged with the FAO-Unesco Digital Soils Map of the World (FAO, 1995) to create the 0°5' (5 arc minutes or approximately 50 km² a side) Soils Program in Global Soil dataset (Global Soil Data Task Group, 2000). Three soil depths were used: 0.1 m, 0.3 m and a variable depth for the third soils layer based on topographic scaling with shallower depths at higher elevations, to a maximum depth limit 1.8 m at low elevation sites (the algorithm was originally designed for estimating soil depths in the University of Washington's DHSVM model). Soil textural classes were extracted directly from the Soils Program database, along with saturated hydraulic conductivity, bulk density, and porosity, adjusted as suggested by Dingman (Figure 6-4 in Dingman, 2002). Field capacity is estimated from soil textures using the formulations of Cosby et al. (1984). Wilting point was estimated based on Soils Program derived estimates that utilizes the van Genuchten equation (Table 5.1.1 in Rawls et al., 1993). Water retention was estimated using the Brooks-Corey calculations as listed in Tables 5.1.1 and 5.3.3 of Rawls et al. (1993). Bubbling pressure and residual water content was based on Brooks and Corey (Table 5.3.3 in Rawls et al. 1993). Soil particle density was obtained from Skopp (Skopp, 2000). Initial soil moisture and residual soil moisture were estimated from a study from British Columbia (Schnorbus et al., 2010). Rooting depths were formulated from recommended values and adjusted to the boreal forest cover (University of Washington's VIC model website <http://www.hydro.washington.edu>, Viereck et al., 1992). The rate of exponential decrease of saturated hydraulic conductivity with soil moisture was taken from Demaria et al. (2007). The infiltration curve rate, and three empirical parameters used in the baseflow generation were calibrated following the common approach for VIC model calibration (University of Washington's VIC model website <http://www.hydro.washington.edu>, Shi et al., 2008).

The frozen ground module in VIC was implemented for select cells in the basins. Where black spruce cover comprised greater than 50% of the grid cell, these grid cells were considered to be 'permafrost dominated' and were subjected to the following conditions; saturated hydrologic conductivity was reduced by a factor of 10 and the sand (quartz) content was set to zero in the first soil layer, following testing of the model in a nearby basin (Endalamaw et al., 2013). Damping depth was set to 10 m following Smith et al. (2010) and 13 soil nodes were utilized. A complete description of the frozen

ground module is described in publications of Cherkauer and Lettenmaier (Cherkauer, 2001; Cherkauer et al., 2003; Cherkauer and Lettenmaier, 1999; Cherkauer and Lettenmaier, 2003). In brief, the thermal fluxes are calculated in the soil column to determine ice content and the heat balance is then calculated based on ice content. Soil moisture fluxes are calculated separately for frozen, unfrozen and thawed soils. Volumetric heat capacity and thermal conductivity are calculated based on the moisture flux solutions. Soil thermal fluxes are solved for each node (n=13) in the soil temperature profile using an explicit finite difference approximation of the soil thermal flux equation. For this application, the finite difference approach was only utilized for the last time step, and the explicit heat flux calculation as described in Liang et al. (1994) were used to reduce computational time, and because testing with and without these settings resulted in no difference to flow estimates.

Vegetation data were generated using a mosaicked vegetation classification map produced by the Alaska Natural Heritage Program that contained estimates of fine forest classifications such as black spruce and alder (<http://aknhp.uaa.alaska.edu/ecology/vegetation-map-and-classification-northern-western-and-interior-alaska/>), considered to be of prime importance for the classification of forest cover in the region. Using this map as a starting point, north facing aspects were combined with elevations < 400 m and intersected with the conifer forest cover from the above mentioned data set to produce an enhanced black spruce class. The final classification contained eight classes where water, burned area, rock outcrops, and perennial snow were treated as bare ground. Leaf Area Index (LAI) values for the region were determined for each vegetation class based on the Global Inventory Modeling and Mapping Studies (GIMMS) Normalized Difference Vegetation Index (NDVI3g) data set (Zhu et al., 2013). The data set is available at a 1/12th of a degree resolution for 15 day intervals, from 1981-2011. For this study, the average monthly 2000-2010 data from the second monthly reading was utilized. Original results appeared to be higher than those observed within the Caribou Poker Creek Research Watershed and thus were corrected downward accordingly (J. Young, pers. comm.). The remainder of the vegetation library parameters was selected based on the University of Washington data set and a study based in British Columbia, adjusted for local vegetation characteristics (Nijssen et al., 2001; Schnorbus et al., 2014; Viereck et al., 1992).

Elevation bands are used to represent sub-grid topography to improve model performance in locations with mountainous terrain where elevation affects snow pack accumulation and ablation. Five elevation bands were populated, with a maximum range of 200 m per band; thus not every band was utilized at all times. Within the elevation bands, temperature change is based a lapse rate of 6.5°C per 1000 m multiplied by the difference between the grid cell elevation and the median elevation of the band. The variation of precipitation with an elevation band is determined by calculating the amount of precipitation occurring in each elevation band as a fraction of the grid cell.

Calibration of the VIC model was applied using the multi objective calibration program MOCOM, which provides an automatic calibration procedure (Yapo et al., 1998). The soil parameter b-infiltration and four parameters governing baseflow generation were used to calibrate the model. Objective functions included the R^2 , Nash Sutcliff efficiency, and the natural log of Nash Sutcliff efficiency. The model simulations are compared with the United States Geological Survey (USGS) streamflow at the Chena River gage (Table 6.1). The calibration period used was 1980-1985. Results for the two basins are provided in Table 6.3.

6.2.4 GCMs

The Coupled Model Intercomparison project version 5 database (CMIP5) of GCMs and emissions scenarios were extracted and applied in this study (Taylor et al., 2012). A subset of six, top performing GCMs were chosen based on their relative performance over the Alaskan domain (Bennett and Walsh, 2014), model availability and completeness of records within the CMIP5 database. In all cases, the first physical realization from the ensemble members was retrieved. The six models selected were the Canadian Earth System Model CanESM2, Centre National de Recherches Météorologiques CNRM-CM5.1, Institut Pierre Simon Laplace Climate Model IPSL-CM5A-LR, Japan's Model for Interdisciplinary Research on Climate (MIROC), Max-Planck Institute Earth System Model MPI-ESM-LR, Japan Meteorological Research Institute's MRI-CGCM3 (see Table 2 in Bennett and Walsh, 2014 for more information on these models). The Community Climate System Model CCSM4 utilized in Bennett and Walsh (2014) was not included in this work due to the requirement for wind speeds to run the VIC hydrologic model; MIROC5 was used as an alternate because it also ranked high in the model comparison for Alaska.

GCMs were downscaled at a monthly resolution using the Bias Correction Spatial Downscaling (BCSD) approach, which is a widely used downscaling technique adopted by many different climate users across the US and North America (Werner, 2011; Wood et al., 2004) and shown to be among the better approaches for representation of extreme values (Bürger et al., 2012; Bürger et al., 2013). The technique uses detrended monthly time scale GCM data and corrects spatially and temporally using a quantile mapping approach. Detrending is applied to ensure that any trend in the GCM is retained through the downscaling procedure. The method bias corrects based on the differences within the monthly quantile maps. Non paired data falling outside the quantile map are estimated based on a Weibull fit for precipitation minimum, and a Gumbel fit for precipitation maximum; a Gaussian fit is applied for temperature (Bürger et al. 2012). The final step is to re-apply the trend and then reduce the GCMs to a daily time step using a temporal disaggregation that matches a monthly time series from the past with

future monthly data values. The downscaling code used in this work was developed by Alex Cannon at the Pacific Climate Impacts Consortium in Victoria, BC, Canada.

Two emission scenarios were analyzed in this work, Representation Concentration Pathway (RCP) 4.5 and 8.5, and are considered to be “low-end” and “high-end” emission scenarios (Moss et al., 2010; Stocker et al., 2013), with the numerical values (2.6, 4.5, etc.) indicating the end-of-century (year 2100) radiative forcing in Watts per m² resulting from anthropogenic inputs to the atmosphere (but not including changes in land use). Regional average minimum and maximum temperature, total precipitation and wind speed for each season are provided for the GCM ensemble for both scenarios as differences from the 1971-2000 climatology (Table 6.5), however for brevity, we focus only on RCP 8.5 for the remaining tables and figures.

6.2.5 Verification

Both hydrologic models were verified by running the calibrated results over an adjacent temporal period to the calibration years. Three verification statistics were utilized, the correlation coefficient (R), Nash-Sutcliff efficiency, and natural log of Nash-Sutcliff efficiency.

$$R = \frac{N \cdot \sum_{i=1}^N S_i \cdot Q_i - \sum_{i=1}^N S_i \cdot \sum_{i=1}^N Q_i}{\left[\left(N \cdot \sum_{i=1}^N S_i^2 - \left(\sum_{i=1}^N S_i \right)^2 \right) \left(N \cdot \sum_{i=1}^N Q_i^2 - \left(\sum_{i=1}^N Q_i \right)^2 \right) \right]^{0.5}} \quad (6-6)$$

$$NSE = 1 - \left(\frac{\sum_{i=1}^N (S_i - Q_i)^2}{\sum_{i=1}^N (\bar{Q} - Q_i)^2} \right) \quad (6-7)$$

$$NSE_l = \log \left[1 - \left(\frac{\sum_{i=1}^N (S_i - Q_i)^2}{\sum_{i=1}^N (\bar{Q} - Q_i)^2} \right) \right] \quad (6-8)$$

where N is equal to the number of data points (i.e. sub-daily streamflow realizations), i is the time step (days), S is the simulated streamflow (m³/s), and Q is the observed streamflow (m²/sec). Results are provided for both models for the calibration, verification and the historical periods of record (1970-2005), respectively, in Table 6.3.

6.2.6 Analysis

The Expert Team on Climate Change Detection and Indices (ETCCDI) developed a set of extreme indices that could be used for analysis of extreme events (Alexander et al., 2006; Frich et al., 2002; Klein Tank et al., 2009; Zhang et al., 2011). The purpose of the ETCCDI indices was to have a compilation of reproducible, common index variables that could be easily calculated and were based on

available daily climate data such as air temperature and precipitation (Zhang and Zwiers, 2013). The ETCCDI indices can be classified into three categories: monthly or annual minimum or maximum values of temperature and maximum daily values of precipitation; counts of the number of days exceeding a specific baseline climatological threshold; and counts of the number of days exceeding a specific fixed threshold. There are 27 ClimDEX indices in total (Zhang and Zwiers, 2013). ClimDEX statistics used in the analysis rely upon most of the major 27 indices described by the ETCCDI (Table 6.4).

The R ClimDEX software package was used to calculate indices for each GCM and scenario using the downscaled gridded 1/16th degree fields, and then results were averaged over the region. Analysis was calculated based on six GCMs, for each emission scenario, averaged over the Chena River basin, upon which ClimDEX statistics were calculated. The median value of all GCMs for RCP 8.5 emission scenario averaged over the Chena basin are presented in Figure 6.3, 6.4, Figure 6.9, and Table 6.6 for the quantile results across individual GCMs. The Fairbanks Airport Global Historical Climate Network (GHCN) level one climate station (USW00026411) is used for comparison to the ClimDEX results for gridded historical observations (Figure 6.4).

Streamflow output was analyzed for the SAC-SMA model and VIC using the same techniques. Values from 1971-2005 were seamed together with future model projections (2006-2099) to ensure all GCMs had the same baseline for correction. Monthly and seasonal minimum, maximum and mean flows were calculated based on this time series for each GCM and hydrologic model. The range of all GCMs and the median are used to present results in figures and tables as described in the figure/table captions.

The GEV analytical approach is outlined in Chapter 3 using the methods described in Cannon (2010; 2011). The statistical approach focused on annual streamflow return intervals. Return intervals were generated for the AICc minimized model results, based on the mean of 100 bootstrapped iterations for 2, 5, 10, 20, 50 and 100 year time periods for the historical (1971-2000), the 2050s and the 2080s. The final return intervals are based on the mean of the covariate (time, i.e. for 1971-2000 this would be 1985).

6.3 Results

6.3.1 Calibration and Verification

The SAC-SMA model calibration, verification and period of record results are provided in Table 6.3 for the Chena River basin. Although calibration and verification periods were not explicitly used during the calibration phase of the SAC-SMA/SNOW17 model, the same range of dates applied in the VIC model calibration are provided for context. The SAC-SMA performs well in this area. The VIC model performs at a lower skill level; flow volume biases and baseflow statistics (Nash-Sutcliff efficiency natural log values) tend to be stronger than the peak flow matching (Nash Sutcliff Efficiency). The

average historical monthly simulations for the SAC-SMA model and the VIC model are plotted against the observed streamflow in Figure 6.5. Timing in SAC-SMA is matched well with the observed in terms of the spring flood peak, while the VIC model does not match the flood peak timing as well (approximately one month late). The VIC model simulates the rainfall peak and under simulates the mean values, while the SAC-SMA model over simulates the maximum (but captures the mean appropriately). Both models tend to underestimate low flows through the summer, fall and winter time periods.

6.3.2 Temperature and Precipitation

Temperature and precipitation gridded data developed for this project provides a reasonable tool by which to examine changes in extreme events across the region. Average gridded historical (1970-2010) daily minimum and maximum temperature and monthly precipitation for the Chena River basin are illustrated in Figure 6.2, and spatially in Figure 6.3. Regionally averaged seasonal results (ensemble) are shown for temperature, precipitation and wind speeds shown as a difference from the historical baseline period for the two time periods, 2041-2070 and 2071-2100 (RCP 8.5) in Table 6.5. Regional spatial variability in temperature results is minimal given the relatively small region and the use of an ensemble average (see standard deviations in Table 6.5, Figure 6.3). However, differences between the two time periods and across the seasons is discernable (Table 6.5). The largest projected changes in minimum temperatures occur during the winter and fall, with increases up to 8°C. Maximum temperatures projections exhibit a similar pattern of change, with increases that are slightly larger in spring on average and slightly smaller in fall on average compared to minimum temperature changes (Table 6.5).

Changes in projected precipitation totals over the seasons have a much more variable spatial pattern across the watersheds (see standard deviations in Table 6.5). The precipitation changes are always positive in the region, with stronger increases projected for the spring and summer. The most notable change occurs during the summer for the 2080s (+82 mm, Table 6.5). Winter increases in precipitation are small in comparison to other seasons but not insignificant (+10 mm, Table 6.5). Precipitation increases are always larger for the 2080s as opposed to the 2050s. Absolute values of precipitation increase strongly in the upper reaches of the adjacent Salcha River basin during spring and summer in the 2050s, but percentage change is greatest in the lowlands (Figure 6.3). However, by the 2080s, widespread increases are noted for all regions of the study area (+73 mm), with the highest absolute increases observed again in the upper elevations. In the fall, larger increases are observed in northwest of the Chena River basin that strengthen in the 2080s.

Changes in extreme temperature and precipitation indices are compared against the changes in minimum and maximum temperature and precipitation based on the median of all GCMs for the Chena River basin in Figure 6.4. The dual lines indicate the different scenarios (RCP 4.5 vs RCP 8.5); dashed

lines illustrate the extremes while the solid lines indicate the mean condition. The emission scenarios for mean maximum, minimum and extreme temperature start to diverge around the 2060s, differences between scenarios have distinct signals after this time period (Figure 6.4). However, minimum extreme temperature and precipitation (bottom panel) have fairly distinct signatures as early as the 2050s. Each value (average or extreme) tends to have a similar trajectory in terms of its trend, although the variability is quite different. The spread in precipitation extremes compared to mean total monthly precipitation is notable, with large deviations observed, particularly around the 2020s. The variability tends to taper somewhat by the end of the 21st century. The historical average values and extreme values (in this case, TXx, TNn, Rx5) considered in comparison to data from the Fairbanks International Airport station show good correspondence to the downscaled gridded extreme values (Figure 6.4). Discrepancies in terms of the variability of extreme precipitation and with respect to a low bias in average extreme maximum temperatures are somewhat expected given that the smoothing over high and low elevations presented by the gridded data for the Chena River basin (Figure 6.4). An additional verification of the data set is the quality results that it produces for streamflow simulation for two separate hydrologic models (Table 6.3).

Annual ClimDEX index values are provided as absolute differences for RCP 8.5 illustrate changing extremes in the Chena River basin (Table 6.6). The results are presented for quantile distributions (0, 50, 75 and 99%) of all six GCMs results to show the spread across models (RCP 8.5). Temperature differences (TXx and TXn and TNn/TXn, see Table 6.4 for definitions) are increasing in the future for most models (50%), with a greater spread across models projected for TNn and TXn values (minimum values for minimum and maximum temperatures). Daily temperature ranges are not projected to change by a large amount, and cold nights and days and warm nights and days are warmer in the future. Summer days increase, while icing and freezing days decrease by a greater amount; overall many more warm spells are projected but cold spells change little (Table 6.6). Precipitation indices, examined as a percentage change from the historical, indicate large increases in the moderately high precipitation (R95Pt, R10mm) indices compared to those changes in R99Pt and R20mm (results not shown). A more muted response is observed for the simple daily intensity index (SDII). Total precipitation is projected to increase with a wide range of responses across GCMs. This finding opposed another study, which reported the largest changes in Rx5, and illustrates the value of downscaling results for local scale studies as discussed by the authors (Sillmann et al., 2013). Notably, for precipitation, there are only small differences in the changes between the 2050s and the 2080s, indicating that precipitation increases will be experienced as soon as the 2050s, and those changes are sustained (and become larger) into the 2080s (Table 6.6).

6.3.3 Streamflow

Streamflow simulations are shown for the historical period (dashed lines) compared to the future time periods (solid lines) in Figure 6.6 and Figure 6.7 for the Chena River basin. Maximum and minimum median values (black line) streamflow estimates are provided for the range of all GCMs (grey envelope) for the RCP 8.5 scenario, and for the 2050s compared to the 2080s. Significant maximum streamflow changes are denoted by open triangles (95% confidence interval). These plots show a dramatically different future scenario for streamflow condition, particularly for maximum streamflow, while minimum streamflow appears to change very little (Figure 6.6, 6.7). The historical streamflow illustrates a classic snowmelt driven system where the peak flow is clearly identified with the melting of over-winter storages of snow and ice in during May and June. The future scenario illustrates a dual-peak system which has comparable peaks for both snowmelt and rainfall seasons in the 2050s for the Chena.

By the 2050s, snowmelt peaks are still larger than the historical in the SAC-SMA however the peak timing has shifted by approximately one month (Figure 6.6, upper panel). By the 2080s, however, the rainfall peak has surpassed the snowmelt peak and is the dominant hydrologic event in the year and occurs in August in the 2050s and reaches a maximum in September in the 2080s (Figure 6.6, lower panel). The VIC model, on the hand, represents a higher rainfall peak in both the 2050s and the 2080s (Figure 6.8). The snowmelt peaks occur in June and has a comparable magnitude, although the melt begins in early March (as opposed to April in the historical data) and appears to be much more protracted in terms of duration. The rainfall peaks occur in August in the 2050s but is spread over August and September during the 2080s (Figure 6.7). Minimum streamflow changes little in both models. The SAC-SMA shows a larger shift upward in low flows while the VIC model shows winter increases and summer declines (Figure 6.6, 6.7).

The range of results illustrated by the grey envelope indicate that changes are more variable and therefore have greater uncertainty around the streamflow maximums and around the peak flow periods, particularly in the 2080s for the SAC-SMA model (Figure 6.6). Both models tend to have greater uncertainty around the snowmelt and rainfall peaks. The minimum flow response has considerably less uncertainty around it compared to the maximum flow response for both models. However even the smallest of the GCM responses in both hydrological models represents a shift away from snowfall peak towards a peak rainfall driven streamflow regime in the Chena (Figure 6.6, 6.7).

Return levels are provided across the range of models to illustrate the annual historical and maximum flow responses at different intervals for the Chena (Figure 6.8). The upper whiskers indicate the maximum of the maximum flow values from a single hydrological/GCMs and tend to have a larger range, while the lower whiskers (minimum maximum flow values) have a much narrower range. The

boxplot results provides the range of responses for all GCMs and both hydrologic models and for each time periods (right is historical, left is 2080s and middle is the 2050s). The historical period has much smaller deviations given that the historical baseline is the same for each model, thus the range within the boxplots represents the differences between the two hydrologic baselines. This range increases as the return interval increases. By the 2050s, all return levels have increased, particularly at the 50 and 100-year return level (Figure 6.8). The ranges in the boxplots are smallest in the 5-year return intervals for the 2050s, but from then on the ranges are fairly similar. The boxplot range illustrates the peak snowmelt representation in the hydrologic models where the sensitivity of snow to changes in temperature and precipitation plays a large role in the boxplot variability (Dickerson-Lange and Mitchell, 2013; Karl et al., 1993; Knowles et al., 2006). However, by the 2080s the rainfall regime shift dominates maximum streamflow return levels and there is more coherence between the hydrologic models (Figure 6.8). Instead, the range in boxplots in the 2080s is accountable to difference between GCMs. Return intervals for the 5, 20 and 50-year events illustrate increases by the 2080s of 1.6 times the historical flow values, while the 100-year return events double by the 2080s.

6.3.4 Median to Maximum Flow Changes

Historical flow magnitudes, exceedances and future changes in exceedances are provided for the 5th, 95th and 99th percentiles compared to the median (50th) percentile annual flows for the median of all GCMs and both hydrologic models under RCP 8.5 (Table 6.7). The 99th percentile increases by 83% by the 2050s and 168% by the 2080s, compared to the 95th percentile which increases by 53% in the 2050s and the 98% by the 2080s. The 5th percentile flows are shown as negative numbers, indicating that historical low flow values are only encountered 2% of the time, and never encountered in the 2080s. The 50th percentile or median flow values, on the other hand, only show moderate increases to the 2050s of 15%, and 34% by the 2080s. The differences in flow responses are five-fold between the 50th and the 99th percentile. Therefore, examining these changes using the mean flow condition would lead to a drastic underestimate of the changes projected for floods. This is important because of the nature of floods to impact property and infrastructure with a single occurrence.

6.3.5 Relationship of Maximum Streamflow to ClimDEX Indices

The relationship between ClimDEX indicators and maximum streamflow was considered by examining correlations and linear relationships between the ClimDEX indices and streamflow maximums at an annual time scale. Figure 6.9 illustrates the correlation matrix between ensemble annual maximum streamflow and linear regression is discussed in the text. Results indicate that streamflow changes are positively and significantly related to temperature indices (TXx, TNn, TNx, TXn, and Tn90p, Tx90p),

while streamflow is negatively and significantly related to temperature indices Tn10p and Tx10p. Summer days and length of dry spells are positively and significantly related to increasing maximum streamflow while icing and freezing days are negatively correlated. The strongest positive relationship is exhibited between streamflow and the percent of days when maximum temperature is greater than the 90th percentile, the annual count of summer days, and the strongest negative relationships are icing days and the percent of days when maximum temperature is greater than the 10th percentile. All precipitation indices are positively related to increasing streamflow maximums with the strongest relationship found for total precipitation amounts.

6.4 Discussion

Future changes in average temperature minimums and maximums have a strong and consistent signal across the region and indicate a pattern of increasing minimum and maximum temperatures through to the 2100s (Table 6.4, Figure 6.4), a finding that is now common knowledge in our understanding of climate change shifts expected in the subarctic and Arctic regions (ACIA, 2005; Stocker et al., 2013). Minimums increase more than maximums by the 2080s under the RCP 8.5 scenario within the Chena River basin, a finding that is reflected in other studies (Bennett and Walsh, 2014; Sillmann et al., 2013). Although historical temperatures have been increasing in the region, and the Arctic as a whole, the projected increase in precipitation is in contrast to historical uncertainty in direction or trend of precipitation change noted in the literature for northern Alaska (Hinzman et al., 2005; McAfee et al., 2013), or moderately increasing trend (+20%) in the past forty years for Fairbanks, Alaska (data 1966-2003, ACIA, 2005; McBean et al., 2004). More recent studies have shown that precipitation for Alaska shows an increase of approximately 10%, with the most amount of change observed in recent decades (Shulski and Wendler, 2007; Stewart et al., 2013). The projections for precipitation indicated herein correspond with precipitation projections in Alaska's Interior region indicating increases of approximately 10-15% by the 2050s and by 20-25% by the 2080s under the A2 CMIP3 ensemble scenario (Stewart et al. 2013).

Maximum streamflow changes in the subarctic snow dominated systems of Interior Alaska are influenced by the changing nature of precipitation and particularly the change in form of precipitation that is projected to occur in these basins. The change in the dominant form of streamflow from snowfall to rainfall indicates a significant and major regime shift for these basins. By the 2050s, the SAC-SMA model projects a maximum streamflow peak from rainfall comparable in magnitude to the snowmelt peak. The range of models response indicates that there are some models that project less severe changes, with the lowest of model scenarios suggesting that the streamflow maximum will be similar; however timing of streamflow in the spring are projected by all GCMs to shift forward by one month (Huntington

et al., 2004; Stewart et al., 2005). The VIC model, on the other hand, reflects larger change in the Chena River hydrograph and depicts the system being more rainfall-than-snowmelt driven by the 2050s. By the 2080s, both hydrologic models show a rainfall peak that is larger than the snowmelt peak. The GCMs range around the peak is greatest during the rainfall season and for the 2080s, however all GCMs agree that the rainfall peak will be larger. The greatest difference between this study and others on changing streamflow volumes is that for many rivers in North America, the change in peak streamflow is associated with declines in SWE/P ratios linked to drought, decline in low flows, and changes in stream temperature (Elsner et al., 2010).

The change in direction of trend or convergence of model estimates towards a projection of increasing precipitation has a strong influence on changing flood levels and reoccurrence intervals projected by hydrologic models for the area. For instance, changes in return intervals by the 2050s indicate that Interior Alaska's snowmelt dominated systems may experience more moderately sized (5-year return interval) flooding related to snowmelt peaks, but this is largely dependent upon the GCM/hydrologic model considered (Figure 6.8). However, the 2080s show consistency across results for these 5-year events that is indicative of the convergence in model agreement towards a rainfall dominant regime where peak floods are associated with summer and fall high flows. However, this is not true of the 20, 50, and 100-year events, which are just as uncertain in the 2050s as the 2080s, likely for different reasons. The uncertainty in the 2050s is due to differences in snowmelt regimes, whereas the uncertainty in the 2080s is linked to uncertainty around precipitation regimes. Return levels are 1.6 times as large in the 2080s for the 5, 20 and 50-year return interval almost twice as large as the historical at the 100-year interval by the 2080s. These increased flow magnitudes and 100-year return intervals are attributed to increased rainfall peaks.

The VIC model's frozen ground and a distributed snowmelt module were utilized in this work. Over half of the Chena cells were permafrost and treated as such in the model. The larger uncertainty present in the model predictions is likely due in part to the variable treatment of frozen ground, and distributed snow. Decreases in summer baseflow values may also be due to increased permeability of the frozen ground layer as the active layer deepens through time with climate change (Romanovsky et al., 2010; Smith et al., 2010). However, the module itself is not without its issues, and testing and comparison to observations at a nearby location indicates an overestimation of the seasonality in the cold front. This may be due to the lack of parameterization of the organic soils in the model. More research is required to determine and correct the issues with frozen ground in this area, and ensure that the model is working as it should be.

Analysis of exceedances compared annual differences across the 99th, 95th, 5th and median (50th) percentiles and illustrate the vast under estimation provided by the mean conditions when considering the

differences between mean flow and maximum flow changes (Table 6.7). Median flows only marginally increase in the future, while future flow conditions in the maximum percentiles are magnified 5-times the median changes (Table 6.7). Because it will only take one flood to cause great damage to a region, the implication here is that for examining changing conditions and future projections of climate change with respect to high flows, a peak flow indicator or statistical approach must be applied. Studies that do not take into account changing maximum flood distributions (based on mean flows) may be dramatically under evaluating the risk potential for impacts within regions. Thus it is recommended that studies on climate change impacts incorporate shifts in extremes as a rule.

The indication, based on the relationship between maximum streamflow increases and ClimDEX indices is that the majority of change in maximum streamflow is largely driven by the bulk volume of precipitation occurring in the system (P_{tot}). ClimDEX indices of precipitation showed the greatest changes in indices representing moderately high indicators (R95mm), followed by R10mm and then the highest indicators, R99 and R20mm, all of which have significant and positive correlations to annual streamflow change. Although physical models are best to describe changes in complex systems such as streamflow – in regions where calibrating models can be challenging due to the lack of station and network observational systems, such as Alaska, a statistical method could have promise. Thus, relationships between indicators in the ClimDEX archive could be explored to generate maps of projected estimates of changing streamflow. Although changes may not be applicable to glacierized basins, a large percentage of the boreal forest region in Alaska is currently snow dominated, and an estimate could be a worthy tool to define at-risk regions.

6.5 Conclusions

This study examined climate change impacts on extreme indices and streamflow for a watershed located in the boreal forest of Interior Alaska. The major findings are that increasing temperatures in conjunction with increasing precipitation is projected to shift streamflow peaks from a snowmelt and rainfall dominated system to a rainfall driven system by the 2080s. GCMs and hydrologic models have a narrower range across estimates of moderately sized (5-year return interval) floods, while 20, 50 and 100 year floods have a wider spread. The median return level estimate for both hydrologic model and all six GCMs indicates that 5-year return interval flows will increase by 1.6 times the historical flow and double in terms of peak streamflow magnitudes associated 100-year floods generated by summer and fall high flows. This represents a major regime shift for the region. This regime shift will have implications for many different aspects of environment and society. Impacts are projected to begin to be experienced as early as the 2050s, and as such planning measures must incorporate these projections where possible.

Two different hydrologic models were applied in this study, a semi-lumped model used currently as the National Weather Service's river flood forecasting tool (SAC-SMA) and a distributed model that explicitly accounts for frozen ground, changes in energy balance and snow across elevation bands (VIC). The SAC-SMA model performed better in the historical ranges, and simulated peak flows more accurately. Both models tended to agree on changes in rainfall peaks however differences were observed in the prediction of peak streamflow around the snowmelt season. In particular, VIC simulated a more distinct rainfall peak by the 2050s, whereas SAC-SMA did not project this shift until the 2080s and the snowmelt peak was retained into the future. Both models indicate however that snowmelt peaks would move forward by approximately one month in the 2050s and retain this pattern into the 2080s. The implications of this difference are likely to be of note to the forecasters and hydrologists attempting to calibrate and validate models if the projected regime shift for the watershed are realized.

Uncertainties in GCM projections of return intervals for 5-year flow events are smaller in the 2080s, indicating coherence in changes for moderately sized events, while the 2050s uncertainty was greater owing to the variable representation of snowmelt peaks by the models. Generally, uncertainty increases at higher return levels, and towards the 2080s. Percentile exceedance comparing results for median (50th) streamflow compared to maximum streamflow (95th and 99th) indicate that large discrepancies between flow projections for mean versus maximum. Analysis of future projected changes in streamflow should focus on maximum distributions in order to fully evaluate the potential for flooding and impacts in regional studies.

Streamflow was correlated and a linear relationship was found between total precipitation and minimum temperature extremes in the ClimDEX archive. Developing a statistical method for identifying at-risk regions in areas such as the subarctic and Arctic, where calibrating models can be challenging due to the lack of station and network observational systems could have promise. Questions that could not be addressed by this study due to limitations also include addressing the changing low flow patterns related to shifts in permafrost that may have consequences for streamflow extremes, the role of antecedent moisture conditions in the systems with regards to peak snowmelt runoff. Future directions for this work include addressing a number of these issues using statistical methods and continued exploration with the VIC model. Finally, the ensemble GCM projections of streamflow in the APRFC CHPS system, which was implemented at the University of Alaska Fairbanks, will be provided as an offline tool for the forecasters to investigate and consider scenarios of change for the basins in Interior Alaska. This may provide a valuable tool to stimulate discussion and planning efforts around future projections of change for this region.

6.6 Figures

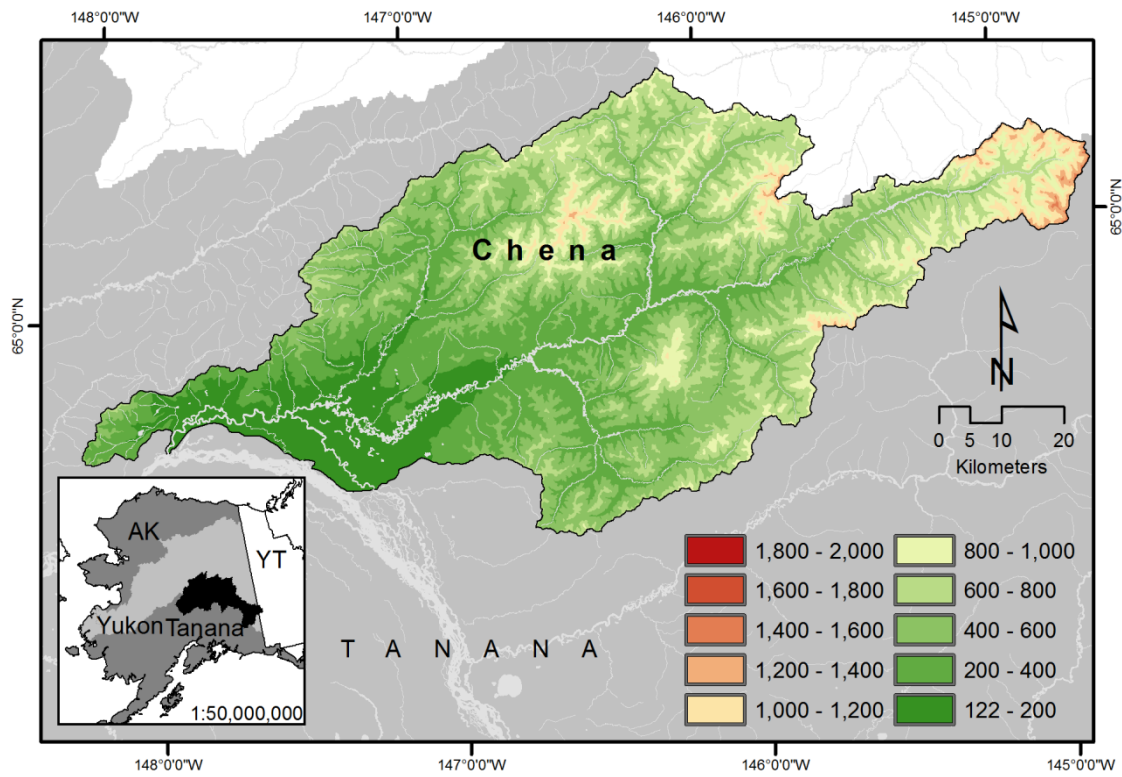


Figure 6.1 Chena River basin, Interior Alaska, U.S.A. The inset illustrates the Tanana and Yukon River basin, Alaska in the context of Yukon Territory, Canada.

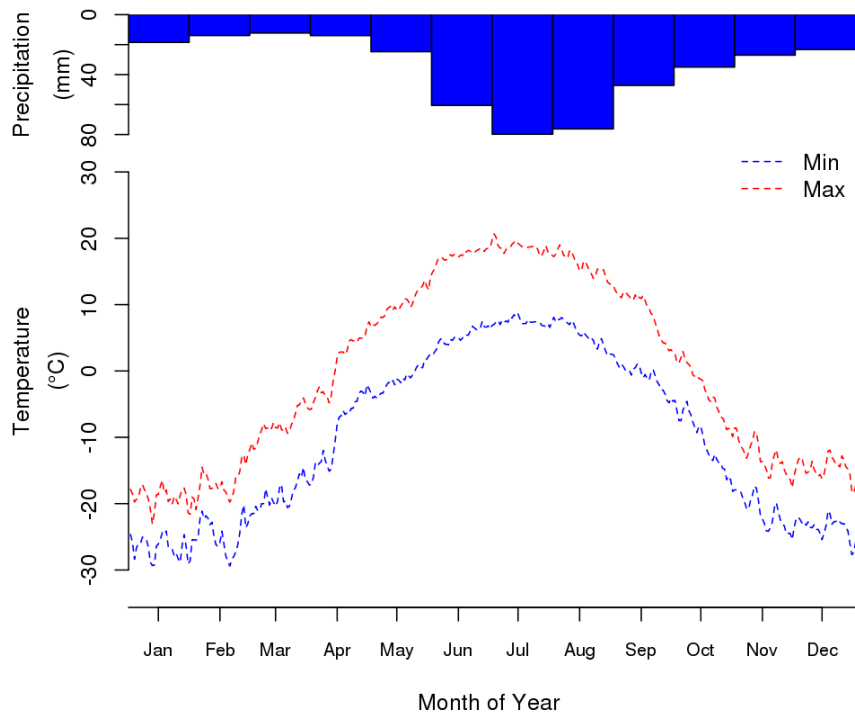


Figure 6.2 Climatological data. Average total monthly precipitation (upper) and average daily minimum and maximum temperature (lower, 1970-2010) for the Chena River basin. Values based on the historical gridded observed data set.

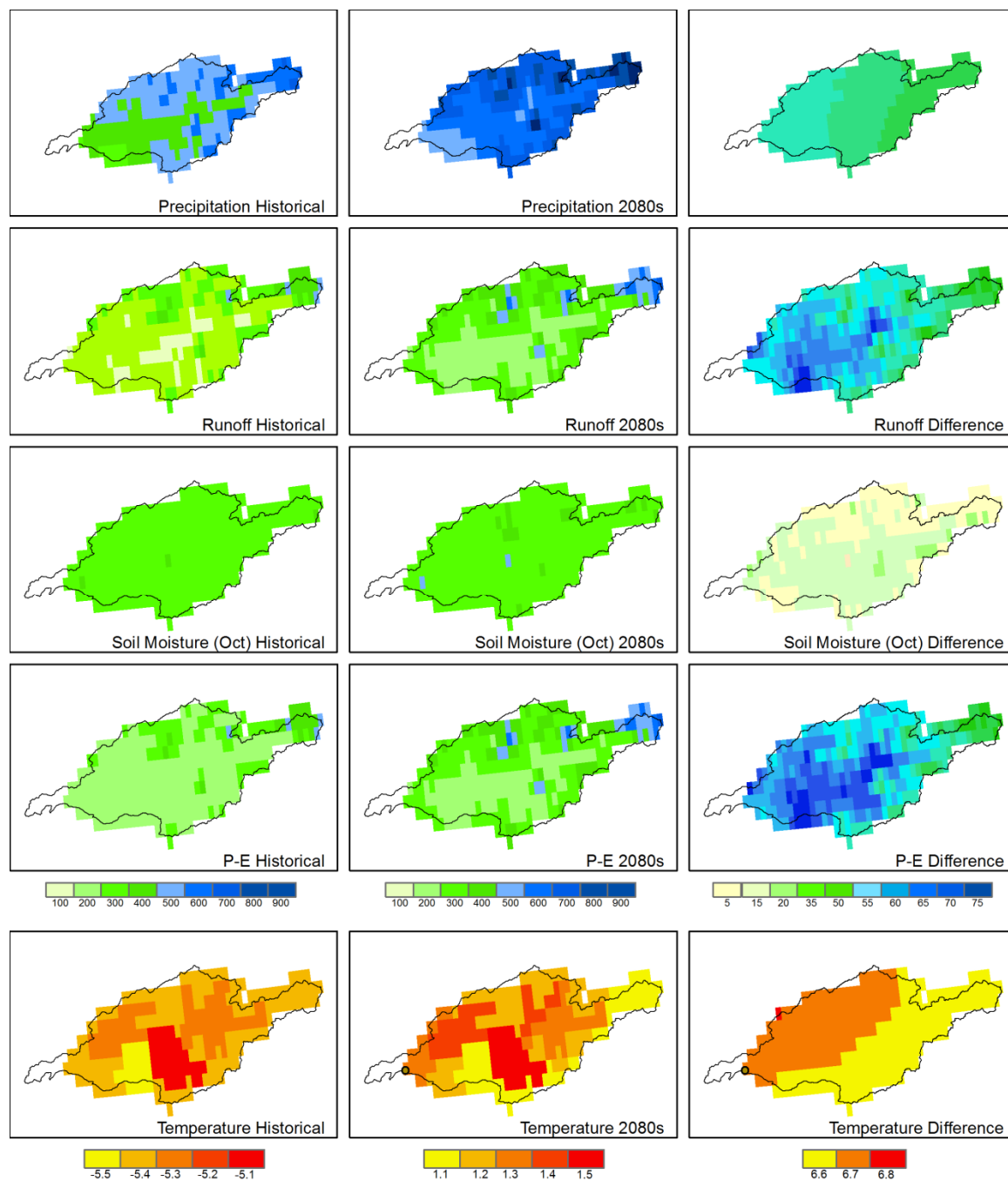


Figure 6.3 Historical and future hydrological variables in the Chena River basin, based on VIC model results.

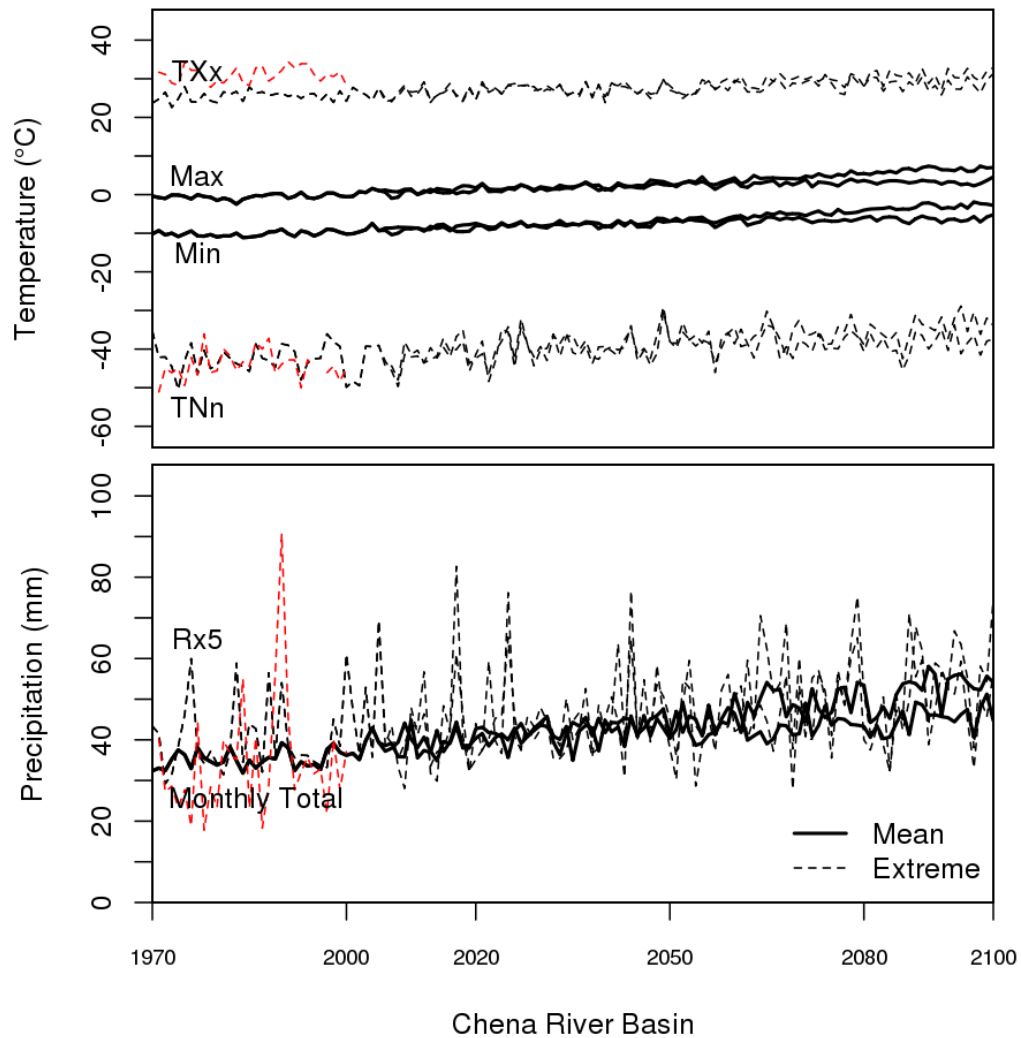


Figure 6.4 Time series of ClimDEX extremes compared to mean values. Average (solid lines) minimum temperature, maximum temperature, and total precipitation compared to extreme values (dashed lines) for annual average (1970-2100) in the Chena River Basin. The ensemble of all GCMs is used. The Fairbanks Airport GHCN climate station data are overlaid on the extreme indices (red lines). TXx, TNn, and Rx5 ClimDEX indices are used as illustrations of extremes; see Table 6.4 for description of indices.

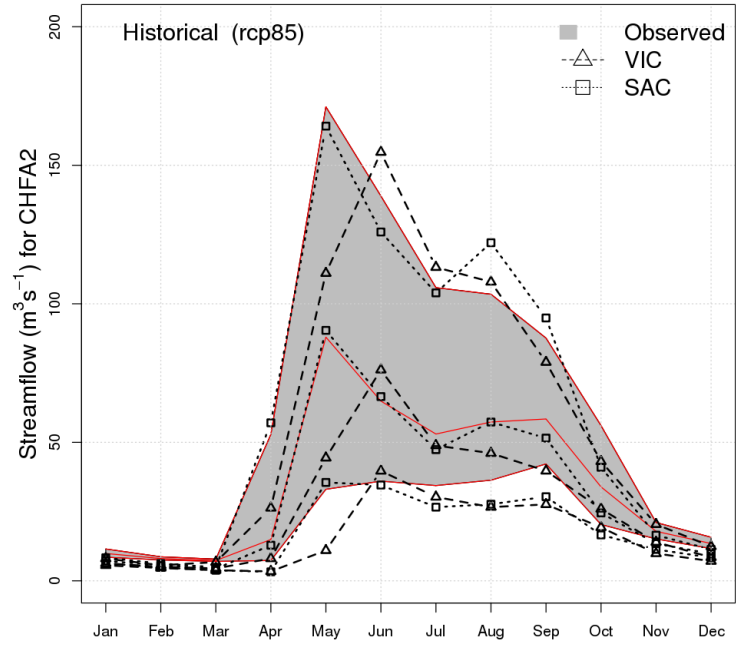


Figure 6.5 Streamflow average historical monthly differences between observed streamflow (red lines, grey fill), SAC-SMA (dotted lines with open boxes) and VIC model simulated streamflow (dashed lines with open triangles) for the 1971-2000 baseline in the Chena River basin.

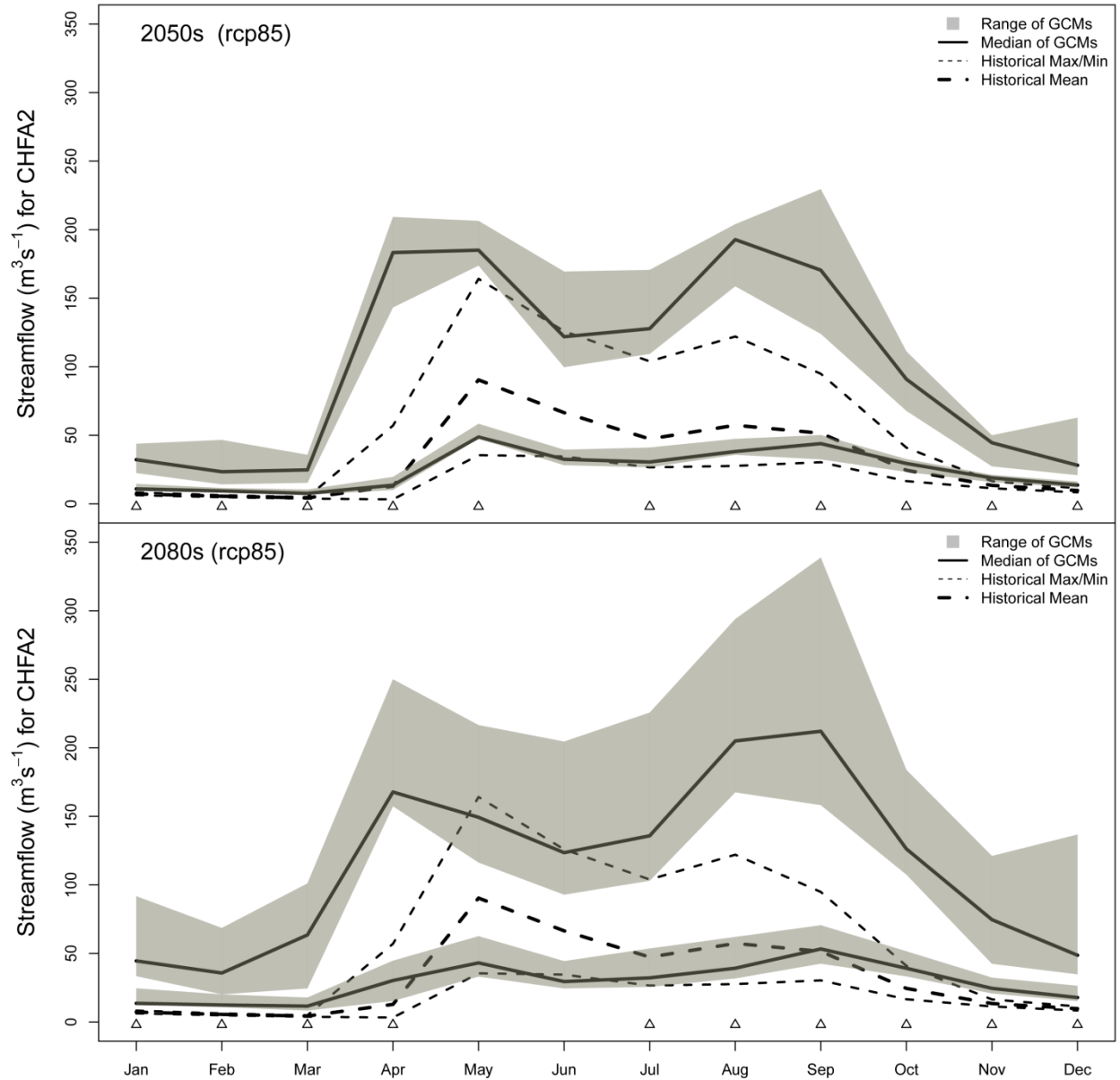


Figure 6.6 Chena River Basin SAC model simulated streamflow ranges for the 2050s (top panel) and the 2080s (bottom panel) for future minimum and maximum streamflow (solid lines) plotted against historical minimum and maximum (dashed lines). Historical mean (thick dashed line) is shown for context. Triangles indicate where future streamflow is significantly different than the historical streamflow by month.

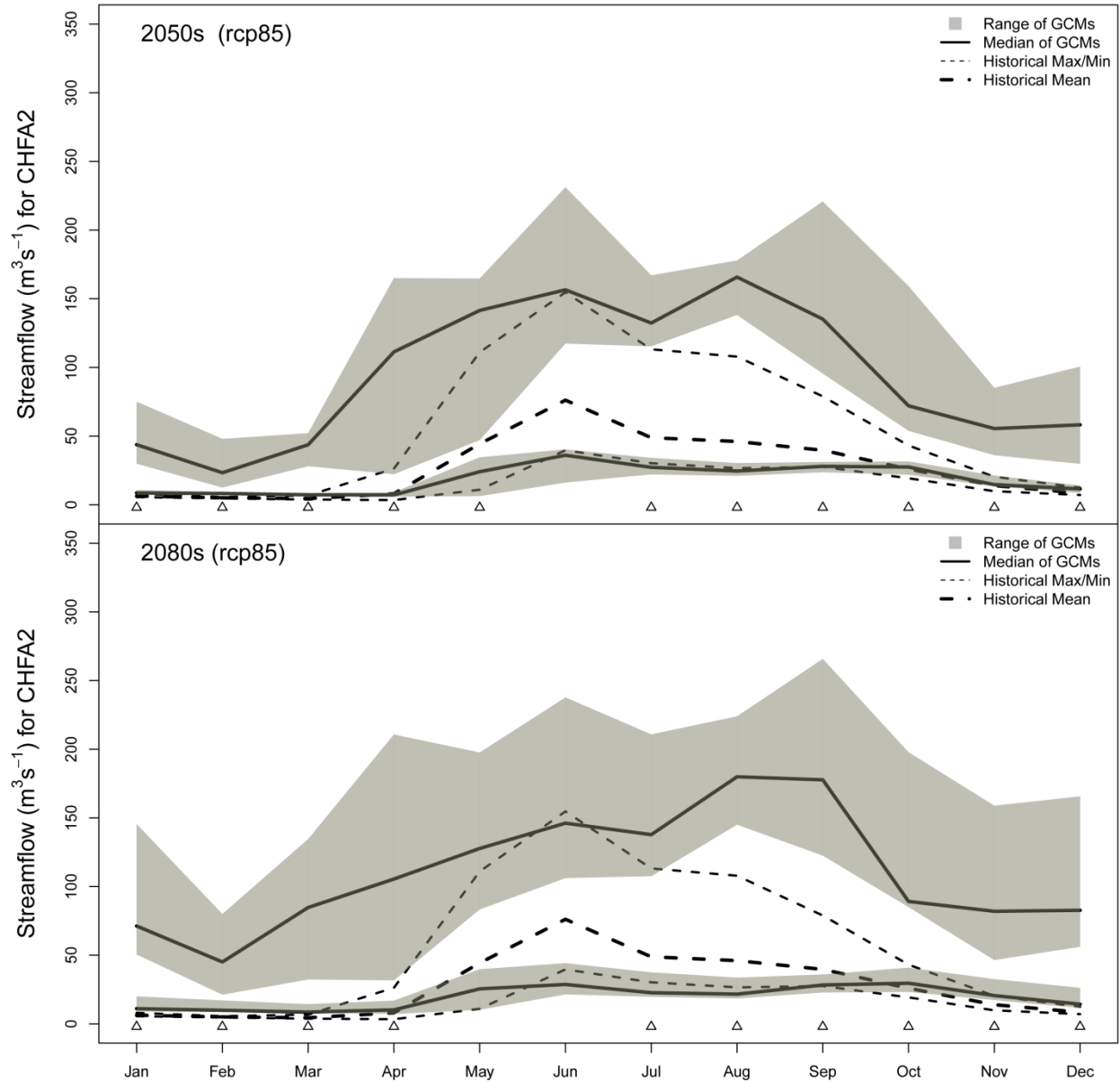


Figure 6.7 Chena River Basin VIC model simulated streamflow ranges for the 2050s (top panel) and the 2080s (bottom panel) for future minimum and maximum streamflow (solid lines) plotted against historical minimum and maximum (dashed lines). Historical mean (thick dashed line) is shown for context. Triangles indicate where future streamflow is significantly different than the historical streamflow by month.

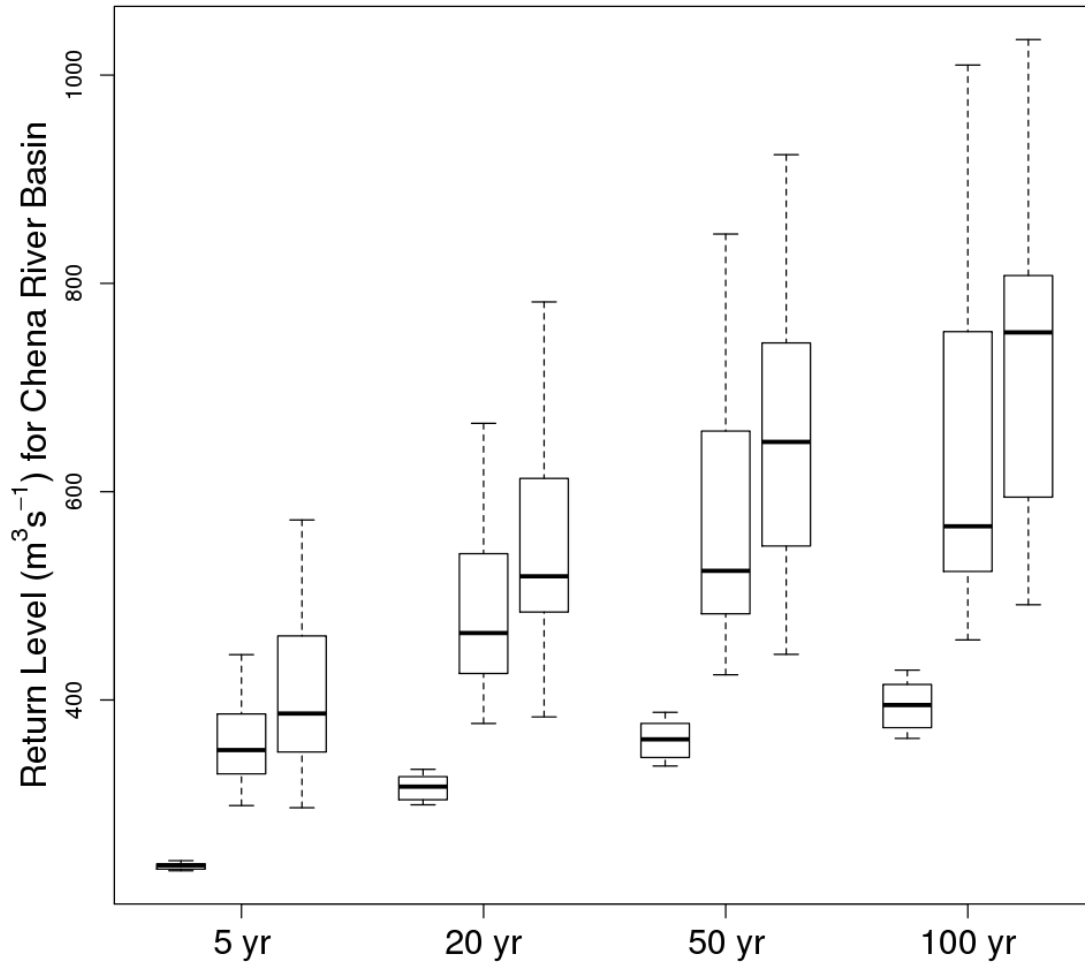


Figure 6.8 Chena River basin return intervals for 5, 20, 50 and 100 year return periods. The impact levels are shown by action (yellow), minor (orange) and major (red) flooding. Boxplots median values are indicated with thick black lines, the range of the data set is the box (the first and third quartiles), and the minimum and maximum values are indicated by dashed lines and whiskers. Outliers are plotted as open circles.

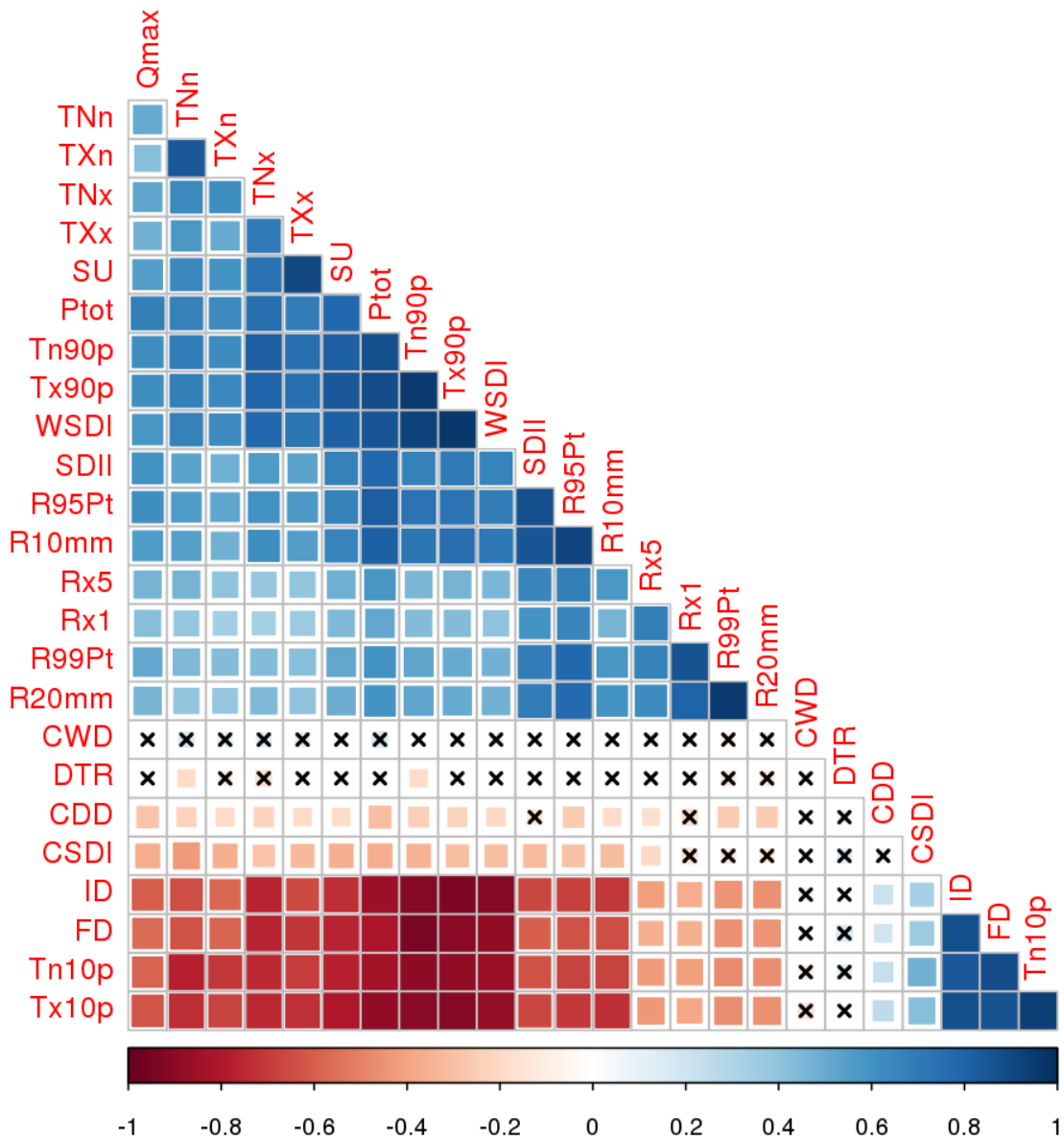


Figure 6.9 ClimDEX indices and streamflow correlation plot for maximum streamflow (ST) against annual indices for the Chena River basin. Blue values indicate positive correlations with streamflow and negative values are indicative of negative correlations and decreased streamflow. Non-significant correlations are denoted with crosses. Lighter values indicate weaker correlations and darker values indicate stronger correlations.

6.7 Tables

Table 6.1 Chena River basin characteristics including gages, sub-basins, area, elevation (Elev), temperature (T), precipitation (P), streamflow (Q) annual averages, and percent land cover (D=deciduous, Bs= black spruce, C=conifers, S=shrubs).

Name	USGS Gage	Area (km ²)	Elev (m)	T (°C)	P (mm)	Q (m ³ /s)	% Land cover
Chena River	15514000	5155	595	12.4 (-21.5)	98 (411)	328	12% D, 59% Bs, 15% C, 12% S

Table 6.2 Maximum and minimum temperature weighting factors used for Alaskan basins. WX=weighted maximum and WN=weighted minimum.

Seasons	WN ₁	WX ₁	WN _{2a}	WX ₂	WN _{2b}	WX ₃	WN ₃	WX ₄	WN ₄
Mar-May	0.78	0.22	0.20	0.69	0.11	0.21	0.79	0.65	0.35
Jun-Aug	0.79	0.21	0.15	0.69	0.16	0.23	0.77	0.68	0.32
Sep-Nov	0.73	0.27	0.23	0.64	0.13	0.31	0.69	0.64	0.36
Dec-Feb	0.61	0.39	0.28	0.53	0.19	0.39	0.61	0.58	0.42

Table 6.3 Calibration and verification results, SAC-SMA and VIC Models

	CHFA2	CHFA2
	SAC-SMA/ SNOW17	VIC
Calibration (1980-1985)		
Correlation Coefficient	0.85	0.79
NS Efficiency	0.66	0.56
NS Efficiency Natural Log	0.77	0.72
Verification (1986-1990)		
Correlation Coefficient	0.85	0.80
NS Efficiency	0.68	0.59
NS Efficiency Natural Log	0.72	0.64
Period of Record (1970-2005)		
Correlation Coefficient	0.87	0.75
NS Efficiency	0.73	0.51
NS Efficiency Natural Log	0.74	0.61

Table 6.4 ClimDEX indices, codes, definitions and units.

Name	Code	Definition	Units
Cold nights	TN10p	Monthly/annual percentage of days when TN < 10 th percentile	%
Cold days	TX10p	Monthly/annual percentage of days when TX < 10 th percentile	%
Warm nights	TN90p	Monthly/annual percentage of days when TN > 90 th percentile	%
Warm days	TX90p	Monthly/annual percentage of days when TX > 90 th percentile	%
Warm spell duration index	WSDI	Annual count of days with at least 6 consecutive days when TX > 90 th percentile	days
Cold spell duration index	CSDI	Annual count of days with at least 6 consecutive days when TN < 10 th percentile	days
Max TX	TXx	Monthly/annual maximum value of daily maximum temperature	°C
Min TX	TXn	Monthly/annual minimum value of daily maximum temperature	°C
Max TN	TNx	Monthly/annual maximum value of daily minimum temperature	°C
Min TN	TNn	Monthly/annual minimum value of daily minimum temperature	°C
Number of frost days	FD	Annual count of days when TN (daily minimum temperature) < 0°C.	days
Number of icing days	ID	Annual count of days when TX (daily maximum temperature) < 0°C.	days
Number of summer days	SU	Annual count of days when TX (daily maximum temperature) > 25°C.	days
Daily temperature range	DTR	Monthly/annual mean difference between TX and TN	°C
Max 1-day precipitation	RX1day	Monthly/annual maximum 1-day precipitation	mm
Max 5-day precipitation	RX5day	Monthly/annual maximum consecutive 5-day precipitation	mm
Simple daily intensity	SDII	Annual simple precipitation intensity index	mm
Heavy precipitation days	R10mm	Annual count of days when PRCP ≥ 10mm	days
Very heavy precipitation days	R20mm	Annual count of days when PRCP ≥ 20mm	days
Precipitation total	Ptot	Annual total precipitation in wet days	mm
Consecutive dry days	CDD	Annual maximum length of dry spell, maximum number of consecutive days with RR < 1mm	days
Consecutive wet days	CWD	Annual maximum length of wet spell, maximum number of consecutive days with RR ≥ 1mm	days
Very wet days	R95p	Annual total PRCP when RR > 95p	mm
Extremely wet days	R99p	Annual total PRCP when RR > 99p	mm

Table 6.5 Regional values for gridded downscaled ensemble of temperature, precipitation and wind speed as differences from the historical baseline period (1971-2000). Results are given for each variable, time period (2050s, 2080s) and RCP for the four seasons.

Variables, Time periods and RCPs	Seasons			
	JFM	AMJ	JAS	OND
Average Daily Minimum Temperature (°C)				
2041-2070 RCP 4.5 (Average)	3.92	2.49	2.17	3.91
2041-2070 RCP 4.5 (SD)	0.08	0.03	0.02	0.09
2071-2100 RCP 4.5 (Average)	4.62	2.99	2.62	4.65
(SD)	0.13	0.07	0.03	0.08
2041-2070 RCP 8.5 (Average)	4.76	3.15	2.8	4.86
(SD)	0.09	0.04	0.03	0.09
2071-2100 RCP 8.5 (Average)	8.07	5.44	4.75	7.76
(SD)	0.21	0.11	0.04	0.14
Average Daily Maximum Temperature (°C)				
2041-2070 RCP 4.5 (Average)	3.81	2.46	2.4	3.73
(SD)	0.07	0.07	0.03	0.09
2071-2100 RCP 4.5 (Average)	4.71	3.2	2.52	4.52
(SD)	0.08	0.05	0.07	0.1
2041-2070 RCP 8.5 (Average)	4.63	3.24	3.01	4.65
(SD)	0.06	0.05	0.02	0.1
2071-2100 RCP 8.5 (Average)	8.14	5.58	4.65	7.63
(SD)	0.16	0.05	0.06	0.15
Average Total Daily Precipitation (mm)				
2041-2070 RCP 4.5 (Average)	9.64	27.86	34.07	19.67
(SD)	2.45	6.1	6.98	4.76
2071-2100 RCP 4.5 (Average)	7.91	32.14	54.35	22.94
(SD)	1.88	7.2	10.93	6.12
2041-2070 RCP 8.5 (Average)	9.91	40	49.29	31.64
(SD)	2.47	7.54	9.96	7.39
2071-2100 RCP 8.5 (Average)	7.89	64.67	81.51	43.37
(SD)	1.96	13.1	15.75	10.71
Average Daily Wind Speed (m/s)				
2041-2070 RCP 4.5 (Average)	6.49	-1.81	0.41	5.22
(SD)	0.3	0.33	0.33	0.35
2071-2100 RCP 4.5 (Average)	7.72	0.47	-1.9	5.41
(SD)	0.79	0.27	0.55	0.52
2041-2070 RCP 8.5 (Average)	5.98	-0.94	2.02	3.88
(SD)	0.62	0.26	0.26	0.76
2071-2100 RCP 8.5 (Average)	14.63	-0.95	4.21	5.04
	1.15	0.17	0.26	0.64

Table 6.6 ClimDEX indices for the 2050s and the 2080s as differences from the historical (1971-2000) for quantiles 0, 50, 75 and 99% probability. Note the variable y-axis scale and the mixing of units (denoted by separate lines in plots, and labels). See Table 4 for ClimDEX indice codes and descriptions.

	2050s Differences				2080s Differences			
	0%	50%	75%	99%	0%	50%	75%	99%
TXx	-4.42	2.94	4.7	9.05	-1.06	5.06	6.88	10.89
TNn	-15.73	4.73	10.01	20.91	-13.71	8.2	12.35	23.24
TNx	-6.04	2.93	4.25	8.46	-3.27	4.58	5.98	9.97
TXn	-16.38	6.39	11.4	22.73	-15.78	9.35	14.09	25.03
DTR	-2.57	0.02	0.43	2.11	-1.64	-0.06	0.32	1.89
Tn10p	-22.57	-7.67	-4.71	2.26	-22.57	-9.18	-6.75	-0.84
Tn90p	-12.65	21.64	30.54	51.36	-2.36	40.71	49.28	68.07
Tx10p	-25.76	-7.95	-4.89	3.61	-27.95	-9.1	-6.74	-1.37
Tx90p	-11.12	19.01	25.93	43.09	3.98	36.05	43.41	62.58
SU	-3	8.5	14	31.91	-2	19	25.75	48.91
ID	-82	-27	-16	13.82	-117	-52	-36	-3
FD	-86	-32.5	-19	14.73	-102	-58	-44.25	-11.18
WSDI	-23	43	62	133.83	3	99	133.75	215.1
CSDI	-26	0	0	14.73	-26	-2	0	6.91
SDII	-1.3	0.77	1.2	2.74	-1.02	1.1	1.53	3.05
Rx1	-29.93	6.35	13.99	38.17	-23.02	8.16	16.68	40.31
Rx5	-46.3	12.12	23.9	68.69	-33.35	15.74	28.94	66.15
CDD	-58	-4	7.75	43.91	-60	-4	5.75	46.73
CWD	-7	0	2	6.91	-10	1	3	8.91
R10mm	-7	5	8	18	-3	8	11	20.82
R20mm	-5	1	3	6	-4	2	3.75	9.91
R95Pt	-135.38	73.46	142.16	299.29	-93.83	118.94	174.69	394.59
R99Pt	-123.46	32.18	68.32	186.89	-97.28	44.14	87.64	270.68
Ptot	-125.79	131.64	201.66	406.59	-78.47	181.14	262.98	573.78

Table 6.7 The 99th, 95th, 5th, and 50th (median) exceedances for historical, 2050s and the 2080s. Calculations based on annual median flow simulations for GCMs and hydrologic models.

	Historical Magnitude (m ³ /s)	Historical Exceedance (count)	2050s Exceedance (count)	2050s Exceedance (%)	2080s Exceedance (count)	2080s Exceedance (%)
99th	158	128	234	83	343	168
95th	98	640	977	53	1266	98
5th	3	640	10	-98	0	-100
50th	17	6392	7335	15	8577	34

6.8 References

- ACIA, 2005. Chapter 6: Cryosphere and Hydrology. In: Walsh, J.E. (Ed.), *The Arctic Climate Impact Assessment*. Cambridge University Press, pp. 1042.
- Alexander, L., Donat, M., Takayama, Y., Yang, H., 2011. The CLIMDEX project: Creation of long-term global gridded products for the analysis of temperature and precipitation extremes, WCRP Open Science conference, Denver.
- Alexander, L.V., Zhang, X., Peterson, T.C., Caesar, J., Gleason, B., Klein Tank, A.M.G., Haylock, M., Collins, D., Trewin, B., Rahimzadeh, F., Tagipour, A., Rupa Kumar, K., Revadekar, J., Griffiths, G., Vincent, L., Stephenson, D.B., Burn, J., Aguilar, E., Brunet, M., Taylor, M., New, M., Zhai, P., Rusticucci, M., Vazquez-Aguirre, J.L., 2006. Global observed changes in daily climate extremes of temperature and precipitation. *Journal of Geophysical Research: Atmospheres* (1984–2012), 111 (D5).
- Allen, M.R., Ingram, W.J., 2002. Constraints on future changes in climate and the hydrologic cycle. *Nature*, 419 (6903): 224-232.
- Anderson, E., 2002. Calibration of conceptual hydrologic models for use in river forecasting. Office of Hydrologic Development, US National Weather Service, Silver Spring, MD.
- Anderson, E.A., 1976. A point energy and mass balance model of a snow cover.
- Arnell, N.W. (Ed.), 2001. Chapter 4: Hydrology and water resources. *IPCC Climate Change 2001: Impacts, Adaptation & Vulnerability, The Third Assessment Report of Working Group II of the Intergovernmental Panel on Climate Change (IPCC)*, J.J. McCarthy, O.F. Canziani, N.A. Leary, D.J. Dokken, White, K.S.(Eds.). Cambridge University Press, Cambridge, UK, 133–191 pp.
- Batjes, N.H. (Ed.), 1995. A homogenized soil data file for global environmental research: A subset of FAO, ISRIC and NRCS profiles (Version 1.0). Working Paper and Preprint 95/10b. International Soil Reference and Information Centre, Wageningen, The Netherlands.
- Beltaos, S., Prowse, T., 2009. River-ice hydrology in a shrinking cryosphere. *Hydrol. Process.*, 23 (1): 122-144.
- Bennett, K.E., Walsh, J., 2014. Spatial and temporal changes in indices of extreme precipitation and temperature for Alaska. *International Journal of Climatology*. DOI: 10.1002/joc.4067.
- Bennett, K.E., Werner, A.T., Schnorbus, M., 2012. Uncertainties in hydrologic and climate change impact analyses in headwater basins of British Columbia. *J. Clim.*, 25 (17): 5711-5730.
- Boyle, D.P., Gupta, H.V., Sorooshian, S., Koren, V., Zhang, Z., Smith, M., 2001. Toward improved streamflow forecasts: Value of semidistributed modeling. *Water Resour. Res.*, 37 (11): 2749-2759.

- Brown, S., Caesar, J., Ferro, C.A., 2008. Global changes in extreme daily temperature since 1950. *Journal of Geophysical Research: Atmospheres* (1984–2012), 113 (D5).
- Bürger, G., Murdock, T., Werner, A., Sobie, S., Cannon, A., 2012. Downscaling extremes-an intercomparison of multiple statistical methods for present climate. *J. Clim.*, 25 (12): 4366-4388.
- Bürger, G., Sobie, S., Cannon, A., Werner, A., Murdock, T., 2013. Downscaling Extremes: An Intercomparison of Multiple Methods for Future Climate. *J. Clim.*, 26 (10): 3429-3449.
- Burn, D.H., 2008. Climatic influences on streamflow timing in the headwaters of the Mackenzie River Basin. *Journal of Hydrology*, 352: 225-238.
- Burnash, R.J.E., Ferral, R.L., McGuire, R.A., 1973. A generalized streamflow simulation system, Joint Federal-State River Forecast Center, Sacramento, CA, pp. 204.
- Cannon, A.J., 2010. A flexible nonlinear modelling framework for nonstationary generalized extreme value analysis in hydroclimatology. *Hydrol. Process.*, 24 (6): 673-685.
- Cannon, A.J., 2011. GEVcdn: An R package for nonstationary extreme value analysis by generalized extreme value conditional density estimation network. *Computers & Geosciences*, 37 (9): 1532-1533.
- Cherkauer, K.A., 2001. Understanding the hydrologic effects of frozen soil, Department of Civil and Environmental Engineering, University of Washington, Seattle, WA.
- Cherkauer, K.A., Bowling, L.C., Lettenmaier, D.P., 2003. Variable infiltration capacity cold land process model updates. *Global Planet. Change*, 38: 151-159.
- Cherkauer, K.A., Lettenmaier, D.P., 1999. Hydrologic effects of frozen soils in the upper Mississippi River basin. *J. Geophys. Res.*, 104 (D16): 19599-19610.
- Cherkauer, K.A., Lettenmaier, D.P., 2003. Simulation of spatial variability in snow and frozen soil. *J. Geophys. Res.*, 108 (D22): 19:1-13.
- Cosby, B.J., Homberger, G.M., Clapp, R.B., Ginn, T.R., 1984. A statistical exploration of the relationships of soil moisture characteristics to the physical properties of soils. *Water Resour. Res.*, 20: 682-690.
- Daly, C., Gibson, W.P., Taylor, G.H., Johnson, G.L., Pasteris, P., 2002. A knowledge-based approach to the statistical mapping of climate. *Clim. Res.*, 22: 99-113.
- Demaria, E.M., Nijssen, B., Wagener, T., 2007. Monte Carlo sensitivity analysis of land surface parameters using the Variable Infiltration Capacity model. *J. Geophys. Res.*, 112.
- Dickerson-Lange, S.E., Mitchell, R., 2013. Modeling the effects of climate change projections on streamflow in the Nooksack River basin, Northwest Washington. *Hydrol. Process.*
- Dingman, S., 2002. *Physical hydrology*. Prentice Hall Englewood Cliffs, NJ.

- Elsner, M.M., Cuo, L., Voisin, N., Deems, J.S., Hamlet, A.F., Vano, J.A., Mickelson, K.E.B., Lee, S.Y., Lettenmaier, D.P., 2010. Implications of 21st century climate change for the hydrology of Washington State. *Clim. Change*, 102 (1-2): 225-260.
- Endalamaw, A.M., Bolton, W.R., Young, J.M., Morton, D., Hinzman, L.D., 2013. Toward Improved Parameterization of a Meso-Scale Hydrologic Model in a Discontinuous Permafrost, Boreal Forest Ecosystem. American Geophysical Union, Fall Meeting 2013, abstract #C53A-0549. <http://adsabs.harvard.edu/abs/2013AGUFM.C53A0549E>.
- FAO, 1995. The Digital Soil Map of the World, Version 3.5. Food and Agriculture Organization of the United States (FAO), Rome, Italy.
- Frich, P., Alexander, L., Della-Marta, P., Gleason, B., Haylock, M., Klein Tank, A., Peterson, T., 2002. Observed coherent changes in climatic extremes during the second half of the twentieth century. *Clim. Res.*, 19 (3): 193-212.
- Gan, T.Y., Burges, S.J., 2006. Assessment of soil-based and calibrated parameters of the Sacramento model and parameter transferability. *Journal of Hydrology*, 320 (1): 117-131.
- Gesch, D., Oimoen, M., Greenlee, S., Nelson, C., Steuck, M., Tyler, D., 2002. The National Elevation Dataset: Photogrammetric Engineering and Remote Sensing. 68 (1): 5-11.
- Gibson, W., 2009. Temperature and Precipitation for Alaska 1971-2000. National Park Service, Alaska Regional Office GIS Team. Geospatial Dataset-2170516. PRISM model, developed by Christopher Daly of the PRISM Climate Group.
- Global Soil Data Task Group, 2000. Global Gridded Surfaces of Selected Soil Characteristics (IGBP-DIS). In: Center., O.R.N.L.D.A.A. (Ed.), Global Gridded Surfaces of Selected Soil Characteristics (International Geosphere-Biosphere Programme - Data and Information System., Oak Ridge, Tennessee, U.S.A.
- Groisman, P.Y., Knight, R.W., Easterling, D.R., Karl, T.R., Hegerl, G.C., Razuvaev, V.N., 2005. Trends in intense precipitation in the climate record. *J. Clim.*, 18 (9): 1326-1350.
- Gupta, H.V., Sorooshian, S., Yapo, P.O., 1998. Toward improved calibration of hydrologic models: Multiple and noncommensurable measures of information. *Water Resour. Res.*, 34 (4): 751-763.
- Haugen, R.K., Slaughter, C.W., Howe, K.E., Dingman, S.L., 1982. Hydrology and climatology of the Caribou-Poker creeks research watershed, Alaska. US Army Corps of Engineers, Cold Regions Research & Engineering Laboratory Hanover, NH.
- He, M., Hogue, T.S., Franz, K.J., Margulis, S.A., Vrugt, J.A., 2011. Characterizing parameter sensitivity and uncertainty for a snow model across hydroclimatic regimes. *Advances in Water Resources*, 34 (1): 114-127.

- Hinzman, L.D., Bettez, N.D., Bolton, W.R., Chapin, F.S., Dyurgerov, M.B., Fastie, C.L., Griffith, B., Hollister, R.D., Hope, A., Huntington, H.P., Jensen, A.M., Jia, G.J., Jorgenson, T., Kane, D.L., Klein, D.R., Kofinas, G., Lynch, A.H., Lloyd, A.H., McGuire, A.D., Nelson, F.E., Oechel, W.C., Osterkamp, T.E., Racine, C.H., Romanovsky, V.E., Stone, R.S., Stow, D.A., Sturm, M.D., Walker, D.A., Webber, P.J., Welker, J.M., Winker, K.S., Yoshikawa, K., 2005. Evidence and implications of recent climate change in northern Alaska and other Arctic regions. *Clim. Change*, 72: 251-298.
- Huntington, T.G., 2006. Evidence for intensification of the global water cycle: Review and synthesis. *Journal of Hydrology*, 319: 83-95.
- Huntington, T.G., Hodgkins, G.A., Keim, B.D., Dudley, R.W., 2004. Changes in the proportion of precipitation occurring as snow in New England (1949-2000). *J. Clim.*, 17 (13): 2626-2636.
- IPCC, 2012. *Managing the Risks of Extreme Events and Disasters to Advance Climate Change Adaptation: A Special Report of Working Groups I and II of the Intergovernmental Panel on Climate Change (IPCC)*, Cambridge University Press, Cambridge, UK, and New York, NY, USA., pp. 582.
- Kalnay, E., Kanamitsu, M., Kistler, R., Collins, W., Deaven, D., Gandin, L., M. Iredell, Saha, S., White, G., Woollen, J., Zhu, Y., Leetmaa, A., Reynolds, R., Chelliah, M., Ebisuzaki, W., W.Higgins, Janowiak, J., Mo, K.C., Ropelewski, C., Wang, J., Jenne, R., D.Joseph, 1996. The NCEP/NCAR 40-Year Reanalysis Project. *B. Am. Meteorol. Soc.*, 77 (3): 437-471.
- Kane, D.L., Hinzman, L.D., Gieck, R.E., McNamara, J.P., Youcha, E.K., Oatley, J.A., 2008. Contrasting extreme runoff events in areas of continuous permafrost, Arctic Alaska. *Hydrology Research*, 39 (4): 287-298.
- Kane, D.L., McNamara, J.P., Yang, D.Q., Olsson, P.Q., Gieck, R.E., 2003. An extreme rainfall/runoff event in Arctic Alaska. *J. Hydrometeorol.*, 4 (6): 1220-1228.
- Karl, T.R., Groisman, P.Y., Knight, R.W., Heim, R.R., 1993. Recent Variations of Snow Cover and Snowfall in North America and Their Relation to Precipitation and Temperature Variations. *J. Clim.*, 6 (7): 1327-1344.
- Kharin, V.V., Zwiers, F.W., Zhang, X., Hegerl, G.C., 2007. Changes in temperature and precipitation extremes in the IPCC ensemble of Global Coupled Model simulations. *J. Clim.*, 20: 1419-1444.
- Klein Tank, A., Zwiers, F., Zhang, X., 2009. Guidelines on analysis of extremes in a changing climate in support of informed decisions for adaptation.—Climate Data and Monitoring WCDMP-No.
- Knowles, N., Dettinger, M., and Cayan, D., 2006. Trends in snowfall versus rainfall for the Western United States. *J. Clim.*, 19 (18): 4545-4559.

- Liang, X., Lettenmaier, D.P., Wood, E.F., Burges, S.J., 1994. A simple hydrologically based model of land surface water and energy fluxes for general circulation models. *J. Geophys. Res.*, 99 (D7): 14,415-14,428.
- Liang, X., Wood, E.F., Lettenmaier, D.P., 1996. Surface soil moisture parameterization of the VIC-2L model: Evaluation and modification. *Global Planet. Change*, 13: 195-206.
- Lins, H.F., Slack, J.R., 1999. Streamflow trends in the United States. *Geophys. Res. Lett.*, 26 (2): 227-230.
- Lohmann, D., Nolte-Holube, R., Raschke, E., 1996. A large-scale horizontal routing model to be coupled to land surface parameterization schemes. *Tellus*, 48A: 708-721.
- Lohmann, D., Raschke, E., Nijssen, B., Lettenmaier, D.P., 1998. Regional scale hydrology: I. Formulation of the VIC-2L model coupled to a routing model. *Hydrological Sciences Journal*, 43 (1): 131-141.
- McAfee, S.A., Guentchev, G., Eischeid, J.K., 2013. Reconciling precipitation trends in Alaska: 1. Station-based analyses. *J. Geophys. Res.: Atmos.*, 118 (14): 7523-7541.
- McBean, G.A., Alekseev, G., Chen, D., Førland, E., Fyfe, J., Groisman, P.Y., King, R., Melling, H., R., V.a., Whitfield, P.H., 2004. The Arctic Climate: – Past and Present, ACIA International Scientific Symposium on Climate Change in the Arctic, Reykjavik, Iceland.
- McCabe, G.J., Wolock, D.M., 1999. General-circulation model simulations of future snowpack in the western United States. *Journal of The American Water Resources Association*, 35 (6): 1473-1484.
- McCabe, G.J., Wolock, D.M., 2002. A step increase in streamflow in the conterminous United States. *Geophys. Res. Lett.*, 29 (24): 38-1-38-4.
- Mölders, N., Kramm, G., 2010. A case study on wintertime inversions in Interior Alaska with WRF. *Atmos. Res.*, 95 (2): 314-332.
- Moss, R.H., Edmonds, J.A., Hibbard, K.A., Manning, M.R., Rose, S.K., van Vuuren, D.P., Carter, T.R., Emori, S., Kainuma, M., Kram, T., Meehl, G.A., Mitchell, J.F.B., Nakicenovic, N., Riahi, K., Smith, S.J., Stouffer, R.J., Thomson, A.M., Weyant, J.P., Wilbanks, T.J., 2010. The next generation of scenarios for climate change research and assessment. *Nature*, 463 (7282): 747-756.
- Nijssen, B., O'Donnell, G.M., Lettenmaier, D.P., Lohmann, D., Wood, E.F., 2001. Predicting the discharge of global rivers. *J. Clim.*, 14: 3307-3323.
- NWSRFC, 2005. Operational Forecast System Mean Areal Temperature Preprocessor Function (MAT). http://www.nws.noaa.gov/oh/hrl/nwsrfs/users_manual/part2/_pdf/27ofs_mat.pdf.
- Orlowsky, B., Seneviratne, S.I., 2012. Global changes in extreme events: regional and seasonal dimension. *Clim. Change*, 110 (3-4): 669-696.

- Pall, P., Allen, M., Stone, D., 2007. Testing the Clausius–Clapeyron constraint on changes in extreme precipitation under CO₂ warming. *Climate Dynamics*, 28 (4): 351-363.
- Peck, E.L., 1976. Catchment modeling and initial parameter estimation for the National Weather Service river forecast system. Office of Hydrology, National Weather Service.
- Peterson, T., Anderson, D., Cohen, S., Cortez-Vázquez, M., Murnane, R., Parmesan, C., Phillips, D., Pulwarty, R., Stone, J., 2008. Why weather and climate extremes matter. Weather and climate extremes in a changing climate. Regions of focus: North America, Hawaii, Caribbean, and US Pacific Islands: 11-33.
- Rawlins, M.A., Steele, M., Holland, M.M., Adam, J.C., Cherry, J.E., Francis, J.A., Groisman, P.Y., Hinzman, L.D., Huntington, T.G., Kane, D.L., Kimball, J.S., Kwok, R., Lammers, R.B., Lee, C.M., Lettenmaier, D.P., McDonald, K.C., Podest, E., Pundsack, J.W., Rudels, B., Serreze, M.C., Shiklomanov, A., Skagseth, O., Troy, T.J., Vorosmarty, C.J., Wensnahan, M., Wood, E.F., Woodgate, R., Yang, D.Q., Zhang, K., Zhang, T.J., 2010. Analysis of the Arctic System for Freshwater Cycle Intensification: Observations and Expectations. *J. Clim.*, 23 (21): 5715-5737.
- Rawls, W.J., Ahuja, L.R., Brakensiek, D.L., Shirmohammadi, A., 1993. Infiltration and Soil Water Movement. In: Maidment, D.R. (Ed.), *Handbook of Hydrology*. McGraw-Hill Inc., New York, pp. 5.1-5.51.
- Regonda, S.K., Rajagopalan, B., Clark, M., Pitlick, J., 2005. Seasonal cycle shifts in hydroclimatology over the Western United States. *J. Clim.*, 18: 372-384.
- Romanovsky, V.E., Smith, S.L., Christiansen, H.H., 2010. Permafrost thermal state in the polar Northern Hemisphere during the international polar year 2007–2009: a synthesis. *Permafrost and Periglacial Processes*, 21 (2): 106-116.
- Rosenzweig, C., G. Casassa, D.J. Karoly, A. Imeson, C. Liu, A. Menzel, S. Rawlins, T.L. Root, B. Seguin, P. Tryjanowski, 2007. Assessment of observed changes and responses in natural and managed systems. *Climate Change 2007: Impacts, Adaptation and Vulnerability*. Contribution of Working Group II to the Fourth Assessment Report of the Intergovernmental Panel on Climate Change, M.L. Parry, O.F. Canziani, J.P. Palutikof, P.J. van der Linden and C.E. Hanson, Eds., Cambridge University Press, Cambridge, UK, 79-131.
- Schaake, J., Henkel, A., Cong, S., 2004. 5.3 Application of PRISM climatologies for hydrologic modeling and forecasting in the Western US, *Proceedings of 84th AMS Meeting, 18st Conference on Hydrology*.
- Schnorbus, M., Bennett, K.E., Werner, A.T., 2010. Quantifying the Water Resources Impacts of Mountain Pine Beetle and Associated Salvage Harvest Operations Across a Range of Watershed

- Scales: Hydrologic Modelling of the Fraser River Basin. Information Report BC-X-423, Canadian Forest Service, Pacific Forestry Centre, Victoria, pp. 64.
- Schnorbus, M., Werner, A., Bennett, K., 2014. Impacts of climate change in three hydrologic regimes in British Columbia, Canada. *Hydrol. Process.*, 28 (3): 1170-1189.
- Serreze, M., Barrett, A., Stroeve, J., Kindig, D., Holland, M., 2009. The emergence of surface-based Arctic amplification. *Cryosphere*, 3 (1): 11-19.
- Serreze, M.C., Barry, R.G., 2011. Processes and impacts of Arctic amplification: A research synthesis. *Global Planet. Change*, 77 (1–2): 85-96.
- Shi, X., Wood, A.W., Lettenmaier, D.P., 2008. How Essential is Hydrologic Model Calibration to Seasonal Streamflow Forecasting? *J. Hydrometeorol.*, 9: 1350-1363.
- Shulski, M., Wendler, G., 2007. *The climate of Alaska*. University of Alaska Press.
- Sillmann, J., Kharin, V., Zwiers, F., Zhang, X., Bronaugh, D., 2013. Climate extreme indices in the CMIP5 multi-model ensemble. Part 2: Future climate projections. *J. Geophys. Res.: Atmos.*
- Skopp, J.M., 2000. Physical properties of primary particles, *Handbook of soil science*. CRC Press, Boca Raton, pp. A3-A17.
- Smith, L.C., 2000. Trends in Russian Arctic river-ice formation and breakup, 1917 to 1994. *Physical Geography*, 21 (1): 46-56.
- Smith, S., Romanovsky, V., Lewkowicz, A., Burn, C., Allard, M., Clow, G., Yoshikawa, K., Throop, J., 2010. Thermal state of permafrost in North America: A contribution to the International Polar Year. *Permafrost and Periglacial Processes*, 21 (2): 117-135.
- Stewart, B., Kunkel, K.E., Stevens, L.E., Sun, L., Walsh, J.E., 2013. Regional Climate Trends and Scenarios for the U.S. National Climate Assessment. Part 7. *Climate of Alaska.*, NOAA/NESDIS, Washington, D.C.
- Stewart, I.T., Cayan, D.R., Dettinger, M.D., 2005. Changes toward earlier streamflow timing across Western North America. *J. Clim.*, 18 (8): 1136-1155.
- Stocker, T., Qin, D., Plattner, G., Tignor, M., Allen, S., Boschung, J., Nauels, A., Xia, Y., Bex, B., Midgley, B. (Eds.), 2013. *Climate Change 2013: The Physical Science Basis*. Contribution of Working Group I to the Fifth Assessment Report of the Intergovernmental Panel on Climate Change (IPCC). Cambridge University Press, Cambridge, UK and New York, NY, USA, 1535 pp.
- Stone, D.A., Weaver, A.J., Zwiers, F.W., 2000. Trends in Canadian precipitation intensity. *Atmosphere-Ocean*, 38 (2): 321-347.
- Taylor, K.E., Stouffer, R.J., Meehl, G.A., 2012. An overview of CMIP5 and the experiment design. *B. Am. Meteorol. Soc.*, 93 (4): 485-498.

- Trenberth, K.E., 1999. Conceptual framework for changes of extremes of the hydrological cycle with climate change, *Weather and Climate Extremes*. Springer, pp. 327-339.
- Trenberth, K.E., Jones, P.D., Ambenje, P., Bojariu, R., Easterling, D.R., Tank, A.K., Parker, D., Rahimzadeh, F., Renwick, J.A., Rusticucci, M., Soden, B., Panmao, Z. (Eds.), 2007. *Observations: Surface and Atmospheric Climate Change*. *Climate Change 2007: The Physical Science Basis*. Contribution of Working Group I to the Fourth Assessment Report of the Intergovernmental Panel on Climate Change, Solomon, S. et al.(Eds.). Cambridge University Press, United Kingdom and New York, NY, USA.
- Vaze, J., Post, D., Chiew, F., Perraud, J.-M., Teng, J., Viney, N., 2011. Conceptual rainfall-runoff model performance with different spatial rainfall inputs. *J. Hydrometeorol.*, 12 (5): 1100-1112.
- Viereck, L., Dyrness, C., Batten, A., Wenzlick, K., 1992. *The Alaska vegetation classification*. Gen. Tech. Rep. PNW-GTR-286. Portland, OR: US Department of Agriculture, Forest Service, Pacific Northwest Research Station. 278 p.
- Wang, J., Zhang, X., 2008. Downscaling and projection of winter extreme daily precipitation over North America. *J. Clim.*, 21 (5): 923-937.
- Werner, A., 2011. *BCSD Downscaled Transient Climate Projections for Eight Select GCMs over British Columbia, Canada*. Pacific Climate Impacts Consortium, University of Victoria, Victoria, BC, 63 pp.
- Wood, A.W., Leung, L.R., Sridhar, W., Lettenmaier, D.P., 2004. Hydrologic implications of dynamical and statistical approaches to downscaling climate model outputs. *Clim. Change*, 62 (1-3): 189-216.
- Yapo, P.O., Gupta, H.V., Sorooshian, S., 1998. Multi-objective global optimization for hydrologic models. *Journal of Hydrology*, 204: 83 - 97.
- Zhang, X., Alexander, L., Hegerl, G.C., Jones, P., Tank, A.K., Peterson, T.C., Trewin, B., Zwiers, F.W., 2011. Indices for monitoring changes in extremes based on daily temperature and precipitation data. *Wiley Interdisciplinary Reviews: Climate Change*, 2 (6): 851-870.
- Zhang, X., Harvey, D.K., Hogg, W.D., Yuzyk, T.D., 2001. Trends in Canadian streamflow. *Water Resour. Res.*, 37 (4): 987-998.
- Zhang, X., Zwiers, F.W., 2013. *Statistical Indices for the Diagnosing and Detecting Changes in Extremes*. In: AghaKouchak, A., Easterling, D., Kuolin, H., Siegfried, S., Soroosh, S. (Eds.), *Extremes in a Changing Climate*. Springer, Dordrecht Heidelberg New York London, pp. 1-14.
- Zhu, Z., Bi, J., Pan, Y., Ganguly, S., Anav, A., Xu, L., Samanta, A., Piao, S., Nemani, R.R., Myneni, R.B., 2013. Global data sets of vegetation leaf area index (LAI) 3g and Fraction of Photosynthetically Active Radiation (FPAR) 3g derived from Global Inventory Modeling and

Mapping Studies (GIMMS) Normalized Difference Vegetation Index (NDVI3g) for the period 1981 to 2011. *Remote Sensing*, 5 (2): 927-948.

CHAPTER 7

7.1 General Discussion

The climate has always changed, but due to recent anthropogenic-forced release of CO₂ in the atmosphere, the climate is changing at a faster rate than ever before encountered in history. Climate change is projected to increase temperature and lead to variations in the hydrosphere, including shifts in hydrologic regimes on a local, regional and global scale (Arnell, 1999; Barnett et al., 2008; Leavesley, 1994; Stocker et al., 2013). Nowhere on earth are the changes in climate more apparent than the high latitude regions, where alterations in snow cover extent, snowmelt timing, permafrost and sea ice couple together to generate strong feedbacks and amplifications of changes that may lead to impacts not only a local scale but regionally and globally as well (Francis and Vavrus, 2012; Hinzman et al., 2005). Higher temperatures increase the water holding capacity of the air, which is the physical underpinnings of the Clausius Clapyron theory, and due to energy limitations is approximated at ~3.4% per 1°C change in temperature (Allen and Ingram, 2002), leading to an intensification of the hydrologic cycle (Huntington 2006, Rawlins et al. 2010). The Clausius Clapyron relationship indicates that larger and more frequent precipitation extremes may occur under warming of the climate system (Lorenz and DeWeaver, 2007; Pall et al., 2007). These extreme events have great propensity to alter the livability of the planet for humans, and to affect infrastructure, economy and social systems in ways that changes in the mean will never do (Katz and Brown, 1992). Thus, there is a pressing need to understand extreme events, and in particular, events in high latitudes basins, so changes may be quantified and planning and adaptation measures may be implemented.

Extreme events have been documented to be changing around the world (Field et al., 2012). Increased warm events have noted to be occurring, while increases and decreases in precipitation extremes are observed (Sillmann et al., 2013a). Future projections for extreme events in Alaska and the Arctic indicate that increased minimum temperatures and five-day maximum precipitation will occur in the future, with larger and more significant shifts occurring in the 2080s compared to the 2050s (Sillmann et al., 2013b; Stewart et al., 2013). Documented changes in high and low streamflow for the globe provide a more varied picture. Changes in the historical patterns of high and low streamflow have been most clearly linked with regards to shifts in snowmelt peak flow timing and snow cover extent, and in small basins of Alaska's North Slope (Brown, 2010; Derksen and Brown, 2012; Foster et al., 2008; Kane et al., 2008; Kane et al., 2003; Stewart et al., 2005; Wang et al., 2013). Low flows have been documented to be increasing as a consequence of thawing permafrost (Smith et al., 2007; St. Jacques and Sauchyn, 2009; Walvoord and Striegl, 2007).

Streamflow responses are variable depending on the regime examined (Fleming et al., 2007; Neal et al., 2002; Whitfield, 2001; Whitfield and Cannon, 2000; Whitfield et al., 2003). Figure 1 illustrates this concept. Climate forcings are passed through nonlinear filters such as glaciers and/or snow pack that alter the characteristics of extreme streamflow response (Fleming and Moore, 2007). For example, adjacent watersheds such as the Salcha and the Chena River basin have variable nonlinear responses to climate forcings that are a consequence of basin hypsometry, although overall they respond similarly to climate variability (i.e. Pacific Decadal Oscillation, PDO) and to changes in snow over time. Streamflow changes in glacier systems do not respond to climate variability, but do respond to changes in spring temperature. Lack of consideration with respect to streamflow regime and filters such glaciers, permafrost, lakes, and geological variability will lead to confusion when attempting to understand trends, and changes in extremes with respect to climate change on hydrology.

Examining extreme hydroclimate events in Alaskan river basins is challenging on a number of fronts. Lack of temporal and spatial consistency in station records and baseline information (i.e. soils, vegetation, elevation) to parameterize, calibrate and validate models hinders analytical approaches and leads to a paucity of studies detailing high latitude hydrology. To address these issues, approaches to input remote sensing tools have been introduced into models to attempt gap filling spatially, although temporally, remote sensing data are generally only available after the 1970s. These approaches can be coupled with distributed models that contain approaches to define frozen ground routines, for example, although these models are generally known to underperform conceptual models developed for flood forecasting in the region due to the lack of information to parameterize them. This presents a confounding issue – does a hydrologist apply a lumped model that performs well or a distributed model with parameterizations for such processes such as frozen ground but that also has greater uncertainty associated with it? This question cannot be resolved in this thesis work but both types of models are explored and their responses are documented.

Historical streamflow trends illustrate a picture of changing conditions within basins that largely represent shifts towards declining streamflow as a result of reduced snowpack, earlier snowmelt peak, and reductions in flow from the glaciers. Future streamflow projections, on the other hand, are towards increased maximum streamflow peaks. These increases in peak streamflow are a consequence of increases in precipitation coupled with increased spring temperatures leading to decreased snowmelt peaks and a marked change in summer and fall flow regimes. For systems such as the Chena River basin, this change represents a major shift away from a snowmelt dominated regime to a rainfall dominated hydrologic regime. These changes were verified by results of not just one, but two different hydrologic models. The projected peak rainfall events were directly linked with increased occurrence of flooding within watersheds, and therefore pose a risk to property and infrastructure in the region.

Our analysis showed that drivers of extreme hydroclimate in Alaska have changed over the past and are projected to change in the future. Global climate models and existing indices of extremes can be used to examine Alaska-wide responses and compare those responses to local stations and reanalysis products. ClimDEX indices calculated based on station data were different from GCMs but these differences are explained by topographic variability between the station and the model grid cells, while the reanalysis products were similar to the GCMs. When considering local changes in extreme events, however, downscaling processing should be applied. Downscaling applied in Chapter 6 revealed that compared to the historical time period, the 2080s RCP 8.5 differences between minimum and maximum extreme temperatures were smaller, indicating a narrowing in the range of results depicted by the coarse scale models for GCM grid boxes nearby Fairbanks, Alaska. Precipitation differences were greater in the downscaled results compared to raw GCM anomalies for Fairbanks. Quantile methods represent an improvement on downscaling processes for extremes, however other more complex methods exist and should be explored to determine if and how downscaling affects the modeling and representation of extremes in Alaska and the interior, in particular.

This work described herein involved collaborations with forecasters at the National Weather Service's Alaska Pacific River Forecast Center (APRFC). The APRFC's forecasting model framework was implemented at the University of Alaska to determine if input of MODIS observed snow cover extent would improve modeled streamflow. The MODIS data were verified against stations data across the region and found to be valid for use in these models. The model framework was altered to accept inputs of MODIS gridded data and the results indicated that sub-basins with poor or limited time series of streamflow could be improved, which has promise for unengaged or under-monitored streamflow throughout the state of Alaska. The next steps in the work will allow for researchers at UAF and collaborators at APRFC to work together to bring these offline tests into an online forecasting mode for use in the daily river forecasting. The model can then be updated on a day-to-day basis with snow cover observations from MODIS during the snowmelt season, a time during which the model simulated areal snow cover estimates are usually considered to be problematic.

The final chapter of this thesis outlines a climate change study of extreme events. The models used for the work did not integrate dynamic vegetation therefore fire activity, plant succession or landscape changes resulting from thermokarst erosion are not incorporated. Dynamic vegetation models exist and may be used to simulate changes in vegetation components, which may yield different answers with respect to changing extreme streamflow projections. Frozen ground models in discontinuous permafrost regions require further testing to determine their adequacy in the area. However, the frozen ground module presents a much larger uncertainty range around the GCMs, compared to the semi-lumped model examined in this work. That uncertainty may be representative of the true uncertainty present in the

system, and therefore ensemble modeling approaches should be undertaken in order to fully consider the range of uncertainty associated with the climate change projections and return level estimates. Finally, the quantitative results provided in this work need to be incorporated into adaptation strategies if the findings are going to make a difference. Because of the high costs associated with these projected impacts, moving forward with planning measures is vital so that resources and management frameworks may be re-allocated appropriately in the future.

7.2 Implications

Changes in hydroclimate extremes in Alaska's boreal region will impact not only natural systems, but also resource and economic development that relies upon, in part, the stability of the environment. Soil structures, erosion rates, and permafrost conditions, all of which will have a direct effect on state infrastructure such as buildings, pipelines, tailings ponds and water retention structures will be impacted. These challenges are discussed in this section to highlight some concerns and indicate where future studies should be focused.

Alterations in permafrost conditions in the boreal zone represent perhaps the greatest threat to infrastructure. Increased warm and decreased cold extremes affect frozen soils regimes, in zones such as the boreal where discontinuous 'warm' permafrost is close to 0°C this may result in the complete degradation of permafrost. Increased temperatures may also lead to increased frost heave, and other processes that affect the structure of the soil. The complicating factor with regards to permafrost change is related largely to the change in hydrology, including changes in snow, vegetation and soil moisture (Riseborough 1990). Snow pack provides insulation from cold waves penetrating deep into soil therefore an increase in snow depth might lead to warming of permafrost (Romanovsky et al. 2010). Organic soils also can protect the ground from thawing in the summer time by insulate the underlying soil from heat fluxes. The presence of water or ice in the ground also changes thermal conductivity of the soils, and latent heat processes can lead to decreased amplitudes of cold waves in the ground (Riseborough 1990). Thus, changing permafrost condition is highly dependent on snow cover, ice and unfrozen water, and vegetation characteristics, all of which can be altered by changing extremes.

Where hydrologic changes result in permafrost degradation and active layer thawing, increased soil moisture storages may lead to decreased runoff, as proposed by some researchers. The addition of this moisture may consequently result in lower soil stability which would impact structural supports. The findings in this work indicate that snow water equivalent (not always an indication of snow depth) will decrease in the future in boreal watersheds. Soil moisture increases slightly, but the largest change is in the increased runoff owing to increased precipitation that overwhelms the changes in evapotranspiration. Frozen ground warms considerably over the century, although the ground remains frozen at the deepest

soil layer to 2100. However, the active layer deepens and all soil layers above this become unfrozen towards the end of the century. Increased runoff and deepened active layers have a considerable effect, and are discussed below.

Unfrozen soils have weaker structures compared to frozen soils. Building supports designed for frozen soils that become unfrozen may collapse, leading to economic loss either in the redesign or abandonment of these structures. Personal property loss may occur if these effects are predominant in populated regions, for example in the town Fairbanks where development on permafrost is common. Since deep ground thaw is not projected to occur, it is likely that mid-sized buildings with pile foundations in the upper soil profile may be the most strongly impacted by these changes (ACIA, 2005). Thawing action in soils can also lead to soil heave, frost piles, settlement and other impacts that would affect structures. Pipelines, which stretch across vast tracts of Interior Alaska, may be particularly susceptible to changes in frozen ground if regional warming and thawing of permafrost occurs. A deeper active layer may also lead to erosional effects such as slope failure which could impact roadways and transmission lines and disrupt communications, energy, transport and emergency access. Pit mining facilities could be affected by changing soil conditions and soil moisture, leading to potential collapse or failure of pit slopes (ACIA 2005).

Summer flooding would have a great effect on infrastructure and settlements located nearby water resources. After the 1967 Fairbanks flood, the Army Corps of Engineers build the Chena River diversion project to capture flood waters and protect the town of Fairbanks. However, the structure has never been tested to withstand a flood similar in size to the 1967 event. Changes to soil characteristics (i.e. strength) caused by changing freeze/thaw regimes may alter the retention capability of the side banks of the Chena Diversion, or other water retention structures. These impacts may limit the ability of the structure to hold and retain flood waters. On the other hand, if the structure was developed to account for these changes, this concern would be mitigated.

Flooding along the upper Chena River basin would affect access to Chena Hot Springs Road River and the popular Chena Hot Springs resort. Summer flooding also affects the Pogo mine airstrip, inundating the airstrip at moderate to high flows on the Salcha, and restricting emergency access and roadways in and out of the mine. Summer flooding could also have implications for tailings ponds located at the Kinross Fort Knox mine site, or the nearby True North gold mine. Flooding could also impact bridges, pipeline river crossings, and lead to culvert blow outs along roadways. High flows in rivers adjacent highways or settlements may undercut structures, leading to loss of integrity. Flooding will impact airports, and army and air force bases such as Fort Wainwright, Eielson and Fort Greely, which are all located adjacent to Interior river systems nearby Fairbanks, Alaska.

7.3 Conclusions

Extreme events in Alaska's Interior boreal forest are projected to change into the future. Peak streamflow is projected by models to be precipitation dominated with lower peaks associated with snowmelt, and an earlier snowmelt peak. Models to simulate changes in streamflows are improved by estimates of remotely sensed snow cover observations in under monitored watersheds. All such improvements should be utilized to project the impacts of changing extremes and attempt to minimize and/or accurately assess uncertainty associated with the climate projections. Basins such as the Chena are susceptible to changing form of precipitation (i.e. snow) due to relatively low elevation gradients, which respond largely to changing precipitation conditions and regime shifts (such as the PDO). Low summer flows are not likely to be an issue, however increasingly high winter baseflows are projected. The major impact, however, will be the shift in flow regime from a snowmelt-rainfall dominated system to a rainfall dominated system, which will have consequence for many components of the boreal forest ecosystem, the community and the economy. These consequences include thawing permafrost, active layer deepening and reduced soil stability, increased erosion, sedimentation and increased liquid soil water content and reduced ice content. These changes will impact infrastructure and in particular, mid-sized buildings, residential homes, highways, bridges, mining tailings ponds and pits, pipelines and military lands. The work presented herein is a first step towards understanding changing extreme events in the boreal forests of Alaska. The changes projected are of a magnitude that can be managed through proper planning and targeted adaptation strategies but the call towards those efforts must be heeded.

7.4 Figures

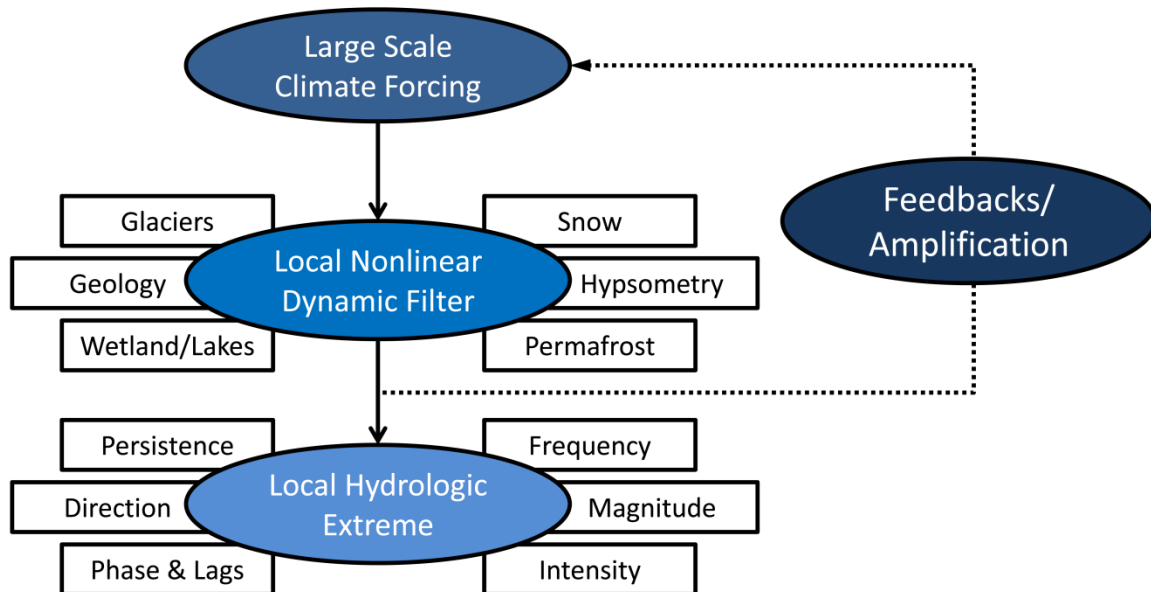


Figure 7.1 Large scale climate forcing when applied through landscape filters (i.e. snow, glaciers, permafrost) alter response and result in variability in hydroclimate response to extreme events, even in adjacent basins. Figure and concepts adapted from Fleming and Moore, 2007.

7.5 References

- ACIA, 2005. Chapter 6: Cryosphere and Hydrology. In: Walsh, J.E. (Ed.), *The Arctic Climate Impact Assessment*. Cambridge University Press, pp. 1042.
- Allen, M.R., Ingram, W.J., 2002. Constraints on future changes in climate and the hydrologic cycle. *Nature*, 419(6903): 224-232.
- Arnell, N.W., 1999. Climate change and global water resources. *Global Environ. Change*, 9: S31–S49.
- Barnett, T.P. et al., 2008. Human-induced changes in the hydrology of the western United States. *Scienceexpress*: 1-4.
- Brown, R.D., 2010. Northern Hemisphere snow cover variability and change, 1915–97. *J. Clim.*, 13: 2339–2355.
- Derksen, C., Brown, R., 2012. Spring snow cover extent reductions in the 2008–2012 period exceeding climate model projections. *Geophys. Res. Lett.*, 39(19): L19504.
- Field, C.B., Barros, V., Stocker, T.F., Dahe, Q., 2012. *Managing the Risks of Extreme Events and Disasters to Advance Climate Change Adaptation: Special Report of the Intergovernmental Panel on Climate Change*. Cambridge University Press.
- Fleming, S., Moore, R.D., 2007. Local-scale controls on hydrologic responses to climate variability. *CMOS Bulletin SCMO*, 36(1).
- Fleming, S.W., Whitfield, P.H., Moore, R.D., Quilty, E.J., 2007. Regime-dependent streamflow sensitivities to Pacific climate modes cross the Georgia–Puget transboundary ecoregion. *Hydrol. Process.*, 21(24): 3264-3287.
- Foster, J.L., Robinson, D.A., Hall, D.K., Estilow, T.W., 2008. Spring snow melt timing and changes over Arctic lands. *Polar Geogr.*, 31(3-4): 145-157.
- Francis, J.A., Vavrus, S.J., 2012. Evidence linking Arctic amplification to extreme weather in mid-latitudes. *Geophys. Res. Lett.*, 39(6): L06801.
- Hinzman, L.D. et al., 2005. Evidence and implications of recent climate change in northern Alaska and other Arctic regions. *Clim. Change*, 72: 251-298.
- Huntington, T.G., 2006. Evidence for intensification of the global water cycle: Review and synthesis. *Journal of Hydrology*, 319: 83-95.
- Kane, D.L. et al., 2008. Contrasting extreme runoff events in areas of continuous permafrost, Arctic Alaska. *Hydrology Research*, 39(4): 287-298.
- Kane, D.L., McNamara, J.P., Yang, D.Q., Olsson, P.Q., Gieck, R.E., 2003. An extreme rainfall/runoff event in Arctic Alaska. *J. Hydrometeorol.*, 4(6): 1220-1228.

- Katz, R.W., Brown, B.G., 1992. Extreme events in a changing climate: variability is more important than averages. *Clim. Change*, 21: 289-302.
- Leavesley, G.H., 1994. Modeling the effects of climate change on water resources-a review. *Clim. Change*, 28(1-2): 159-177.
- Lorenz, D.J., DeWeaver, E.T., 2007. The response of the extratropical hydrological cycle to global warming. *J. Clim.*, 20(14).
- Neal, E.G., Walter, M.T., Coffeen, C., 2002. Linking the Pacific decadal oscillation to seasonal stream discharge patterns in Southeast Alaska. *Journal of Hydrology*, 263: 188-197.
- Pall, P., Allen, M., Stone, D., 2007. Testing the Clausius–Clapeyron constraint on changes in extreme precipitation under CO₂ warming. *Climate Dynamics*, 28(4): 351-363.
- Rawlins, M.A. et al., 2010. Analysis of the Arctic system for freshwater cycle intensification: Observations and expectations. *J. Clim.*
- Riseborough, D.W. 1990. Soil latent heat as a filter of the climate signal in permafrost. *Proceedings of the Fifth Canadian Permafrost Conference, Collect. Nordicana*, 54: 199-205.
- Romanovsky, V.E., Smith, S.L., Christiansen, H.H. 2010. Permafrost thermal state in the polar Northern Hemisphere during the international polar year 2007–2009: A synthesis. *Permafrost and Periglacial Processes*, 21(2): 106-116.
- Sillmann, J., Kharin, V., Zhang, X., Zwiers, F., Bronaugh, D., 2013a. Climate extremes indices in the CMIP5 multi-model ensemble. Part 1: Model evaluation in the present climate. *J. Geophys. Res.: Atmos.*
- Sillmann, J., Kharin, V., Zwiers, F., Zhang, X., Bronaugh, D., 2013b. Climate extreme indices in the CMIP5 multi-model ensemble. Part 2: Future climate projections. *J. Geophys. Res.: Atmos.*
- Smith, L.C., Pavelsky, T.M., MacDonald, G.M., Shiklomanov, A.I., Lammers, R.B., 2007. Rising minimum daily flows in northern Eurasian rivers: A growing influence of groundwater in the high-latitude hydrologic cycle. *Journal of Geophysical Research: Biogeosciences*, 112(G4): G04S47.
- St. Jacques, J.-M., Sauchyn, D.J., 2009. Increasing winter baseflow and mean annual streamflow from possible permafrost thawing in the Northwest Territories, Canada. *Geophys. Res. Lett.*, 36(1): L01401.
- Stewart, B., Kunkel, K.E., Stevens, L.E., Sun, L., Walsh, J.E., 2013. Regional Climate Trends and Scenarios for the U.S. National Climate Assessment. Part 7. Climate of Alaska., NOAA/NESDIS, Washington, D.C.

- Stewart, I.T., Cayan, D.R., Dettinger, M.D., 2005. Changes toward earlier streamflow timing across Western North America. *J. Clim.*, 18: 1136-1155.
- Stocker, T. et al., 2013. IPCC, 2013: climate change 2013: the physical science basis. Contribution of working group I to the fifth assessment report of the intergovernmental panel on climate change.
- Walvoord, M.A., Striegl, R.G., 2007. Increased groundwater to stream discharge from permafrost thawing in the Yukon River basin: Potential impacts on lateral export of carbon and nitrogen. *Geophys. Res. Lett.*, 34(12): L12402.
- Wang, L., Derksen, C., Brown, R., Markus, T., 2013. Recent changes in pan-Arctic melt onset from satellite passive microwave measurements. *Geophys. Res. Lett.*, 40(3): 522-528.
- Whitfield, P.H., 2001. Linked hydrologic and climate variations in British Columbia and Yukon. *Environ. Monit. Assess.*, 67: 217-238.
- Whitfield, P.H., Cannon, A.J., 2000. Recent variations in climate and hydrology in Canada. *Can. Water Resour. J.*, 25: 19-65.
- Whitfield, P.H., Wang, J.Y., Cannon, A.J., 2003. Modelling Future Streamflow Extremes - Floods and Low Flows in Georgia Basin, British Columbia. *Can. Water Resour. J.*, 28(4): 633 - 656.